



**Palaeoproterozoic eclogite formation in Tanzania: a structural, geochronological, thermochronological and metamorphic study of the Usagaran and Ubende orogenic belts.**

Rachael A. Brick

Geology & Geophysics  
School of Earth & Environmental Science

University of Adelaide

Submitted – 8<sup>th</sup> April, 2011

---



# TABLE OF CONTENTS

---

Abstract	i.
Acknowledgements	iii.
Declaration	v
<b>Chapter 1 - Tectonic settings of Palaeoproterozoic eclogites</b>	<b>1.1</b>
1.1 Introduction	
1.1.1 Eclogite or not eclogite, what is the difference?	
1.1.2 Problems in dating eclogites	
1.1.3 Precambrian plate tectonics	
1.1.4 Problems of P-T determination	1.2
1.2. Eclogite types and their tectonic settings	1.3
1.3 Tectonic scenarios for Palaeoproterozoic eclogite-hosting orogens	
1.3.1 Tanzania	
1.3.1.1 Usagaran Orogen	
1.3.1.2 Ubende Orogen	
1.3.2 Snowbird tectonic zone, Canada	1.4
1.3.3 Lapland Granulite Belt	1.5
1.3.4 North China Craton	
1.3.5 Sare Sang, Afghanistan	
1.3.6 Archaean Eclogites and high-P rocks	
1.3.6.1 Belomorian Eclogites	
1.3.6.2 Barberton granitoid-greenstone terrane	
1.4. Discussion	1.6
1.5. Scope of this project	1.7
<b>Chapter 2 - Characterising the crustal evolution of the Tanzanian Craton using LA-ICPMS U-Pb and Lu-Hf analyses of detrital zircon</b>	<b>2.1</b>
2.1 Introduction	
2.2 Geology and geochronology of the Tanzanian Craton	
2.3 Samples and analytical techniques	2.2
2.3.1 Sampling strategy	
2.3.2 Sample preparation	2.3
2.3.3 Analytical technique – LA-ICPMS U-Th-Pb geochronology	
2.3.4 Analytical technique – LA-MC-ICPMS Hf isotope analysis	
2.4 Results	2.4
2.4.1 TC2 – Zira River, Mbeya district	
2.4.2 TC3 – Durumo River, Singida district	
2.4.3 TC4 – Malagarasi River, Uvinza township	2.5
2.4.4 Albsong-05	
2.5 Discussion	
2.5.1 The significance of concordant Archaean U-Pb ages	
2.5.2 The significance of Archaean Lu-Hf data	2.7
2.5.3 Post-Archaean crustal evolution of the Tanzanian Craton	
2.6 Conclusions	2.8

---

<b>Chapter 3 - <math>^{40}\text{Ar}/^{39}\text{Ar}</math> Thermochronology and U-Pb geochronology of the eclogite-hosting Ubende Belt, Tanzania</b>	<b>3.1</b>
3.1 Introduction	
3.2. Geological Background	
3.3. Structure	3.2
3.4. Sample details and analytical procedure	3.3
3.4.1 Zircon U-Pb geochronology	
3.4.2 <i>Hornblende <math>^{40}\text{Ar}/^{39}\text{Ar}</math> thermochronology</i>	
3.5. Results	3.8
3.5.1 U-Pb results	
3.5.2 $^{40}\text{Ar}/^{39}\text{Ar}$ results	3.9
3.6. Discussion	3.12
3.6.1 Source of Ubende sediments	
3.6.2 Timing of sedimentation, metamorphism and exhumation	3.14
3.6.3 <i>Significance of Hadean aged zircons</i>	3.16
3.7. Conclusions	
<b>Chapter 4. Architecture of a Palaeoproterozoic subduction zone: a structural and geochronological traverse through the Usagaran Orogen, Tanzania</b>	<b>4.1</b>
4.2 Crustal Architecture and temporal evolution	
4.3 Lithology	4.2
4.3.1 Tanzanian Craton	
4.3.2 Konse Group	
4.3.3 Isimani Suite	
4.3.3.1 Luhomero lithodeme	4.3
4.3.3.2 The Mbunga River lithodeme	
4.4 Structural traverse	4.4
4.4.1 Domains of contrasting deformational style	
4.4.1.1 Tanzanian Craton	
4.4.1.2 Konse Domain	4.5
4.4.1.3 Luhomero Domain	
4.4.1.4 Jede Domain	4.8
4.4.1.5 Chogola Shear	
4.4.1.6 Kikuyu domain	
4.4.1.7 Kinusi domain	
4.4.1.8 Wazaganza domain	
4.4.1.9 Idodoma domain	4.9
4.4.1.10 Ruaha-Mbuyuni domain	
4.4.2 Deformational phases	
4.4.2.1 D <sub>1</sub> deformation	
4.4.2.2 D <sub>2</sub> deformation	4.11
4.4.2.3 D <sub>3</sub> deformation	
4.4.2.4 D <sub>4</sub> deformation	4.12
4.4.4 Distribution of bulk strain and strain type	
4.5 U-Pb Geochronology	
4.5.1 Analytical methods – LA-ICPMS geochronology	
4.5.2 Sample details	
4.5.3 Geochronology results	4.13
4.6 Discussion	4.17
4.6.1 Geochronology	
4.6.1.1 Timing of sediment deposition	
4.6.1.2 Provenance of sediments	4.18
4.6.1.3 Timing of Usagaran deformation and metamorphism across the orogen	4.19
4.6.1.4 Timing of “East-African” metamorphism	
4.6.2 Structural evolution of the Usagaran orogenic belt	4.20
4.6.3 Tectonic models	4.22
4.7 Conclusions	

---



<b>Chapter 5 - P-T-t evolution of the 2.0 Ga eclogite-hosting Usagaran orogenic belt, Tanzania</b>	<b>5.1</b>
5.1 Introduction	
5.2 Geological setting	
5.2.1 Previous metamorphic studies	5.2
5.3 Metamorphic petrology	5.3
5.3.1 Abbreviations	
5.3.2 Eclogites and mafic rocks	
5.3.3 Metapelites	5.5
5.4 Analytical procedures	
5.4.1 Electron Microprobe	
5.4.1.1 Garnet profiles	5.6
5.4.2 Thermobarometry	
5.4.2.1 THERMOCALC overview	
5.4.2.2 P-T calculations	5.7
5.4.3 Trace element thermometry	5.8
5.4.3.1 Quartz temperature estimates	5.9
5.4.3.2 Rutile temperature estimates	5.10
5.4.3.3 Zircon temperature estimates	
5.4.3.4 U-Pb-Th LA-ICPMS analyses	
5.5 Discussion	5.11
5.5.1 Ti in zircon thermometry	
5.5.2 Eclogites and intercalated rocks	
5.5.3 Garnet zoning	5.13
5.5.3.1 Garnet-biotite diffusion modeling	
5.5.3.2 Thermal History software	5.14
5.5.3.3 Cooling rates of pelites	
5.5.4 Cooling rates	5.15
5.5.5 P-T evolution	5.16
5.6 Conclusions	5.17
<b>Chapter 6 - Archaean to Proterozoic crustal evolution of the orogenic belts surrounding the Tanzanian Craton: constraints from combined U-Pb and Lu-Hf analyses of detrital zircon</b>	<b>6.1</b>
6.1 Introduction	
6.1.1 Regional geology	
6.2 Sampling strategy and analytical techniques	
6.2.1 LA-ICPMS U-Pb-Th analysis	6.3
6.2.2 LA-ICPMS Lu-Hf analysis	
6.3 Results	
6.3.1 Usagaran orogenic belt	6.4
6.3.2 Ubende orogenic belt	6.7
6.3.3 Songea District stream sediments samples	6.9
6.4 Discussion	
6.4.1 Crustal evolution studies of other East African orogenic belts	
6.4.2 Crustal evolution of Ubende and Usagaran belts	6.10
6.4.3 Do the Usagaran and Ubende belts form one contiguous orogenic belt?	
6.5 Conclusions	6.12
<b>Chapter 7 – Conclusions</b>	<b>7.1</b>
7.1 Crustal evolution	
7.2 Ubende Orogen	
7.3 Usagaran Orogen	
7.3.1 <i>Structure</i>	
7.3.2 <i>Timing of Metamorphism</i>	
7.3.3 <i>Geochronology</i>	
7.3.4 <i>Metamorphic Conditions</i>	
7.4 Conclusions	
<b>References</b>	<b>8.1</b>

<b>Appendices</b>	9.1
Appendix 1 – U-Pb data for sample AlbSong-05	
Lu-Hf data for sample AlbSong-05	9.2
Appendix 2 – Representative AX output file. File is for sample T01-22, peak assemblage	9.3
Representative THERMOCALC output file. File is for sample T01-22, peak assemblage	
Appendix 3 – U-Pb data for sample AlbSong-01 – AlbSong-04	9.6
Lu-Hf data for sample AlbSong-01 – AlbSong-04	9.14

## Abstract

---

Eclogites and other high-P low-T rocks have been used to understand changing tectonic regimes and the processes which have shaped the Earth. Uncertainty exists over the tectonic setting of Palaeoproterozoic high-pressure rock formation with several workers proposing that deep subduction, the most commonly inferred method for modern high-pressure metamorphism, was not functioning at the time these rocks formed. Tanzania hosts two of the oldest *in-situ* eclogites in the 2.0 Ga Usagaran and 1.85 Ga Ubendian orogenic belts, with km-scale eclogite & retrograde-eclogite sheets in these locations interlayered with felsic gneisses and amphibolites. These orogenic belts form the south-eastern and south-western margins of the Tanzanian Craton. Based on detrital zircon study on stream sediments the Tanzanian Craton formed between 2850 – 2500 Ga with magmas derived from an evolved ( $T_{DM}$  crustal = 3.2 Ga) source.

Lu-Hf studies on metasedimentary rocks show the Ubende and Usagaran Belt's crustal material formed between 1850 – 2050 Ma from a more evolved magma source ( $T_{DM}$  crustal = 2.6 Ga) that also reworked some Archaean material from the Tanzanian Craton. The Ubende and Usagaran belts have similar but not identical crustal evolution histories through the Archaean and Palaeoproterozoic, but the Mesoproterozoic evolution of the Ubende diverges from the Usagaran. The Songea district, situated at the junction of these orogenic belts, has a separate crustal evolution and does not form the link between the two orogens. The youngest zircon population (1.0 – 1.2 Ga) may be derived from the Irumide Belt, and has a mixed ( $T_{DM}$  crustal = 2.1 and 1.3 Ga) magma source. Thus the belts, sometimes referred to as a continuous orogenic system, are in fact distinguishable by their crustal evolution and the timing of sedimentation and metamorphism.

Ubendian eclogites have been dated using  $^{40}\text{Ar}/^{39}\text{Ar}$  at  $1848 \pm 6$  Ma (Boven et al., 1999).  $^{40}\text{Ar}/^{39}\text{Ar}$  thermochronology on a suite of five samples coupled with U-Pb geochronology yields a new metamorphic age for the Ubende Belt. An age of ~1070 Ma is preserved in zircon within metasedimentary rocks with cooling below ~500 °C at ~1020 Ma.

Structures in the Usagaran Belt are consistent with sinistral transpression associated with collision between the Tanzanian craton and an unknown continent. The metasedimentary rocks of the eastern Usagaran rocks are inconsistent with being derived from the Tanzanian Craton, indicating the existence of an as yet unidentified continental block as part of the collisional event. Rocks from the western Usagaran are more consistent with being derived from the craton, with some input of sediment derived from local igneous activity, possibly a volcanic arc.

Two metamorphic events were recognised in the Usagaran belt. Usagaran metamorphism occurred over ~20 My between 2007 and 1991 Ma. The East African orogen affected these rocks during the Neoproterozoic, and is recorded in zircon growth in the east of the orogen at  $577 \pm 17$  Ma. Peak eclogite-facies P-T conditions in the Usagaran Orogeny ( $17.2 \pm 3.6$  kbar,  $839 \pm 173$  °C) were slightly higher temperature than previously published. Lithologies intercalated with eclogite in the eclogite body experienced conditions of at least  $13.4 \pm 2$  kbar,  $920 \pm 130$  °C, however there is no evidence of pelitic rocks having experienced the 17 kbar which the eclogites saw. Fe-Mg diffusion modeling on garnet-biotite shows that country-rock pelites cooled at ~1-2 °C/My, compared to 25°C/My for eclogites between 1999 and 1991 Ma.

All of these facts are consistent with the eclogite body having formed during subduction of Palaeoproterozoic sea-floor which became intercalated with metasediments and other metaigneous rocks during exhumation. The surrounding blocks of the Isimani suite did not experience eclogite-facies metamorphism but were tectonically juxtaposed during exhumation. All this strongly supports a Palaeoproterozoic subduction-related origin for eclogites in the Usagaran Belt.

---



## Acknowledgements

---

This work was funded by Australian Research Council Discovery grant DP0774019 to Alan Collins, Martin Hand, Graham Heinson and Karin Barovich. Thanks for letting me be a part of this awesome project. Alan Collins, Martin Hand and Steve Reddy are particularly thanked for supervising me through this project, and Alan for keeping pushing me the whole way through.

U-Pb-Th analyses, CL imaging and EMP analyses were conducted at Adelaide Microscopy, and couldn't have been completed without the assistance of many of the staff there, particularly Angus Netting, Ben Wade, Peter Self, and the rest of the team there. You guys have been awesome. Thanks also to Fred Juordan at the Western Australian Argon Isotope Facility at Curtin University for his invaluable assistance with  $^{40}\text{Ar}/^{39}\text{Ar}$  analyses. Lu-Hf analyses were conducted at Macquarie University and comprise a contribution from the ARC National Key Centre for the Geochemical Evolution and Metallogeny of Continents (<http://www.els.mq.edu.au/GEMOC>). This study was supported by funding to the Macquarie University geochemical node of the AuScope NCRIS and used instrumentation funded by ARC LIEF and DEST Systematic Infrastructure Grants, Macquarie University and Industry.

Albidon Limited is gratefully thanked for allowing me access to the results from their study of stream sediments in the Songea District of Tanzania which have enhanced the discussion of the crustal evolution of the orogenic belts surrounding the Tanzanian Craton.

Professor Abdul Mruma and the Geological Survey of Tanzania are thanked for logistical support, especially Aniset Mundi and Philip Momburi for spending time out in the field and translating on those numerous occasions when my Swahili just couldn't cut it.

CERG-tank crew, without your company over the years I'd either have gone totally nuts, or got more work done, or given up... possibly a bit of all. Particular thanks to Cuttsy, Ailsa, Yee, Katie, De... you were brilliant. My family and friends have supported me so much through this whole process. Finally you can ask "are you finished yet". Thanks for putting up with me.

Karen Hennekam is thanked for helping me get through. Without her support (emotional, physical and fiscal) I'd never have gotten this far. Thank you.

---



This work contains no material which has been accepted for the award of any other degree or diploma in any university or other tertiary institution to Rachael A. Brick and, to the best of my knowledge and belief, contains no material previously published or written by another person, except where due reference has been made in the text.

I give consent to this copy of my thesis, when deposited in the University Library, being made available for loan and photocopying, subject to the provisions of the Copyright Act 1968.

I also give permission for the digital version of my thesis to be made available on the web, via the University's digital research repository, the Library catalogue, the Australasian Digital Theses Program (ADTP) and also through web search engines, unless permission has been granted by the University to restrict access for a period of time.

Rachael A. Brick

Date - 8/4/2011

---





# Chapter 1 - Tectonic settings of Palaeoproterozoic eclogites.

## 1.1 Introduction

Eclogites and other high-pressure rocks have been used by various authors to interpret changing tectonic regimes of the earth (Maruyama and Liou, 1998b; O'Brien and Rötzler, 2003) because the pressure conditions of their formation are equivalent to those at mantle depths while the temperatures recorded by the mineral assemblages are cooler than those found within the mantle. Eclogites form at high-pressures, and require relatively fast exhumation to preserve their mineral assemblage. The mechanism for transporting rocks to mantle depths then rapidly exhuming them to mid-crustal levels is commonly considered to be subduction, because it is within known subduction zones that modern eclogites are found.

Eclogitic rocks are relatively rare in the geological record (Figure 1.1), and are more common in the Phanerozoic earth than the Proterozoic or older. The paucity of eclogites in the geological record may be because:

- the pressure-temperature (P-T) conditions to form eclogites are rare;
- preservation of eclogite during exhumation is rare;

or due to a combination of all these factors.

This chapter aims to summarise the current literature on Palaeoproterozoic eclogites and their tectonic settings, and to propose a methodical framework for investigating one of these occurrences.

### 1.1.1 Eclogite or not eclogite, what is the difference?

Eclogite, *sensu stricto*, consists of garnet and omphacitic clinopyroxene, and may contain relatively small amounts of amphibole, kyanite, quartz, talc, rutile, zoisite or clinozoisite and white mica (Newton, 1986). They have the bulk-rock geochemical characteristics of gabbro and experimental studies have confirmed that eclogite can form from gabbro submitted to high pressures (Green and Ringwood, 1972; Ringwood and Green, 1966)

The term 'eclogite-facies', used to describe metamorphism at high-pressure with (relatively) low-temperature (Eskola, 1929) includes garnet peridotites and whiteschists as well as eclogites. Since it is the P-T conditions of their formation that makes eclogites unusual this paper will consider all eclogite-facies rocks.

### 1.1.2 Problems in dating eclogites

The dating of metamorphism is always problematical in rocks, since we can only date certain events. Radiometric dating provides an age based on when accumulation of radiogenic daughter isotopes in minerals begins. Accumulation of daughter isotopes begins when the mineral becomes a closed system, which occurs when the mineral is cooled to a temperature such that diffusion of atoms is no longer possible. Since retention is related to temperature, we are actually dating the "closure temperature" of a mineral. The most robust technique for dating high-grade metamorphism is U-Pb dating, however U-rich minerals such as zircon are rare in mafic eclogites, so they are commonly dated using the Sm-Nd method. The closure temperature for Sm-Nd in garnet is 600 – 700 °C (Burton et al., 1995; Mezger et al.,

1992), so the dates obtained by this method are usually cooling dates associated with exhumation or later metamorphic events. Sm-Nd chronometry can also be affected by isotopic disequilibrium in the Sm-Nd system within garnets, which can lead to ambiguous ages arising from REE-rich inclusions (i.e. apatite, zircon etc.), variations in lattice concentrations (i.e. (Anczkiewicz et al., 2002; DeWolf et al., 1996)) or HREE zoning within garnets, with Sm partitioning into late phases of growth (Lapen et al., 2002; Schmitz et al., 2002). The U-Pb method can also be applied to monazite, titanite and rutile if they are present in the rocks to be dated.

For example, in a recent study of the Mariánské Lázně Complex (Czech Republic), Timmerman (2004) found that U-Pb single-grain zircon analyses (TIMS) from mafic rocks gave a concordant age of 540 Ma while metamorphic zircon from mafic rocks, monazite from orthogneiss and titanite in leucosomes gave ages around 380 Ma, which is interpreted to be the age of exhumation. Eclogitization was previously dated at  $487 \pm 13$  Ma, however this age was re-interpreted as the age of an igneous event. Sm-Nd dating of the garnet in eclogite yields ages of  $377 \pm 7$  Ma and  $367 \pm 4$  Ma (Beard et al., 1995). These dates likely represent the cooling age during exhumation. None of these ages represent the high-pressure metamorphic event.

Some suggestions for how to accurately date HP metamorphism are:

- SHRIMP or LA-ICPMS on zircon inclusions in HP garnets.
- LA-ICPMS or SHRIMP on monazite inclusions in HP garnets.
- Lu-Hf ICP-MS on REE-rich garnet – avoiding Hf-rich inclusions (Duchine *et al.*, 1997; Scherer *et al.*, 2002)

Considering the difficulty of dating eclogites it is important when reading eclogite geochronology papers to be aware of exactly what has been dated. There are numerous examples in the literature (i.e. (Beard et al., 1995; Cao and Zhu, 1995; Timmermann et al., 2004)) of dates for eclogites which have been subsequently revised to reflect much younger eclogitization ages.

### 1.1.3 Precambrian plate tectonics

The questions of when Earth first developed a modern style plate tectonic systems, differences in tectonic processes over time, and the reasons for these differences (i.e. changes in mantle temperatures, geothermal gradients, plate sizes, etc) have been the subject of debate over the last decade or more (eg. (Brown, 2007a, b; Maruyama and Liou, 1998a; Sizova et al., 2010; Stern, 2005a)). There is general consensus that recycling of crustal material has been in operation since at least 3.0-3.2 Ga (Cawood et al., 2009; Cawood et al., 2006; Condie, 2008; Windley and Garde, 2009). Paired high-P-low-T and high-T-low-P tectonothermal environments (Miyashiro, 1973) requiring plate subduction, have been recognized as far back as the Neoproterozoic (Brown, 2007a, b), although differences in

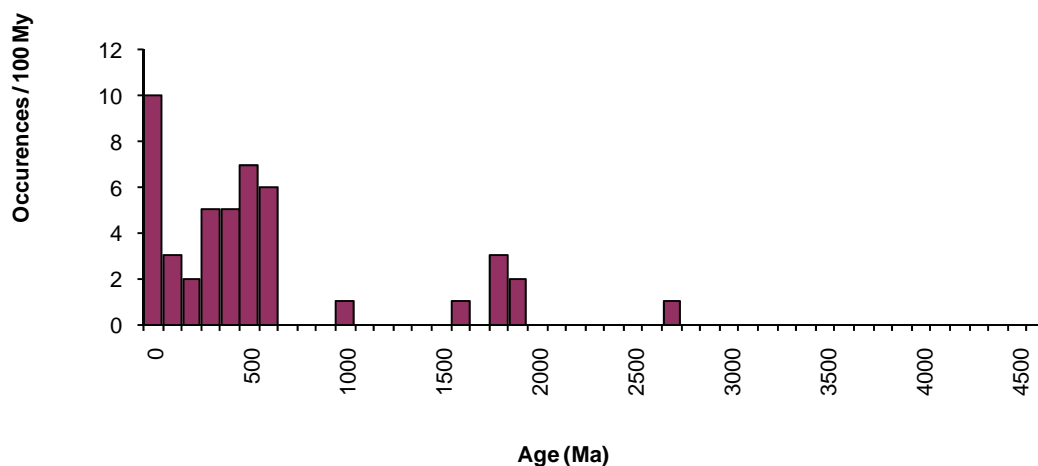


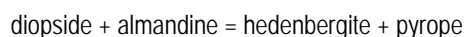
Figure 1.1 Frequency of eclogite occurrences through time.

the style of metamorphism have been recognised. The Neoarchaean-Proterozoic plate tectonics regime is characterised by high-pressure granulites and ultra-high-temperature metamorphism while the modern (Neoproterozoic-current) plate tectonics regime is characterised by high-pressure to ultra-high-pressure metamorphism (Brown, 2007a).

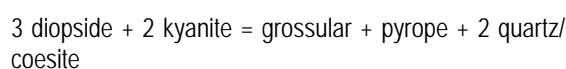
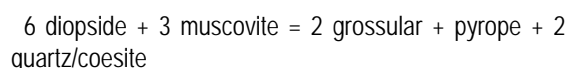
#### 1.1.4 Problems of P-T determination

One of the most common methods for estimating the P-T conditions of a rock is to analyse the distribution of elements between different minerals in an assumed equilibrium assemblage and use these as geobarometers and geothermometers. In the past many authors (El-Shazly et al., 1990; Kienast, 1991 #337; Oh, 1990 #338; Sklyarov, 1998 #14; Zhao, 2000 #153) have used the Fe-Mg exchange garnet-clinopyroxene geothermometers in conjunction with the albite-jadeite-quartz equilibria to get an estimation of temperature and minimum pressure, however this estimation is only of the minimum pressure, and the albite-jadeite-quartz equilibria cannot be accurately used where albite is absent.

A common reaction used for geothermometry is the Fe-Mg exchange between garnet and clinopyroxene, according to the reaction



with an exchange coefficient ( $K_d$ ) defined as  $(\text{Fe}^{2+}/\text{Mg}^{2+})_{\text{grt}}/(\text{Fe}^{2+}/\text{Mg}^{2+})_{\text{cpx}}$  (Krogh, 1988). The main issue with this involves large errors introduced by the recalculation of  $\text{Fe}^{2+}$  and  $\text{Fe}^{3+}$  from microprobe analyses. Two thermobarometers which are relatively independent of Fe exchange are:



which can be applied using activity models provided by Ravna and Terry (Ravna and Terry, 2004) and operate in the K-Ca-Mg-Al-Si-H (KCMASH) system.

Recent work has been done on the application of rutile thermometry to eclogites (Zack and Luvizottow, 2006). Rutile thermometry is based on the Zr content in rutile

coexisting with quartz and zircon and analysis is done using secondary ion mass spectrometry (SIMS). Temperature results from this study gave results within error of those obtained by previous P-T studies, but were more internally reproducible on a thin-section scale, and are interpreted by Zack and Luvizottow (Zack and Luvizottow, 2006) to allow better determination of metamorphic gradients within an eclogite terrain. This technique is relatively unproven at this time, however could prove a useful tool in conjunction with other systems. If used in conjunction with U-Pb geochronology of rutile this could be powerful in dating metamorphism.

Thermocalc pseudosections, which are used effectively for P-T determination of many rock types, are often ineffective on eclogites as they tend to have low mineral variance, meaning mineral assemblages are stable over large P-T ranges.

#### 1.2. Eclogite types and their tectonic settings

Several classifications of eclogites have been proposed, with older divisions based on their geological setting (ie. xenolithic eclogite, ophiolitic eclogite, and eclogite within gneiss (Coleman, 1965; Smulikovski, 1964)), while more recent work has focussed on a division based on temperature or pressure. This paper considers all non-xenolithic Palaeoproterozoic eclogites and eclogite facies rocks. It also includes some granulite facies rocks, which have been interpreted as retrograde eclogites.

Ophiolitic eclogites are associated with glaucophanites and form high-P belts in orogenic belts. They are commonly considered remnants of palaeo-subduction zones (Godard, 2001). Eclogites within gneisses are more enigmatic as they form at significantly higher P-T conditions than the surrounding gneisses. There is a tendency to consider that eclogite-facies assemblages are more easily preserved in eclogite than in gneisses where the combined effects of fluid, plasticity and kinetics lead to recrystallisation during retrogression (Rubie, 1986; Schmadicke et al., 1992) however recent work focussed on identifying the P-T paths of eclogites and the surrounding gneisses has shown that some eclogites are tectonically intercalated into the surrounding gneisses during exhumation (Štípska et al., 2006a). Modern theories regarding the formation of these rock suites include subducted crust being

subsequently incorporated into orogenic belts during collisions, high-P metamorphism of sialic crust, and tectonic emplacement of mantle eclogites into the crust.

A classification of eclogites based on the temperatures indicated by their mineral assemblages was introduced by Carswell (1983) and refined by Newton (1986). These classifications are:

- low-temperature (450-500°C) containing pseudomorphs of clinozoisite, epidote and white mica after lawsonite;
- intermediate-temperature (500-600°C);
- high-temperature (600-750°C) defined by reaction of clinocllore and quartz to talc and kyanite in eclogite or co-metamorphic pelites.

A more recently recognised sub-type of eclogites is the ultrahigh-pressure (UHP) eclogite, in which coesite (a silica polymorph) and micro-diamond are found. UHP metamorphism occurs at pressures of greater than 20 kbar, with pressure of up to 60 kbar suggested for metamorphism in some areas (Parkinson, 2000). The oldest known UHP eclogites are ~620 Ma (Jahn et al., 2001; Maruyama and Liou, 1998b).

The formation of non-xenolithic eclogites requires rapid exhumation from depth. Some models allowing exhumation in a compressive setting (Figure 1.2 ) include: (1) forces applied external to the metamorphic terrain (i.e. extrusion, strike slip faulting, channel flow (Chemenda et al., 1995)); (2) buoyancy forces caused by density differences (eclogite is denser than surrounding rocks, but if eclogite lenses in pelitic gneisses had low enough density this mechanism might work (i.e. England and Holland, 1979b); (3) extensional processes caused by gravitational difference (this mechanism only works to depths of about 30km) (Platt, 1993). Exhumation driven by extensional processes should also be considered in eclogite exhumation as compressional orogens can have extensional phases (i.e. subduction rollback where the descending slab breaks off.)

### 1.3 Tectonic scenarios for Precambrian eclogite-hosting orogens

Palaeoproterozoic eclogites are relatively rare, but a number of well-studied examples exist, along with some less well-documented examples (figure 1.3). Figure 1.7 shows the P-T conditions at which these Precambrian orogens.

#### 1.3.1 Tanzania

There are two Palaeoproterozoic orogenic belts in Tanzania in which eclogite occurrences have been documented. These are the Usagaran Orogen, dated at ~2.0 Ga (Collins et al., 2004b; Möller et al., 1995) and the Ubende Orogen (Sklyarov et al., 1997; Sklyarov et al., 1998). These orogenic belts occur to the SE and SW of the Tanzanian Craton (Figure 1.5 ), and have been dated at ~2.0 Ga.

##### 1.3.1.1 Usagaran Orogen

The Usagaran Orogen, located to the SE of the ~2.7 Ga Tanzanian craton, consists of the Konse Group, a greenschist facies metasedimentary package

#### NOTE:

This figure is included on page 1.3 of the print copy of the thesis held in the University of Adelaide Library.

Figure 1.2. Exhumation models for eclogite formation. From Stuwe 1997

immediately adjacent to the Craton, and the Isimani Suite, a series of medium to high-grade gneisses and amphibolites with a few pockets of granulite. Some pods of eclogite are preserved within the gneisses of the Isimani Suite which was exposed to conditions of ~18 kbar & ~750 °C (Möller et al., 1995). The most recent geochronological work, addressed in detail in chapter 4, suggests the eclogites formed during the D<sub>1</sub> at 1999.1±1.1 Ma and were subsequently exhumed at ~25°C/Ma, 0.06-0.22GPa/Ma (Collins et al., 2004b). This date was obtained from SHRIMP U-Pb zircon analysis of zircon in eclogite. Stern (2005b) suggests that these eclogites may in fact be a product of the East African orogen rather than the Palaeoproterozoic orogen, however this suggestion is not supported by the available data.

The structural setting of these eclogites is uncertain with Reddy et al. (Reddy et al., 2004a; Reddy et al., 2003) suggesting that the Usagaran Orogen formed during subduction of a stretched or rifted continental margin with subsequent sinistral oblique convergence while Fritz et al. (Fritz et al., 2005) suggest that formation was associated with strike-slip tectonics in an island arc regime.

A magnetotelluric survey has investigated the deep crustal architecture between the Tanzanian Craton and the Usagaran Orogen. This survey shows structures consistent with west-dipping subduction underneath the Tanzanian Craton (Selway, unpb.). A study on the geochemical characteristics of mafic rocks within the Usagaran eclogite body has shown that most rocks have a enriched mid-ocean-ridge basalt (eMORB) signature, although some intercalated ultramafics have an island-arc basalt (IAB) signature (Lau, 2009b).

The Neoproterozoic East African orogeny has affected the east coast of Tanzania (Stern, 1994a), and the boundary between the Usagaran Orogen and East African Orogen is poorly defined. The East African orogeny in the Tanzania area reached greenschist facies P-T conditions, although in the Mozambique Orogen of Malawi eclogites of Ediacaran to Cambrian age (~530-500 Ma) have been reported (Ring et al., 2002). Rb-Sr and K-Ar ages for granites and gneisses around the Usagaran (Wendt et al., 1972) give younger ages towards the east of the orogen, which are likely the result of a East African overprint on the earlier Usagaran rocks.

##### 1.3.1.2 Ubende Orogen

Mafic and ultramafic high-pressure granulites and rare eclogite lenses and blocks occur in the Ubende Orogen within sheared amphibolite facies country rock (Boven et al., 1999). The timing of eclogite facies metamorphism in

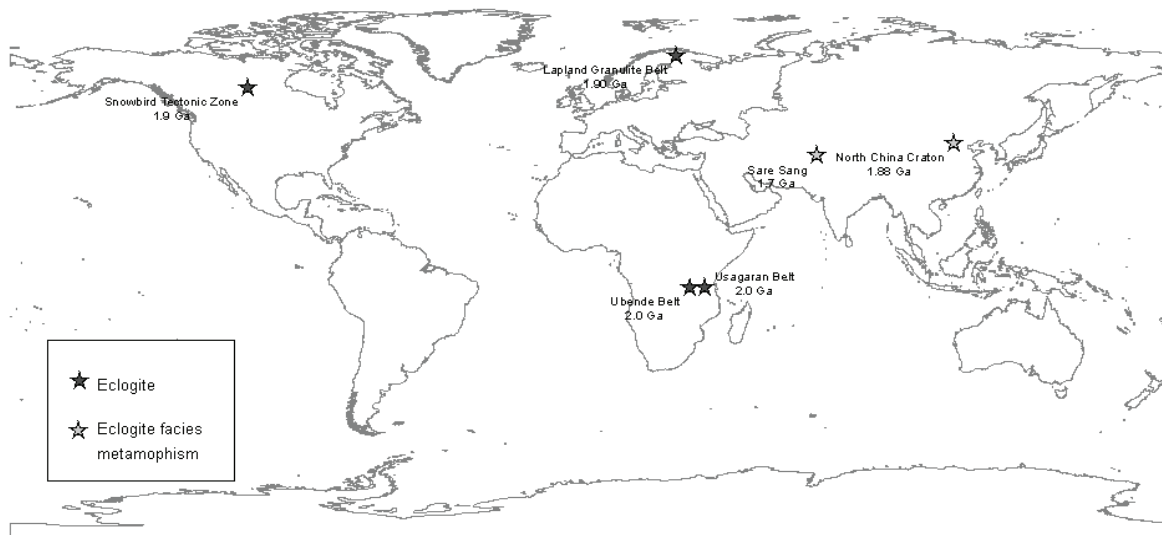


Figure 1.3. Global occurrences of Palaeoproterozoic eclogite (filled stars) and eclogite-facies rocks (unfilled stars).

the Ubende Orogen is poorly constrained. The Ubende Orogen has been assumed by some authors to be the synchronous with the Usagaran Orogen (Sklyarov et al., 1998; Wendt et al., 1972) however recent geochronological work (Rb-Sr whole rock isochrons and U-Pb whole-zircon TIMS on granites assumed to be syn-orogenic) suggests that metamorphism in the Ubende Orogen may have occurred at 1.95-1.85 Ga (Lenoir et al., 1994b) making the granites younger than the Usagaran Orogen. Eclogite occurs as constituents of basic dismembered tectonic units (Ubende & Ikulu series) and as rare small lenses in felsic gneiss (Daly, 1988).

The tectonic setting of these eclogites, based on *P-T* paths, has been interpreted to be initial subduction of an oceanic slab under the Tanzanian Craton ( $T=720^{\circ}\text{C}$ ,  $P=17.1$  kbar), followed by exhumation ( $T=800-500^{\circ}\text{C}$ ,  $P=11-15$  kbar), later exhumation ( $25\text{bar}/^{\circ}\text{C}$ ) either slower or with higher *T* gradient during orogenesis, final exhumation at near isothermal decompression ( $500-600^{\circ}\text{C}$ ,  $5-10\text{kbar}$ ) (Sklyarov et al., 1998). *P-T* studies on HP mafic granulite supports multiple stages of exhumation and suggest that exhumation is related to dextral lateral shear deformation (Boven et al., 1999). The Usagaran orogen is bounded to the west by Lake Tanganyika, which is part of the African Rift Complex. Rift-related faults are common within the Ubende, and make it difficult to interpret structures.

### 1.3.2 Snowbird Tectonic Zone, Canada

The Snowbird Tectonic Zone (STZ) is a 3000km long boundary between the Archaean Rae and Hearn Provinces of Northern Canada (Figure 1.5). Basement exposure along most of the STZ is poor, but it is well exposed in the East Athabasca Mylonite Triangle (EAMT).

The STZ was active from the Middle Archaean to the mid-Proterozoic, with left-lateral strike-slip deformation (Hanmer, 1997) in an arc-related setting at  $\sim 3.2$  Ga (Hanmer et al., 1994; Williams et al., 1995). Metamorphic mineral assemblages associated with this deformation suggest temperatures of  $750-850^{\circ}\text{C}$  and pressures of  $\sim 10$  kbars (Williams et al., 1995). It is suggested that this event was related to subduction in

a continental margin setting (Kopf, 2002)

The STZ underwent a period of granulite facies metamorphism and strike-slip deformation (Hanmer, 1997; Hanmer et al., 1994) in the Late Archaean at 2620-2600 Ma (Hanmer et al., 1994). This date is based on U-Pb ages of syntectonic granites within the contact region. *P-T* conditions were between  $700-800^{\circ}\text{C}$ ,  $8-10$  kbar in the Mary gneiss, (Williams et al., 2000) and greater than  $1000^{\circ}\text{C}$  and  $15\text{kbars}$  in the EAMT (Snoeyenbos et al., 1995). Hanmer et al. (1995a, b) argue from the geometry of the mylonite belt, the proximity to a 2.66 Ga greenstone basin and the similarity of Nd model ages either side of the STZ that in the Late Archaean the STZ was an intra-plate shear zone.

Kopf (2002) suggested that the STZ was not active after the Archaean, although it was noted that granulite facies metamorphism and right-lateral strike slip deformation had affected the neighbouring Rae Province at 1880-1840 Ma. However subsequent work (Baldwin et al., 2003; Baldwin et al., 2004) on eclogites and other high-pressure rocks in the Southern Domain of the STZ indicates that there was an eclogite forming metamorphic event at  $\sim 1.9$  Ga with temperatures of  $920-1000^{\circ}\text{C}$  and pressures of at least  $1.8-2.0$  GPa (Baldwin et al., 2004). The composition of these eclogites is consistent with transport of continental crust to mantle depths followed by rapid buoyancy-driven exhumation to lower mantle. Tectonic settings that have been suggested for the STZ include a Palaeoproterozoic suture, and an Archaean (2.55-2.52) suture that has experienced a component of Palaeoproterozoic convergence and metamorphism. Both these models involve transport to mantle depths, exposure to mantle temperatures and major regional shortening at 1.90 Ga (Baldwin et al., 2004). If we accept that the STZ was a subduction zone in the Middle Archaean (Kopf, 2002) and an intra-plate shear zone in the Late Archaean (Hanmer et al., 1995a 1995b) then one possible tectonic setting for Palaeoproterozoic metamorphism is renewed convergence along the Middle Archaean subduction-related suture. This, however, would require Early Palaeoproterozoic break-up of these continents, with subsequent reassembly along the same suture.



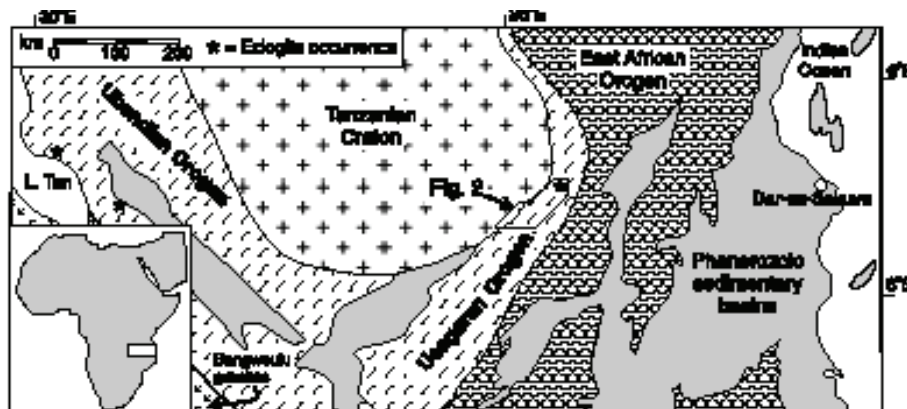


Figure 1.4 Map showing location of Usagaran & Ubendian Orogens in Tanzania.

### 1.3.3 Lapland Granulite Belt

Although eclogites have been identified in the Lapland Granulite Belt (Tuisku and Huhma, 1998) there has been little published work on them. The published data indicates peak metamorphism at 1905-1888 Ma with peak P-T conditions of 12 kbar and 650-700°C, roughly equivalent to a depth of 40km. The orogen is interpreted as a subduction zone between two colliding plates; the Inari Kola in the northeast and the Karelian Craton in the southwest (Tuisku and Huhma, 1998).

### 1.3.4 North China Craton

The North China Craton (NCC) can be divided into three units; the Eastern & Western Blocks and the Central Zone (Figure 1.6). The Central Zone contains pods of high-pressure rocks which record varying P-T conditions (Figure 1.7). The entire SSW-NNE trending zone, which is 100-400 km wide and ~1000km long, represents the zone of collision between two major blocks resulting in assembly of NCC (Zhao et al., 2001) between 2.0 – 1.85 (or 1.80) Ga. Subsequent intracratonic rift basin formation at Yanshan-Taihangshan Aulacogen suggests that the assembly of the NCC was complete by  $1840 \pm 14$  Ma (Songnian et al., 2002). The interpreted sequence of events in the Hengshan Complex is initial crustal thickening, subsequent exhumation, cooling and retrogression (Zhao et al., 2001). Rocks are interpreted to have reached depths of ~50 km (Kröner et al., 2005) at around 1.88 Ma (Kröner et al., 1998), with anatectic melting & decompression at ~1860 Ma (Zhao et al., 2001). Although the P-T conditions are variable within the Central Zone they are consistent with formation in the closure of an ancient ocean and collision of the Eastern and Western Blocks of the NCC (Zhao et al., 2000).

### 1.3.5 Sare Sang, Afghanistan

While there is no record of eclogites being found in the Sare Sang region of Kazakhstan there are metapelites and metabasites containing lapis lazuli deposits and whiteschists which metamorphic studies show to have undergone metamorphism at P-T conditions at or nearly at eclogite facies. The only published geochronological work on the Badakhshan Block is in Russian (Horeva et al., 1971) and provides a protolith age of 2700-2400 Ma (U-Pb) and ages of  $1675 \pm 100$  Ma (K-Ar) and 1720-1750 Ma (Rb-Sr) for a phlogopite deposit in the area. Peak metamorphic conditions of 12-13 kbar at 730-740 °C are suggested by mineral chemistry. The tectonic setting of this metamorphism is interpreted as crustal

thickening due to a compressional event, followed by rapid exhumation associated with expansion. The lapis lazuli deposits are interpreted to have formed post peak metamorphism during decompression (Faryad, 1999).

### 1.3.6 Archaean Eclogites and high-P rocks

Archaean ages have been proposed for four eclogite terranes; Glenelg in Scotland (Alderman, 1936) which was subsequently dated at ~1.08 Ga (Storey et al., 2003), the Snowbird Tectonic Zone in Canada, which is discussed earlier in the document, the Dabie-Shan coesite-bearing eclogite in China (Cao and Zhu, 1995) and the Belomorian Mobile Belt in the Baltic / Fennoscandian shield (Volodichev et al., 2004). The 2.77 Ga age published for the Dabieshan eclogites is contradicted by later U-Pb zircon and Ar-Ar work indicating that these rocks underwent UHP metamorphism between 260-245 Ma (Faure et al., 2003; Hacker et al., 2000). This later date is consistent with the occurrence of other UHP eclogites only within the last 630 Ma.

#### 1.3.6.1 Belomorian Eclogites

The Belomorian Mobile Zone in Russia is reported to have undergone three episodes of high-pressure metamorphism, in the Late Archean (~2.7 Ga) and Palaeoproterozoic (~2.45 Ga and 1.9-1.8 Ga). Eclogites have been reported from three localities within the Belomorian Mobile Belt, including Gridino and Salma. Those from the vicinity of Gridino have been dated at  $2720 \pm 8$  Ma and  $2416.1 \pm 1.3$  Ma (Volodichev et al., 2004). These eclogites contain high-Ca-garnet and low-Na-clinopyroxene+zoisite which is not typical of true eclogite. The P-T conditions are reported as 690°C and at least 9.5-11 kbar (Slabunov et al., 2003). Eclogites in the Salma area (Kola Peninsula) formed at  $2695 \pm 26$  Ma with prograde metamorphism at ~700°C, 14-15 kbar, and retrograde metamorphism at  $727 \pm 24$ °C at  $10.7 \pm 0.7$  kbar at 1.89 Ga (Kaulina et al., 2006). It is unfortunate that the majority of work on the Belomorian eclogites has been published either in Russian (Volodichev, 1977, 1990, 1997) or as brief abstracts (Bibikova et al., 2005; Kaulina et al., 2006; Slabunov et al., 2003).

#### 1.3.6.2 Barberton granitoid-greenstone terrane

Garnet-albite bearing amphibolites have been reported in the Barberton granitoid-greenstone terrain, South Africa, which have been dated at 3.23 Ga (Dziggel et al., 2006). These rocks indicate peak metamorphic conditions of 600-650 °C and 12-15 kbar, with retrograde metamorphism at 580-650 °C and 8-10 kbar, and are

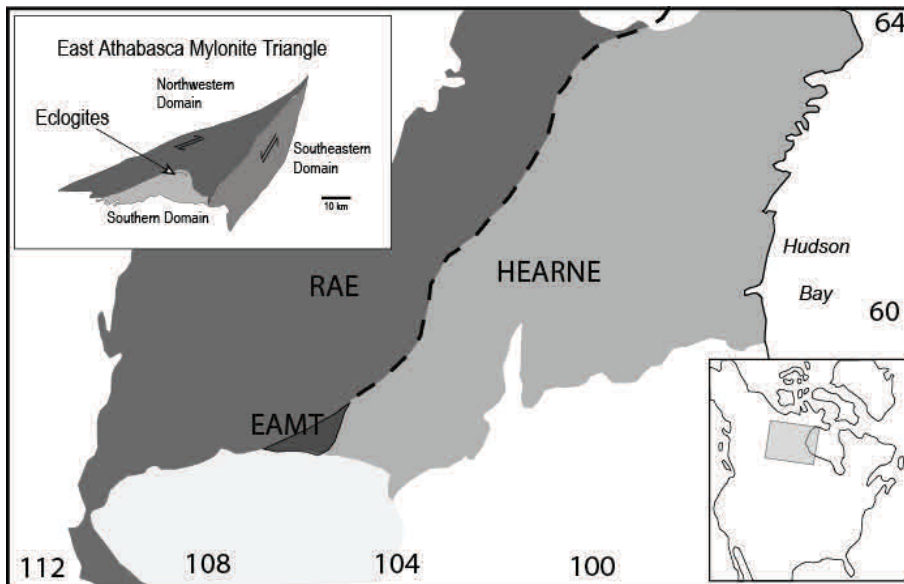


Figure 1.5. Location map of the Snowbird tectonic zone (dashed line) relative to major Archaean and Proterozoic features of the Central Canadian Shield. Inset shows location of map area, and location of eclogite outcrop within the East Athabasca Mylonite Triangle (EAMT). Numbers on the margins refer to longitude and latitude.

interpreted as evidence for cold strong lithosphere and active subduction (Moyen *et al.*, 2006).

#### 1.4. Discussion

One of the reasons for researching Palaeoproterozoic eclogite-facies rocks is to answer the question of whether the Precambrian earth functioned in the same way as the modern earth. How long plate tectonics has been operating has been debated (Eriksson *et al.*, 2004; Kröner, 1981) as has whether mechanisms like subduction operated in the same way (Stern, 2005b).

Evidence for the existence of Precambrian plate tectonics (Cawood *et al.*, 2006) include: palaeomagnetic data indicating differential movements of continents; ophiolite, island-arc and accretionary complexes in Palaeoproterozoic rocks (Trans-Hudson orogen in the Canadian Shield, Svecofennian orogen in SW Finland, Mazatzal-Yavapai orogens in SW Laurentia) with trace-element signatures similar to those found in modern equivalents; the presence of Archaean ore-deposits formed by subduction related processes; and mid-Archaean island-arc volcanics (Cawood *et al.*, 2006). Cawood *et al.* (Cawood *et al.*, 2006) include the discovery of eclogites of Palaeoproterozoic and inferred Archaean ages in his evidence for Precambrian plate tectonics.

Some recent work has suggested that early plate tectonics were fundamentally different from modern tectonics. According to some models plate movement in the Archaean was driven by more active lithospheric convection or hot spots (Kröner, 1981; Lambert, 1981). Some authors argue for higher geothermal gradient due to higher heat production from the radiogenic decay of K, Th and U (Bickle, 1984) while others suggest that continental geotherms were not significantly different from those in the modern earth, but that major orogenic events were hotter (Percival, 1992). Other factors which are considered to potentially impact the style of plate tectonics in the Precambrian include hotter and weaker continental crust due to higher heat loss from the mantle (McKenzie and Weiss, 1975; Richter, 1985), more vigorous mantle convection leading to more delamination, denser supracrustal rocks changing the geometry of deformation (Marshak, 1999) and higher erosion rates due to increased and more corrosive

atmosphere leading to faster exhumation and higher crustal isotherms (Winslow *et al.*, 1995). Subduction in the Precambrian has been suggested to be shallower because oceanic plate was not cold/dense enough for slab pull to be a major factor (Stern, 2005b). However the transport mechanism for the formation and exhumation of modern eclogites in steep subduction zones is already the topic of debate (Froitzheim *et al.*, 2003), and eclogite formation without subduction is problematical.

Based on the occurrence of eclogites and granulites in the Palaeoproterozoic and high-pressure rocks in the Archaean it seems clear that some form of plate movement and orogenesis did occur in the Palaeoproterozoic and earlier. Does this mean that modern-style subduction was operating? If this is not evidence of subduction, what evidence would be required to prove the existence of subduction? How do we prove whether 2.0 Ga rocks were formed during subduction?

- Is it possible to use mapping to find typical subduction features? (ie. ophiolites, back-arc volcanics, etc). In some older instance such features may not still be recognisable after subsequent tectonic or volcanic events.
- Can we use metamorphic petrology to sufficiently constrain the P-T-t path of rocks, and hence prove burial and exhumation at rates comparable to those in modern subduction (Camacho *et al.*, 2005). This may be difficult due to the issues in P-T determinations discussed earlier in this review.
- Can we use geophysical methods to image any remnant crustal structures? Recent magnetotelluric work in central Australia (Selway *et al.*, 2006a; Selway *et al.*, 2006b) has successfully imaged the remnants Proterozoic subduction related structures.
- Can geochemical signatures of associated igneous rocks prove subduction? i.e. If we can identify a suite of volcanic rocks suitably situated within an orogen which are the same age as eclogite-facies metamorphism, and such rocks have bulk-rock and isotope signatures characteristic of back-arc volcanics.

Figure 1.6. Outline tectonic map of China showing the major Precambrian blocks (inset); Tarim Craton (TC), North China Craton (NCC), South China Craton (SCC), Yangtze Block (YB) and Cathaysia Block (CB). Late Neoproterozoic and Palaeozoic fold belts indicated by dashed lines. Main map shows the distribution of the basement rocks in the North China Craton. The Central Zone, bounded by the Huashan-Lishi-Datong-Duolun (HLDD) fault to the east and the Xinyang-Kaifeng-Shijiazhuang-Jianping (XKSJ) fault to the west, includes the Dengfeng (DF), Fuping (FP), Hengshan (HS), High-Pressure Granulite (HPG), Huaian (HA), Lüliang (LL), Northern Hebei (NH), Taihua (TH), Wutai (WT), Zhanhuang (ZH) and Zhongtiao (ZT) domains. (modified after (Zhao et al., 2000))

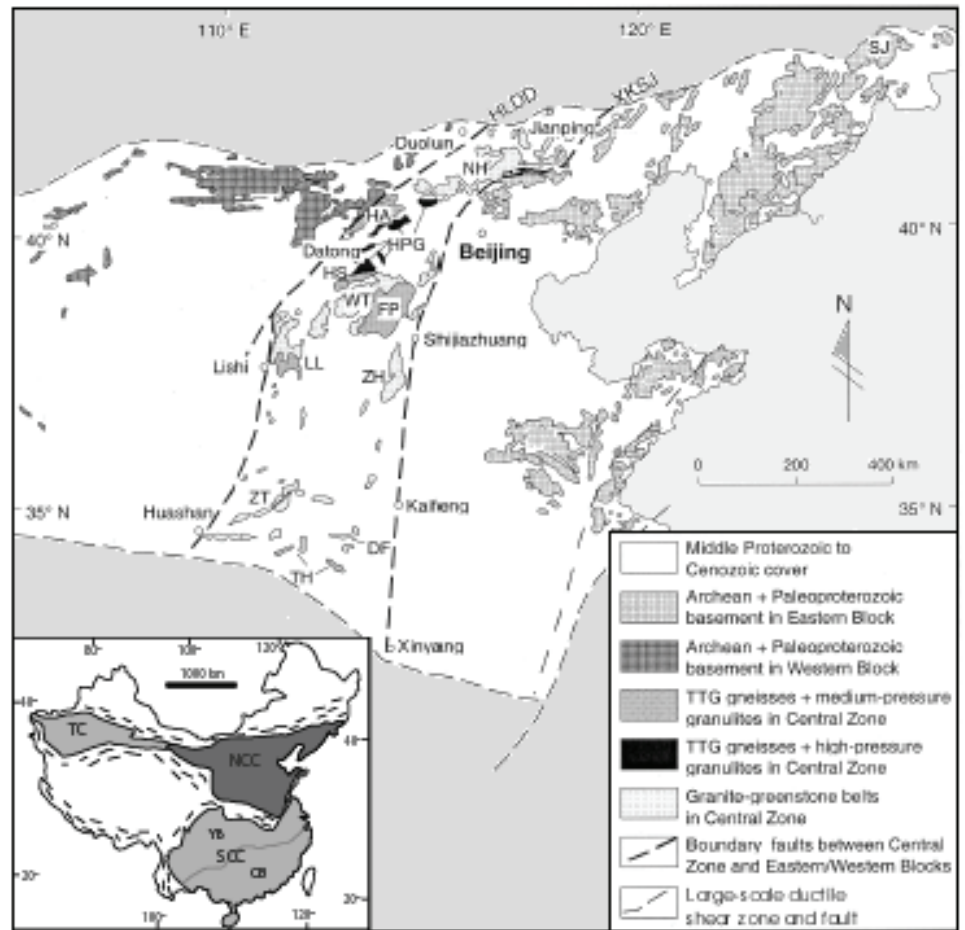
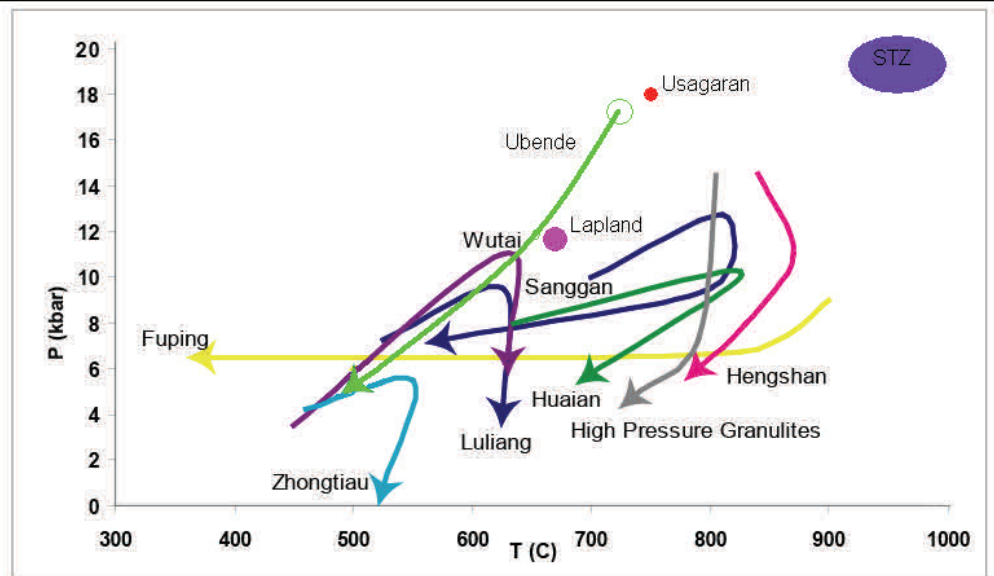


Figure 1.7. Preserved P-T paths from the Central Zone of the North China Craton. All rocks are interpreted as having formed during the collision between the East and West Blocks. The High Pressure Granulites are interpreted as retrograde eclogites.



The other question of interest is, if these Palaeoproterozoic rocks did not form during subduction, how did they form?

### 1.5. Scope of this project

Based on the published literature about Palaeoproterozoic eclogite-facies rocks it is not possible to answer conclusively the question of precisely how plate tectonics operated at that time. However the number of eclogite-facies rocks of this age indicates that plate tectonics was operating in some manner in the

Palaeoproterozoic. In order to prove that subduction was operational in the formation of eclogite-facies rocks it would be necessary to study one or more of these occurrences using a multifaceted approach which could incorporate geochronology, metamorphic petrology, mapping and structural analysis, geochemistry and geophysics.

With geochemical and geophysical investigations of the Usagaran terrane already completed (Selway, 2008; Lau, 2009) this study is broken down in to six subsections, the main aims of which are to :

- Characterising the isotope chemistry of the Tanzanian Craton using U-Pb and Lu-Hf in order to obtain a good data set to for comparison in the investigation of the provenance of sediments in the Usagaran and Ubende Orogens.
- Better constrain the structure and timing of eclogite formation Ubende Orogen using U-Pb geochronology and  $^{40}\text{Ar}/^{39}\text{Ar}$  thermochronology.
- Complete a full structural traverse through the Usagaran Orogen, from the Archaean Craton into the Neoproterozoic rocks of the Mozambique Belt.
- Investigate the provenance of metasediments in the Usagaran and Ubende Orogens to determine whether the metasediments are sourced from the Tanzanian Craton, or from some other source.
- Conduct a metamorphic study of the Usagaran Orogen to more fully constrain the P-T-t history of eclogites and surrounding gneisses and to establish whether they have shared or separate metamorphic histories.
- A crustal evolution study of the Usagaran and Ubende Orogens using Lu-Hf to investigate the input of new crustal material and crustal reworking in the orogenic Orogens.

Two field seasons were conducted by the candidate. During the first season in November of 2006 a magnetotelluric study was conducted (Selway, 2008), structural data and samples were collected from the Tanzanian Craton and Konse Group north-west of Yalumba Hill, from an location with cropping out eclogite at the foot of Yalumba Hill, and from the Ngengerengengere Gorge on the Great Ruaha River. This field work was in the company of Alan Collins, Martin Hand, Kate Selway and a geologist from the Geological Survey of Tanzania, Philip Momburi who acted as translator. The second field season, through May-June 2007, was in the company of Philip Momburi from the Geological Survey of Tanzania who again acted as translator for most of the field season, and six days were spent working with Alan Collins. Six weeks were spent completing a traverse from the Tanzanian Craton (NW of Yalumba Hill) through to the village of Ruaha-Mbuyuni which was considered to be within the Mozambique Belt. Data and samples collected in these field seasons, along with data from three samples collected previously by Alan Collins and Steve Reddy in a 2001 field season, form the basis of chapters four and five of this thesis. The remaining two weeks of that season were spent collecting stream sediment samples, data from which are presented in chapter two.

Chapter three of this thesis is based on structural data and samples collected by Alan Collins and Steve Reddy in a 2004 traverse through the Ubende Orogen accompanied by Professor Abdul Mruma of the Geological Survey of Tanzania. Separation of hornblende for Ar-Ar analysis was performed by Alan Collins. Thermochronological, geochronological, and Lu-Hf isotopic data collection and interpretation and structural data interpretation was performed by the candidate.

Stream sediment samples from the Songea district were

collected the Albidon Limited, a gold mining company, and analysis and initial interpretation of these samples were performed by Elena Belousova, but not published. Data from these samples, labelled AlbSong-01 to Albsong-05 are included in this thesis for discussion, and were reinterpreted by the candidate as part of the wider dataset. These data are discussed in chapters two and six. They form a part of the two papers to be submitted as a product of this thesis. Elena Belousova is to be listed as a co-author on these two papers, co-authorship of papers derived from each other chapter will reflect those who participated in the field-work.



## Chapter 2 – Characterising the crustal evolution of the Tanzanian Craton using LA-ICPMS U-Pb and MC-LA-ICPMS Lu-Hf analyses of detrital zircon

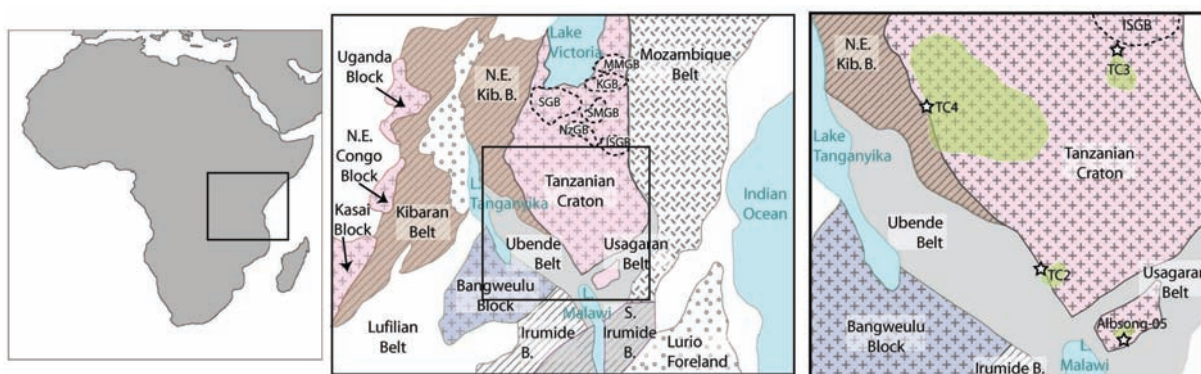


Figure 2.1. Location diagram showing Archaean cratons and Proterozoic orogenic belts in East Africa and location of green-stone belts on the Tanzanian Craton (SGB = Sukumaland Greenstone Belt, MMGB = Musumo-Mara Greenstone Belt, KGB = Kilimafedha Greenstone Belt, SMGB = Shinyanga-Malita Greenstone Belt, NzGB = Nzega Greenstone Belt, ISGB = Iramba-Sekenke Greenstone Belt). Enlargement shows sample sites for this study with modern drainage areas indicated in white.

### 2.1 Introduction

Radiogenic isotopic analysis of impurities in zircon (e.g. U-Th-Pb and Lu-Hf) provides information about the timing of continental crust formation (Amelin et al., 1999; Harrison et al., 2005; Hawkesworth and Kemp, 2006; Kinny and Maas, 2003; Scherer et al., 2007; Zeh et al., 2008). By coupling data on the age of zircon crystallization provided by U-Th-Pb isotopes and the age of crustal residence of the source magma to the zircon, provided by Lu-Hf isotopes, understanding of the timing of crust/craton formation and the role of crustal recycling in crust forming events can be improved (Amelin et al., 1999; Condie et al., 2005; Harrison et al., 2005; Howard et al., 2009; Patchett et al., 1981). These data also provide valuable information on whether the zircon grains form from melts formed in the depleted mantle, in a more enriched mantle, reworked older crust or mixture of these sources (Davis et al., 2005; Hawkesworth and Kemp, 2006; Vervoort and Blichert-Toft, 1999; Zeh et al., 2008).

Zircon provides an ideal target mineral for isotopic studies because it can be accurately dated using the U-Pb isotope system (Collins et al., 2004b; Compston et al., 1984). Zircon also incorporates high concentrations of Hf but only minor Lu (average initial Lu/Hf = 0.0016) (Patchett et al., 1981) allowing initial Hf concentrations to be obtained with high precision (Griffin et al., 2004). *In situ* analytical techniques (i.e. secondary ion mass spectrometry (SIMS) and laser ablation inductively coupled plasma mass spectrometer (LA-ICPMS)) allow for high precision spot analyses within zoned crystals allowing different episodes of zircon formation to be recognized and analysed.

In this study we present LA-ICPMS U-Pb and LA-MC-ICPMS (MC= Multicollector) Lu-Hf zircon analyses from stream sediment samples obtained from four locations on the Tanzanian Craton. Stream sediments are used because they capture a broad spectrum of the rock types and ages within the stream system.

### 2.2 Geology and geochronology of the Tanzanian Craton

The Tanzanian Craton is one of seven Archaean cratonic blocks in southern and central Africa (Figure 2.1). It is commonly grouped with the Kasai, Angola, NE Congo and Uganda Blocks and the Gabon Craton into a unit called the Congo Craton (or Congo-Tanzania-Bangweulu Block of Collins and Pisarevsky (2005)), which is believed to have been assembled by the Mesoproterozoic, and possibly as early as the Palaeoproterozoic (Boven et al., 1999; Collins et al., 2004b; DeWaele et al., 2008). The ~2.0 Ga Usagaran Orogen formed to the south-east of the Tanzanian craton (Collins et al., 2004; Möller et al., 1995; Reddy et al., 2003) and the ~1.85 Ga Ubende Orogen formed between the Tanzanian Craton and the Bangweulu Block to the south-west of the craton (Boven et al., 1999; Lenoir et al., 1994a). In the Mesoproterozoic the 1.4 – 1.0 Ga Kibaran Orogen (Kokonyangi et al., 2004; Tack et al., 2002) formed between the Tanzanian Craton/Bangweulu Block and the Kasai/NE Congo/Uganda blocks and the 1.2-1.0 Ga Irumide Orogen formed to the south-east of the Bangweulu Block (DeWaele, 2005; DeWaele et al., 2006a; DeWaele et al., 2006b).

The Tanzanian Craton consists of Archaean terranes accreted between at least 2.93 to 2.53 Ga, and may contain an older (~ 3.2 Ga) terrane to the south (Pinna et al., 1999). The Tanzanian Craton has been subdivided into two domains, the Dodoman in the south and the Victorian Orogen to the north. The cratonic margins are caught up in the Usagaran and Ubende Orogens.

The published geochronological data for the craton, summarized in Table 2.1, are sparse. In the Victorian Belt four greenstone belts have been investigated by various methods, while in the Dodoman only five Sm-Nd model ages have been published for granitoids close to the Great Ruaha River. In the Kilimafedha Greenstone Belt  $^{207}\text{Pb}$ - $^{206}\text{Pb}$  zircon analyses dated rhyolite sequences at  $2712 \pm 5$  and  $2720 \pm 5$  Ma and granites at  $2692 \pm 11$  and  $2643 \pm 11$  Ma (Wirth et al., 2004b). Dating of the Musoma-Mara Greenstone Belt (MMGB) using the U-Pb zircon SIMS

Kilimafedha Greenstone Belt	rhyolite sequences	2712 ± 5 and 2720 ± 5 Ma	<sup>207</sup> Pb- <sup>206</sup> Pb zircon	Wirth et al., 2004
	granites	2692 ± 11 and 2643 ± 11 Ma		
Musoma-Mara Greenstone Belt	mafic volcanism	2676-2669 Ma	U-Pb zircon SIMS	Manya et al., 2006
	felsic volcanism	2668-2667 Ma		
	post-orogenic granites	2649 ± 36 Ma		
	hornblende-rich granitoids	2610 ± 80 Ma	Rb-Sr whole rock	Bell and Dodson, 1981
	granitoids intruding the greenstone sequence	2490 ± 60 Ma		
Iramba-Sekenke Greenstone Belt	back-arc volcanic suite	2742 ± 27 Ma (εNd = 2.3)	Sm-Nd	Manya and Maboko, 2008
Sukumaland Greenstone Belt	Nyanzian mafic volcanism	~2820 Ma εNd=-2.7	Sm-Nd wholerock	(Manya and Maboko,
	Upper Nyanzian pyroclastics	2808 ± 3 and 2780 ± 3 Ma	U-Pb single zircon TIMS	Borg and Krogh, 1999
	Trachyandesites at Geita	2699 ± 9 Ma		
	Na-rich granitoid	2620 ± 30 Ma		
	granitoids	2680 ± 3 Ma	U-Pb single zircon TIMS	Manya & Maboko, 2003
	leucocratic and aplitic dykes cross-cutting greenstone	2544 ± 15 Ma	Sm-Nd garnet & whole-rock	Cloutier et al., 2005
	granitoids	2570 ± 50 and 2530 ± 30 Ma	Rb-Sr whole-rock	Rammlmair et al. (1990)
Dodoman terrane		T <sub>DM</sub> = 3.0 – 3.1 Ga	Sm-Nd wholerock	Rammlmair et al. (1990)

Table 2.1 Summary of published geochronological data from the Tanzanian Craton

method shows mafic volcanism (2676-2669 Ma) followed by felsic volcanism (2668-2667 Ma) and emplacement of post-orogenic granites at 2649 ± 36 Ma (Manya et al., 2006). These ages are in accord with a Rb-Sr whole rock isochron giving an age of 2610 ± 80 Ma for hornblende-rich granitoids near Musoma (Bell and Dodson, 1981). Bell and Dodson (1981) also published a Rb-Sr isochron age of 2490 ± 60 Ma for granitoids intruding the greenstone sequence at Utegi. Sm-Nd dating of the Iramba-Sekenke Greenstone Belt shows that the volcanic suite was emplaced at 2742 ± 27 Ma (εNd = 2.3), and the geochemistry of these rocks is consistent with formation in a back-arc setting (Manya and Maboko, 2008). The most geochronological data exists for the Sukumaland Greenstone Belt (SGB). Nyanzian mafic volcanism has been dated at ~2820 Ma (initial εNd=-2.7) using the Sm-Nd whole rock isochron method (Manya and Maboko, 2003). Upper Nyanzian pyroclastics are also dated at 2808 ± 3 and 2780 ± 3 Ma by U-Pb single zircon TIMS (Borg and Krogh, 1999). Trachyandesites at Geita and a Na-rich granitoid have been dated by U-Pb single zircon TIMS at 2699 ± 9 Ma and 2620 ± 30 Ma respectively (Borg & Krogh 1999). The granitoids contain trace zircon dated at 2680 ± 3 Ma which may be representative of some precursor to the granites (Manya & Maboko, 2003). The host greenstone at the Tulawaka gold deposit is cross-cut by leucocratic and aplitic dykes dated by the Sm-Nd garnet-whole-rock method at 2544 ± 15 Ma (Cloutier et al., 2005). Rb-Sr whole-rock ages of 2570 ± 50 and 2530 ± 30 Ma were obtained for SGB granitoids by Rammlmair et al. (1990). For the Dodoman terrane, 5 whole-rock Sm-Nd model ages were calculated by Möller et al. (1998a) and

yielded T<sub>DM</sub> = 3.0 – 3.1 Ga.

## 2.3 Samples and analytical techniques

### 2.3.1 Sampling strategy

Sample sites were selected using the river drainage and geology shown on the geology and mineral map of Tanzania (Pinna et al., 2004) in combination with road maps. Sample sites were selected targeting spatially distant zones of the Tanzanian Craton, where rivers had the largest possible drainage area that covered only the Tanzanian Craton, and that were accessible by road.

Sample TC2 is taken from the Zira (or Sira) River in the Mbeya region (33°02'33.312, 8°30'44.641). The Zira River flows into the south end of Lake Rukwa along the base of a major NW-SE normal fault associated with the East Africa Rift system. The modern catchment includes Palaeoproterozoic to Neoproterozoic granitoids, Palaeoproterozoic (Ubendian) metaigneous and sedimentary rocks and Cenozoic sediments of the Rift Valley. Sample TC3 comes from the Durumo River in the Singida region (34°33'33.312, 4°19'00.142). The Durumo flows north into the Wenbere Steppe (an eastern branch of the Rift Valley system). The catchment area includes Neoproterozoic orthogneisses, granitoid, migmatites, ultramafics, mafics, banded ironstones, greenstone belts and syenites as well as younger (Cenozoic) conglomerates, cherts and alluvium. Sample TC4 comes from the Malagarasi River at the township of Uvinza (5°06'37.887, 30°23'25.556). The catchment of the Malagarasi River includes Neoproterozoic TTG granitoids and sediments, the Nyanzian greenstone belts and may

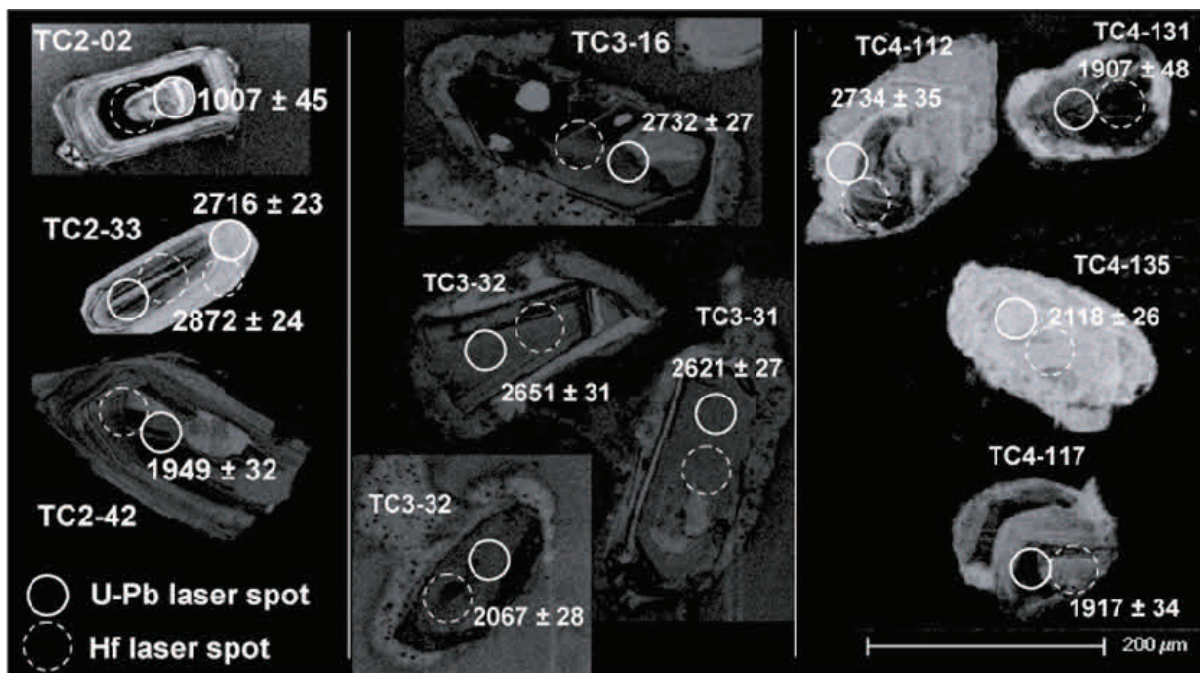


Figure 2.2 Representative CL images for samples TC2, TC3 and TC4 with analysis name and Pb/Pb ages shown.

also include some Meso- to Neo-proterozoic volcano-sedimentary sequences from the north-eastern Kibaran Orogen. Sample Albsong-05 comes from a river on an outlying unit of Archaean granitoids south of the main Tanzanian Craton. This sample was collected by Albison Limited, and analytical work was conducted by Belousova (unpublished). Results for this sample are given in Appendix 1.

### 2.3.2 Sample preparation

Samples are heavy mineral concentrates of sand samples from modern river drainages. Zircons were separated from stream sediment samples by sieving, magnetic and heavy liquid separation, then grains were handpicked and mounted in epoxy discs. The mounts were carbon coated then imaged using a cathodoluminescence (CL) detector fitted to a Phillips XL20 scanning electron microscope at a working distance of 13.5mm and using an accelerating voltage of 10kV.

### 2.3.3 Analytical technique – LA-ICPMS U-Th-Pb geochronology

Zircon U-Th-Pb analyses were undertaken by LA-ICPMS at Adelaide Microscopy, University of Adelaide on an Agilent 7500cs ICPMS fitted with a New Wave 213 nm neodymium–yttrium–aluminium-garnet (Nd-YAG) laser. Beam diameter was set at 30 μm using a repetition rate of 15 Hz. Sample bracketing was used to correct for instrumental drift over the course of a session. U-Pb fractionation was corrected using the GEMOC GJ-1 zircon (TIMS normalization data  $^{207}\text{Pb}/^{206}\text{Pb} = 608.3 \text{ Ma}$ ,  $^{206}\text{Pb}/^{238}\text{U} = 600.7 \text{ Ma}$ ,  $^{207}\text{Pb}/^{235}\text{U} = 602.2 \text{ Ma}$  (Jackson et al., 2004)). Standard GJ-1 was run 4 times at the beginning and end of each run, interspersed by two analyses of the in-house Sri Lankan zircon standard (BJWP-1,  $^{207}\text{Pb}/^{206}\text{Pb} = 720.9 \text{ Ma}$  (Wade et al., 2008)) and ten analyses of unknowns. Total acquisition time per analysis was 90 seconds; 50 seconds background measurement followed by 40 seconds of sample ablation. Data was processed using GLITTER software (Van

Achterbergh et al., 2001). The cut off for concordant data was 90-110%.

### 2.3.4 Analytical technique – LA-MC-ICPMS Hf isotope analysis

Zircon Lu-Hf analyses were undertaken at Macquarie University at GEMOC on a Nu Plasma multi-collector ICPMS details coupled with a New Wave 213 nm Nd-YAG laser. Beam diameter was set at 40-55 μm using a repetition rate of 5 Hz. Total acquisition time per analysis was 200 seconds, with 30 seconds background measurement. The “Lu-Hf laser spot” was drilled next to the “U-Pb laser spot” within the same domain as constrained by the CL images. The reference zircons Mud Tank ( $^{176}\text{Hf}/^{177}\text{Hf} = 0.282530 \pm 30$ ) (Griffin et al., 2007) and Harvard 91500 ( $^{176}\text{Hf}/^{177}\text{Hf} = 0.282280 \pm 120$ ) (Weidenback et al., 1995; Weidenback et al., 2004) were analysed at the beginning and end of each session, with Mud Tank samples also run between sets of ten analyses.

Measurement of accurate  $^{176}\text{Hf}/^{177}\text{Hf}$  ratios in zircon requires correction for interferences of  $^{176}\text{Lu}$  and  $^{176}\text{Yb}$  on  $^{176}\text{Hf}$ . Because the Nu Plasma multi-collector ICPMS mass bias instrument is independent of mass over the mass range considered here this correction is relatively straightforward. Interference of  $^{176}\text{Lu}$  on  $^{176}\text{Hf}$  was corrected by measuring the intensity of the interference-free  $^{175}\text{Lu}$  isotope and using  $^{176}\text{Lu}/^{175}\text{Lu} = 0.02669$  to calculate the intensity of  $^{176}\text{Lu}$ . Similarly, the interference of  $^{176}\text{Yb}$  on  $^{176}\text{Hf}$  was corrected by measuring the interference-free  $^{172}\text{Yb}$  isotope and using  $^{176}\text{Yb}/^{172}\text{Yb}$  to calculate the intensity of  $^{176}\text{Yb}$ . The appropriate value of  $^{176}\text{Yb}/^{172}\text{Yb}$  (0.5865) was determined by successively spiking the JMC475 Hf standard (100 ppb solution) with Yb (10–80 ppb), and determining the value of  $^{176}\text{Yb}/^{172}\text{Yb}$  required to yield the value of  $^{176}\text{Hf}/^{177}\text{Hf}$  obtained on the pure Hf solution (Griffin et al., 2004; Pearson et al., 2008). More detailed discussions regarding the overlap corrections for  $^{176}\text{Lu}$  and  $^{176}\text{Yb}$  can be found in Griffin et al. (2007) and Pearson et al. (2008).



The measured  $^{176}\text{Lu}/^{177}\text{Hf}$  ratios of the zircons have been used to calculate initial  $^{176}\text{Hf}/^{177}\text{Hf}$  ratios. These age corrections are very small, and the typical uncertainty on a single analysis of  $^{176}\text{Lu}/^{177}\text{Hf}$  (+1%) contributes an uncertainty of  $<0.05$   $\epsilon\text{Hf}$  unit. For the calculation of  $\epsilon\text{Hf}$  values, representing the per mil difference between the sample and the chondritic reservoir (CHUR) at the time of intrusion, we have adopted a decay constant for  $^{176}\text{Lu}$  of  $1.865 \times 10^{-11}$  and the chondritic values of  $^{176}\text{Hf}/^{177}\text{Hf}$  and  $^{176}\text{Lu}/^{177}\text{Hf}$  derived by (Scherer et al., 2001). The accuracy and precision of the method are discussed in further detail by Griffin et al. (2004; 2000).

## 2.4 Results

### 2.4.1 TC2 – Zira River, Mbeya district

This sample contained abundant prismatic zircon with aspect ratios between 2:1 and 5:1. Most grains were unbroken although grain terminations were commonly rounded (Figure 2.2). CL imaging illustrates well defined growth zoning. Analyses of 110 U-Pb spots were carried out on 109 grains (Table 2.1). Age data from this stream sediment sample, shown in Figure 2.3 (a & b), are loosely grouped into at least three populations ( $\sim 2720$  Ma,  $\sim 1950$  Ma, and  $\sim 1050$  Ma) based on their  $^{207}\text{Pb}/^{206}\text{Pb}$  ages. The Archaean population cannot be resolved to a single crystallization event, with the major age peak at  $2724 \pm 8$  Ma (MSWD = 2.5) and a minor older peak at  $2804 \pm 28$  Ma (MSWD = 13). The relatively high MSWD for both of these peaks suggests that neither of these populations can be interpreted to represent a single rock source or to give an unique rock age. It is mostly likely that each of these populations represents major crust forming or metamorphic events with multiple rock sources represented that formed over an interval of a number of million years. Similarly the Palaeoproterozoic zircon ages can be separated to show two age peaks at  $1865 \pm 35$  Ma and  $2011 \pm 27$  (MSWD = 7.1 and 8.5 respectively) but again, neither of these peaks indicates a single rock source. Four  $> 90\%$  concordant zircon grains yielded Mesoproterozoic  $^{207}\text{Pb}/^{206}\text{Pb}$  ages with a peak at  $1066 \pm 82$  Ma (MSWD = 4.0) which does not appear to indicate a single rock source. One 91% concordant grain yielded a Cambrian  $^{206}\text{Pb}/^{238}\text{U}$  age of  $507 \pm 7$  Ma.

Lu-Hf analysis of 39 spots on 38 grains yielded distinct clusters (figure 2.4, a., b. & c.).  $^{176}\text{Hf}/^{177}\text{Hf}$  values for the Archaean zircons yielded  $T_{\text{DM}}$  values of  $\sim 3.2$  Ga. The  $^{176}\text{Hf}/^{177}\text{Hf}$  values for the Palaeoproterozoic grains are higher and are clustered in an inverted "L" shape, suggesting an initial injection of new magmatic material at  $\sim 2000$  Ma with a  $T_{\text{DM}}$  crustal value of 2.76 Ga, followed by reworking of newer and older crustal material at  $\sim 1865$  Ma. Mesoproterozoic grains have higher  $^{176}\text{Hf}/^{177}\text{Hf}$  and similar  $\epsilon\text{Hf}$  when compared to the older grains, indicating injection of more juvenile material with a  $T_{\text{DM}}$  crustal of 2.1 Ga.

### 2.4.2 TC3 – Durumo River, Singida district

This sample contained abundant elongate prismatic zircons with rounded pyramidal terminations. Many zircons were fragmented. In fact grains commonly preserve aspect ratios of 2:1 to 4:1. CL images illustrate sector zoning and oscillatory growth zoning in most grains. Some grains preserve oscillatory zones cut off by transgressive recrystallised domains.

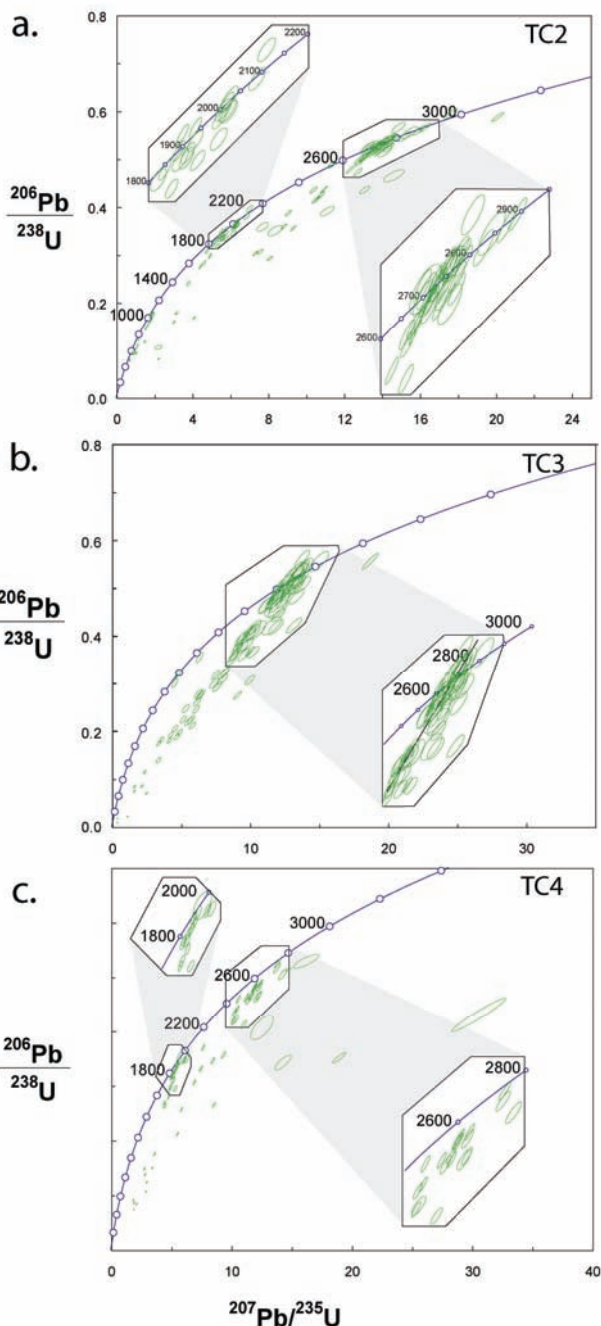


Figure 2.3 U-Pb concordia plots for all samples from this study and probability density plots for all samples, with  $^{207}\text{Pb}/^{206}\text{Pb}$  ages plotted on the x-axis, light grey curves representing 90-110% concordant data and dark grey curves representing all data. No concordia is presented for sample AlbSong-05 as data on correlation coefficients was unavailable.

U-Pb analysis of 104 spots was carried out on 97 grains (Table 2.2). Most of the data from this sample, shown in Figure 2.3 (e & f), form a discordia drawn down from  $\sim 2.65$  Ga, with a few  $>90\%$  concordant grains of younger ages. The Archaean grains have  $^{207}\text{Pb}/^{206}\text{Pb}$  ages that spread between 2600 and 2750 Ma, with a weighted average of  $2661 \pm 19$  Ma (MSWD = 15). The large MSWD strongly suggests that these data cannot be resolved into individual rock ages, but appear to represent multiple rock sources with broadly similar ages. Lu-Hf analysis of 28 spots on 28 grains gave  $^{176}\text{Hf}/^{177}\text{Hf}$  results with a narrow range of values.  $T_{\text{DM}}$  crustal ages of  $\sim 3.2$  Ga were obtained for the main cluster of Archaean grains, while the

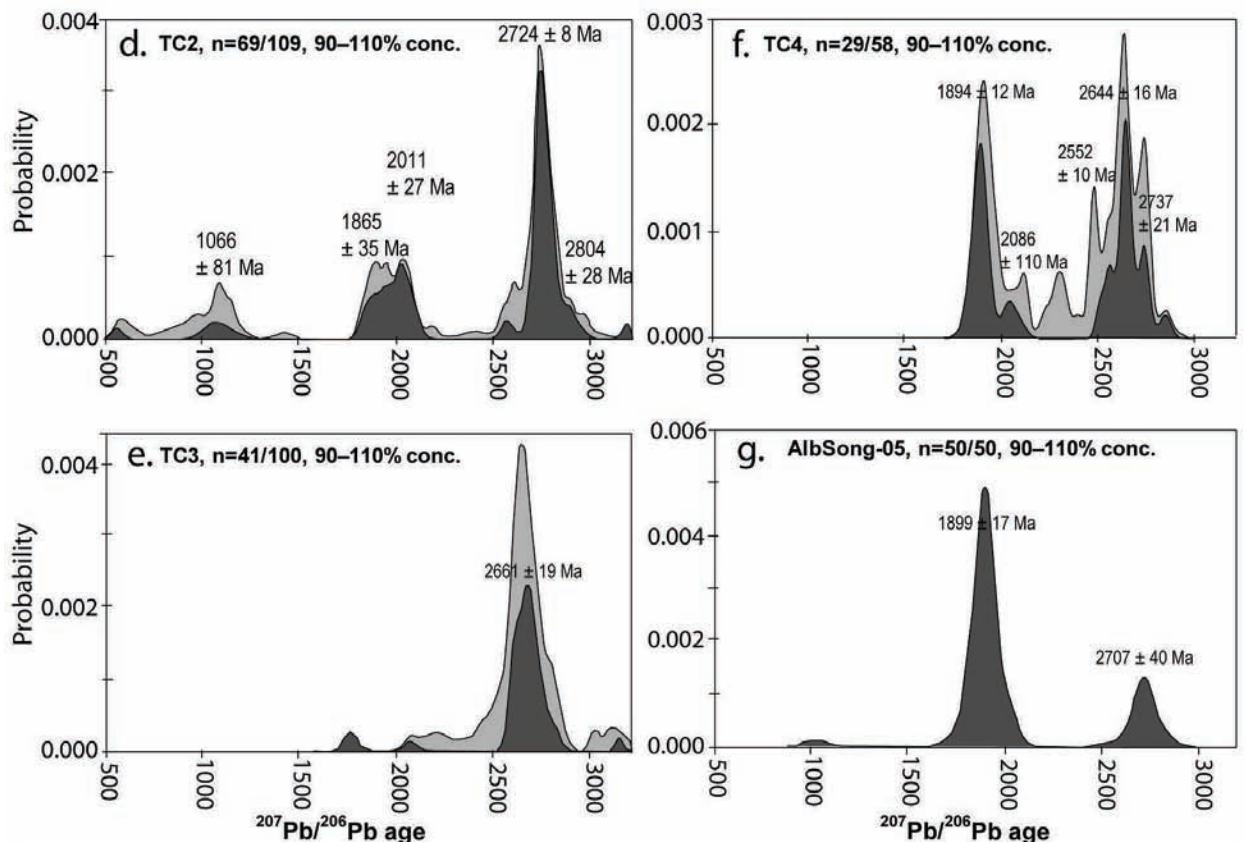


Figure 2.3 (continued)

Palaeoproterozoic zircon appears to have formed from reworking of this older crust, with U-Pb ages reflecting Pb loss.  $\epsilon_{\text{Hf}}$  values are consistent with an initial relatively juvenile Archaean source ( $\epsilon_{\text{Hf}} = 5$  to  $-10$ )

#### 2.4.3 TC4 – Malagarasi River, Uvinza township

This sample contained abundant zircon with heterogeneous morphologies ranging from sub-rounded to prismatic grains. Prismatic grains are commonly broken and where terminations are preserved they are rounded pyramids. Aspect ratios of such grains range from 2:1 to 5:1. CL imaging illustrates that rounded grains commonly show no zonation. Prismatic grains preserve some oscillatory growth zoning although in some grains zoning is overprinted by transgressive recrystallised domains.

Analysis of 63 U-Pb spots was carried out on 63 grains (Table 2.2). Figure 2.3 (g & h) shows two populations, one plotting along a discordia with an upper intercept of  $\sim 2700$  Ma and a second group plotting on a discordia with an upper intercept of  $\sim 1900$  Ma. When only  $< 90\%$  concordant grains are considered  $^{207}\text{Pb}/^{206}\text{Pb}$  age peaks can be resolved into three Archaean peaks at  $2737 \pm 21$  Ma (7 grains, MSWD = 3.6),  $2644 \pm 16$  Ma (11 grains, MSWD = 5.4) and  $2552 \pm 10$  Ma (4 grains, MSWD = 5.0), and two Palaeoproterozoic peaks at  $2086 \pm 110$  Ma (3 grains, MSWD = 8.0) and  $1894 \pm 12$  Ma (18 grains, MSWD = 1.9). Based on grain morphology and their Th/U all zircons appear to have an igneous origin (Corfu et al., 2003; Rubatto, 2002), however none of these groups can be refined sufficiently by grain morphology or other characteristics to indicate a single rock source.

Lu-Hf analysis of 29 spots on 29 grains yields a population

of Archaean grains with similar  $^{176}\text{Hf}/^{177}\text{Hf}$  values and a  $T_{\text{DM}}$  crustal age of  $\sim 3.2$  Ga. The Palaeoproterozoic grains show a mixture of reworked Archaean zircon ( $\epsilon_{\text{Hf}} = -15$  to  $-18$ ) and an input of more juvenile crust ( $T_{\text{DM}}$  crustal = 2.6 Ga,  $\epsilon_{\text{Hf}} = 5$  to  $-5$ ).

#### 2.4.4 Albsong-05

This sample was collected by Albidon Ltd, and data was collected by Belousova and Griffin (2006). These data have been reprocessed and interpreted for this study. No CL images of this sample are available.

Analysis of 50 zircons yielded 50 concordant  $^{207}\text{Pb}/^{206}\text{Pb}$  ages (Appendix 1) with strongly bimodal populations at  $2707 \pm 40$  Ma (MSWD = 2.0) and  $1899 \pm 17$  Ma (MSWD = 1.3) with one Mesoproterozoic grain ( $1004 \pm 58$  Ma). All these grains were analysed for Lu-Hf. The Archaean grains have similar  $^{176}\text{Hf}/^{177}\text{Hf}$  values (0.28210 to 0.28212) and a  $T_{\text{DM}}$  crustal age of  $\sim 3.2$  Ga. Palaeoproterozoic grains have a spread of  $^{176}\text{Hf}/^{177}\text{Hf}$  values indicating a mixture of more evolved Archaean crust with new juvenile material. The single Mesoproterozoic grain records a relatively juvenile signature with  $\epsilon_{\text{Hf}}$  of about  $+8$  and a  $T_{\text{DM}}$  crustal of 2.1 Ga.

## 2.5 Discussion

### 2.5.1 The significance of concordant Archaean U-Pb ages

Of the concordant U-Pb grains, 59% of the ages fall between 2500 - 2850 Ma, while 37% occur between 1800 - 2100 Ma. These Archaean grains support the existing geochronological data from the craton indicating that the main period of cratonic growth occurred between 2850 and 2500 Ma. Detailed investigation of the modern drainage

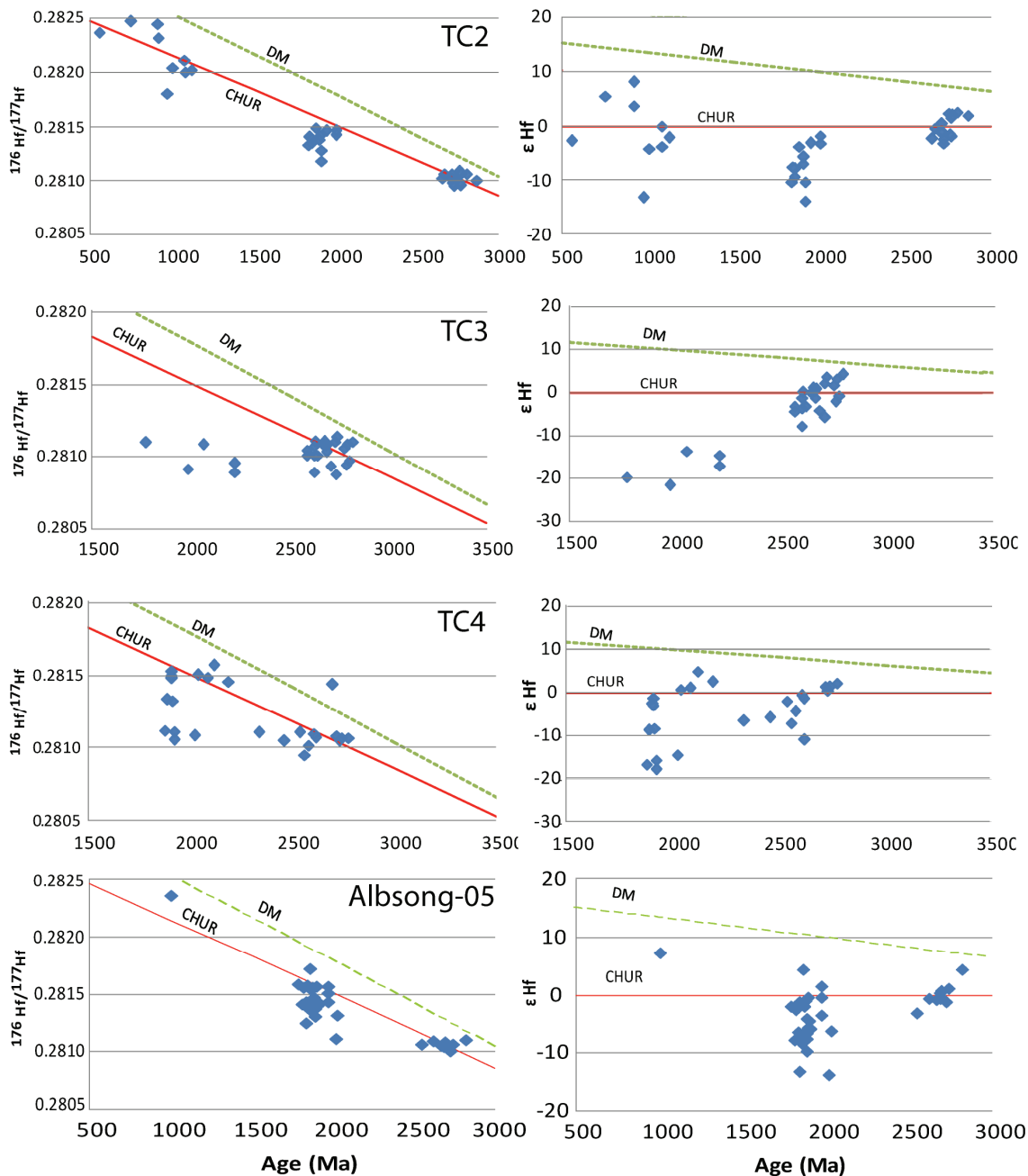


**Figure 2.4** Results of combined Lu-Hf and U-Pb zircon spot analyses from all stream sediment samples presented as  $^{176}\text{Hf}/^{177}\text{Hf}(t)$  vs  $^{207}\text{Pb}/^{206}\text{Pb}$  age,  $\epsilon\text{Hf}(t)$  vs  $^{207}\text{Pb}/^{206}\text{Pb}$  age and  $T_{\text{DM}}$  vs  $^{207}\text{Pb}/^{206}\text{Pb}$  age.  $^{176}\text{Hf}/^{177}\text{Hf}(t)$  is initial  $^{176}\text{Hf}/^{177}\text{Hf}$  calculated at the time of crystallisation.

area of each river using LandsatTM images reveals that the outer edges of the drainage area for three of the four samples (TC2, TC4 and Albsong-05) are in areas which the Tanzanian geological map (Pinna et al., 2004) describes as being Palaeoproterozoic (Ubendian) metaigneous and metasedimentary rocks. This readily explains the presence of post-Archaean zircons in these samples, however even sample TC3 for which the modern drainage area is wholly within the craton contains two younger grains. These younger peaks could be indicative of the presence of some younger crust within the modern craton, they could be the result of zircon transport in an ancient drainage system (as suggested by the presence of Cenozoic basins), they could reflect aeolian transport, or may indicate that younger crust that has now eroded away existed above the modern craton surface (i.e. a nappe from the Usagaran or Mozambique Orogens). It is important to realize that a long

distance or ancient transport model need only be invoked to explain a few grains in one sample, but this explanation does raise the issue that if these grains have been transported then allowance must be made for the possibility that some of the Archaean grains may also have originated outside the present drainage basin.

A review of published data from other Archaean cratons shows peaks in age spectra from igneous rocks between 2500 and 2850 Ma on, amongst others, the Yilgarn, Congo, Superior, Karelia, Wyoming, São Francisco, Nain, and Kaapvaal cratons (Batumike et al., 2009; Condie et al., 2009b; Davis et al., 2005; Zeh et al., 2008). At around 2700 Ma there is a global peak in U-Pb zircon age spectra, with some cratons showing up to 5 resolvable peaks near 2700 Ma (i.e. Superior Craton), and some age peaks recorded on up to six cratons (Condie et al., 2009b). Elimination of

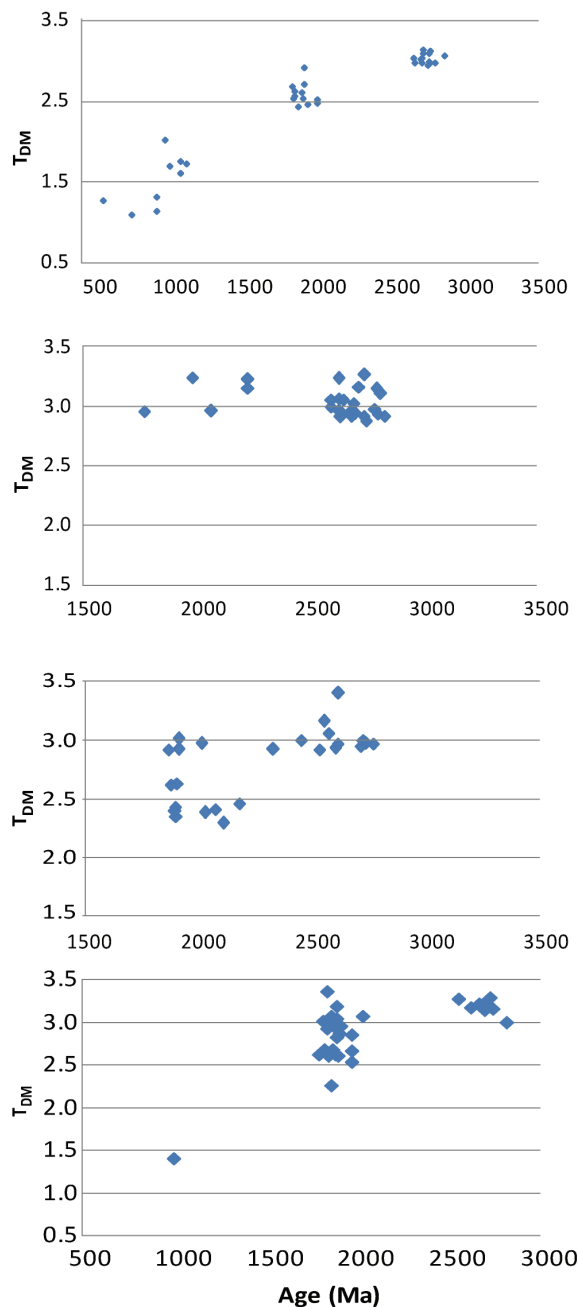


**Figure 2.4 Continued**

those cratons with significantly older or younger peaks and those whose peaks do not cover most of the 2500 – 2850 Ma range seen in this study leaves the Kaapvaal, Slave and São Francisco cratons as potential sources for zircons of similar ages to those seen here. The Kaapvaal and Slave cratons have similar granitoid ages, and have been grouped together by Condie et al. (2009b), suggesting a similar history of plutonism and possible geographic proximity during the late Archaean. Fluvial zircon transport has been invoked to explain peaks in U-Pb age spectra from up to 2000 km from the source (Cawood and Nemchin, 2001; Rainbird et al., 1992; Rainbird et al., 1997; Riggs et al., 1996). A study of zircon distribution in a modern river system, however, suggests that over a distance of ~125 km from a source region the detritus can be largely obscured by zircon ages reflecting the units through which the river flows (Cawood et al., 2003). If these materials have been transported over long distances it would have to be through rock units with ages which reflect

those seen in this study.

The location of the Tanzanian craton with respect to other Archaean cratons throughout history is enigmatic. During the Archaean it may have been part of the supercontinent Ur (Williams et al., 1991) or one of a number of smaller independent supercratons (Bleeker, 2008) however its position relative to other cratons has not been postulated. Many Proterozoic supercontinent reconstructions exclude the Tanzanian/Congo craton from their models (Hou et al., 2008; Kröner and Cordani, 2003; Pisarevsky et al., 2003), while others offer contradictory locations within models (Li et al., (2008) Hoffman, (1991)). For instance, in reconstructions of the Mesoproterozoic supercontinent of Rodinia Li *et al.* (2008) place the Congo next to the Kalahari while Hoffman (1991) places it on the opposite side of the continent next to Laurentia). Thus the Precambrian position of the Tanzanian Craton is largely unconstrained until the Neoproterozoic, and almost any Archaean craton could be invoked as a some-time neighbour.

### 2.5.2 The significance of Archaean Lu-Hf data

Lu-Hf data from all Archaean zircons in this study yield similar results ( $^{176}\text{Hf}/^{177}\text{Hf} = 0.2808 - 0.28125$ ;  $\epsilon_{\text{Hf}} = 5$  to  $-10$ ;  $T_{\text{DM}} = 3.0$  to  $3.4$  Ga). These data suggest that the craton protolith may have crystallized from a moderately evolved reservoir that separated from the depleted mantle around 0.5 Gy before craton formation, forming an older (~3.2 Ga) crust that was reworked to form the presently exposed craton at ~2.7 Ga. This idea is supported by the presence in these samples of a few zircons with U-Pb ages of ~3.2 Ga, however no 3.2 Ga crust has been identified within the craton. Alternatively the source magma from these rocks may not have been characteristic of the depleted mantle, but instead came from the lower mantle (possibly via a mantle plume) and had a more enriched signature with little or no contribution from the depleted mantle. This model has been proposed for the Emeishan large igneous province in southwestern China (Shellnutt et al., 2009) however the paucity of mafic rocks within the Tanzanian craton does not support the idea of a mantle plume. Batumike et al. (2009) propose a model for the Congo craton (based on zircons with Hf  $T_{\text{DM}} \approx 3.6$  Ga and  $^{207}\text{Pb}/^{206}\text{Pb}$  ages ~2.7 Ga) in which a thus-far unrecognized ~3.6 Ga crust underwent partial melting producing crustal rocks which record zircon crystallization between ~2900–2500 Ma. Application of this model to this data set would suggest a ~3.2 Ga crust, unrecognized within the Tanzanian Craton but hinted at by rare ~3.2 Ga zircons, underwent late Archaean reworking and recrystallisation between 2.85 – 2.5 Ga.

### 2.5.3 Post-Archaean crustal evolution of the Tanzanian Craton

Post-Archaean zircon populations in the stream sediment samples are probably sourced from the orogens surrounding the craton. These younger grains are seen in the samples from the south and west of the craton where it is bounded by the Ubende Orogen. Timing of metamorphism in the Ubende Orogen is poorly-constrained, but is generally considered to have occurred in the Palaeoproterozoic, at around ~1850 Ma (Boven et al., 1999). Numerous Ubendian granites have been dated by U-Pb TIMS zircon, with ages as follows;  $2066 \pm 8$  Ma,



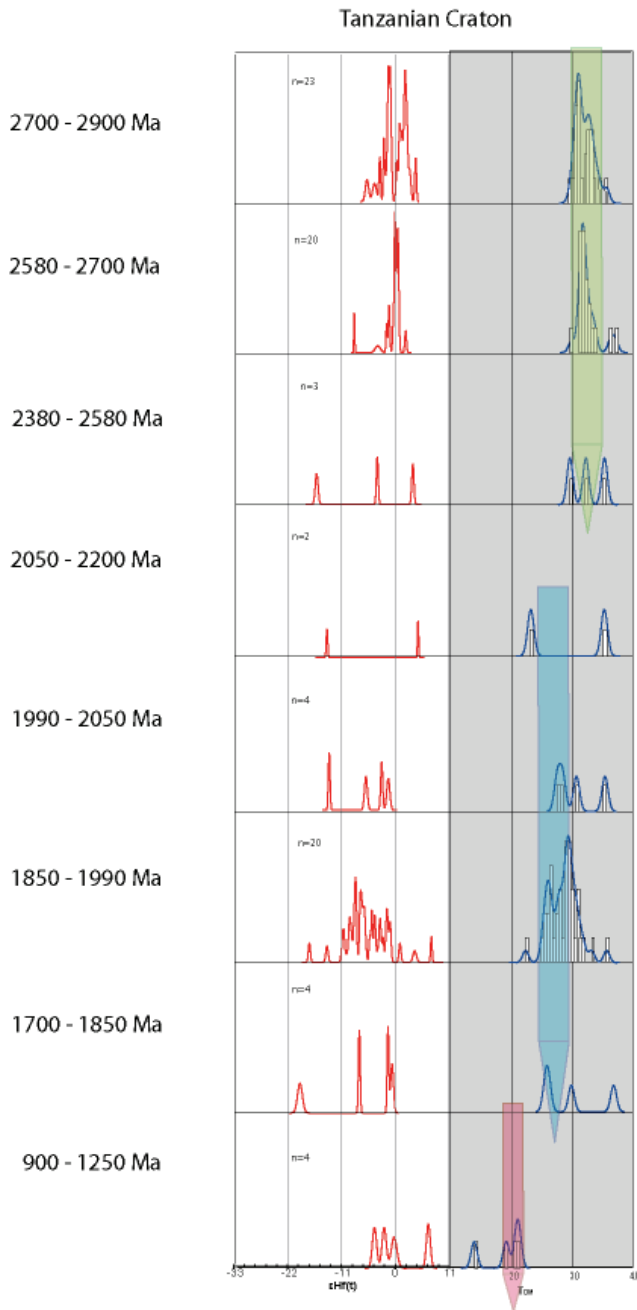


Figure 2.5 Probability density plots showing  $\epsilon_{\text{Hf}}$  and  $T_{\text{DM}}$  crustal at times of peak crust formation.

1864 ± 32 Ma, 1847 ± 37 Ma, 1838 ± 86 Ma, 1723 ± 41 Ma, 842 ± 80 Ma, 724 ± 6 Ma (Lenoir et al., 1994a). Although these data must be treated with caution as their errors are relatively large for TIMS data and are probably due to unrecognised complexity in the zircons analysed, the ages do mostly match up well with the 1850 – 2050 Ma U-Pb ages seen in this study, suggesting that the Ubende Orogen is the most likely proximal source for these Palaeoproterozoic grains. The Palaeoproterozoic peak in the age spectra for sample TC2 occurs at ~2050 Ma, compared to ~1890 Ma in TC4 and Albsong-05. This ~2050 Ma peak can be accounted for by Ubendian magmatism, although the absence of younger zircons suggests these zircons may be related to the Usagaran Orogeny in which eclogite facies metamorphism occurred at ~2.0 Ga (Collins et al., 2004b; Möller et al., 1995) as opposed to the later metamorphism and intrusions seen in the Ubende Orogen.

The  $T_{\text{DM}}$  crustal for these grains forms two groups (figure

2.5 ), a large population with  $T_{\text{DM}}$  crustal = 2.6 Ga and a smaller group with  $T_{\text{DM}}$  crustal = 3.2 Ga. This suggests an injection of new material at ~1.9 Ga derived from a slightly evolved reservoir that separated from the mantle at ~ 2.6 Ga and incorporated and reworked some older crustal material, possible from the craton.

The minor Mesoproterozoic peak in U-Pb age spectra is seen only in the two southern-most samples and may represent either younger rock units within the Ubende Orogen or transport of materials from either the 1.2 – 1.0 Ma Irumide Orogen or the 1.4 – 1.0 Ga Kibaran Orogen. The Irumide Orogen is the most proximal potential source. These grains show a mixture of an evolved and juvenile source ( $T_{\text{DM}}$  crustal = 2.1 and 1.3 Ga respectively).

It should be noted that the U-Pb age spectra data from all samples preserve no >90% concordant zircon ages between 2490 and 2150 Ma. This is consistent with a 250 My gap been seen at this time (2.2 – 2.45 Ga) in Palaeoproterozoic terranes globally and has been interpreted to indicate a lull in crust formation, possibly related to a shutdown of subduction zones and magmatism during this period (Condie et al., 2009c).

## 2.6 Conclusions

Based on the data from this study the Tanzanian Craton formed between 2850 – 2500 Ga with magmas derived from an evolved ( $T_{\text{DM}}$  crustal = 3.2 Ga) source. Within the Ubende Orogen and Usagaran Orogen crustal material formed between 1850 – 2050 Ma from a more evolved magma source ( $T_{\text{DM}}$  crustal = 2.6 Ga) that also reworked some Archaean material from the Tanzanian Craton. The youngest zircon population (1.0 – 1.2 Ga) seen in the southern samples may be derived from the Irumide Orogen, and have a mixed ( $T_{\text{DM}}$  crustal = 2.1 and 1.3 Ga) magma source.



# Chapter 3— $^{40}\text{Ar}/^{39}\text{Ar}$ Thermochronology and U-Pb geochronology of the eclogite-hosting Ubende Orogen, Tanzania

---

## NOTE:

This figure is included on page 3.1 of the print copy of the thesis held in the University of Adelaide Library.

Figure 3.1 Location diagram showing Ubende orogenic belt, major geological domains and known localities of eclogite outcropping. Map modified after Coolen (1980)

### 3.1. Introduction

Modern tectonic processes are driven by dissipation of the internal heat of the Earth; as the latter changed over time, so tectonic processes also changed. The manner and timing of these changes are highly controversial, but Archaean (>2.5 billion years - Ga) tectonic processes are clearly different from those active after ~1.6 Ga (see review of Brown, 2007b). Eclogites and other high-pressure rocks have been used by various authors to interpret changing tectonic regimes of the earth (Maruyama and Liou, 1998; O'Brien and Rötzler, 2003) because the pressure conditions of their formation are equivalent to those at mantle depths while the temperatures recorded by the mineral assemblages are cooler than those found within the mantle. Eclogites require relatively fast burial and exhumation to preserve their mineral assemblage. The mechanism for transporting rocks to mantle depths then rapidly exhuming them to mid-crustal levels is commonly considered to be subduction, because it is within known subduction zones that modern eclogites are found. These rocks are relatively rare in the geological record (Figure 1.1), and are more common in the Phanerozoic earth than the Proterozoic or older.

The earliest onset of plate tectonics has been a topic of some debate in the literature, as has the criteria which could be used to identify plate tectonics.

Amongst the world's oldest known *in situ* eclogite occurrences is in the Ubende Orogen of western Tanzania. The Ubende Orogen has been assumed by some authors to be the synchronous with the Usagaran Orogen (Priem et al., 1979; Quennel et al., 1956) however recent geochronological work suggests that metamorphism in the Ubende Orogen may have occurred at 1.95-1.85 Ga (Boven et al., 1999) making it ~50-150 Myr younger than the 2.0 Ga Usagaran orogeny.

### 3.2. Geological Background

The Ubende Orogen is north-west south-east trending, is over 600 km long and 200 km wide and comprises the south-western margin of the Archaean Tanzanian Craton (Figure 3.1). The Ubende Orogen is bounded to the west by Lake Tanganyika, part of the East African Rift system. To the north and west of the Ubende Orogen lies the Mesoproterozoic Kibaran Orogen. To the south west of the Ubende Orogen lies the Bangweulu Block, a series of Palaeoproterozoic granites, and south of these lies the Irumide Orogen, a Mesoproterozoic Orogen transecting the southern end of the Ubende terrane.

The Ubende Orogen comprises eight structural blocks (Figure 3.1, table 3.1) comprised of high-grade metamorphic rocks; mainly amphibolites, granulites and gneisses. The structural blocks are separated by ductile shears zones up to 600 km in length (Sutton et al., 1954) with mainly NW dextral strike slip displacement (Lenoir et al., 1994a; Nanyaro et al., 1983). Mafic and ultramafic high-pressure granulites and rare eclogite lenses and blocks occur in the Ubende Orogen within sheared amphibolite facies country rock. Eclogite occurs as constituents of basic dismembered tectonic units (Ubende & Ikulu blocks) and as rare small lenses in felsic gneiss. The timing of eclogite facies metamorphism in the Ubende Orogen is poorly constrained, but is considered to be Palaeoproterozoic, at around 1850 Ma (Boven et al., 1999; Lenoir et al., 1994). This age is inferred from whole zircon SIMS U-Pb dating of granites which are assumed to be syn-orogenic (Lenoir et al., 1994) and from  $^{40}\text{Ar}/^{39}\text{Ar}$  thermochronology of barroisite (amphibole) from a blastomylonite situated near the northern Ubendian eclogites (Boven et al., 1999). These dates are discussed in section 3.6.2.

The tectonic setting of these eclogites, based on *P-T* paths, has been interpreted to be initial subduction of an oceanic slab under the Tanzanian Craton (Lenoir et al.,

NOTE:

This figure is included on page 3.2 of the print copy of the thesis held in the University of Adelaide Library.

Figure 3.2 Geological map showing sample locations and structural trends – base geology modified from Pinna et al. (2004)

1994a) ( $T=720^{\circ}\text{C}$ ,  $P=17.1$  kbar), followed by exhumation ( $T=800\text{-}500^{\circ}\text{C}$ ,  $P=11\text{-}15$  kbar), later exhumation (25bar/ $^{\circ}\text{C}$ ) either slower or with higher T gradient during orogenesis, final exhumation at near isothermal decompression (500-600 $^{\circ}\text{C}$ , 5-10kbar) (Boven et al., 1999). P-T studies on HP mafic granulite supports multiple stages of exhumation and suggest that exhumation is related to dextral lateral shear deformation (Boven et al., 1999).

The Kibaran Orogen is a SW-NE trending orogenic Orogen, the north-eastern end of which which transects the northern end of the Ubende Orogen. Three tectonic phases have been recognized in the Kibaran: (1&2) the Usagaran (2.04–1.95 Ga) and the Ubendian phase (1.88–1.85 Ga) phase is recognized predominantly along the southern margin of the Congo Craton rather than the north-eastern Kibaran Orogen and is interpreted as relating to metacratonic reactivation or convergence; (3) the Lukamfwa phase at around 1.6–1.4 Ga is intracontinental, and can be observed in almost all parts of the Kibaran Orogen with ages of around 1.4 Ga in the north eastern section (Pohl, 1994) and ages up to 1.5 Ga in the central part (Tack et al., 1994). A fourth phase ranging from 1.3 to 1.2 Ga has been reported by (Buchwaldt et al., 2007; Klerkx et al., 1987; Pohl, 1994; Tack et al., 1994) in the northeastern and in the north central part of the Kibaran Orogen, but not been reported in the southern part, and interpreted as associated with orogenic extensional collapse; a final phase of post orogenic magmatic activity in the Kibaran Orogen throughout the Irumide period (1.1–0.9 Ga) has been attributed to large scale reworking of the crust along

conjugate margins (DeWaele et al., 2006b; Klerkx et al., 1987).

The Irumide Orogen is situated along the southern margin of the Bangweulu block and transects the southern end of the Ubende Orogen. It consists of deformed basement and metasediments and granitoid intrusions. The basement is mostly Palaeoproterozoic ( $2049 \pm 6$  to  $1927 \pm 10$  Ma) (Rainaud et al., 1999; 2002; Rainaud, 2003; DeWaele, 2005; DeWaele et al., 2006a; 2006b) with minor Archaean granite gneiss ( $2726 \pm 36$  Ma) (DeWaele, 2005; DeWaele et al., 2006a; DeWaele et al., 2006b). This is overlain by sedimentary package with a maximum depositional age of  $\sim 1.8$  Ga based on detrital zircon U-Pb age data with local marine volcanic units aged  $1879 \pm 13$  and  $1856 \pm 4$  Ma (DeWaele, 2005; DeWaele and Fitzsimons Ian, 2007; DeWaele and Fitzsimons, 2004; Rainaud, 2003). These units are intruded by granitoids aged between  $1664 \pm 4$  and  $1551 \pm 33$  Ma (DeWaele, 2005; DeWaele et al., 2006b).

The Bangweulu Block has not been directly dated, though many of the intrusive rocks are considered to be of equivalent age to Ubendian intrusive rocks (Lenoir et al., 1994). Other rock age constraints come from dating of surrounding metasedimentary sequences which are assumed to have been sourced from the Bangweulu block (Rainaud et al., 2005).

### 3.3. Structure

Structural data was collected from the Ubende Orogen following approximately the same transect as that followed by the UNESCO survey team (Nanyaro et al., 1983). This data is shown in Figure 3.2. The data

**Table 3.1.** Geological characteristics of the Ubendian terranes (modified after Daly 1988)

**NOTE:**

This table is included on page 3.3 of the print copy of the thesis held in the University of Adelaide Library.

collected was consistent with the model described in that report. The relationships between the tectonic blocks are illustrated in a schematic block diagram of the relationship between different blocks along the transect (Figure 3.3).

The southwestern-most unit in this transect is the Ufipa block, comprised of Palaeoproterozoic ( $1864 \pm 32$  Ma; U-Pb zircon; (Lenoir et al., 1994a)) granites and granite gneisses dipping steeply to the northeast with lineations trending to the north west (or rarely to the south east). The boundary between the Ufipa and Ikulu blocks is defined by a southeast-northwest trending shear zone containing amphibolites and chlorite phyllites with intense and steep shear-parallel foliation. Northeast of this shear is the Ikulu block, comprised of strongly foliated amphibolites with boudins of eclogite- and granulite-facies rock and carbonatite. Small (cm-scale) sub-soclinal folds with east-west striking axial planes and east trending lineations are seen in the amphibolites but not in the boudins of eclogite and granulite. These small folds are overprinted by steep northeast dipping foliation which is also seen in the eclogite and granulite.

The Ubende block is mostly comprised of amphibole gneisses and quartzites, with some small boudins of mafic and ultramafic rocks. Foliations in this unit are generally less steep than in the Ikulu block, dipping moderately to the north-northeast, becoming steeper in the northeast of the block. Mineral lineations dip predominantly to the east. The contact between the Ikulu and Ubende blocks is not well exposed in this section, however Boven *et al.* (1999) indicate the boundary to be a steep northeast-dipping reverse fault. The boundary between the Ubende and the Wakole block to the northeast is also poorly exposed. The country rock of both blocks is amphibolite gneiss, but in the Wakole block boudins are of granulite rather than mafic and ultramafic rocks. The foliation is defined by compositional banding with boudins of granulite. The foliation strikes consistently northwest-southeast, but undulates between shallow southwest and steep northeast dips.

#### 3.4. Sample details and analytical procedure

##### 3.4.1 Zircon U-Pb geochronology

Three samples were selected for zircon separation and analyses. T04-07 is a kyanite-garnet-biotite-muscovite-plagioclase-ilmenite metapelite from the Wakole block (S

$6^{\circ}30'21.5''$  E  $30^{\circ}44'11.9''$ ) with minor quartz and inclusions in garnet of biotite, sillimanite, staurolite, ilmenite (Figure 3.4 a & b). T04-12b is a kyanite-biotite-garnet-quartz- gneiss from close to the boundary between the Ubende and Wakole blocks (S  $6^{\circ}39'37.8''$ , E  $30^{\circ}39'28.4''$ ) with minor muscovite and sillimanite associated with coarse grained kyanite (figure 3.4 c & d). The boundary between these blocks is poorly defined and the sample could be from either terrane, but based on the lithology is probably part of the Wakole block. Sample T04-39 is a quartz-muscovite psammitic schist (figure 3.4 e & f) from the Ubende Orogen (S  $6^{\circ}43'52.5''$ , E  $30^{\circ}33'21.5''$ ).

Zircons were separated from crushed rocks samples by magnetic and heavy liquid separation, then grains were handpicked and mounted in epoxy discs. The mounts were carbon coated then imaged using a CL detector fitted to a Phillips XL20 scanning electron microscope at a working distance of 13.5mm and using an accelerating voltage of 10kV. Zircon U-Th-Pb analyses were undertaken by LA-ICPMS at Adelaide Microscopy, University of Adelaide on an Agilent 7500cs ICPMS fitted with a New Wave 213 nm neodymium–yttrium–aluminium-garnet (Nd-YAG) laser. Beam diameter was set at 30  $\mu\text{m}$  using a repetition rate of 15 Hz. U-Pb fractionation was corrected using the GEMOC GJ-1 zircon (TIMS normalization data  $^{207}\text{Pb}/^{206}\text{Pb} = 608.3$  Ma,  $^{206}\text{Pb}/^{238}\text{U} = 600.7$  Ma,  $^{207}\text{Pb}/^{235}\text{U} = 602.2$  Ma (Jackson et al., 2004)). Standard GJ-1 was run 4 times at the beginning and end of a run, interspersed by two analyses of the in-house Sri Lankan zircon standard (BJWP-1,  $^{207}\text{Pb}/^{206}\text{Pb} = 720.9$  Ma (Wade et al., 2008)) and ten analyses of unknowns. Total acquisition time per analysis was 90 seconds; 50 seconds background measurement followed by 40 seconds of sample ablation. Data was processed using GLITTER software (Van Achtenbergh et al., 2001). Fractionation corrections etc are discussed in more detail in chapter 2.

##### 3.4.2 Hornblende $^{40}\text{Ar}/^{39}\text{Ar}$ thermochronology

Five hornblende-bearing samples from widely separated sites within the traverse section were selected. T04-05 is an amphibolite from the Wakole block (S  $6^{\circ}33'21.0''$ , E  $30^{\circ}48'33.3''$ ). T04-14b is a coarse grained massive amphibolite-clinopyroxene-plagioclase-quartz-ilmenite rock from the Wakole- block (S  $6^{\circ}38'55.5''$ , E  $30^{\circ}38'58.5''$ ) (figure 3.4 g). T04-26b is a coarse grained garnet-

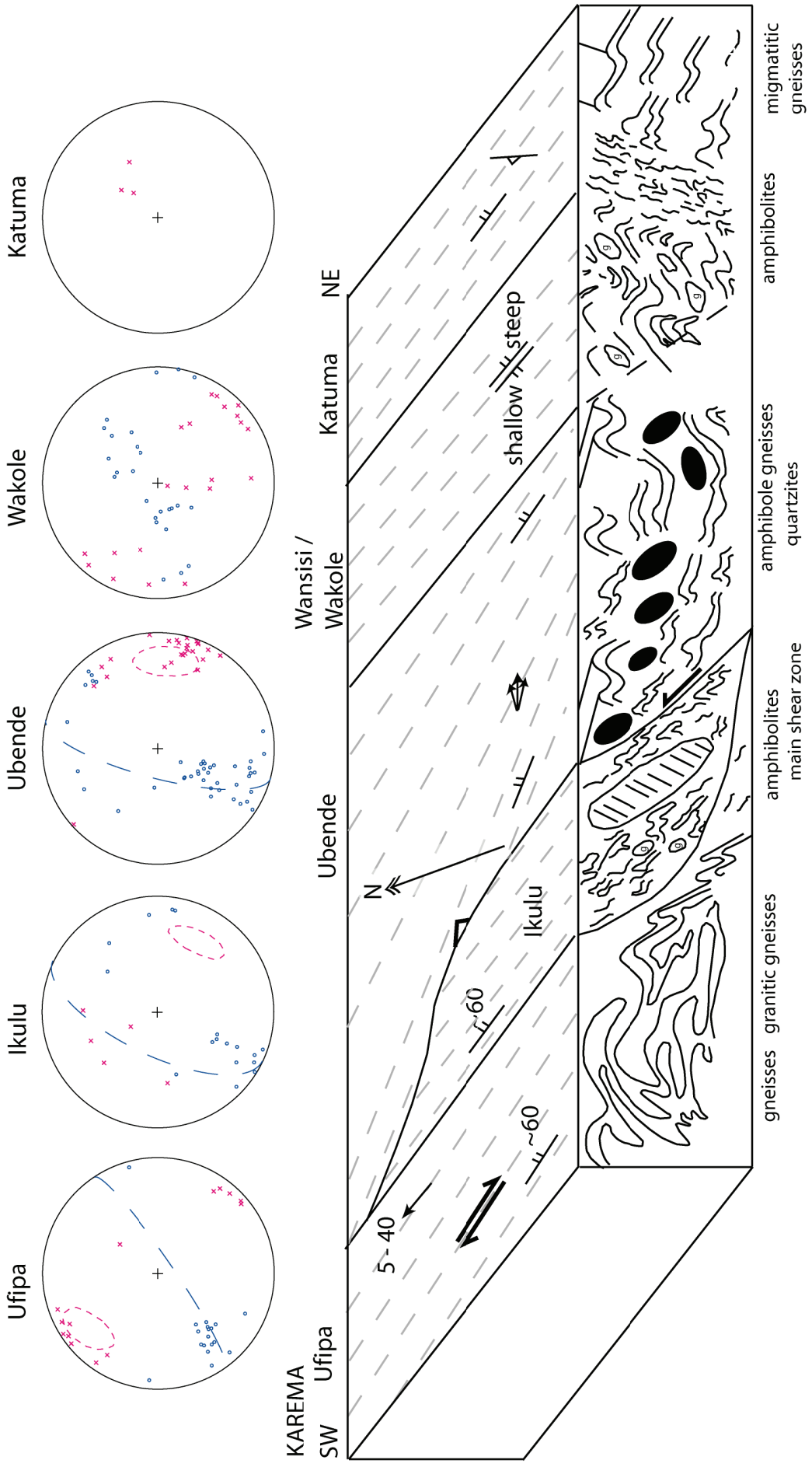


Figure 3.3 Schematic block diagram showing a section SW – NE from Karema. Stereographic projections (equal area, lower hemisphere) show mineral elongation lineations (pink cross) and poles to foliations (blue dot). Dashed lines indicate major trends in data from Boven et al. (1999).



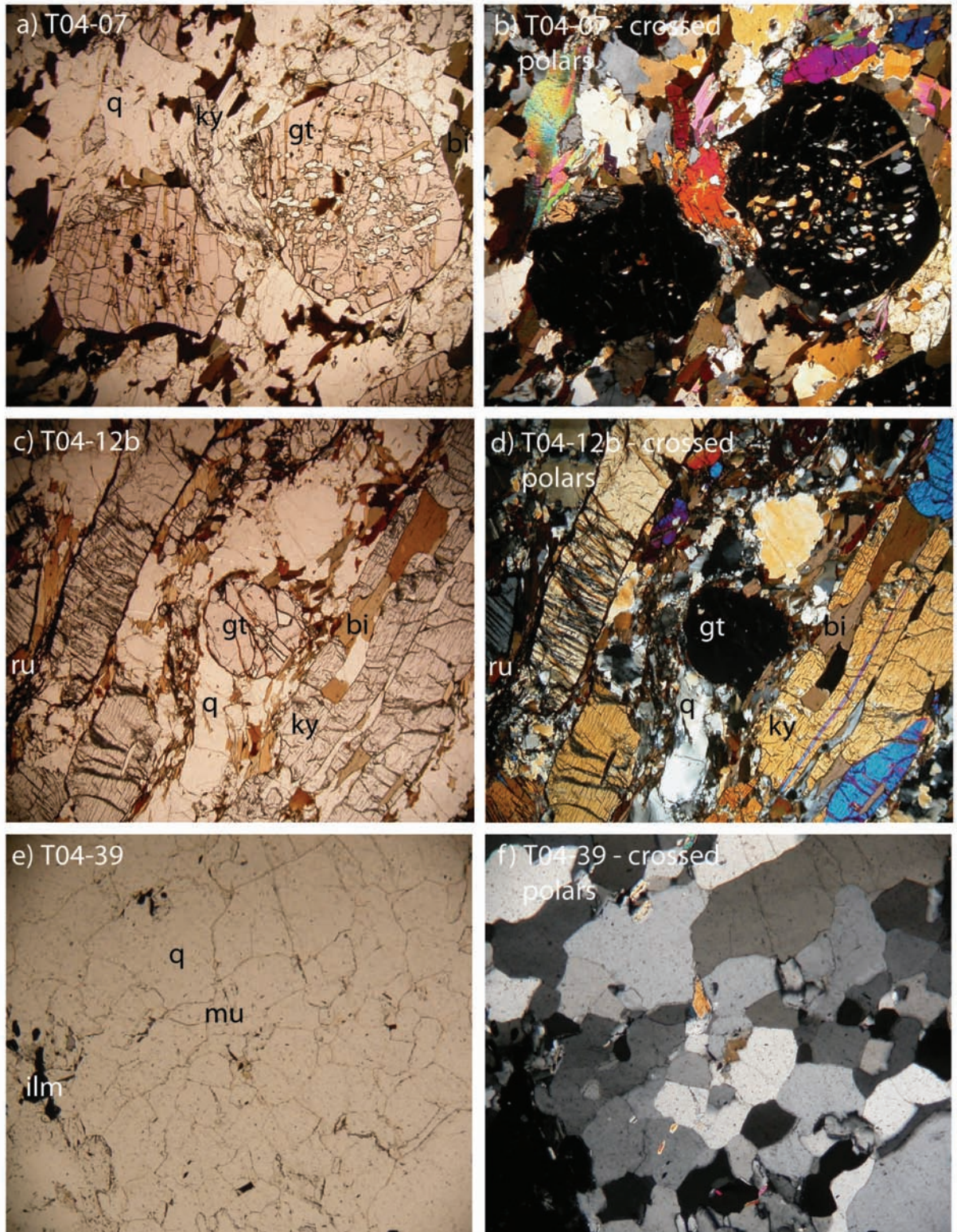


Figure 3.4 a) – f) - Photomicrographs of metasedimentary samples used for U-Pb zircon geochronology.

clinopyroxene-titanite eclogite with mm-scale retrograde actinolite-muscovite shears from an eclogitic boudin within the Ikulu block (1km along Ikola-Mpanda Rd from S 6° 44'18.9" E 30° 24'19.6") (figure 3.4 h & i). T04-33 is a coarse grained massive garnet bearing amphibolite (figure 3.4 j) with minor k-feldspar from the Ikulu block (S 6°45'35.9", E 30°26'52.2"). T04-43 is a coarse grained amphibolite with a weak foliation developed in discrete zones (figure 3.4 k) the Ubende block (S 6°41'48.0", E 30°36'25.1").

From these samples unaltered, optically transparent, hornblende were separated. These minerals were separated using a Frantz magnetic separator, and then carefully hand-picked under a binocular microscope. The selected hornblende minerals were further leached in diluted HF for one minute and then thoroughly rinsed with distilled water in an ultrasonic cleaner.

Samples were loaded into 5 large wells of one 1.9 cm diameter and 0.3 cm depth aluminium disc. These wells were bracketed by three small wells that included Hb3gr hornblende used as a neutron fluence monitor for which



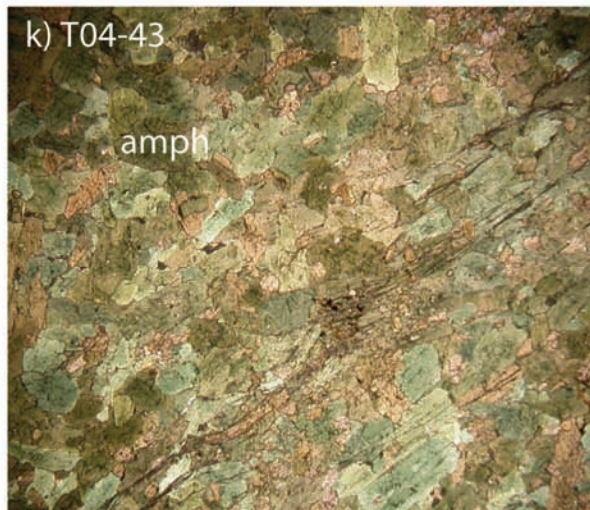
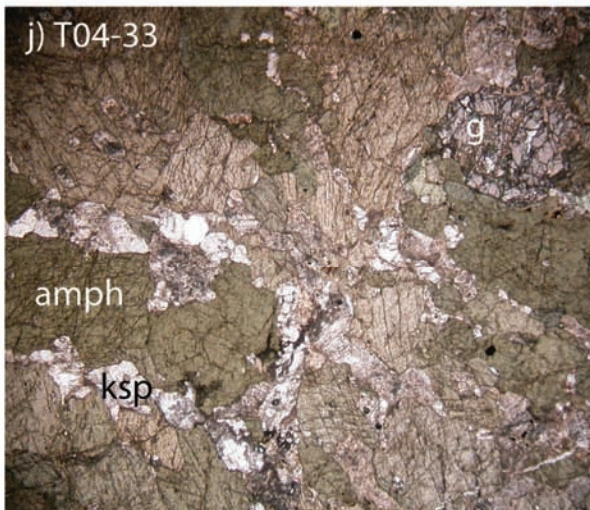
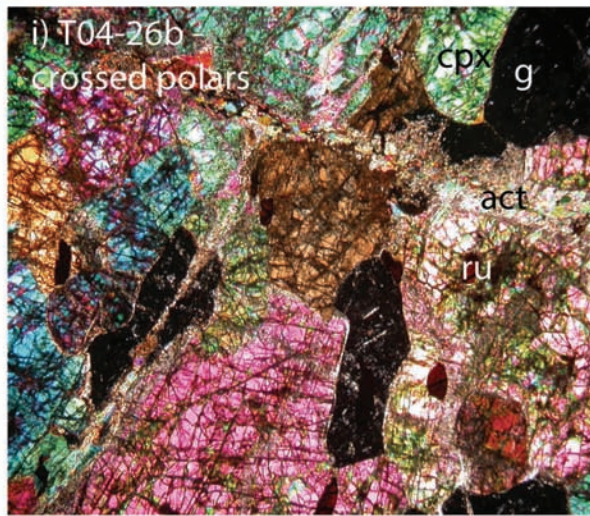
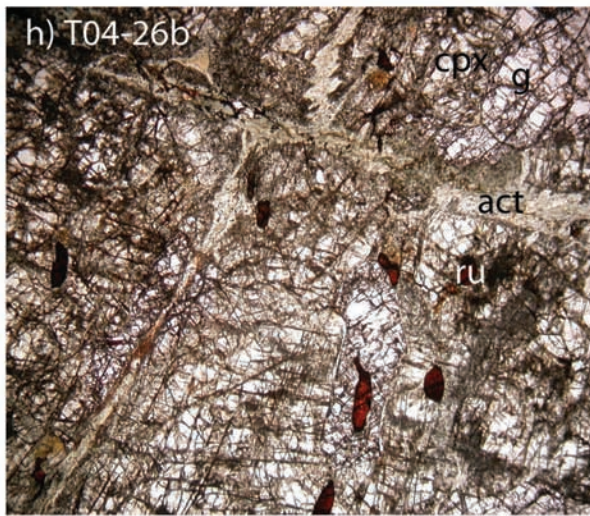
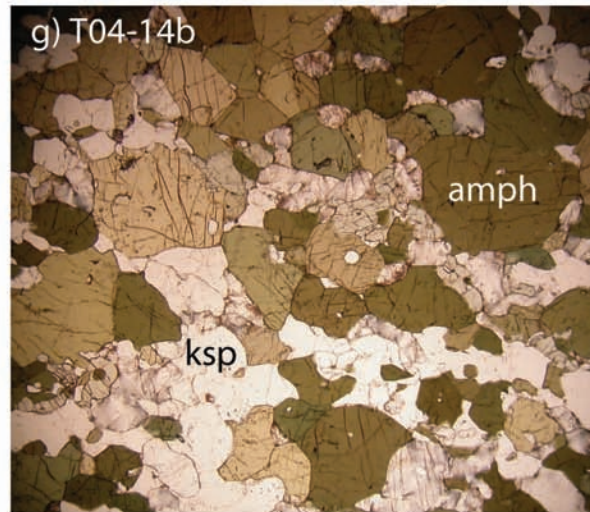


Figure 3.4 g) – k) - petrology of metaigneous rock samples used for Ar-Ar thermochronology.

an age of  $1072 \pm 11$  Ma was adopted (Jourdan et al., 2006; Turner et al., 1971) and a good in-between-grains reproducibility has been demonstrated (Jourdan and Renne, 2007; Jourdan et al., 2006). The discs were Cd-shielded to minimize undesirable nuclear interference reactions and irradiated for 25 hours in the Hamilton McMaster University nuclear reactor (Canada) in position 5C. The J-value computed for all samples was  $0.008951 \pm 0.0000313$  (0.35%) determined as the average and standard deviation of J-values of the small wells for each irradiation disc. Mass discrimination was monitored using

an automatic air pipette and provided a mean value of  $1.004665 \pm 0.27$  per dalton (atomic mass unit). The correction factors for interfering isotopes were  $(^{39}\text{Ar}/^{37}\text{Ar})_{\text{Ca}} = 7.30 \times 10^{-4} (\pm 11\%)$ ,  $(^{36}\text{Ar}/^{37}\text{Ar})_{\text{Ca}} = 2.82 \times 10^{-4} (\pm 1\%)$  and  $(^{40}\text{Ar}/^{39}\text{Ar})_{\text{K}} = 6.76 \times 10^{-4} (\pm 32\%)$ .

The  $^{40}\text{Ar}/^{39}\text{Ar}$  analyses were performed at the Western Australian Argon Isotope Facility at Curtin University, operated by a consortium consisting of Curtin University and the University of Western Australia. The samples were step-heated using a 110 W Spectron Laser Systems, with a continuous Nd-YAG (IR; 1064 nm) laser





Figure 3.5. Cathodoluminescence images of zircons from T04-07 and T04-39

rastered over the sample during 1mn to ensure an homogenously distributed temperature. The gas was purified in a stainless steel extraction line using three SAES AP10 getters and a liquid nitrogen condensation trap. Ar isotopes were measured in static mode using a MAP 215-50 mass spectrometer (resolution of  $\sim 600$ ; sensitivity of  $2 \times 10^{-14}$  mol/V) with a Balzers SEV 217 electron multiplier mostly using 9 to 10 cycles of peak-hopping. The data acquisition was performed with the Argus program written by M.O. McWilliams and ran under a LabView environment. The raw data were processed using the ArArCALC software (Koppers, 2002) and the ages have been calculated using the decay constants recommended by (Steiger and Jäger, 1977). More accurate calibrations of standard monitors that yield ages about 0.7% and 1.0% older than previously proposed have recently been suggested (Kuiper et al., 2008; Renne et al., 2010)). Systematic errors of this magnitude in decay constants could have an effect on our result. For instance, the study of Renne et al. (2010) recalculates the age of the Hb3gr standard used in this study from  $1072 \pm 11$  Ma to  $1080.4 \pm 1.1$  Ma. However as no consensus on calibration of standards and decay constants has yet been reached in the literature this

study uses the decay constants recommended by (Steiger and Jäger, 1977).

Blanks were monitored every 3 to 4 steps and typical  $^{40}\text{Ar}$  blanks range from  $1 \times 10^{-16}$  to  $2 \times 10^{-16}$  mol. Ar isotopic data corrected for blank, mass discrimination and radioactive decay are given in table 3.3. Individual errors in table 3 are given at the  $1\sigma$  level. Our criteria for the determination of plateau are as follows: plateaus must include at least 70% of  $^{39}\text{Ar}$ , and the plateau should be distributed over a minimum of 3 consecutive steps agreeing at 95% confidence level and satisfying a probability of fit (P) of at least 0.05. Mini-plateaus are defined similarly except that they include between 50% and 70% of  $^{39}\text{Ar}$ . Plateau ages (Table 3 and Fig. 6) are given at the  $2\sigma$  level and are calculated using the mean of all the plateau steps, each weighted by the inverse variance of their individual analytical error. Integrated ages ( $2\sigma$ ) are calculated using the total gas released for each Ar isotope. Inverse isochrons include the maximum number of steps with a probability of fit  $\geq 0.05$ . The uncertainties on the  $^{40}\text{Ar}^*/^{39}\text{Ar}$  ratios of the monitors are included in the calculation of the integrated and plateau age uncertainties, but not the errors on the age of the

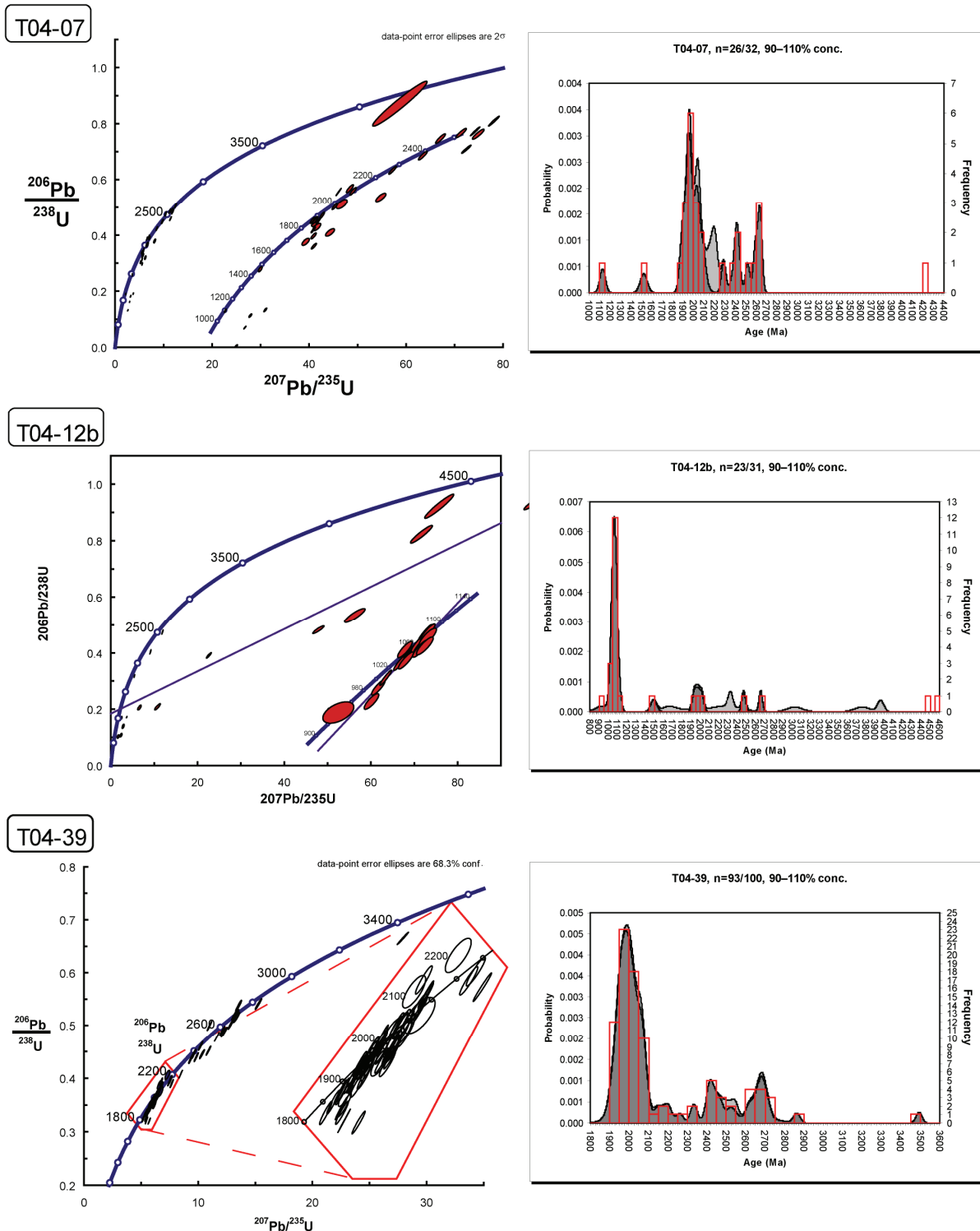


Figure 3.6. U-Pb concordia plots and probability density plots for all samples, with  $^{207}\text{Pb}/^{206}\text{Pb}$  ages plotted on the x-axis, light grey curves representing 90-110% concordant data and dark grey curves representing all data.

monitor and on the decay constant (internal errors only, see discussion in (Min et al., 2000).

### 3.5. Results

#### 3.5.1 U-Pb results

Zircon U-Pb-Th data for all samples are reported in appendix 2.1 and plotted as concordia and probability density plots in figure 3.5.6. Representative cathodoluminescence (CL) images are shown in figure 3.5.

Sample T04-07, a kyanite-biotite pelite, contained few zircon grains, mostly fragments of apparently prismatic grains with rounded terminations. CL imaging revealed

well developed oscillatory growth zoning. One small rounded grain had unzoned high CL response. Analysis of 32 U-Pb spots was conducted on 29 grains (Table 3.2). Figure 3.6 (a & b) shows concordia and probability density plots, with a spread in the  $^{207}\text{Pb}/^{206}\text{Pb}$  age spectra between 1.9 Ga and 2.75 Ga and three apparently concordant grains outside of this grouping. When only > 90 % concordant grains are considered the Palaeoproterozoic grouping can be resolved into two peaks at  $1947 \pm 24$  Ma (10 grains, MSWD = 7.8) and  $2045 \pm 37$  Ma (5 grains, MSWD = 4.9). The Archaeaean data can be resolved at  $2416 \pm 14$  Ma (3 grains, MSWD = 1.3) and  $2622 \pm 42$  Ma (4 grains, MSWD = 7.2). Grains



Table 3.3.  $^{40}\text{Ar}/^{39}\text{Ar}$  data summary

Sample N°		Z-05	Z-14b	Z-26b	Z-33	Z-43
Coordinates		S 6°33'21.0" E 30°48'33.3"	S 6°38'55.5" E 30°38'58.5"	S 6°44'18.9" E 30°24'19.6"	S 6°45'35.9" E 30°26'52.2"	S 6°41'48.0" E 30°36'25.1"
Unit		Wakole	Ubende	Ikulu	Ikulu	Ubende
Integrated age (Ma, $\pm 2\sigma$ )		1058 $\pm$ 8	1169 $\pm$ 7	2997 $\pm$ 16	979 $\pm$ 7	1089 $\pm$ 8
Plateau characteristics	Plateau /mini-plateau* age (Ma, $\pm 2\sigma$ )	1035 $\pm$ 9	1023 $\pm$ 7 *	-	1019 $\pm$ 9	960 $\pm$ 9 *
	Total $^{39}\text{Ar}$ released (%)	72.2	62.2		78	63.3
	MSWD	1.68	1.12		1.72	1.2
	P	0.063	0.35		0.11	0.35
Isochron characteristics	Isochron age (Ma, $\pm 2\sigma$ )	1039 $\pm$ 10	1023 $\pm$ 8	-	1017 $\pm$ 11	954 $\pm$ 9
	n	13	6		7	5
	$^{40}\text{Ar}/^{36}\text{Ar}$ Intercept ( $\pm 1\sigma$ )	283 $\pm$ 29	64 $\pm$ 6		271 $\pm$ 44	78 $\pm$ 1
	MSWD	1.8	1.16		1.78	0.61
	P	0.18	0.33		0.12	0.61

aged 1131  $\pm$  27 Ma, 1525  $\pm$  34 Ma, 2291  $\pm$  21 Ma, 2521  $\pm$  22 Ma and 4210  $\pm$  119 Ma did not fit into these populations. Hadean aged grains will be addressed in the discussion of this chapter. Based on grain morphology and Th/U ratio > 0.07 all grains appear igneous (Corfu et al., 2003; Rubatto, 2002).

Multiple U-Pb spots were targeted on four grains, one with distinct sector zoning, and three grains with cores and rims. Of the three grains with cores and rims analysed one yielded identical results for each (within error) while the remaining two rim yielded discordantly ages, younger than the cores suggesting some resetting of the U-Pb system. The sector zoned grain yielded distinctly different concordant  $^{207}\text{Pb}/^{206}\text{Pb}$  ages of 4210  $\pm$  119 Ma and 1914  $\pm$  29 Ma.

Sample T04-12b, a kyanite-biotite pelite, contained few zircon grains. Analysis of 37 spots was conducted on 34 grains. The results are presented in table 3.2, and plotted in figure 3.6 (c & d). There was a significant peak in the  $^{207}\text{Pb}/^{206}\text{Pb}$  age spectra at 1068  $\pm$  11 Ma (16 grains, MSWD 2.8), a minor Palaeoproterozoic peak at 1973  $\pm$  100 Ma (3 grains, MSWD = 15) and individual grains aged 4567  $\pm$  44 Ma, 4489  $\pm$  54 Ma, 2658  $\pm$  19 Ma, 2473  $\pm$  21 Ma and 1494  $\pm$  32 Ma. All of the grains in the Mesoproterozoic peak have Th/U ratio < 0.07, and typically metamorphic zircon morphology, indicating that this peak represents metamorphic zircon growth (Corfu et al., 2003; Rubatto, 2002).

Sample T04-39 yielded abundant prismatic zircon grains, rarely fractured, with preserved pyramidal terminations. Aspect ratios range from 2:1 to 5:1. CL imaging illustrates well developed oscillatory growth zoning in most grains while the remainder have sector zoning. There is no

evidence of metamorphic rims or overgrowths. Results from U-Pb analysis of 100 spots on 97 grains are presented in table 3.2 and figure 3.6 (e & f). When only > 90 % concordant data is considered a large peak is seen in the  $^{207}\text{Pb}/^{206}\text{Pb}$  age spectra at 1975  $\pm$  9 Ma (46 grains, MSWD = 8.5) with smaller peaks at 2059  $\pm$  8 Ma (17 grains, MSWD = 3.0), 2334  $\pm$  12 Ma (2 grains, MSWD = 0.38), 2436  $\pm$  22 Ma (8 grains, MSWD = 8.4), 2538  $\pm$  39 Ma (2 grains, MSWD = 4.3), 2631  $\pm$  29 Ma (4 grains, MSWD = 2.6) and 2691  $\pm$  17 (7 grains, MSWD = 3.3) and individual grains aged 2791  $\pm$  27 and 3368  $\pm$  31 Ma. Six of these analyses were from three sector zoned zircons, with one spot in each zone (zircon 10-11, 16-17 and 40-41). The results from within each grain were within error of each other. Ratios of U/Th in all grains combined with their shape and zoning characteristics, were indicative of igneous crystallisation (Corfu et al., 2003; Rubatto, 2002).

### 3.5.2 $^{40}\text{Ar}/^{39}\text{Ar}$ results

Five samples underwent  $^{40}\text{Ar}/^{39}\text{Ar}$  analysis, results of which are summarised in table 3.3, detailed in Appendix 2.2 and plotted in respect to cumulative  $^{39}\text{Ar}\%$  in figure 3.7. For each sample age (calculated from  $^{40}\text{Ar}/^{39}\text{Ar}$ ) and K/Ca ratios are plotted. Changes in K/Ca ratios are indicative of alteration of the sample, although high K/Ca ratios are often found in the first few steps as fine-grained K-rich phyllosilicate inclusions are ablated (McDougall and Harrison, 1999). Each step-heating profile represents the analysis of a package of 10 hornblende grains.

Hornblende from sample T04-05 yields a straight relatively flat  $^{40}\text{Ar}/^{39}\text{Ar}$  age spectrum (figure 3.7 e) in which 72% of gas released defines a plateau age of 1035  $\pm$  9 Ma (MSWD = 1.7, p = 0.063). Sample T04-33

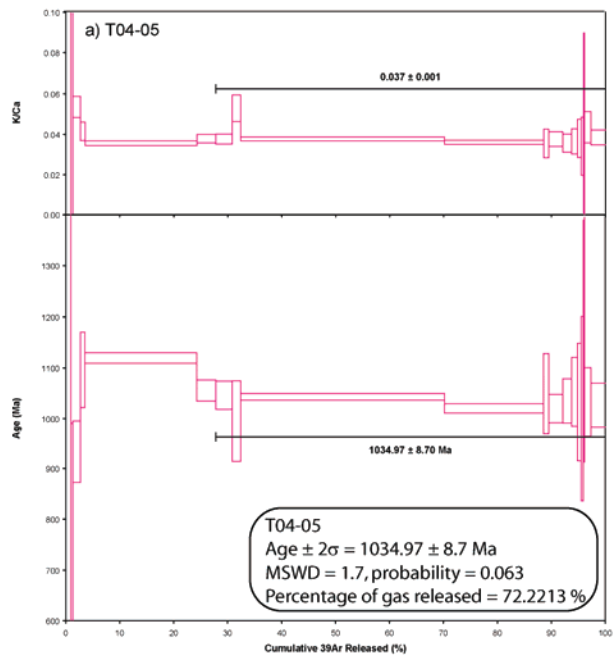
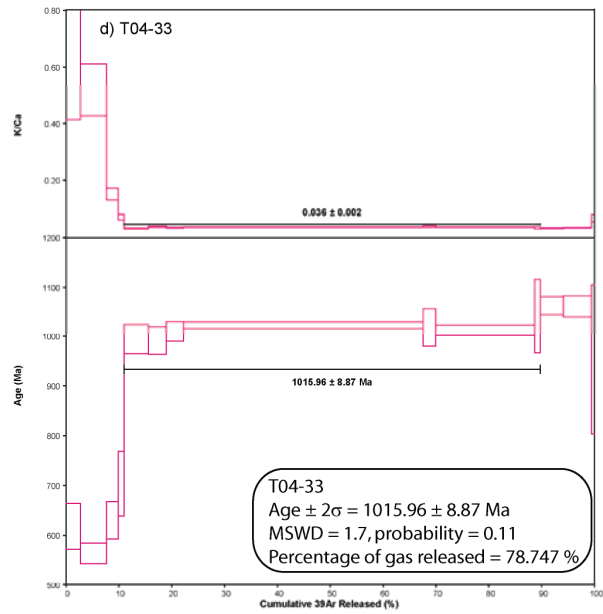
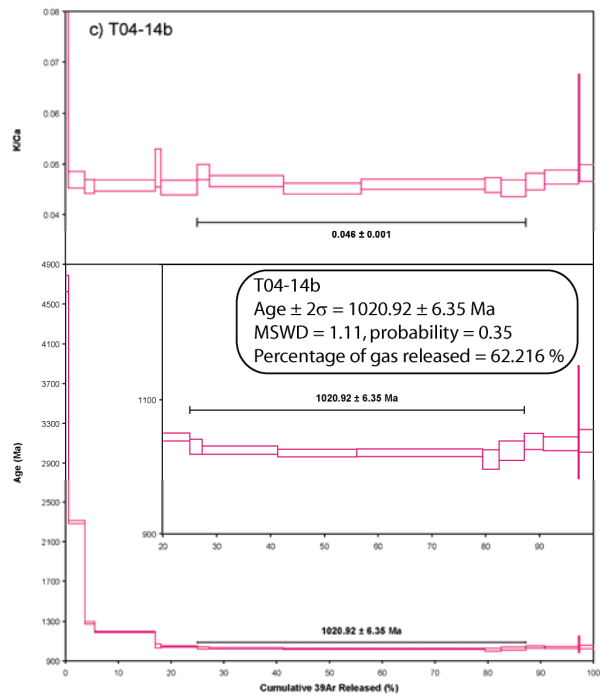
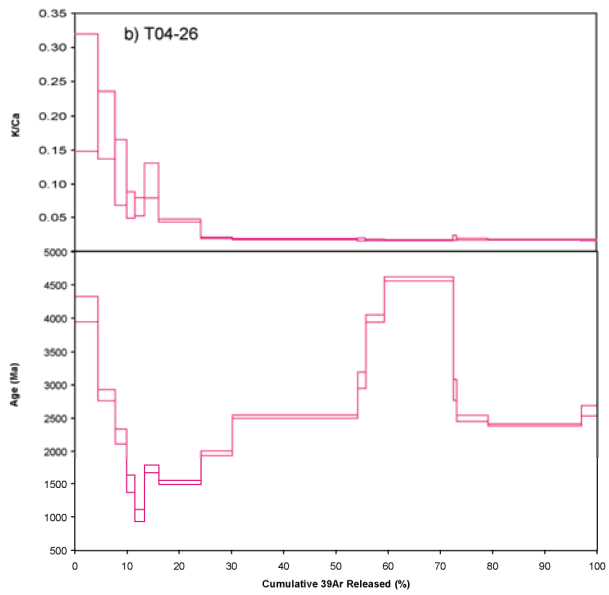
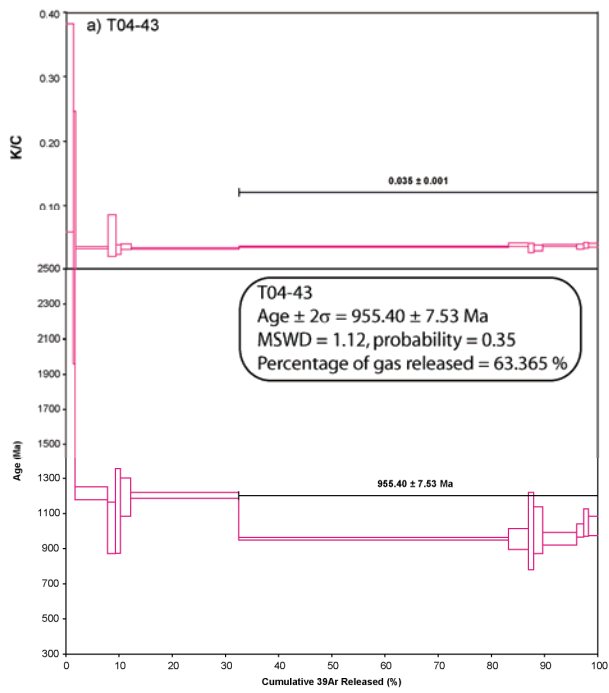


Figure 3.7. Ar laser step-heating profiles for each sample. (a) Z-43 (b) Z-26 (c) Z-14b (d) Z-33 (e) Z-05. Inverse isochrons for each sample presented on next page.

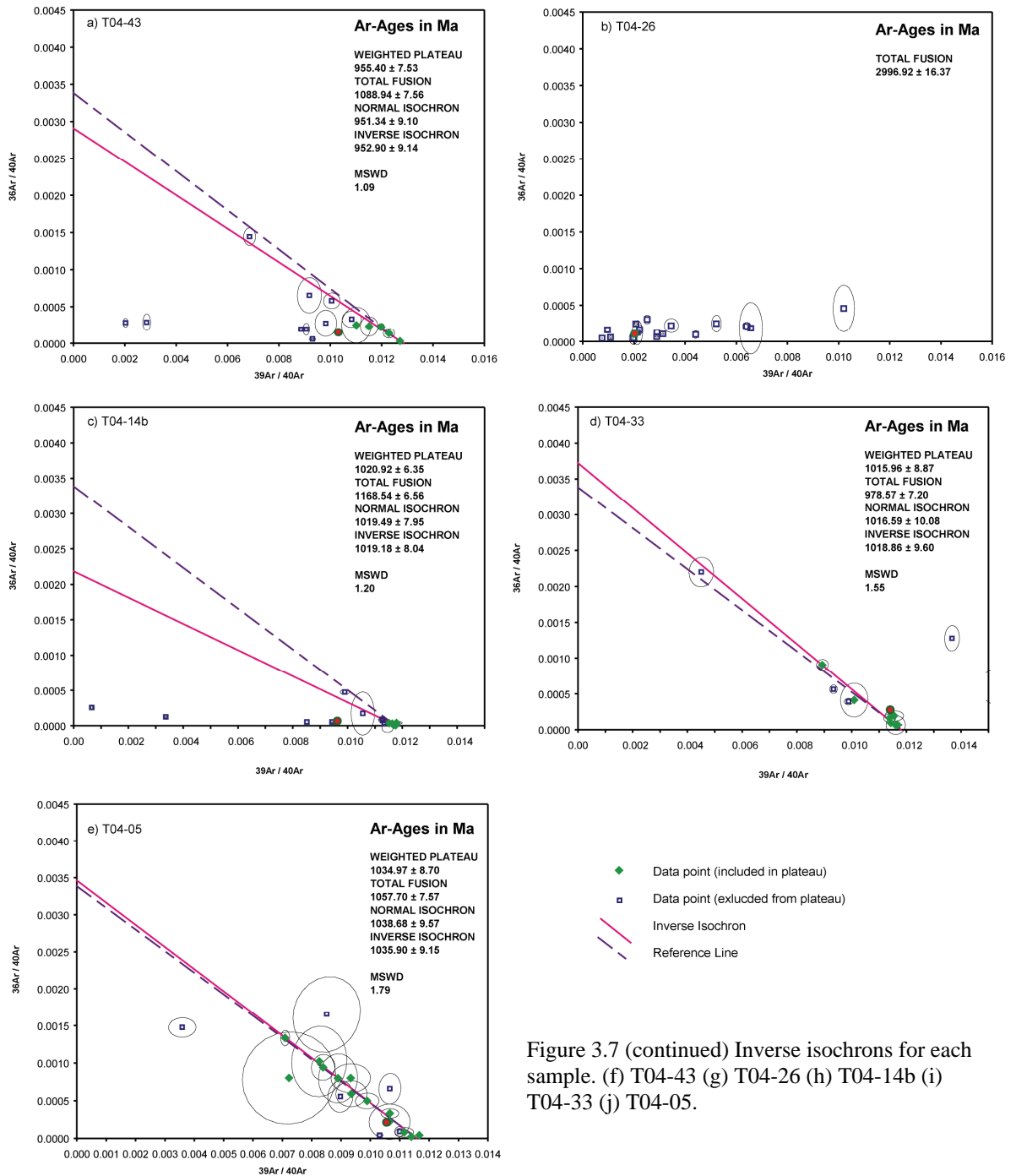


Figure 3.7 (continued) Inverse isochrons for each sample. (f) T04-43 (g) T04-26 (h) T04-14b (i) T04-33 (j) T04-05.

displays a different  $^{40}\text{Ar}/^{39}\text{Ar}$  age spectrum (figure 3.7 d) with the first 4 steps yielding Neoproterozoic ages (~650 Ma) then the next 7 steps defining a plateau age of  $1019 \pm 9$  Ma (MSWD = 1.7,  $p = 0.11$ , 78% data). The last the heating steps yielded marginally older ages. This step heating pattern may indicate mixing of two  $^{40}\text{Ar}/^{39}\text{Ar}$  domains with initial gas released from a younger, less retentive domain formed at during the Neoproterozoic, then subsequent release of gas from a more retentive domain formed during the Mesoproterozoic (Forster & Lister, 2004).

Sample T04-14b yielded an  $^{40}\text{Ar}/^{39}\text{Ar}$  age spectrum (figure 3.7 c) with ages generally decreasing as more gas was released, and a mini-plateau defined by 62.2 % of gas at age  $1023 \pm 7$  Ma. Sample T04-43 yielded an  $^{40}\text{Ar}/^{39}\text{Ar}$  age spectrum steps mostly decrease in age (figure 6a). The first two heating steps yielded Archaean

ages (~2.8 Ga), the next 5 steps yielded ~1.2 Ga ages, then 63.3 % of the data yielded a mini-plateau age of  $960 \pm 9$  Ma (MSWD = 1.2). The pattern of gas release in both these samples suggests initial gas release from an older, more retentive domain, followed by release from the Mesoproterozoic domain with some minor mixing between the domains.

Sample T04-26, an actinolite-eclogite, yields a more complex  $^{40}\text{Ar}/^{39}\text{Ar}$  age spectrum (figure 3.7b) Despite a relatively flat plateau in the K/Ca the sample failed to yield a plateau age. Three non-consecutive steps, representing 42.8 % of released gas, yielded ages close to 2.43 Ga, however this age has no statistical validity and does not correlate to any known magmatic, tectonic or thermal events in the region. Plotting the data on an inverse isochron does not illustrate any systematic shift in Ar values, suggesting that this age spectra may represent

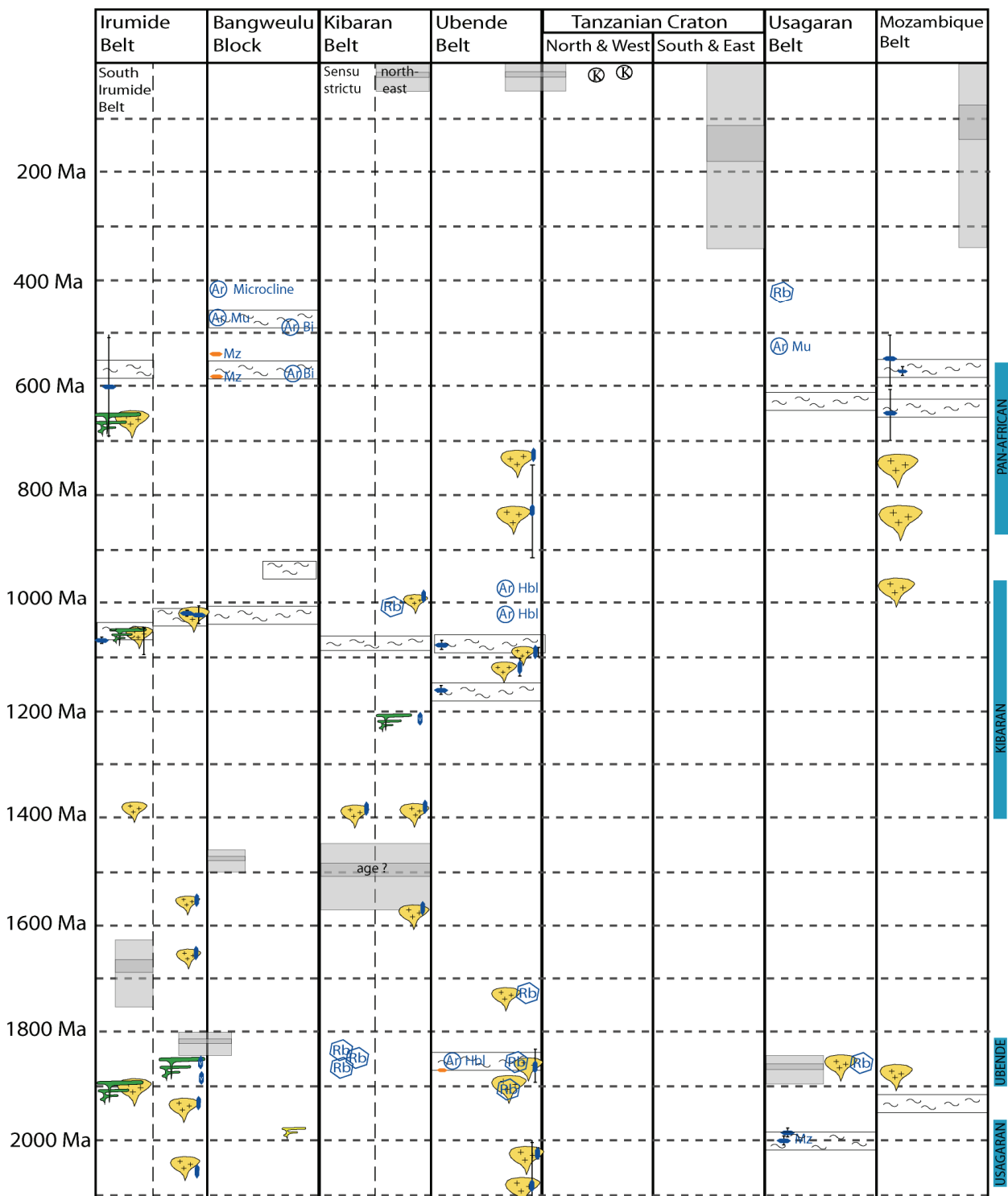


Figure 3.8. Time space plot for the Tanzanian Craton, the Ubende, Kibaran, Irumide and Usagaran Orogenic Belts, and the Bangweulu Block. Data from (Borg and Krogh, 1999; Boven et al., 1999; Brewer et al., 1979; Buchwaldt et al., 2007; Cahen et al., 1984; Collins et al., 2004a; DeWaele, 2005; DeWaele and Fitzsimons Ian, 2004; DeWaele and Fitzsimons, 2007; DeWaele et al., 2008; DeWaele et al., 2006b; DeWaele et al., 2003; Johnson and Oliver, 2004; Johnson et al., 2005; Kabengele et al., 1990; Kokonyangi et al., 2005; Lenoir et al., 1994a; Many and Maboko, 2003; Oliver et al., 1998; Rainaud et al., 2005; Reddy et al., 2004c; Reddy et al., 2003; Ring et al., 1999; Schandelmeyer, 1983; Tack et al., 1990; Tack et al., 2002; Tack et al., 1994; Wirth et al., 2004a)

mixing of two or more Ar reservoirs with differing retentive properties (Forster and Lister, 2004). The minimum age obtained from the sample was ~1020 Ma, matching the age obtained for all other samples T04-05, T04-14b and T04-33, but not sample T04-43 which is also from the Ikulu.

### 3.6. Discussion

#### 3.6.1 Provenance of Ubende sediments

Zircon age data is presented as comparative probability density plots in figure 3.6. Age population peaks occur at 1070 Ma, 1950 Ma, 1985 Ma, 2020 Ma, 2070 Ma, 2420 Ma, 2625 Ma and 2680 Ma, with all but the 1070 Ma and 2680 Ma peaks occurring in both the felsic gneiss and

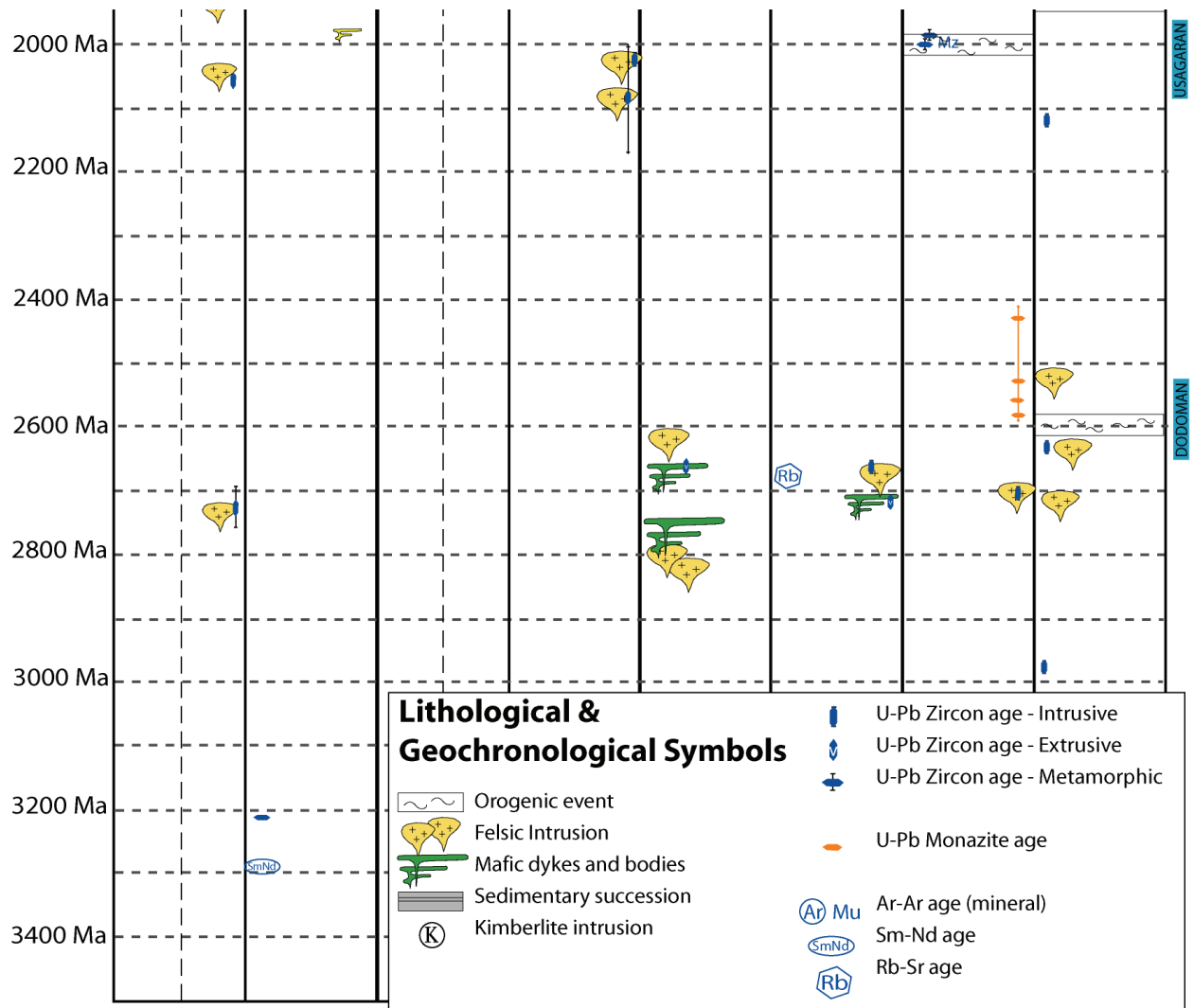


Figure 3.8 (continued)

metapelite samples. The 1070 peak is comprised of zircon considered, based on grain morphology and Th/U ratios to be of metamorphic origin, and hence can be disregarded in discussion of sediment provenance. Any source region would need to contain the same age peaks to be considered viable.

For this study the most obvious source regions to consider are the adjacent Tanzanian Craton for Archaean zircons and both the Bangweulu Block and the Ubende Orogen itself for Palaeoproterozoic grains. Published geochronological data for these terranes is summarised in figure 3.8. Given the lack of direct geochronology data for the Bangweulu block it will be excluded from this discussion. The Tanzanian Craton experienced rock forming events at ~2680 Ma and 2625 Ma; however even when the published data is supplemented by the Tanzanian Craton stream sediment geochronology data presented in chapter two of this thesis (figure 2.4) there is no indication of a source for the 2420 Ma zircons seen in the Ubende samples. It should be noted that some Neoproterozoic igneous rock units have been mapped within the Ubende Orogen (ref for map), however these rocks have not been dated so their age is in doubt. Significant Palaeoproterozoic igneous rocks have been identified in the Ubende Orogen (figure 3.8); the dated rocks include granite intrusion in the south of the belt which broadly account for the 1950 Ma, 1985 Ma, 2020

Ma and 2070 Ma peaks seen in the age spectra (Lenoir et al., 1994; Ring et al., 1997). This leaves the 2420 Ma peak seen in samples T04-39 and T04-07 unaccounted for in surrounding cratons and orogenic belts, a peak occurring during what Condie et al. (2009c) describes a widespread magmatic shutdown globally between ~2.25 and 2.45 Ga, and a time at which no magmatism has been identified on the Tanzanian Craton, Ubende Orogen, or any surrounding orogens.

When looking outside the modern surrounds of the Ubende Orogen for a sediment source for these sediments it is necessary to consider possible sediment sources from around the globe as both the timing of sedimentation and the relative position of the Ubende at the time are poorly constrained. Global data on granitoid events from the Archaean to Mesoproterozoic is presented in figure 3.9 (Condie et al., 2009a), with the ages identified in the studied highlighted in green. There are granitoid events on a number of cratons which match some of these age peaks, including the Hearne, Wyoming, Slave, Superior and Kaapvaal cratons for the Archaean peaks, the Karelia and West Africa cratons for the early Palaeoproterozoic peak, and Laurentia and the São Francisco cratons for the mid Palaeoproterozoic peaks. Based on this data source which best accounts for all of these peaks is the Hearne craton on the modern north-western margin of Laurentia, however

Dated unit	Rb/Sr	U/Pb	Source
Mbozi Syenite	743 ± 30 Ma		Brock, 1963
Kapalugulu	1239 ± 50		Cahen and Snelling, 1966
Nyika granite	1930 ± 30 Ma		Dodson et al., 1975
Songwe syenite	685 ± 62 Ma		Ray, 1974
Kate Granite		1838 ± 86 Ma	Schandelmeier, 1983
	1725 ± 48 Ma		Lenoir et al. 1994
	1723 ± 41 Ma		Lenoir et al. 1994
Mpanda gneiss	1902 ± 73 Ma		Lenoir et al. 1994
Mpanda granite	1847 ± 37 Ma		Lenoir et al. 1994
Mbarali granite		2026 ± 8 Ma	Lenoir et al. 1994
Ukenju gneiss		2084 ± 86 Ma	Lenoir et al. 1994
Kalunduru granite		724 ± 6 Ma	Lenoir et al. 1994
Ufipa granite		1864 ± 32 Ma	Lenoir et al. 1994
Kwamanga granite		842 ± 80 Ma	Lenoir et al. 1994

**Table 3.5 Summary of published geochronological data from the Ubende orogenic belt**

palaeomagnetic data suggests that these cratons were separated by a large longitudinal gap between 1100-1050 Ma (D'Agrella-Filho et al., 2004).

### 3.6.2 Timing of sedimentation, metamorphism and exhumation

Conventional models for the formation of the Ubende Orogen would indicate that Ubendian sedimentary rocks underwent metamorphism during the Palaeoproterozoic. Based on zircon U-Pb data in this study the maximum depositional age for sample T04-39, calculated based on the youngest population of igneous zircons, is 1975 ± 9 Ma (youngest grain 1905 ± 20 Ma). This age does not contradict the Palaeoproterozoic metamorphism model, however both metapelitic samples from the Wakole terrane contained younger concordant grains. There are two ~1.5 Ga grains in these samples (1525 ± 34 Ma and 1494 ± 32 Ma), suggesting that metamorphism occurred after ~1.5 Ga. This age, however, is indicated by only one grain in each sample. Sample T04-07 has a significant Palaeoproterozoic population aged 1947 ± 24 Ma (youngest grain aged 1885 ± 23) which provides a more robust maximum depositional age, and is consistent with sample T04-39. Sample T04-12b has only two grains of this age, the youngest of which, at 1973 ± 100 Ma, provides an only slightly more robust maximum depositional age which is in accordance with the other two samples.

Metamorphic zircon, identified mainly in the metapelitic sample T04-12b, indicates metamorphism at above ~700° at 1068 ± 11 Ma. The temperature at which hornblende becomes closed to Ar diffusion is accepted to be 500 – 550 °C, thus the results of this study indicate that these samples cooled to this temperature at 1026 ± 15 Ma, with cooling at slightly different times in different blocks. Cooling of rock systems is usually related either to the end of a magmatic thermal event (ie. nearby granite intrusion) or exhumation of the terrane from below 25 km (assuming a geothermal gradient of 20°C/km). This raises two questions about these results: is the cooling related to a thermal event or to exhumation; and what is the significance of the 66 Myr younger cooling age obtained from sample T04-43.

No Mesoproterozoic ages have been proposed for any

large igneous bodies within the Ubende Orogen. The Kwamanga and Kalundru granites, about 300 km southwest of the study area, have been dated at 842 ± 80 Ma and 724 ± 6 Ma respectively (U/Pb zircon: (Lenoir et al., 1994a). A few older rocks have been identified in the north eastern Kibaran Orogen of Burundi and north western Tanzania, with one granite dated at 1137 ± 39 Ma (Rb-Sr whole rock: (Tack et al., 1990) and A-type granitoid intrusion at 1275 ± 11 Ma and 1249 ± 8 Ma (U-Pb zircon: (Tack et al., 1994)). In the north-eastern Irumide Orogen several granites and granite gneisses have been dated at between 942 ± 9 Ma and 1015 ± 14 Ma (DeWaele et al., 2009) providing the best age fit to this data. None of these rocks is in close proximity to the study area, however one granite body (~5 km exposed) of unknown age (presumed Archaean) has been mapped in the vicinity of the study area about 15km south of sample T04-43. If this, or some other granite, were intruded in the Mesoproterozoic it could have involved a thermal event. This would also account for the differences in cooling age of each sample with the younger ages closer to the granite body. However no granite of this age has been identified in the region.

There is no direct indication of metamorphism at ~1850 Ma seen in either the U-Pb zircon or <sup>40</sup>Ar/<sup>39</sup>Ar hornblende data, only the robust maximum sediment deposition age of 1900 Ma supports this metamorphic age. The presence of two ~ 1.5 Ga zircons in the metapelitic samples could be used to argue that sedimentation post-dated this 1.85 Ga metamorphism, though more data would be needed to confirm this.

Between 1.5 – 0.95 Ga the Kibaran and Irumide Orogens experienced a series of compressional events, associated with the assembly of Rodinia whereby the already connected Tanzanian and Congo Cratons collided with the Kaapvaal and Kalahari Cratons along the modern southern margin of the Bangweulu Block (Cordani et al., 2003; Klerkx et al., 1987; Pohl, 1994) or perhaps relating to accretion of a series of island arcs (DeWaele et al., 2008). It has been suggested that this compressional phase (1.5-1.4 Ga) was followed by extensional collapse between 1.3 – 1.2 Ga (Buchwaldt et al., 2007; Klerkx et al., 1987; Pohl, 1994; Tack et al., 1994) followed in the Kibaran by a post-orogenic



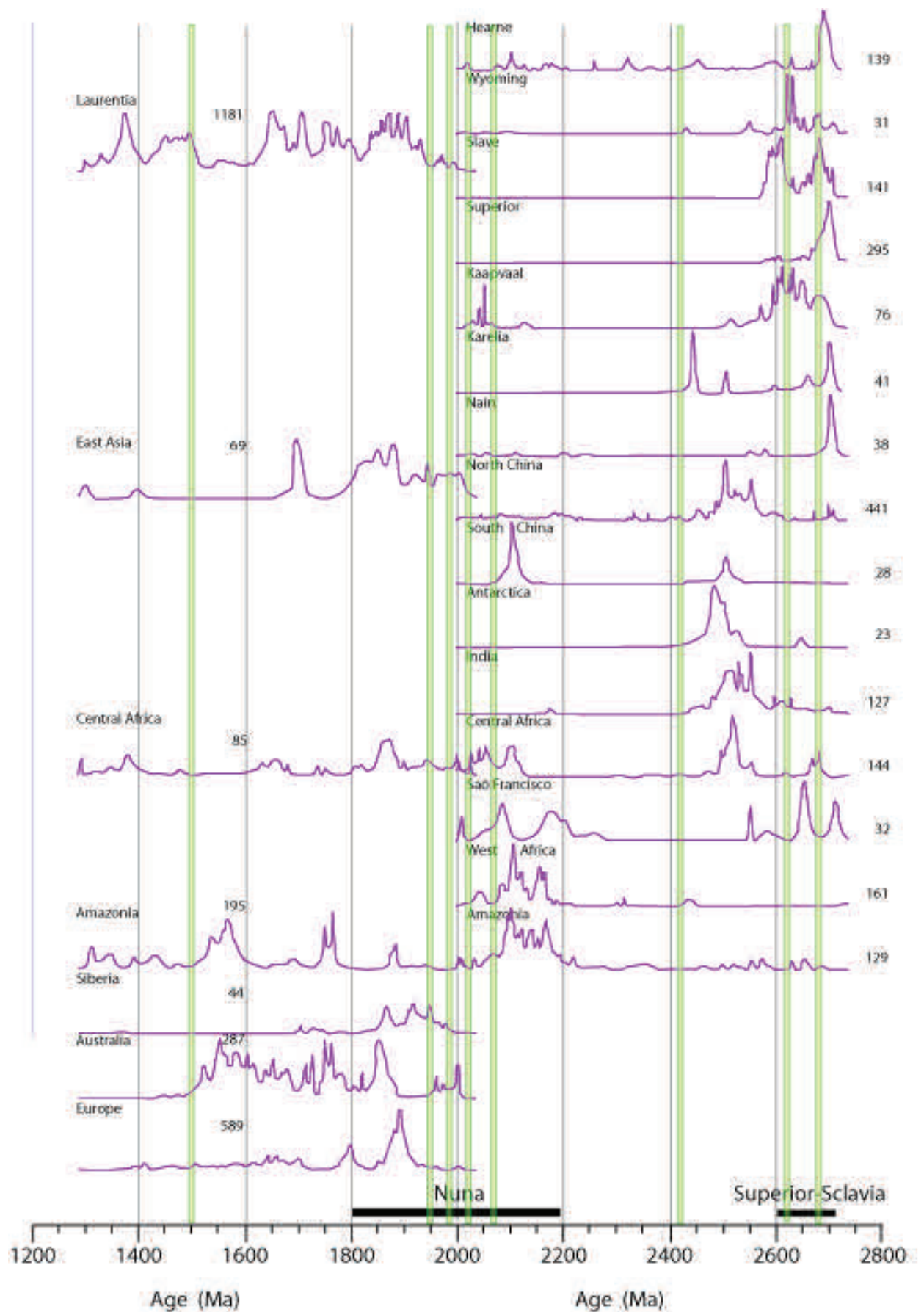


Figure 3.9. Global detrital zircon record for discussed cratonic blocks (source - Condie et al., 2009a). Green lines represent peaks in the detrital zircon age spectra from this study. Numbers indicate the number of zircon analyses represented in each region.

magmatic activity (1.1–0.9 Ga) attributed crustal to reworking along conjugate margins (DeWaele et al., 2006b; Klerkx et al., 1987); recent extensive U-Pb dating of extensive granites in the Irumide Orogen shows widespread emplacement of both deformed and undeformed granites between  $1053 \pm 14$  and  $942 \pm 9$  Ma (DeWaele et al., 2009) consistent with the timing of peak metamorphism in that terrane at  $1020 \pm 20$  Ma during compressional orogenesis (DeWaele, 2005). Many SW-NE oriented structures in the Kibaran and Irumide Orogens accommodated compression as part of this event, and it is likely that the SE-NW trending structures in the Ubende Orogen also experienced compressional movement leading to exhumation of some blocks.

The samples in this study come from three tectonic blocks, the Wakole, Ubende and Ikulu blocks. There is an ~80 My difference between the  $^{40}\text{Ar}/^{39}\text{Ar}$  age from the Ubende Block and those from the blocks on either side. This age difference could relate to proximity to an as yet unidentified heat source such as a granite intrusion, or could be related to exhumation of the Ubende block either from greater depth or later in the compressional event.

### **3.6.3 Significance of Hadean aged zircons**

Three concordant zircons of Hadean are reported from

the metapelitic rocks in this study. One grain, aged  $4210 \pm 119$  Ma, is of a similar age to those from Jack Hills, Western Australia (Amelin et al., 2000; Nemchin et al., 2006; Wilde et al., 2001). Globally, the oldest reported zircon age,  $4,404 \pm 8$  Ma, is also from the Jack Hills metasediments (Wilde et al., 2001). Two of the ages obtained in this study are older than this, however they were obtained using less precise dating methods than the U-Pb SHRIMP dating used on the Jack Hills zircons. Because the LA-ICPMS method is quite destructive of the sample it was not possible to repeat the analysis to more precisely resolve the age. It is also possible that the apparently concordant Hadean age was the result of mixing of different aged zones within grains. The presence of apparently Hadean aged zircon does suggest the presence of early Archaean zircon in the source region for these sediments, and warrants further investigation.

### **3.7. Conclusions**

A new metamorphic age for the Ubende Orogen of ~1070 Ma is preserved in zircon within metasedimentary rocks, with cooling below ~500 °C occurring at ~1020 Ma. Although the Ubende Orogen is currently considered to be a Palaeoproterozoic suture between the Tanzanian Craton and an unidentified Archaean (~3.3 Ga) basement



Spot No. Core / Rim	Isotope Ratios						Ages (Ma)				Conc (%)		
	<sup>207</sup> Pb/ <sup>206</sup> Pb	1σ	<sup>207</sup> Pb/ <sup>235</sup> U	1σ	<sup>206</sup> Pb/ <sup>238</sup> U	1σ	<sup>207</sup> Pb/ <sup>206</sup> Pb	1σ	<sup>207</sup> Pb/ <sup>235</sup> U	1σ		<sup>206</sup> Pb/ <sup>238</sup> U	1σ
Sample T04-07													
Z-07_01	0.12905	0.00355	0.36121	0.00645	6.42625	0.17135	2085.1	47.6	1987.9	30.6	2035.9	23.4	97.6
Z-07_02	0.12278	0.00283	0.2977	0.00475	5.03915	0.11425	1997.0	40.4	1679.9	23.6	1825.9	19.2	91.4
Z-07_03	0.13726	0.00193	0.18405	0.00242	3.48304	0.05247	2193.0	24.3	1089.1	13.2	1523.4	11.9	69.5
Z-07_04	0.12288	0.00276	0.32243	0.00509	5.4624	0.12102	1998.5	39.3	1801.6	24.8	1894.7	19.0	94.8
Z-07_05	0.11721	0.00192	0.33423	0.0046	5.40112	0.09206	1914.1	29.0	1858.8	22.2	1885.0	14.6	98.5
Z-07_06	0.48982	0.0414	0.86947	0.06618	58.7143	4.61647	4210.9	119.4	4033.2	228.2	4152.5	78.5	98.6
Z-07_07	0.11894	0.00247	0.32929	0.00499	5.39975	0.11277	1940.4	36.7	1834.9	24.2	1884.8	17.9	97.1
Z-07_08	0.09485	0.00175	0.25183	0.00353	3.29282	0.0626	1525.0	34.5	1447.9	18.2	1479.4	14.8	97.0
Z-07_09	0.12039	0.00135	0.33273	0.00416	5.52246	0.07246	1962.0	19.9	1851.6	20.1	1904.1	11.3	97.0
Z-07_10	0.1174	0.00151	0.33222	0.00428	5.37679	0.07708	1917.0	22.9	1849.1	20.7	1881.2	12.3	98.1
Z-07_11	0.12084	0.00182	0.17469	0.00233	2.91021	0.04646	1968.7	26.6	1037.9	12.8	1384.6	12.1	70.3
Z-07_12	0.12507	0.00159	0.35735	0.00461	6.16156	0.08762	2029.8	22.4	1969.6	21.9	1999.0	12.4	98.5
Z-07_13	0.13825	0.00321	0.31339	0.00515	5.97301	0.136	2205.4	39.8	1757.4	25.3	1971.9	19.8	89.4
Z-07_14	0.12025	0.00152	0.342	0.00439	5.66982	0.08029	1960.0	22.4	1896.3	21.1	1926.8	12.2	98.3
Z-07_15	0.12169	0.00139	0.31761	0.00399	5.3285	0.07047	1981.1	20.3	1778.1	19.5	1873.4	11.3	94.6
Z-07_16	0.17939	0.00202	0.4536	0.00573	11.2128	0.14637	2647.2	18.5	2411.3	25.4	2541.0	12.2	96.0
Z-07_17	0.11531	0.00147	0.33372	0.0043	5.30345	0.07552	1884.8	22.8	1856.4	20.8	1869.4	12.2	99.2
Z-07_18	0.1663	0.00219	0.48074	0.0064	11.0185	0.16041	2520.7	22.0	2530.5	27.9	2524.7	13.6	100.2
Z-07_19	0.12656	0.00145	0.15469	0.00196	2.69869	0.03582	2050.7	20.1	927.2	10.9	1328.1	9.8	64.8
Z-07_20	0.1733	0.00187	0.48357	0.00611	11.5523	0.14833	2589.8	17.9	2542.8	26.6	2568.8	12.0	99.2
Z-07_21	0.07738	0.00107	0.1827	0.00237	1.94904	0.02972	1131.0	27.3	1081.7	12.9	1098.1	10.2	97.1
Z-07_22	0.14528	0.00179	0.41835	0.00547	8.37958	0.1172	2291.1	21.0	2253.0	24.9	2273.0	12.7	99.2
Z-07_23	0.12576	0.00188	0.3076	0.00421	5.33348	0.08534	2039.5	26.1	1728.9	20.8	1874.2	13.7	91.9
Z-07_24	0.15425	0.00312	0.37286	0.00593	7.93034	0.16066	2393.6	34.0	2042.8	27.8	2223.1	18.3	92.9
Z-07_25	0.15617	0.00207	0.44306	0.006	9.54077	0.14091	2414.6	22.4	2364.3	26.8	2391.5	13.6	99.0
Z-07_26	0.15727	0.00215	0.47132	0.00654	10.2213	0.15487	2426.6	23.0	2489.3	28.7	2455.0	14.0	101.2
Z-07_27	0.13374	0.00184	0.29043	0.00399	5.3555	0.0816	2147.6	23.9	1643.7	20.0	1877.8	13.0	87.4
Z-07_27	0.17681	0.00256	0.47876	0.00686	11.6723	0.18415	2623.2	23.9	2521.9	29.9	2578.5	14.8	98.3
Z-07_28	0.11963	0.00129	0.38216	0.00498	6.30344	0.08258	1950.8	19.1	2086.4	23.3	2018.9	11.5	103.5
Z-07_29	0.17785	0.00208	0.50059	0.00675	12.2741	0.16916	2632.9	19.3	2616.3	29.0	2625.6	12.9	99.7
Z-07_30	0.12978	0.00179	0.38329	0.00532	6.85742	0.1053	2095.0	24.0	2091.7	24.8	2093.2	13.6	99.9
Z-07_31	0.12616	0.00192	0.38758	0.00555	6.74033	0.11116	2045.2	26.6	2111.6	25.8	2077.9	14.6	101.6
Z-07_32	0.13886	0.0023	0.12364	0.0018	2.36641	0.04092	2213.0	28.4	751.5	10.4	1232.5	12.3	55.7
Sample T04-12b													
Z-12b_1	0.07519	0.0009	0.18245	0.00212	1.891	0.0244	1073.6	23.9	1080.4	11.6	1078.1	8.6	100.
Z-12b_10	0.36277	0.02034	0.21135	0.00855	10.56	0.48808	3761.5	82.6	1236.0	45.5	2486.0	42.8	66.1
Z-12b_11	0.07491	0.0009	0.17627	0.00213	1.820	0.02412	1066.1	23.9	1046.6	11.7	1052.8	8.7	98.8
Z-12b_12	0.0748	0.00105	0.16074	0.002	1.657	0.02479	1063.0	28.0	960.9	11.1	992.4	9.5	93.4
Z-12b_13	0.11856	0.00137	0.3132	0.00381	5.119	0.06607	1934.7	20.5	1756.4	18.7	1839.3	11.0	95.1
Z-12b_14	0.07456	0.00086	0.173	0.00209	1.778	0.02308	1056.3	23.3	1028.6	11.5	1037.5	8.4	98.2
Z-12b_15	0.10198	0.0046	0.17321	0.00388	2.435	0.10353	1660.5	81.3	1029.8	21.3	1253.0	30.6	75.5
Z-12b_17	0.07485	0.00083	0.18215	0.0022	1.879	0.02395	1064.4	22.3	1078.7	12.0	1073.9	8.5	100.
Z-12b_18 c	0.12117	0.00139	0.32436	0.00398	5.418	0.07049	1973.5	20.4	1811.0	19.4	1887.7	11.2	95.7
Z-12b_19 r	0.12409	0.00151	0.31813	0.00396	5.442	0.07363	2015.9	21.4	1780.6	19.4	1891.6	11.6	93.8
Z-12b_2	0.07402	0.00094	0.16519	0.00194	1.685	0.0227	1041.9	25.3	985.6	10.8	1003.1	8.6	96.3
Z-12b_20	0.07506	0.00086	0.175	0.00213	1.811	0.02357	1070.2	22.7	1039.6	11.7	1049.4	8.5	98.1
Z-12b_21	0.07518	0.00097	0.17887	0.00226	1.854	0.02667	1073.4	25.6	1060.8	12.4	1065.1	9.5	99.2
Z-12b_22 c	0.4144	0.00958	0.38879	0.00781	22.21	0.47191	3962.2	34.2	2117.2	36.3	3193.3	20.6	80.6
Z-12b_23 r	0.14892	0.01604	0.11331	0.00603	2.326	0.22582	2333.6	173.6	691.9	34.9	1220.5	68.9	52.3
Z-12b_24	0.07567	0.00087	0.17837	0.00222	1.861	0.0248	1086.4	22.9	1058.1	12.2	1067.4	8.8	98.3
Z-12b_25	0.07614	0.00097	0.17728	0.00224	1.861	0.02657	1098.7	25.3	1052.1	12.3	1067.4	9.4	97.2
Z-12b_26	0.07657	0.00103	0.17816	0.00227	1.880	0.02783	1109.9	26.6	1056.9	12.4	1074.3	9.8	96.8
Z-12b_27	0.11962	0.01237	0.10777	0.00519	1.777	0.16791	1950.5	174.1	659.8	30.2	1037.2	61.4	53.2
Z-12b_28	0.07524	0.00094	0.17363	0.00219	1.801	0.0255	1074.9	24.8	1032.1	12.1	1045.9	9.2	97.3
Z-12b_29	0.07449	0.00085	0.17761	0.00222	1.824	0.02441	1054.5	23.2	1053.9	12.2	1054.1	8.8	100.
Z-12b_3	0.07407	0.00081	0.16816	0.00194	1.717	0.02077	1043.5	21.9	1002.0	10.7	1015.0	7.8	97.3
Z-12b_30	0.14847	0.00223	0.17619	0.00239	3.606	0.05731	2328.3	25.5	1046.1	13.1	1551.0	12.6	66.6
Z-12b_31	0.07583	0.00107	0.18093	0.00233	1.891	0.02923	1090.7	28.0	1072.1	12.7	1078.2	10.3	98.9
Z-12b_32	0.0701	0.00247	0.15726	0.00276	1.519	0.0521	931.3	70.8	941.5	15.4	938.4	21.0	100.
Z-12b_33	0.14405	0.01089	0.14397	0.00555	2.859	0.19621	2276.5	124.8	867.1	31.3	1371.2	51.6	60.2
Z-12b_35	0.09334	0.00161	0.24816	0.00341	3.193	0.05754	1494.7	32.3	1429.0	17.6	1455.5	13.9	97.4
Z-12b_5 r	0.16171	0.002	0.40123	0.00492	8.944	0.11823	2473.6	20.7	2174.7	22.6	2332.4	12.1	94.3
Z-12b_6	0.625	0.0191	0.81196	0.02475	69.95	2.01146	4567.2	43.6	3831.8	88.0	4327.7	28.8	94.8
Z-12b_7	0.59224	0.02246	0.90695	0.03434	74.04	2.6812	4489.1	54.1	4161.2	116.1	4384.5	36.3	97.7
Z-12b_8	0.0736	0.00095	0.17707	0.00213	1.796	0.02496	1030.6	25.7	1050.9	11.7	1044.2	9.1	101.
Z-12b_9	0.22657	0.01197	0.20908	0.00693	6.530	0.30283	3027.9	82.3	1223.9	37.0	2050.0	40.8	67.7

Table 3.2 LA-ICPMS U-Pb geochronological data obtained at Adelaide Microscopy.  
<sup>1</sup>Concordance = <sup>206</sup>Pb/<sup>238</sup>U / <sup>207</sup>Pb/<sup>206</sup>Pb

Spot No.	Isotope Ratios						Ages (Ma)						Conc <sup>(1)</sup> %
	<sup>207</sup> Pb/ <sup>206</sup> Pb	1σ	<sup>207</sup> Pb/ <sup>235</sup> U	1σ	<sup>206</sup> Pb/ <sup>238</sup> U	1σ	<sup>207</sup> Pb/ <sup>206</sup> Pb	1σ	<sup>207</sup> Pb/ <sup>235</sup> U	1σ	<sup>206</sup> Pb/ <sup>238</sup> U	1σ	
Sample Z-39-													
Z-39-1	0.12259	0.00134	0.36004	0.00432	6.08454	0.07555	1994.3	19.3	1982.3	20.5	1988	10.8	99.7
Z-39-2	0.30477	0.00311	0.68631	0.00817	28.8355	0.34098	3494.7	15.7	3368.5	31.2	3447.9	11.6	98.7
Z-39-3	0.11942	0.00135	0.35018	0.00422	5.76505	0.07312	1947.6	20.1	1935.5	20.2	1941.2	11.0	99.7
Z-39-4	0.18685	0.00206	0.51737	0.00627	13.3263	0.16541	2714.6	18.0	2688	26.6	2703.1	11.7	99.6
Z-39-5	0.1255	0.00143	0.39679	0.0048	6.86494	0.08744	2035.9	20.1	2154.3	22.1	2094.1	11.3	102.9
Z-39-6	0.12787	0.00146	0.38094	0.00461	6.71509	0.0856	2068.9	20.0	2080.7	21.5	2074.6	11.3	100.3
Z-39-7	0.12194	0.00135	0.36381	0.00436	6.11611	0.07621	1984.8	19.6	2000.2	20.6	1992.5	10.9	100.4
Z-39-8	0.14865	0.00152	0.40328	0.00475	8.26413	0.09764	2330.4	17.5	2184.1	21.8	2260.4	10.7	97.0
Z-39-9	0.12691	0.00131	0.20133	0.00237	3.52236	0.04172	2055.6	18.1	1182.4	12.7	1532.2	9.4	74.5
Z-39-10	0.1217	0.00137	0.3625	0.00435	6.08178	0.07655	1981.2	20.0	1994	20.6	1987.6	11.0	100.3
Z-39-11	0.11955	0.00157	0.33679	0.00417	5.55089	0.07764	1949.5	23.3	1871.2	20.1	1908.5	12.0	97.9
Z-39-12	0.20475	0.00224	0.54202	0.00651	15.3000	0.18728	2864.4	17.7	2791.9	27.2	2834.1	11.7	98.9
Z-39-13	0.12173	0.00148	0.36292	0.00441	6.09082	0.08052	1981.7	21.5	1996	20.9	1988.9	11.5	100.4
Z-39-14	0.12061	0.00125	0.32963	0.00386	5.48113	0.06476	1965.2	18.4	1836.6	18.7	1897.6	10.2	96.6
Z-39-15	0.1262	0.00133	0.36099	0.00423	6.28112	0.07476	2045.7	18.4	1986.9	20.1	2015.8	10.4	98.5
Z-39-16	0.16099	0.00177	0.4622	0.00551	10.2589	0.12605	2466.1	18.5	2449.3	24.3	2458.4	11.4	99.7
Z-39-17	0.15964	0.00169	0.50067	0.0059	11.0195	0.13151	2451.8	17.8	2616.7	25.3	2524.8	11.1	103.0
Z-39-18	0.12518	0.00138	0.37155	0.00439	6.4127	0.07862	2031.4	19.3	2036.7	20.7	2034	10.8	100.1
Z-39-19	0.16584	0.00166	0.40572	0.0047	9.27696	0.10675	2516.1	16.8	2195.3	21.6	2365.7	10.6	94.0
Z-39-20	0.12306	0.00125	0.28896	0.00335	4.90301	0.05686	2001.1	17.9	1636.3	16.8	1802.8	9.8	90.1
Z-39-21	0.15796	0.00162	0.36522	0.00426	7.95293	0.09293	2434	17.3	2006.9	20.1	2225.7	10.5	91.4
Z-39-22	0.1265	0.00148	0.37344	0.00449	6.512	0.08342	2049.8	20.6	2045.5	21.1	2047.5	11.3	99.9
Z-39-23	0.12945	0.00141	0.32241	0.00381	5.75334	0.06997	2090.5	19.0	1801.5	18.6	1939.4	10.5	92.8
Z-39-24	0.11797	0.00131	0.33752	0.004	5.48913	0.06772	1925.8	19.8	1874.7	19.3	1898.9	10.6	98.6
Z-39-25	0.17642	0.00182	0.48012	0.00562	11.6764	0.13688	2619.5	17.1	2527.8	24.5	2578.8	11.0	98.4
Z-39-26	0.12164	0.00136	0.32737	0.00388	5.48939	0.06797	1980.4	19.8	1825.6	18.9	1898.9	10.6	95.9
Z-39-27	0.12778	0.00139	0.35587	0.0042	6.26827	0.0762	2067.6	19.0	1962.5	20.0	2014	10.7	97.4
Z-39-28	0.12399	0.00141	0.3593	0.00428	6.14127	0.07696	2014.4	20.0	1978.9	20.3	1996.1	10.9	99.1
Z-39-29	0.18556	0.00215	0.5219	0.00635	13.3496	0.16935	2703.2	19.0	2707.2	26.9	2704.7	12.0	100.1
Z-39-30	0.13773	0.00162	0.39506	0.00477	7.50035	0.09632	2198.8	20.3	2146.2	22.0	2173	11.5	98.8
Z-39-31	0.12126	0.00128	0.36568	0.00438	6.11399	0.07441	1974.9	18.7	2009.1	20.7	1992.2	10.6	100.9
Z-39-32	0.13335	0.00145	0.32524	0.00393	5.97963	0.07406	2142.5	18.8	1815.3	19.1	1972.9	10.8	92.1
Z-39-33	0.1642	0.00171	0.22987	0.00276	5.20395	0.06261	2499.4	17.4	1333.8	14.4	1853.3	10.3	74.1
Z-39-34	0.1229	0.00158	0.30681	0.00385	5.19902	0.07232	1998.8	22.6	1725	19.0	1852.5	11.9	92.7
Z-39-35	0.11659	0.00129	0.33268	0.00403	5.3476	0.06721	1904.5	19.7	1851.4	19.5	1876.5	10.8	98.5
Z-39-36	0.16843	0.00189	0.44689	0.00549	10.3776	0.1315	2542.1	18.7	2381.4	24.5	2469.1	11.7	97.1
Z-39-37	0.1838	0.00209	0.52184	0.00648	13.224	0.16948	2687.4	18.7	2707	27.4	2695.8	12.1	100.3
Z-39-38	0.1204	0.00132	0.34336	0.00417	5.69953	0.07119	1962.1	19.3	1902.8	20.0	1931.3	10.8	98.4
Z-39-39	0.11959	0.0013	0.34368	0.00417	5.66679	0.07071	1950.1	19.4	1904.4	20.0	1926.3	10.8	98.8
Z-39-40	0.15584	0.00157	0.4373	0.00524	9.39542	0.11155	2411	17.0	2338.5	23.5	2377.4	10.9	98.6
Z-39-41	0.15702	0.00166	0.44752	0.00552	9.68733	0.12096	2423.9	17.9	2384.2	24.6	2405.5	11.5	99.2
Z-39-42	0.15539	0.00169	0.43806	0.00544	9.38405	0.11912	2406.1	18.4	2341.9	24.4	2376.3	11.7	98.8
Z-39-43	0.18278	0.0021	0.4888	0.00618	12.3171	0.16145	2678.3	18.9	2565.5	26.8	2628.9	12.3	98.2
Z-39-44	0.1241	0.00139	0.3693	0.00459	6.31824	0.08171	2015.9	19.8	2026.1	21.6	2021	11.3	100.3
Z-39-45	0.12832	0.00139	0.37997	0.00469	6.72199	0.08497	2075.1	18.9	2076.2	21.9	2075.5	11.2	100.0
Z-39-46	0.12391	0.00127	0.32325	0.00395	5.52222	0.06745	2013.2	18.1	1805.6	19.2	1904.1	10.5	94.6
Z-39-47	0.11965	0.00132	0.34933	0.00433	5.76276	0.0738	1951	19.6	1931.4	20.7	1940.8	11.1	99.5
Z-39-48	0.12089	0.00145	0.35069	0.00442	5.84534	0.07902	1969.4	21.2	1937.9	21.1	1953.2	11.7	99.2
Z-39-49	0.12211	0.00126	0.36135	0.00442	6.08356	0.07474	1987.2	18.3	1988.6	20.9	1987.9	10.7	100.0
Z-39-50	0.1275	0.00155	0.38107	0.00483	6.69909	0.09121	2063.8	21.2	2081.3	22.5	2072.5	12.0	100.4
Z-39-51	0.1189	0.0013	0.35206	0.00421	5.77161	0.07115	1939.8	19.4	1944.4	20.1	1942.2	10.7	100.1
Z-39-52	0.12389	0.00138	0.37186	0.00447	6.35206	0.07944	2013	19.7	2038.1	21.0	2025.7	11.0	100.6
Z-39-53	0.1202	0.00139	0.35912	0.00435	5.95196	0.07628	1959.2	20.5	1978	20.6	1968.9	11.1	100.5
Z-39-54	0.12179	0.00146	0.34151	0.00417	5.73518	0.07544	1982.6	21.3	1893.9	20.0	1936.7	11.4	97.7
Z-39-55	0.13812	0.00165	0.39983	0.0049	7.61505	0.09978	2203.8	20.6	2168.3	22.6	2186.6	11.8	99.2
Z-39-56	0.18268	0.00216	0.53888	0.00668	13.5742	0.17602	2677.3	19.4	2778.8	28.0	2720.5	12.3	101.6
Z-39-57	0.12777	0.00137	0.387	0.0046	6.81834	0.08276	2067.5	18.8	2108.9	21.4	2088.1	10.8	101.0
Z-39-58	0.1206	0.00142	0.35764	0.00434	5.94777	0.07698	1965.2	20.8	1971	20.6	1968.2	11.3	100.2
Z-39-59	0.12745	0.00136	0.38807	0.0046	6.82046	0.0822	2063.1	18.6	2113.9	21.4	2088.4	10.7	101.2

Table 3.2 (Continued)

Z-39-60	0.12033	0.00128	0.29766	0.00352	4.93951	0.05937	1961.2	18.8	1679.7	17.5	1809	10.2	92.2
Z-39-61	0.1833	0.00439	0.38516	0.00659	9.73517	0.22138	2683	39.1	2100.4	30.7	2410	20.9	89.8
Z-39-62	0.12604	0.00163	0.35733	0.00432	6.21037	0.08506	2043.5	22.8	1969.5	20.5	2005.9	12.0	98.2
Z-39-63	0.12379	0.00178	0.35449	0.00443	6.05114	0.08989	2011.6	25.3	1956	21.1	1983.2	12.9	98.6
Z-39-64	0.123	0.00198	0.35703	0.00464	6.05542	0.09877	2000.1	28.3	1968.1	22.0	1983.9	14.2	99.2
Z-39-65	0.12405	0.00173	0.39991	0.00496	6.84078	0.09967	2015.2	24.6	2168.6	22.9	2091	12.9	103.8
Z-39-66	0.12589	0.00188	0.34795	0.0044	6.04063	0.09263	2041.4	26.2	1924.8	21.0	1981.7	13.4	97.1
Z-39-67	0.18253	0.00219	0.50982	0.0061	12.8325	0.16549	2676	19.8	2655.8	26.1	2667.4	12.2	99.7
Z-39-68	0.12238	0.00148	0.30545	0.0036	5.15515	0.0668	1991.2	21.3	1718.3	17.8	1845.2	11.0	92.7
Z-39-69	0.12343	0.00265	0.37262	0.00555	6.34271	0.13351	2006.4	37.7	2041.7	26.1	2024.4	18.5	100.9
Z-39-70	0.11819	0.00156	0.23586	0.00283	3.84451	0.05329	1929.1	23.5	1365.1	14.8	1602.1	11.2	83.0
Z-39-71	0.169	0.00173	0.35292	0.00425	8.22785	0.09948	2547.7	17.1	1948.5	20.2	2256.4	11.0	88.6
Z-39-72	0.11949	0.00129	0.33594	0.00408	5.53721	0.06902	1948.6	19.1	1867.1	19.7	1906.4	10.7	97.8
Z-39-73	0.12457	0.00138	0.36238	0.00443	6.22647	0.07913	2022.6	19.5	1993.4	21.0	2008.2	11.1	99.3
Z-39-74	0.12441	0.0013	0.35765	0.00433	6.13707	0.07516	2020.3	18.5	1971	20.6	1995.5	10.7	98.8
Z-39-75	0.11919	0.00133	0.35444	0.00435	5.82629	0.07443	1944.1	19.8	1955.8	20.7	1950.3	11.1	100.3
Z-39-76	0.12268	0.00135	0.37277	0.00457	6.30676	0.07983	1995.5	19.4	2042.4	21.4	2019.4	11.1	101.2
Z-39-77	0.11907	0.00125	0.33912	0.00412	5.56822	0.06832	1942.3	18.6	1882.4	19.8	1911.2	10.6	98.4
Z-39-78	0.11716	0.00122	0.34488	0.00419	5.57159	0.0682	1913.3	18.6	1910.1	20.1	1911.7	10.5	99.9
Z-39-79	0.13522	0.00161	0.34018	0.00426	6.34231	0.08444	2166.9	20.6	1887.5	20.5	2024.3	11.7	93.4
Z-39-80	0.14931	0.00153	0.3884	0.00471	7.99502	0.09674	2338	17.5	2115.4	21.9	2230.5	10.9	95.4
Z-39-81	0.15643	0.00176	0.44709	0.00565	9.64097	0.12585	2417.4	19.0	2382.3	25.2	2401.1	12.0	99.3
Z-39-82	0.14287	0.00152	0.39183	0.00487	7.71705	0.09724	2262.3	18.2	2131.3	22.5	2198.6	11.3	97.2
Z-39-83	0.12523	0.00147	0.37328	0.00472	6.4442	0.08661	2032.1	20.7	2044.8	22.2	2038.3	11.8	100.3
Z-39-84	0.16205	0.00176	0.44151	0.00551	9.86285	0.12564	2477.1	18.2	2357.4	24.6	2422	11.7	97.8
Z-39-85	0.12783	0.00157	0.35251	0.0045	6.212	0.08571	2068.4	21.5	1946.6	21.4	2006.1	12.1	97.0
Z-39-86	0.17961	0.00196	0.49097	0.00614	12.1568	0.15545	2649.3	18.0	2574.9	26.6	2616.6	12.0	98.8
Z-39-87	0.12265	0.0014	0.34575	0.00433	5.84597	0.07692	1995.1	20.1	1914.3	20.7	1953.3	11.4	97.9
Z-39-88	0.12815	0.00154	0.3679	0.00466	6.49972	0.08845	2072.8	21.0	2019.5	22.0	2045.9	12.0	98.7
Z-39-89	0.12334	0.0013	0.18465	0.00227	3.13986	0.03926	2005.1	18.6	1092.3	12.4	1442.5	9.6	71.9
Z-39-90	0.1219	0.00135	0.3536	0.00439	5.94247	0.07664	1984.3	19.6	1951.7	20.9	1967.5	11.2	99.2
Z-39-91	0.11914	0.00279	0.35529	0.00497	5.83108	0.12538	1943.4	41.2	1959.8	23.7	1951	18.6	100.4
Z-39-92	0.1745	0.00449	0.46753	0.00749	11.2371	0.26419	2601.3	42.3	2472.7	32.9	2543	21.9	97.8
Z-39-93	0.17788	0.00361	0.43206	0.00556	10.5849	0.19429	2633.2	33.3	2315	25.0	2487.4	17.0	94.5
Z-39-94	0.12897	0.00317	0.19941	0.00285	3.54167	0.07862	2083.9	42.6	1172.1	15.3	1536.6	17.6	73.7
Z-39-95	0.12249	0.00351	0.34232	0.00554	5.77404	0.15115	1992.7	50.1	1897.8	26.6	1942.5	22.7	97.5
Z-39-96	0.11798	0.00316	0.32072	0.00487	5.21078	0.1269	1925.9	47.2	1793.3	23.8	1854.4	20.8	96.3
Z-39-97	0.19062	0.00599	0.51364	0.01017	13.4823	0.38435	2747.5	50.8	2672.1	43.3	2714	27.0	98.8
Z-39-98	0.11719	0.00328	0.34591	0.00542	5.58249	0.1419	1913.9	49.4	1915	26.0	1913.4	21.9	100.0
Z-39-99	0.12978	0.00341	0.34773	0.00526	6.21489	0.14703	2095	45.5	1923.7	25.2	2006.5	20.7	95.8
Z-39-100	0.12103	0.00348	0.3607	0.0058	6.01222	0.15643	1971.5	50.3	1985.5	27.5	1977.6	22.7	100.3

Table 3.2 (Continued)

Table 3.4 (next page) complete Ar-Ar data for all Ubende samples

Laser intensity (W)	$^{40}\text{Ar} \pm \sigma$ (nA)	$^{39}\text{Ar} \pm \sigma$ (nA)	$^{38}\text{Ar} \pm \sigma$ (nA)	$^{37}\text{Ar} \pm \sigma$ (nA)	$^{36}\text{Ar} \pm \sigma$ (nA)	$^{40}\text{Ar}^*$ (%)	$^{39}\text{Ar}$ released (%)	$^{40}\text{Ar}^{39}\text{ArK} \pm \sigma$	Age $\pm \sigma$								
<b>T04-12b</b>																	
61	1.681438	0.001669	0.000026	0.000127	0.000009	0.000123	0.000010	0.000470	0.000019	92.41	0.56	1396.16	-	33.55	4706.09	$\pm$	80.5
64	1.844599	0.000967	0.000026	0.000163	0.000008	0.001668	0.000022	0.000284	0.000007	96.30	3.12	286.43	-	1.53	2298.08	$\pm$	13.9
64.5	0.433912	0.000700	0.000013	0.000082	0.000005	0.001022	0.000009	0.000068	0.000006	98.47	1.83	115.62	$\pm$	0.76	1284.69	$\pm$	12.1
64.5	2.425836	0.002848	0.000055	0.000439	0.000011	0.006216	0.000039	0.000225	0.000008	98.47	11.50	104.38	$\pm$	0.42	1193.03	$\pm$	7.0
65.1	0.192034	0.000542	0.000016	0.000033	0.000006	0.000560	0.000019	0.000035	0.000005	100.90	1.05	88.05	$\pm$	1.14	1050.98	$\pm$	20.7
65.5	1.216805	0.002088	0.000012	0.000241	0.000014	0.003771	0.000047	0.000107	0.000006	99.17	6.90	87.43	$\pm$	0.33	1045.31	$\pm$	6.0
65.5	0.409209	0.001325	0.000016	0.000080	0.000006	0.001209	0.000013	0.000061	0.000005	98.94	2.32	85.86	-	0.62	1031.02	$\pm$	11.3
65.6	2.389146	0.001079	0.000067	0.000484	0.000014	0.007405	0.000043	0.000137	0.000008	99.65	14.02	85.30	$\pm$	0.33	1025.91	$\pm$	6.1
65.68	2.488439	0.001259	0.000059	0.000510	0.000014	0.008015	0.000050	0.000133	0.000008	99.80	14.70	84.85	$\pm$	0.31	1021.72	$\pm$	5.7
65.8	3.967693	0.007527	0.000056	0.000829	0.000018	0.012513	0.000059	0.000199	0.000003	99.73	23.45	84.90	$\pm$	0.31	1022.20	$\pm$	5.7
65.8	0.523406	0.001706	0.000045	0.000113	0.000005	0.001666	0.000016	0.000077	0.000005	98.79	3.05	83.79	$\pm$	0.78	1011.97	$\pm$	14.5
66.3	0.805996	0.002812	0.000070	0.000190	0.000007	0.002564	0.000033	0.000091	0.000007	99.11	4.67	85.22	$\pm$	0.79	1025.17	$\pm$	14.5
66.9	0.630625	0.000954	0.000043	0.000132	0.000005	0.001896	0.000024	0.000109	0.000005	97.80	3.54	86.70	$\pm$	0.65	1038.67	$\pm$	11.9
67.7	1.143833	0.002219	0.000065	0.000246	0.000008	0.003361	0.000031	0.000183	0.000006	97.30	6.45	86.33	$\pm$	0.56	1035.30	$\pm$	10.1
68.5	0.045347	0.000190	0.000006	0.000020	0.000004	0.000120	0.000004	0.000050	0.000005	94.86	0.20	89.87	$\pm$	4.66	1067.35	$\pm$	83.6
72	0.535044	0.001740	0.000037	0.000144	0.000007	0.001368	0.000015	0.000308	0.000008	85.94	2.63	86.81	$\pm$	0.91	1039.67	$\pm$	16.5
<b>T04-26b</b>																	
61	0.829732	0.005074	0.000047	0.000055	0.000005	0.000070	0.000007	0.000177	0.000010	95.17	3.97	987.28	$\pm$	59.14	4124.42	$\pm$	194.2
63.5	0.273605	0.000865	0.000016	0.000037	0.000004	0.000070	0.000004	0.000087	0.000008	95.11	2.95	427.34	$\pm$	12.97	2839.32	$\pm$	86.8
65	0.122630	0.000306	0.000015	0.000029	0.000003	0.000076	0.000008	0.000069	0.000004	93.49	1.96	270.11	$\pm$	11.62	2217.19	$\pm$	109.8
66	0.052812	0.000206	0.000009	0.000014	0.000003	0.000090	0.000007	0.000053	0.000007	94.56	1.42	143.92	$\pm$	9.40	1493.38	$\pm$	132.7
66.5	0.042893	0.000189	0.000005	0.000022	0.000002	0.000105	0.000006	0.000060	0.000004	86.51	1.70	84.79	$\pm$	4.97	1018.77	$\pm$	91.3
67	0.102227	0.000346	0.000008	0.000042	0.000004	0.000098	0.000006	0.000068	0.000004	92.68	2.43	177.41	$\pm$	4.61	1715.47	$\pm$	57.5
67.5	0.233376	0.000637	0.000016	0.000494	0.000013	0.000466	0.000006	0.000096	0.000005	93.73	7.20	146.30	$\pm$	2.24	1510.07	$\pm$	31.3
67.8	0.253999	0.000521	0.000013	0.001038	0.000013	0.000778	0.000020	0.000075	0.000005	97.19	5.42	220.08	$\pm$	3.39	1963.79	$\pm$	36.8
68.1	1.488783	0.004144	0.000036	0.0005984	0.000030	0.003300	0.000042	0.000174	0.000005	98.08	21.49	339.46	$\pm$	3.29	2518.28	$\pm$	26.3
68.4	0.149932	0.000467	0.000010	0.000497	0.000010	0.000237	0.000009	0.000057	0.000005	98.62	1.38	498.42	$\pm$	21.20	3062.77	$\pm$	125.4
68.5	0.593411	0.002305	0.000010	0.001130	0.000030	0.000525	0.000014	0.000067	0.000005	98.19	3.21	905.57	$\pm$	15.64	3985.04	$\pm$	55.5
68.6	3.110636	0.001424	0.000019	0.004156	0.000031	0.001931	0.000021	0.000187	0.000005	98.66	11.83	1302.90	$\pm$	11.41	4579.88	$\pm$	29.1
68.7	0.059896	0.000332	0.000004	0.000167	0.000008	0.000095	0.000005	0.000033	0.000004	96.31	0.58	451.67	$\pm$	24.53	2918.97	$\pm$	157.1
68.7	0.371362	0.000896	0.000017	0.001102	0.000013	0.000813	0.000021	0.000080	0.000006	96.30	5.34	332.07	$\pm$	5.77	2488.49	$\pm$	46.9
69.5	1.030510	0.002448	0.000011	0.005066	0.000037	0.002520	0.000021	0.000164	0.000006	96.90	16.07	309.74	$\pm$	1.85	2395.32	$\pm$	15.9
70	0.219909	0.000670	0.000013	0.000804	0.000012	0.000458	0.000010	0.000100	0.000006	90.97	2.67	361.45	$\pm$	9.95	2604.11	$\pm$	75.9
73	1.004355	0.003143	0.000022	0.000391	0.000039	0.001992	0.000032	0.000298	0.000006	92.76	10.39	446.67	$\pm$	5.45	2902.88	$\pm$	35.2

Laser intensity (W)	$^{40}\text{Ar} \pm \sigma$ (nA)	$^{39}\text{Ar} \pm \sigma$ (nA)	$^{38}\text{Ar} \pm \sigma$ (nA)	$^{37}\text{Ar} \pm \sigma$ (nA)	$^{36}\text{Ar} \pm \sigma$ (nA)	$^{40}\text{Ar}^+ (\%)$	$^{39}\text{Ar}$ released (%)	$^{40}\text{Ar}^{39}\text{Ar}/\text{K} \pm \sigma$	Age $\pm \sigma$									
T04-33																		
61	0.133438	0.000507	0.000170	0.000011	0.000043	0.000012	0.000047	0.000005	0.000193	0.000010	62.22	2.76	45.52	±	2.00	616.57	±	45.9
64	0.169496	0.000419	0.003127	0.000022	0.000060	0.000004	0.000093	0.000005	0.000155	0.000007	77.32	4.89	40.86	±	0.87	562.32	±	20.6
65	0.081825	0.000231	0.001442	0.000018	0.000047	0.000004	0.000134	0.000007	0.000062	0.000005	86.76	2.23	46.58	±	1.64	628.66	±	37.5
65.5	0.051107	0.000319	0.000725	0.000013	0.000038	0.000003	0.000139	0.000007	0.000056	0.000004	82.09	1.10	53.13	±	2.94	701.88	±	64.5
66.2	0.332535	0.000628	0.002980	0.000033	0.000302	0.000006	0.001131	0.000012	0.000340	0.000011	73.17	4.61	81.92	±	1.62	992.28	±	30.2
66.4	0.192568	0.000364	0.002205	0.000030	0.000182	0.000008	0.000708	0.000020	0.000070	0.000005	94.32	3.41	81.62	±	1.53	989.46	±	28.5
66.6	0.186593	0.000856	0.002107	0.000013	0.000196	0.000012	0.000730	0.000010	0.000064	0.000002	95.26	3.25	83.65	±	1.12	1008.26	±	20.6
66.9	2.508695	0.001318	0.028977	0.000085	0.002780	0.000052	0.009427	0.000034	0.000360	0.000008	97.26	45.31	85.07	±	0.37	1021.39	±	6.8
66.95	0.136870	0.000538	0.001562	0.000020	0.000130	0.000009	0.000495	0.000014	0.000041	0.000007	98.10	2.40	84.47	±	2.10	1015.90	±	38.7
67.1	1.018046	0.002245	0.011991	0.000067	0.001153	0.000013	0.003950	0.000037	0.000137	0.000007	98.03	18.71	83.91	±	0.61	1010.69	±	11.2
68	0.073346	0.000216	0.000714	0.000014	0.000083	0.000008	0.000261	0.000012	0.000059	0.000006	87.78	1.06	86.94	±	4.12	1038.47	±	74.8
69	0.286257	0.000744	0.002833	0.000017	0.000296	0.000012	0.001033	0.000017	0.000152	0.000004	88.40	4.38	89.38	±	1.00	1060.44	±	17.9
70	0.367243	0.000822	0.003441	0.000020	0.000372	0.000018	0.001199	0.000019	0.000249	0.000010	83.35	5.33	89.24	±	1.17	1059.22	±	20.9
72	0.087325	0.000477	0.000400	0.000016	0.000055	0.000004	0.000091	0.000004	0.000211	0.000006	34.99	0.57	77.63	±	7.90	951.81	±	150.5
T04-43																		
63	0.425642	0.001916	0.000878	0.000020	0.000035	0.000013	0.000071	0.000007	0.000157	0.000012	91.76	1.39	457.96	±	29.59	2945.91	±	187.9
63	0.094425	0.000170	0.000272	0.000006	0.000011	0.000004	0.000050	0.000006	0.000057	0.000004	92.85	0.42	353.31	±	79.64	2578.87	±	619.3
64.8	0.429740	0.001167	0.003829	0.000017	0.000086	0.000006	0.001478	0.000029	0.000122	0.000004	94.72	6.17	106.97	±	2.19	1214.54	±	36.3
65.2	0.092531	0.000383	0.000978	0.000015	0.000032	0.000005	0.000251	0.000068	0.000054	0.000003	92.20	1.55	84.51	±	7.94	1018.62	±	146.4
65.5	0.064704	0.000476	0.000619	0.000011	0.000010	0.000003	0.000261	0.000010	0.000041	0.000004	93.79	0.93	95.16	±	13.75	1114.17	±	240.4
65.9	0.140728	0.000558	0.001273	0.000005	0.000036	0.000004	0.000472	0.000013	0.000054	0.000004	94.63	1.97	104.36	±	6.52	1192.87	±	109.1
66.2	1.335980	0.004983	0.012582	0.000065	0.000272	0.000011	0.005019	0.000040	0.000154	0.000003	98.24	20.23	105.53	±	0.98	1202.61	±	16.3
66.5	2.437923	0.001086	0.031339	0.000074	0.000600	0.000008	0.011610	0.000084	0.000215	0.000009	99.06	50.57	77.90	±	0.38	956.62	±	7.2
66.55	0.195877	0.000527	0.002373	0.000018	0.000050	0.000004	0.000812	0.000015	0.000067	0.000005	94.97	3.69	77.68	±	3.14	954.53	±	59.9
66.8	0.065363	0.000170	0.000682	0.000015	0.000017	0.000003	0.000269	0.000007	0.000050	0.000006	89.98	0.97	82.51	±	11.81	1000.09	±	219.9
67.5	0.101055	0.000574	0.001089	0.000018	0.000033	0.000004	0.000430	0.000008	0.000060	0.000005	92.03	1.73	83.10	±	7.15	1005.55	±	132.8
67.9	0.333879	0.000682	0.003993	0.000015	0.000094	0.000007	0.001403	0.000013	0.000122	0.000007	93.26	6.39	77.85	±	1.88	956.16	±	35.9
68.2	0.086063	0.000284	0.000831	0.000011	0.000026	0.000003	0.000314	0.000014	0.000082	0.000003	82.99	1.30	82.92	±	2.05	1003.88	±	38.0
69.1	0.065326	0.000199	0.000570	0.000012	0.000020	0.000004	0.000208	0.000010	0.000074	0.000006	80.49	0.87	87.82	±	4.28	1048.88	±	77.6
72	0.168601	0.000307	0.001118	0.000020	0.000063	0.000006	0.000395	0.000013	0.000276	0.000009	57.07	1.81	85.67	±	3.04	1029.24	±	55.7

Laser intensity (W)	$^{40}\text{Ar} \pm \sigma$ (nA)	$^{39}\text{Ar} \pm \sigma$ (nA)	$^{38}\text{Ar} \pm \sigma$ (nA)	$^{37}\text{Ar} \pm \sigma$ (nA)	$^{36}\text{Ar} \pm \sigma$ (nA)	$^{40}\text{Ar}^*$ (%)	$^{39}\text{Ar}$ released (%)	$^{40}\text{Ar}^{r/39}\text{Ar}_K \pm \sigma$	Age $\pm \sigma$									
T04-05																		
61	0.153679	0.000567	0.000550	0.000034	0.000058	0.000005	0.000040	0.000004	0.000250	0.000008	56.43	0.93	157.16	$\pm$	11.65	1588.20	$\pm$	156.7
63	0.033205	0.000109	0.000241	0.000012	0.000021	0.000004	0.000036	0.000004	0.000075	0.000005	51.12	0.38	60.07	$\pm$	10.10	778.08	$\pm$	212.7
64.5	0.081534	0.000234	0.000825	0.000009	0.000060	0.000005	0.000221	0.000008	0.000086	0.000006	80.52	1.40	75.51	$\pm$	3.18	933.70	$\pm$	61.4
65.5	0.060535	0.000076	0.000515	0.000007	0.000050	0.000007	0.000175	0.000006	0.000066	0.000004	83.57	0.84	93.07	$\pm$	4.20	1095.79	$\pm$	74.2
66	1.137414	0.001347	0.011829	0.000050	0.000204	0.000008	0.004380	0.000043	0.000124	0.000008	98.77	20.75	95.75	$\pm$	0.58	1119.38	$\pm$	10.1
66	0.185828	0.000265	0.002021	0.000009	0.000035	0.000006	0.000711	0.000016	0.000058	0.000004	97.36	3.48	88.52	$\pm$	1.14	1055.24	$\pm$	20.6
66.1	0.162702	0.000397	0.001788	0.000021	0.000028	0.000004	0.000631	0.000016	0.000054	0.000003	97.63	3.06	87.51	$\pm$	1.51	1046.08	$\pm$	27.4
66.2	0.104518	0.000519	0.000951	0.000030	0.000028	0.000004	0.000251	0.000010	0.000114	0.000008	76.40	1.58	81.88	$\pm$	4.29	994.18	$\pm$	80.1
66.4	1.871444	0.001785	0.021515	0.000047	0.000295	0.000012	0.007513	0.000040	0.000144	0.000007	99.37	37.77	87.19	$\pm$	0.37	1043.10	$\pm$	6.8
66.5	0.889487	0.002096	0.010460	0.000041	0.000137	0.000010	0.003788	0.000026	0.000095	0.000005	98.80	18.37	84.67	$\pm$	0.52	1020.13	$\pm$	9.5
66.6	0.056513	0.000260	0.000571	0.000012	0.000015	0.000002	0.000220	0.000010	0.000038	0.000005	93.51	0.96	87.79	$\pm$	4.39	1048.55	$\pm$	79.6
67.5	0.143776	0.000401	0.001510	0.000016	0.000033	0.000003	0.000535	0.000017	0.000077	0.000003	90.25	2.61	84.64	$\pm$	1.52	1019.81	$\pm$	28.0
67.6	0.099286	0.000363	0.000957	0.000014	0.000027	0.000002	0.000363	0.000012	0.000077	0.000004	85.35	1.63	86.30	$\pm$	2.39	1035.00	$\pm$	43.6
67.8	0.072271	0.000231	0.000649	0.000013	0.000027	0.000004	0.000246	0.000008	0.000071	0.000005	82.52	1.08	88.24	$\pm$	3.74	1052.65	$\pm$	67.6
68.6	0.052299	0.000226	0.000439	0.000009	0.000021	0.000002	0.000166	0.000006	0.000069	0.000007	76.46	0.71	85.93	$\pm$	6.38	1031.70	$\pm$	116.8
68.9	0.033964	0.000273	0.000257	0.000005	0.000021	0.000003	0.000112	0.000007	0.000061	0.000006	69.79	0.39	84.52	$\pm$	9.90	1018.70	$\pm$	182.5
69.2	0.022183	0.000059	0.000143	0.000004	0.000001	0.000004	0.000059	0.000005	0.000046	0.000003	76.32	0.19	105.55	$\pm$	17.43	1202.84	$\pm$	290.1
69.7	0.087820	0.000483	0.000718	0.000011	0.000028	0.000006	0.000228	0.000007	0.000115	0.000006	72.16	1.20	85.99	$\pm$	3.74	1032.20	$\pm$	68.4
72	0.219765	0.000428	0.001561	0.000010	0.000069	0.000005	0.000537	0.000017	0.000331	0.000010	60.60	2.68	85.38	$\pm$	2.36	1026.59	$\pm$	43.3



# Chapter 4—Architecture of a Palaeoproterozoic subduction zone: a structural and geochronological traverse through the Usagaran Orogen, Tanzania

## 4.1 Introduction

Eclogites and other high-pressure rocks have been used by various authors to interpret changing tectonic regimes of the earth (Brown, 2006, 2007a, b; Maruyama and Liou, 1998b; O'Brien and Rötzler, 2003; Stern, 2005b) because the pressure conditions of their formation are equivalent to those at mantle depths while the temperatures recorded by the mineral assemblages are cooler than those found within the mantle. Eclogites form at high-pressures, and require relatively fast exhumation to preserve their mineral assemblage. These rocks are relatively rare in the geological record, and are much more common in the Phanerozoic earth than the Proterozoic or older (Brown, 2007a).

The mechanism for transporting rocks to mantle depths is commonly considered to be subduction, because it is within known subduction zones that modern eclogites are found. Once transported to depth these rocks must return to mid-crustal levels relatively quickly otherwise they would be heated to granulite-facies conditions. The tectonic setting for exhumation of high-pressure metamorphic rocks is more complicated, and various models have been proposed based on the characteristics of different occurrences of high-pressure metamorphic rocks. Models range from, and sometimes include several of, erosion (transportation of material from the surface by atmospheric processes), ductile flow (horizontal stretching of the orogenic wedge resulting in vertical shortening), normal faulting (removal of overlying material by tectonic processes which may be associated with rifting, subduction zone roll-back or orogenic collapse), and extrusion of material by deep-seated channel flow within the subduction trench.

The oldest eclogites identified are the ~2.7 Ga eclogites in the Belomorian region of north-western Russia (Volodichev et al., 2004), however these occur as 1-10 m scale boudins within a highly deformed mobile belt. The Usagaran Orogen in Central Tanzania contains eclogite which formed at 2.0 Ga (Collins et al., 2004b; Möller et al., 1995) at pressures of ~18 kbar and temperatures of ~750 °C (Möller et al., 1995) and are the oldest identified eclogites occurring within a well preserved orogenic belt.

For this study a full structural traverse through the Usagaran Orogen, from the Archaean Craton into the Neoproterozoic rocks of the Mozambique Orogen was completed. Samples were taken to investigate the metamorphic history of the orogen, which will be discussed in chapter 5, and to investigate the provenance of metasediments in the Usagaran and Ubende Orogens to determine whether the metasediments are derived from the Tanzanian Craton, or from some other source.

## 4.2 Crustal Architecture and temporal evolution

The Usagaran Orogen (figure 4.1) is located to the southeast of the ~2.7 Ga Tanzanian craton and consists

of the Konse Group, a greenschist-facies metasedimentary package immediately adjacent to the Craton, and the Isimani Suite, a series of medium to high-grade gneisses and amphibolites with a few pockets of granulite (Mruma, 1989a). Some pods of eclogite are preserved within the a body of mafic rocks within the Isimani Suite which was exposed to conditions of ~18 kbar & ~750 °C (Möller et al., 1995) and are exposed at Yalumba Hill. The most recent geochronological work suggests the eclogites formed during the D<sub>1</sub> at 1999.1±1.1 Ma and were subsequently exhumed at ~25°C/Ma, 0.06-0.22GPa/Ma (Collins et al., 2004b; Möller et al., 1995). Stern (2005b) suggests that these eclogites may in fact be a product of the Pan-African orogen rather than the Palaeoproterozoic orogen, however this suggestion is not supported by the available data.

Structural mapping of the Usagaran Orogen south of Yalumba Hill was conducted by Mruma (1989). A more detailed ~10km structural traverse along the Great Ruaha River by Reddy et al. (2003), running from the Archaean Craton and crossing the tail of the eclogite-hosting mafic body identified 5 stages of deformation and described their affect on five different structural domains. The initial stage (D<sub>1</sub>) occurred at high pressure conditions and resulted in formation of recumbent folds and compositional bandings (Mruma, 1989; Reddy *et al.*, 2003). The eclogite and granulite facies mineral assemblages are considered to have developed at this stage (Mruma, 1989). The second stage (D<sub>2</sub>) took place at amphibolite facies conditions and overprinted the previous D<sub>1</sub> deformations and mineral assemblages (Reddy *et al.*, 2003). The third stage (D<sub>3</sub>) probably only affected the area in a short time and the metamorphic grade of the D<sub>3</sub> fabrics are indistinguishable from those developed during D<sub>2</sub> which indicated that it is probably associated with the later stages of D<sub>2</sub> (Reddy *et al.*, 2003). D<sub>3</sub> may represent the phase that the direction of shortening changes from SE to S during the orogeny (Reddy *et al.*, 2003). The last two stages involved extension (D<sub>4</sub>) followed by thrusting (D<sub>5</sub>) under greenschist facies condition that thrust the Isimani Suite over the Konse Group (Reddy *et al.*, 2003). The ages of the D<sub>4</sub> and D<sub>5</sub> deformation phases are poorly constrained and may reflect deformation during Palaeoproterozoic exhumation of the Usagaran Orogen or during the late Neoproterozoic East African orogeny (Reddy *et al.*, 2003). The overall tectonic setting of the eclogites is uncertain with Reddy et al. (2004a; Reddy et al., 2003) suggesting the Usagaran formed during subduction of a stretched or rifted continental margin with subsequent sinistral oblique convergence while Fritz et al. (2005) suggest that formation was associated with strike-slip tectonics in an island arc regime.

The Usagaran Orogen contains post-orogenic granites, some of which have been dated by whole rock Rb-Sr and SHRIMP zircon U/Pb at ~1.87 Ga (Reddy et al.,

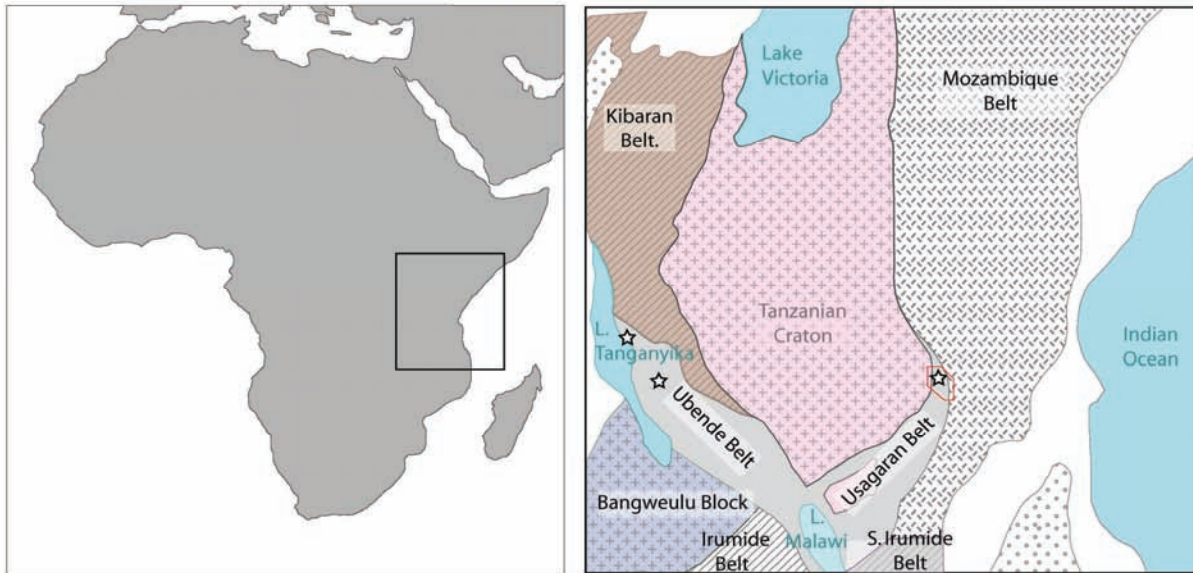


Figure 4. 1 Location diagram, showing Tanzanian orogenic belts. Red outline shows study area. Stars mark eclogite localities.

2003; Wendt et al., 1972). The Neoproterozoic East-African orogen has affected the east coast of Tanzania, and the boundary between the Usagaran and East-African orogens is poorly defined. The East-African orogen in the Tanzania area reached greenschist facies P-T conditions, although in the Mozambique Orogen of Malawi eclogites of Pan-African age (~530-500 Ma) have been reported (Ring et al., 2002). Rb-Sr and K-Ar ages for granites and gneisses around the Usagaran (Wendt et al., 1972) give younger ages towards the east of the orogen, which are likely the result of a Pan-African overprint on the earlier Usagaran rocks. Muscovite  $^{40}\text{Ar}/^{39}\text{Ar}$  data from an Isimani Suite orthogneiss at the western edge of the orogen yielded an age of  $535 \pm 3$  Ma indicating some thermal reworking occurred during the East-African orogeny (Reddy et al., 2004b).

A structural traverse within the Mozambique Orogen was conducted by Vogt et al. (2006) along the Great Ruaha River downstream of Kidete Dam, about 50km SE of the eastern end of the traverse in this study. They identify the earliest preserved fabric ( $S_0$ ) as seen only in mafic boudins and associated with high-pressure granulite facies metamorphism. A second fabric ( $S_1$ ) is associated with partial melting of granitoid gneisses. This fabric is folded by isoclinal folds ( $F_2$ ), and is preserved only in fold hinges and boudins. A second foliation ( $-S_2$ ) is axial planar to  $F_2$  folds. These earlier fabrics are only locally, generally overprinted by the main fabric,  $S_3$ , a dipping moderate- to steeply to the north or south and associated with minor  $F_3$  folding and regional dextral shearing (Vogt et al., 2006).

#### 4.3 Lithology

Outcrop is sparse on the easily accessible parts of the traverse conducted in this study. Plains are covered by an unconsolidated sedimentary sequence which ranges from 1m to at least 4m in places. Rock is exposed in incised rivers and drainage channels, and on densely vegetated hill slopes. At the southern end of this traverse a dirt road leads into the hills between Kinusi and Wazaganza exposing some outcrop on and to the sides of the track before descending to the Great Ruaha River

floodplain. For this reason there are sometimes gaps of several kilometers between outcrops. The area covered in this study was mapped in the 1950's and 1960's by the Tanganyika Bureau of Mines (Grainger and Fozzard, 1966; King, 1955; Whittingham, 1959) and more recently an area just south of this traverse was mapped and the lithology described in detail by Mruma (1989). This lithology is summarized in figure 4.2.

##### 4.3.1 Tanzanian Craton

The rock units that occur within this structural traverse include Archaean granitoids of the Tanzanian Craton, a pre-tectonic igneous suite including metadolerite (pyroxene-hornblende±garnet) and granite gneisses, the Isimani Suite, the Konse Group and a post-tectonic igneous suite (figure 4.2). The Tanzanian craton in this section is comprised of variably deformed, foliated, felsic granites with minor mafic enclaves and tonalite trondjemite granodiorites. Narrow shear bands commonly contain chlorite and sericite. Undeformed (late) felsic dykes are common. Ages from the Tanzanian Craton are discussed in detail in section 2.2.

##### 4.3.2 Konse Group

A detailed description of rock types in the Konse Group is given by Mruma (1995) and it is interpreted as a peripheral foreland basin along the margin of the Tanzanian Craton during the main phase of the Usagaran Orogen (Mruma, 1989a; Mruma, 1995). The traverse in this study passed through only a few metres of exposed Konse Group metasediments, with narrow (10 cm – 1m) beds of quartzites, marble and metapelites. The metapelitic rocks were very fine grained, with a weak foliation defined by alignment of muscovite, chlorite and epidote in a matrix of quartz and plagioclase. Epidote was observed to be nucleated around titanite (figure 4.3 a) in this sample.

##### 4.3.3 Isimani Suite

The Isimani Suite has been subdivided into three members (lithodemes) by Mruma (1989). The Iguruba member, containing sillimanite-biotite±garnet/cordierite gneisses and banded biotite-hornblende-garnet gneiss, is

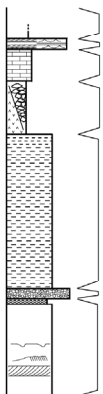
<b>Post-tectonic Igneous Suite</b>	Mu-bi granite Hornblende granite	olivine-hornblende metabasite serpentinite	pyroxene-hornblende gabbro pyroxene dolerite	olivine-pyroxene dolerite
<b>Konse Group</b> 	Ifwambo Formation	metabasite		
	Mhwana Formation	chert-like quartzite, quartz-manganese-silicate schist, quartz-mica schist		
	Ihumbirisa Formation	viridine-pneumontite-phlogopite quartzite pseudoconglomerate, BIF magnetite-quartzite		
	Kikuyu Formation	dolomite, marble & calc-silicate basic metatuff & basic metalava		
	Killimbe Formation	mica quartzite & quartz-mica schist		
	Ruaha River Formation	matrix supported polymictite conglomerate Grey quartzite member		
Mkulula Formation	orthoquartzite			
<b>Pre-tectonic Igneous Suite</b>	metadolerite (garnet-pyroxene-hornblende) muscovite pegmatite microcline granite gneiss			
<b>Isimani Suite</b>	<b>Iguruba Lithodeme</b>	<b>Mbunga River Lithodeme</b>	<b>Luhomero Lithodeme</b>	
	cordierite-sillimanite-biotite gneiss garnet-sillimanite-biotite gneiss biotite-hornblende gneiss with garnet porphyroblasts (banded)	grunerite-magnetite-quartzite kyanite-garnet-biotite gneiss epidote- and garnet-amphibolites with pyroxene bearing pockets garnet amphibolite leucocratic muscovite-feldspar gneiss muscovite-biotite gneiss porphyroclastic microcline gneiss	eclogite & associated garnetiferous gneisses of Yalumba	
<b>Tanzanian Craton</b>	tonalite trondjemite gneiss granitoid gneiss		metadolerite late felsic dykes	

Figure 4. 2 Lithology diagram showing the lithology of the northern Usagaran orogenic belt. Grey text indicates the lithology as described by Mruma (1989), black text shows additional units described in this study.

reported to occur south of this structural section and was not observed in this traverse. This section lies outside the area mapped by Mruma (1989), however both the Luhomero Member and Mbunga River Member defined by Mruma continue north into this section.

#### 4.3.3.1 Luhomero Member

The Luhomero Member is described by Mruma (1989a) as a 35 km long 1-3 km wide unit with faulted tectonic contacts between it and the enclosing Mbunga River Member. It comprises mostly foliated coarse-grained garnet amphibolite with some diopside-bearing lenses tens of meters thick and hundreds of meters long. The northern end of the unit is significantly wider than the southern end, and in addition to garnet amphibolite also contains intercalated eclogite, lherzolite, ultrabasics and felsic gneiss. These bodies form a complex mélangé with boudins of different rock types occurring on scales ranging from 10 to 100m.

Eclogitic rocks at Yalumba Hill occur as 10 – 100 m bodies. They have a primary mineral assemblage of garnet and clinopyroxene, with minor fine grained ilmenite and rare primary plagioclase and quartz. Amphibole forms a reaction texture with secondary plagioclase and ilmenite between garnet and clinopyroxene. Accessory phases include zircon, rutile and apatite. Garnet-pyroxene rocks are sometimes cut by actinolite shears and felsic mylonites zones. Foliation is seen in some eclogitic rocks and is defined by an alignment of amphibole crystals. Within each body the margins display more developed secondary mineralogy while in the centre the primary mineralogy is more prevalent.

Felsic rocks are commonly intercalated with the eclogites lenses, and are well foliated. Bodies range from 1 cm to 100 m wide. The main mineralogy is plagioclase and quartz with minor amphibole in some locations. Ultrabasic and lherzolite bodies are 10 – 20 m wide and up to 100 m long. Ultrabasics are medium grained with a mineralogy of pyroxene and amphibole ± olivine. Lherzolite, also medium grained, have a mineralogy of orthopyroxene, clinopyroxene, plagioclase, olivine with rare quartz. Pyroxenes generally have well preserved crystal shapes and cleavages, though some breakdown of pyroxene to amphibole and ilmenite has occurred. There is no indication that these rocks have seen eclogite facies metamorphism despite being within the same mélangé as the eclogites themselves. The lherzolite bodies are relatively undeformed, and Sm-Nd isotope data suggests that they may have been intruded or intercalated with the eclogite in the latest stages of the Usagaran Orogeny (Lau, 2009a). Intercalated metapelitic rocks have also been reported within the eclogite body (Möller et al., 1995) but were not observed in this study.

#### 4.3.3.2 The Mbunga River Member

The Mbunga River Member is the most spatially dominant unit in this section of the Usagaran Orogen. Mruma (1989) describes six rock types in this unit: muscovite-biotite gneiss, porphyroclastic microcline gneiss, leucocratic muscovite-feldspar gneiss, garnet amphibolites, epidote- and garnet-amphibolites with pyroxene bearing pockets, kyanite-garnet-biotite gneiss and grunerite-magnetite-quartzite. All but the grunerite-magnetite-quartzite were observed in the traverses



covered in this study. In addition geological mapping during the 1950's and 1960's identified interlayered biotite gneiss with interlayered amphibolites, migmatitic biotite-kyanite±garnet gneiss, granite migmatite and basic and ultrabasic rocks (Grainger and Fozzard, 1966; King, 1955; Whittingham, 1959).

The most common rock unit found in this traverse is an interlayered package of felsic and pelitic gneisses and amphibolite. Relative abundance of the three rock types was spatially variable, as was the composition of the felsic- and pelitic-gneisses. All units are migmatitic with garnet sometimes associated with melt leucosomes. The felsic gneiss contains quartz and plagioclase with muscovite, biotite and k-feldspar sometimes present. Biotite abundances range from 0 – 70 %. Chlorite is sometimes seen in the felsic gneisses, generally associated with late shearing. Amphibolite layers are generally narrow, but range from 0.2 – 10 m. Amphibolite mineralogy is generally amphibole and plagioclase with minor quartz and biotite. Garnet occurs in some amphibolites, and is commonly associated with melt leucosomes. Where interlayering of amphibolites and felsic gneiss is clearly visible layers are parallel to compositional variation in the felsic gneiss, suggesting that the protolith to the amphibolites was intruded as sills. A body of metamorphosed mafic rocks occurs within this package, with a mineralogy of plagioclase and orthopyroxene with garnet forming a reaction texture between the two minerals. Pegmatite occurs within this rock package, especially near the village of Chogola. The main mineralogy of pegmatites is quartz-feldspar-muscovite-biotite with rare 2-3 cm tourmaline crystals.

Pelitic gneisses contain biotite, quartz, feldspar, kyanite and garnet. Kyanite and garnet are relatively rare in the north-west, but coarse grained and common in the southwestern part. A layering parallel to foliation is sometimes defined by variations in the size and quantity of garnet in the rocks. Garnet ranges from 0.2 – 2 cm in diameter. In the south of the area garnet is commonly rimmed by a reaction texture where garnet and quartz are breaking down to biotite, kyanite and plagioclase. In some areas there are large (10-30cm) feldspar porphyroblasts and zones containing abundant elongate kyanite.

The Mang'alisa Plateau displays some variations within this basic lithology. Mang'alisa means "place of sparkles" in the local dialect, and micaceous minerals are abundant. While the main rock type remains a biotite-quartz-plagioclase±kyanite gneiss there are layers with up to 80% green kyanite while others contain 80-90% coarse grained biotite and/or muscovite, and muscovite books of 20 – 30 cm are common. Abundant coarse grained sphalerite (1 – 15 cm) is found in some locations. In the hills below the plateau, northeast of Kinusi village, a narrow 2-3 m long body of 90% graphite with minor biotite and plagioclase was identified in the biotite-felsic gneiss.

Metagranitic rocks outcrop through ~1km of the traverse between Chogola and Kikuyu (-E 217730, N 9227190) and on the Mang'alisa plateau (-E 211841, N 9215528). Near Kikuyu the rock is weakly foliated, with some outcrops preserving a well lineated tectonite-type fabric. Mineralogy is quartz+plagioclase+biotite. Melt

leucosomes in this granite are common, and contain rare garnet. On the Mang'alisa Plateau the granite has the same mineralogy, however no foliation or lineation was observed.

From the point where the road approaches the Sasimo River (loc 193, E 0223582, N 9208244) we move into a package of interlayered felsic and amphibolites gneisses. The felsic gneiss contains quartz-plagioclase-biotite-K feldspar gneiss with no kyanite present. This is most likely a metaigneous rock. Amphibolite is interlayered with the felsic gneiss. This amphibolite is different from the amphibolites further north in that, while still containing minor plagioclase, it has no garnet. Small shears in the amphibolites contain actinolite.

There is a large break in outcrop between the descent from the Usagara Mountains and the foothills of the Udzungwa Mountains. The Sasimo and Ruaha Rivers merge in this valley and agriculture on the flood plain is intensive. The Udzungwa Mountain foothills are composed of felsic gneiss with a foliation defined by alignment of biotite, and interlayered amphibole ± plagioclase ± garnet ± pyroxene gneiss. Layering occurs at variable scale with thicknesses of 20-60 cm in some locations, ranging up to 10 – 15 m in other locations. Amphibolite sometimes forms boudins within the felsic gneiss.

#### 4.4 Structural traverse

The structural traverse (Figure 4.4) starts on the eastern margin of the Tanzanian craton and runs roughly south east as far as the village of Chogola, then approximately follows the road south to Ruaha-Mbuyuni where the Iringa-Morogoro road crosses the Great Ruaha River. Outcrop was found mostly in river beds and by on the slopes of steep sided hills which protrude from the alluvial plains. River channels are deeply incised into the plain and generally expose 2-4 m of alluvium and laterite.

##### 4.4.1 Domains of contrasting deformational style

Reddy et al. (2003) identified 5 phases of deformation and observed differing expression of those stages in five domains, which they numbered 1-5. Ten distinctly different zones of deformation were observed along the traverse undertaken in this study. To avoid confusion in the discussion of domains this study is labeling the domains based on village names or landforms within the domains rather than numbers. Only the domain 1 of the Reddy et al. (2003) study is exposed in this traverse, the others are covered by recent sediments. This unit is here referred to as the Luhomero domain as it comprises only the Luhomero lithodeme of Mruma (1989). This study will describe the deformation seen in different domains (Figures 4.4 and 4.5) before trying to relate it back to the phases of deformation identified by Reddy et al. (2003).

##### 4.4.1.1 Tanzanian Craton

The western-most part of this traverse includes variably foliated and unfoliated granitic rocks of the Tanzanian Craton. Where present foliations dip steeply to the south (mean foliation=80°/172, n=37, var=0.45). Lineations trend steeply to the east (mean=74°/098, n=15, var=0.07). Narrow shear zones are common, and often contain chlorite and sericite. Shear zones are nearly vertical and trend either ENE-WSW or form conjugate



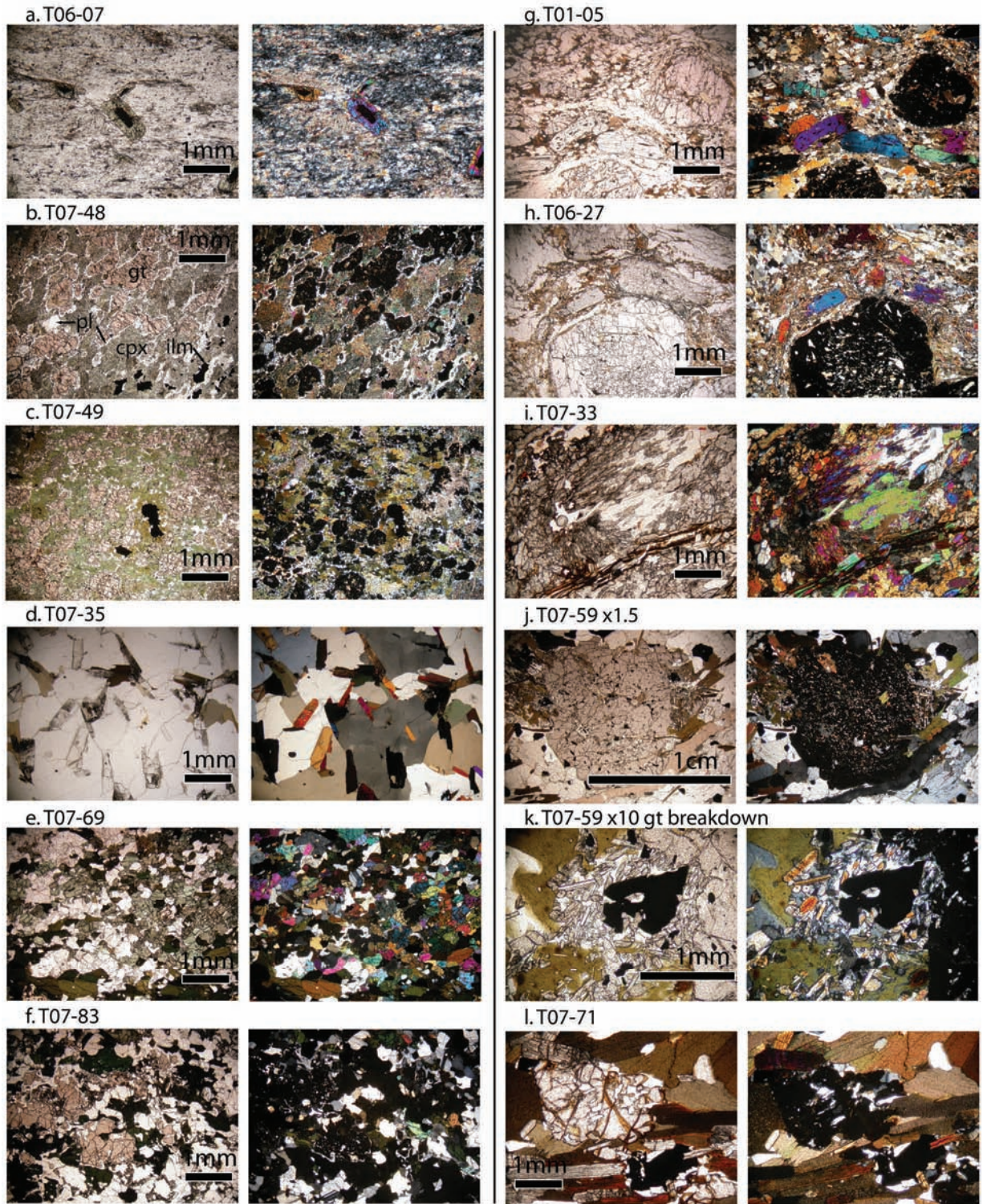


Figure 4.3 Petrology photomicrographs

sets trending E-W and SSE-NNW.

#### 4.4.1.2 Konse Domain

The Konse group is exposed over ~30 m in this section, and bedding and cleavage are consistent throughout the exposure. Bedding dips steeply (~80°) to the south-east, with subparallel cleavage dipping slightly less steeply (~70°) in the same direction. The contact between the Konse Group and cratonic rocks is not exposed in this section, nor is the contact between the Konse and the Isimani Suite. There are no exposed rocks between the Konse group and the eclogitic rocks of the Luhomero lithodeme which is exposed at Yalumba Hill.

#### 4.4.1.3 Luhomero Domain

Domain 1 of Reddy et al. (2003), here called the Luhomero domain, has generally ENE dipping  $S_2$  foliations and NNW-SSE trending  $L_2$  lineations where exposed by the Great Ruaha River. At Yalumba Hill, 30km north of that section, foliations dip between 20-50° to the SE (mean foliation = 42°/143, n=40, var=0.09). Rare lineations are defined by amphiboles and plunge to the E. Towards the northern edge of this domain small (1-2 cm) actinolite bearing shears cut the compositional banding and within sheared felsic layers CS fabrics indicate top to west thrust movement.

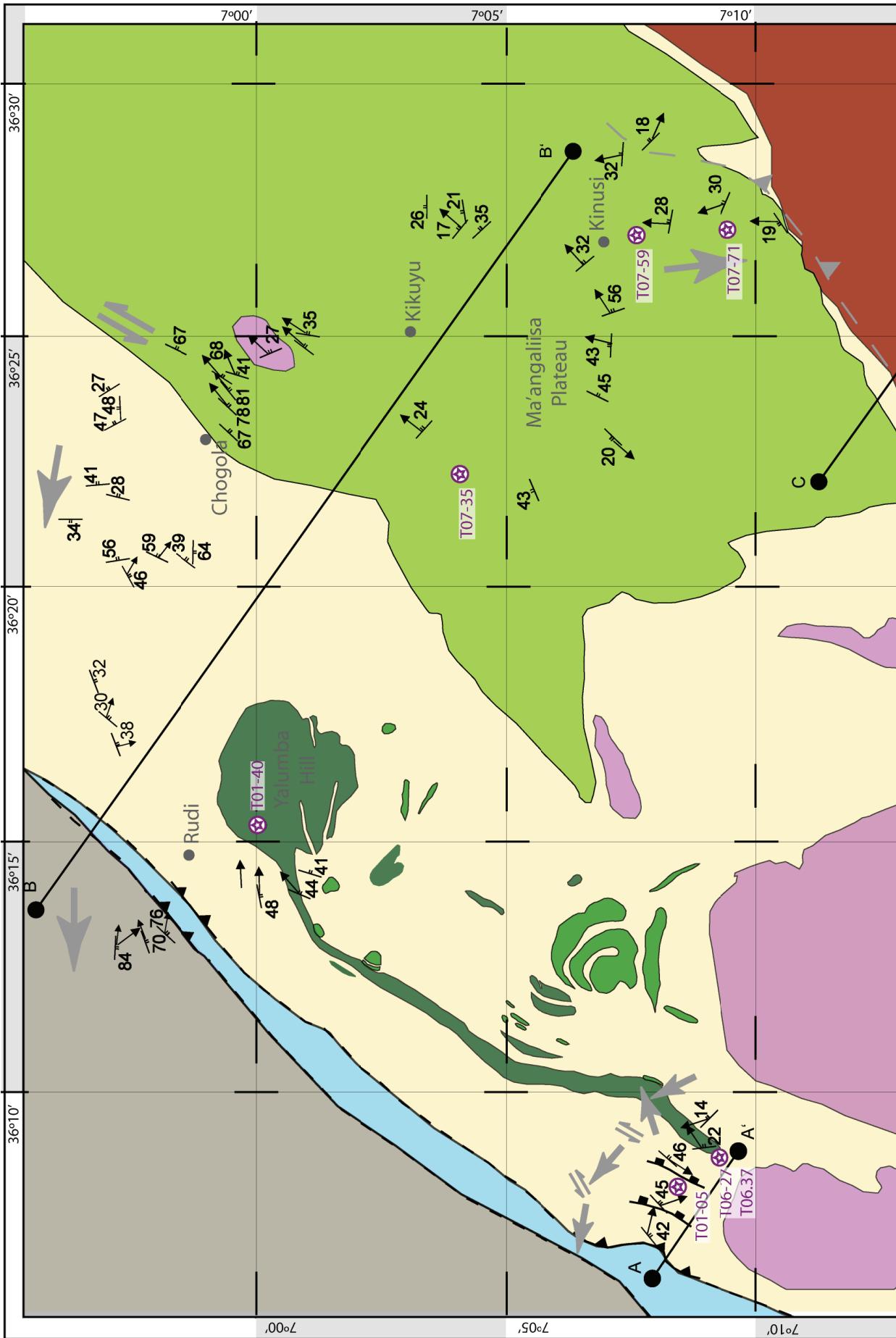
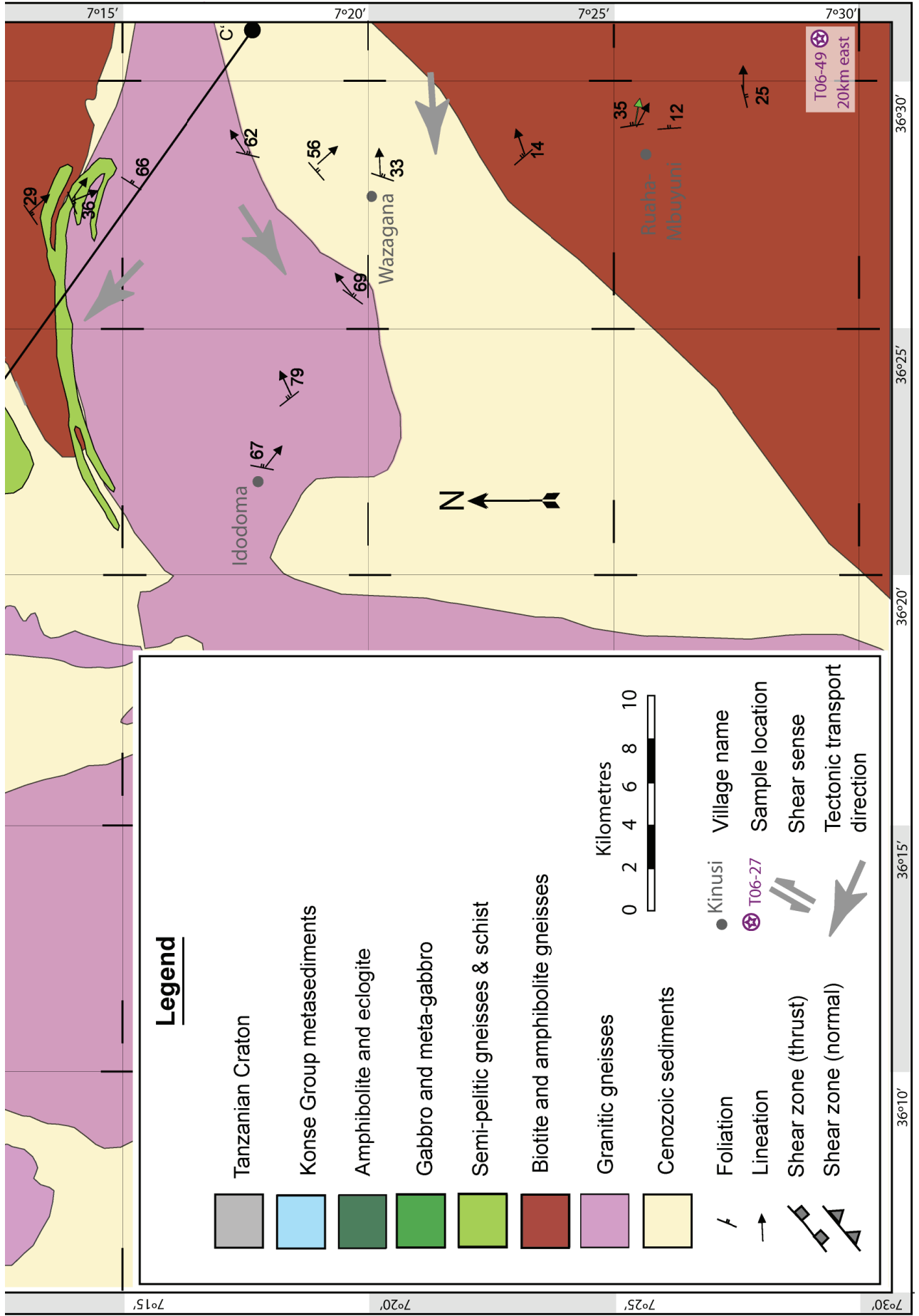


Figure 4.4 Map showing representative structural data, sample locations and place names referred to in this study. Base geology is from Tanzanian geological survey maps (King, 1955; Meinhold and Venzlaff, 1965; Whittingham, 1959) .





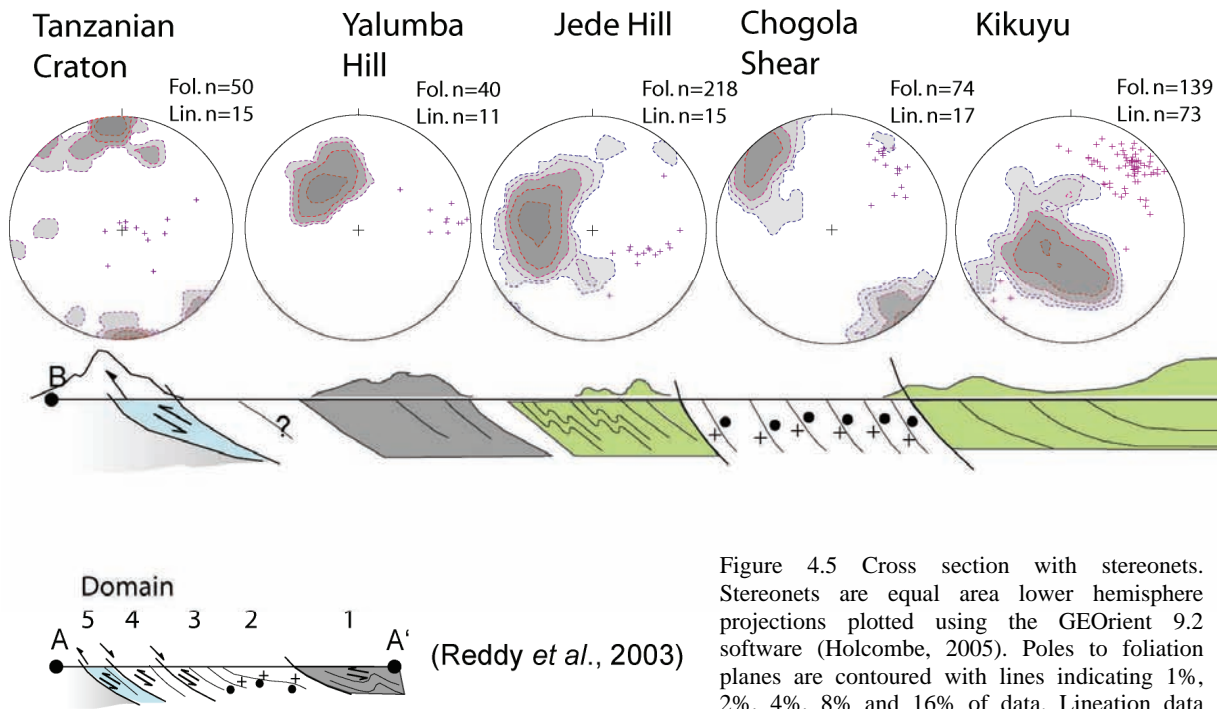


Figure 4.5 Cross section with stereonets. Stereonets are equal area lower hemisphere projections plotted using the GEORient 9.2 software (Holcombe, 2005). Poles to foliation planes are contoured with lines indicating 1%, 2%, 4%, 8% and 16% of data. Lineation data indicated by purple +.

#### 4.4.1.4 Jede Domain

The next domain east is the Jede domain, in which biotite bearing felsic gneiss is the dominant rock type. Foliations are generally ESE dipping (mean foliation= $41^{\circ}/095$ ,  $n=218$ ,  $var=0.14$ ) and sub-parallel to compositional banding. Mineral lineations are poorly developed but where seen plunge to the E (mean lineation= $46^{\circ}/112$ ,  $n=15$ ,  $var=0.07$ ). Kinematic indicators seen in the western part of this domain include extensional crenulation cleavage fabrics (figure 4.6 b) and in the center of the domain folded gneissic layering with hinges plunging to the SE while lineations trend to the E (figure 4.6 a), both indicative of top to the west movement. In the east of this domain the foliation is axial planar to rare isoclinal folds (figure 4.6 a), and dips moderately to the SE. Fold hinges plunge moderately to the SE. Crenulation of the main east-dipping foliation is sometimes visible, producing a fabric which dips steeply ( $\sim 60^{\circ}$ ) to the SSE.

#### 4.4.1.5 Chogola Shear

South-west of Jede is the Chogola shear, an 8-10 km wide zone in which exposure is sparse, but where seen foliations plunge at  $75-85^{\circ}$  to the SE (mean foliation= $81^{\circ}/137$ ,  $n=74$ ,  $var=0.55$ ). The transition into this zone from the north involves a dextral rotation of foliations from dipping SE to S. Lineations are commonly well developed and trend towards the northeast (mean lineation= $26^{\circ}/043$ ,  $n=17$ ,  $var=0.03$ ). No kinematic indicators were observed. The rotation of foliations as you enter this zone suggests a zone of mostly dextral strike-slip movement. The timing of shearing is uncertain, but must be syn- or post-formation of the foliation. as the fabrics at the margins are rotated into the shear.

#### 4.4.1.6 Kikuyu domain

The Kikuyu domain is south of the Chogola shear. Foliations dip shallowly ( $10 - 50^{\circ}$ ) to the north and

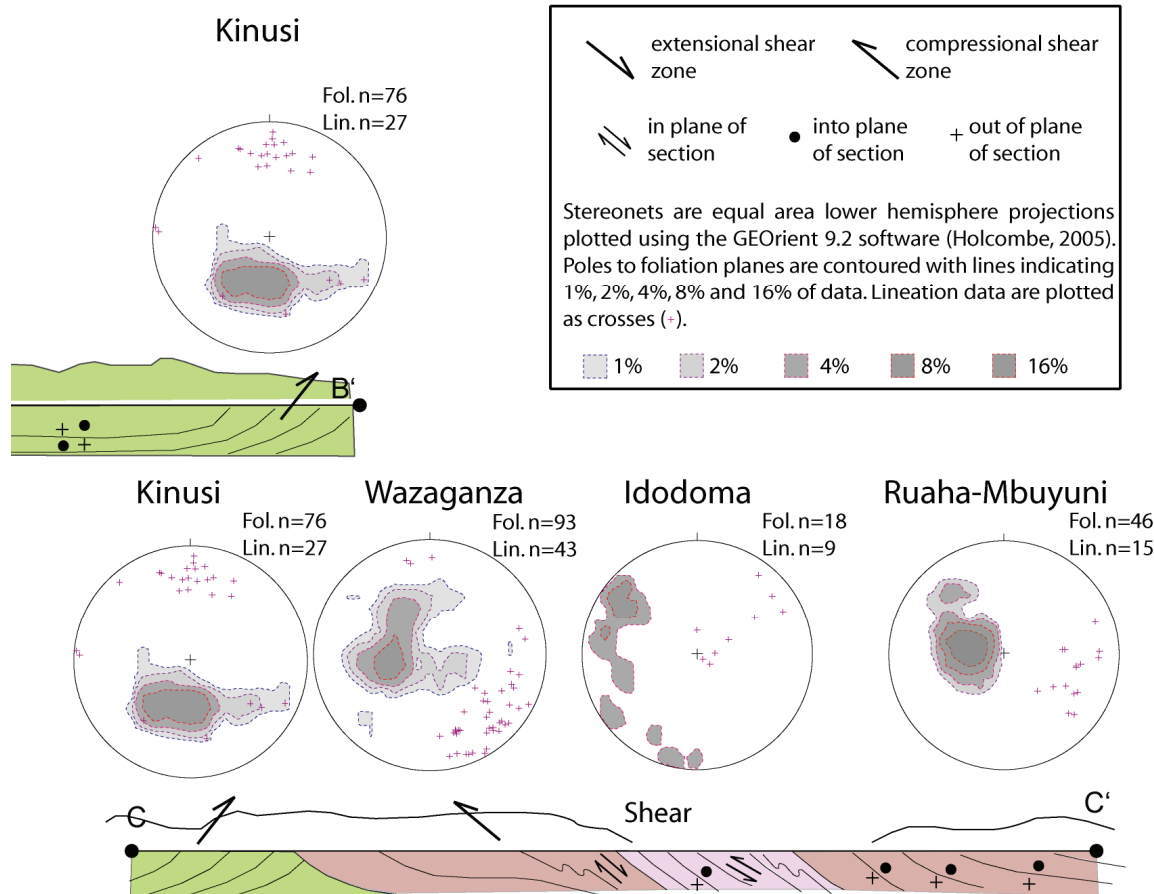
northeast (mean foliation= $23^{\circ}/018$ ,  $n=139$ ,  $var=0.13$ ). Lineations plunge shallowly towards the northeast (mean lineation =  $25^{\circ}/042$ ,  $n=73$ ,  $var=0.10$ ). A secondary cleavage overprinting these foliation is visible in places. This cleavage is near vertical ( $80 - 90^{\circ}$ ) and strikes roughly NNE-SSW. A body of granitic rock in this zone displays a nearly mylonitic fabric with a foliation dipping shallowly to the ENE and a very well developed lineation plunging shallowly to the NE. Intruded leucocratic melts are sometimes parallel to and at other times transgress the foliation.  $\delta$ - and  $\sigma$ -porphyroclasts are the most common kinematic indicators, however in the Kikuyu domain they are poorly developed and some suggest movement to the northeast while others indicate the opposite. In the south of the domain kinematic indications in the form of  $\sigma$ -porphyroclasts and cs fabrics indicated top-to-northeast movement, while some foliation parallel shears with rotated fabrics and dislocated melt veins indicated top-to-southwest movement.

#### 4.4.1.7 Kinusi domain

The Kinusi domain is defined by a change in orientation of foliations and lineations from the village of Kinusi south. Foliations dip moderately to the north or slightly northwest (mean foliation= $32^{\circ}/013$ ,  $n=76$ ,  $var=0.10$ ), and lineations trend to the north (mean lineation= $22^{\circ}/358$ ,  $n=27$ ,  $var=0.33$ ). Coarse grained garnet-biotite-kyanite gneiss is interlayered with quartz-feldspar  $\pm$  biotite gneiss. The felsic layers often preserve isoclinal folds, with the axial surface parallel to foliation and hinges plunging moderately to the NNE. In places the felsic gneiss displays clearly metaigneous textures with porphyroclasts of feldspar in a fine grained matrix.  $\delta$  and  $\sigma$ -prohyroclasts indicate top to S movement (figure 4.5 c).

#### 4.4.1.8 Wazaganza domain

The Wazaganza domain is named after the closest



village which is situated at the southern end of the mountain pass. The transition between the Sasimo and Wazaganza domains is gradual and is seen in a separation of low-strain and high-strain fabrics over 2-3 km's, with fabrics switching from low- to high-strain. This separation could be clearly seen within single outcrops, and is shown in figure 4.6 b. The low strain event produced the earlier foliation with steeply dipping fabrics dipping generally to the E or ENE (mean foliation=63°/79, n=57, var=0.11) and sometimes overturned to dip to the west. A weak lineation is associated with this fabric. A second later fabric was formed by a higher strain event in this zone, with a foliation dipping moderately to the southeast (mean foliation=27°/142, n=24, var=0.14) and lineations defined by elongation of plagioclase also trending to the southeast (mean lineation=20°/142, n=31, var=0.24). Earlier low-strain fabrics are folded by the high strain event, and rotated into the high-strain fabric. Kinematics of the high-strain event are indicated by  $\sigma$ -porphyroclasts and indicate top-to-northeast movement. Syn-deformational melt formation is associated with the later high strain fabric with melt leucosomes parallel to the fabric and folded by the event (figure 4.5 d).

#### 4.4.1.9 Idodoma domain

The Idodoma is characterised by moderate to steep east-southeast dipping foliations (mean foliation=63°/106, n=18, var=0.28) and northeast dipping lineations (mean lineation=55°/55, n=9, var=0.14). Top to west kinematics are indicated by  $\sigma$ - and  $\delta$ -porphyroclasts (figure 4.5 e). No folding or secondary cleavages were observed.

#### 4.4.1.10 Ruaha-Mbuyuni domain

Outcrop becomes sparse for approximately 10km's between the base of the Usagara Mountains and the start of the Udzungwa mountains. In the Udzungwa mountains foliations dip moderately to steeply towards the east (mean foliation=28°/102, n=46, var=0.05) and lineations trend to the east (mean lineation=35°/107, n=15, var=0.06). Poorly developed kinematics indicate top to the west movement. Amphibolite layers are sometimes boudinaged within the layered and foliated felsic gneiss. Amphibolite layers vary from cm- to m-scale, and sometimes stacked layering of amphibolite is seen (figure 4.5 e & f). In some locations (ie. road cuttings on Iringa-Morogoro Road) mafic melt can be seen to have intruded the felsic package, been subsequently deformed with top to NW kinematics indicated by  $\delta$  shaped boudins, anatectic melt has formed within the boudins and been subsequently deformed, and a later generation of mafic melt which also intruded the felsic volcanics displays a weak foliation (figure 4.6 c). Brittle deformation of mafic dykes is seen in some road cuttings (figure 4.5 h).

#### 4.4.2 Deformational phases

##### 4.4.2.1 D<sub>1</sub> deformation

The first phase of deformation stage produced a compositional layering (S<sub>1</sub>) seen throughout this section wherever subsequent deformational overprinting is weak, such as in the hinges of D<sub>2</sub> folds. In the Kikuyu, Wazaganza and Ruaha-Mbuyuni domains compositional banding in igneous rocks, seen at a cm to meter scale is interpreted to be tectonic in origin. This is similar to the





Figure 4.6. a) Jede domain 1-2 m isoclinal folds and b) ECC fabrics and shear sense are consistent with transpression during oblique convergence. c) Kinusi domain top-to-S kinematics. d) small scale folding and shearing with syn-deformational melt formation in the Wazaganza domain. e) Top-to-E kinematics in Idodoma domain. f) 30m high stacked amphibolite dykes, g) multi-phase plastic deformation and h) brittle deformation in the Ruaha-Mbuyuni domain.



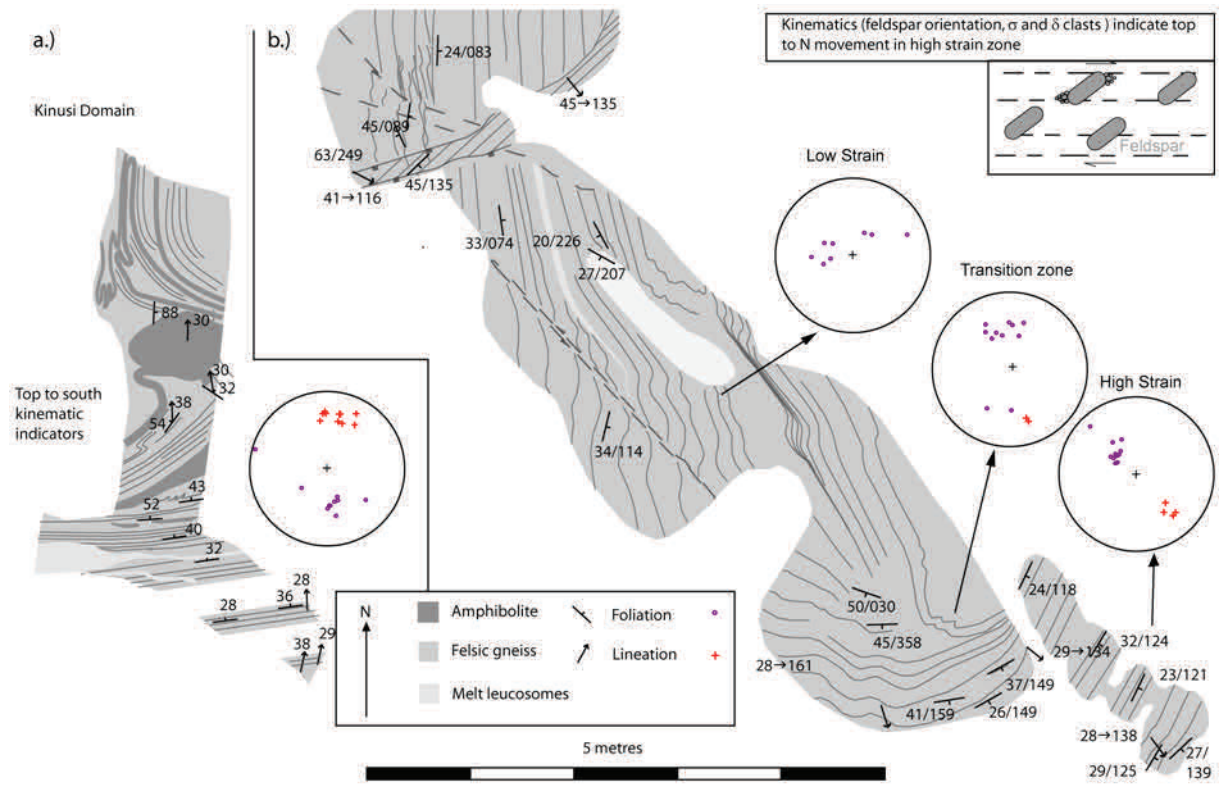
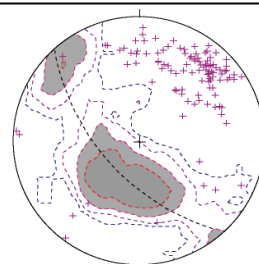


Figure 4. 7 Outcrop sketches for the a) Kinusi and b) Wazaganza domains showing general trend of foliations and relationship of melt leucosomes. c) Stereonet showing combined structures for the Kikuyu and Kinusi domains



Fol. n=289

Mean Principal Direction = 63-198  
 Mean Resultant dir'n = 68/221  
 Mean Resultant length = 0.72  
 (Variance = 0.28)  
 Calculated. girdle: 66/227

Lin. n=117

Mean Principal Direction = 25-037  
 Mean Resultant dir'n = 30/036  
 Mean Resultant length = 0.83  
 (Variance = 0.17)  
 Calculated. girdle: 25/035

$D_1$  described by Mruma (1989) and Reddy et al. (2003).

#### 4.4.2.2 $D_2$ deformation

The second phase of deformation seen by each domain is compressional producing a well defined foliation ( $S_2$ ) mylonitic in places and often accompanied by a lineation ( $L_2$ ) defined by elongate kyanite, plagioclase and amphibole. This foliation is axial planar to tight isoclinal folds ( $F_2$ ) in the Jede and Kinusi domains which affect  $S_1$  compositional banding. No systematic relationship was observed between fold hinges and lineations. Where seen pegmatites are sometimes parallel to  $S_2$ , while in other locations they occur both refolded by and axial planar to  $F_2$  folds indicating that melt formation was syn-deformational.

The orientation of  $D_2$  structures is highly variable from domain to domain. In the Jede domain  $D_2$  produced shortening in a WNW-ESE direction with overall top to WNW movement. The Chogola domain experienced shearing, most likely at this time but possibly as a result of  $D_5$ . In the Kikuyu and Kinusi domains shortening produced a large 10-20 km scale fold, with the Kinusi forming the southern limb of a NE plunging antiform, the northern limb of which is affected by shearing in the Chogola domain. Top to S kinematics in the Kinusi domain are the result of flexural slip between metasedimentary layers. Ambiguous kinematics in the core of the fold are due to SW-NE stretching.

The Wazaganza, Idodoma and Ruaha-Mbuyuni domains also experienced  $D_2$  shortening, however the orientation of structures varies between domains, with NW-SE shortening in the Wazaganza domain, WSW-ENE shortening in the Idodoma and E-W in the Ruaha-Mbuyuni domain. The timing of  $D_2$  in these domains is uncertain, as they fall between the dated Usagaran fabrics in the Kinusi domain and the East African metamorphism further south-east. Deformation could have occurred during either the Usagaran or East African orogens.

#### 4.4.2.3 $D_3$ deformation

The third phase of deformation phase described by Reddy et al. (2003) produced meter scale tight overturned NW verging isoclinal folds which refolded  $S_2$  and  $F_2$  in domains 1 & 2 of their traverse. Domain 1 is precisely equivalent to the Luhomero domain of this study and domain 2 roughly equivalent to the Jede domain of this study however no  $F_3$  folding was observed in the northern exposure of these domains. In both the Luhomero and western Jede domains  $D_3$  CS' fabrics were observed, indicating top-to-NW movement in both domains. In the eastern Jede domain  $S_2$  fabrics were crenulated by a steep SE dipping crenulation cleavage ( $S_3$ ).

In the eastern end of this traverse the third deformation phase produced a high-strain fabric ( $S_3$ ) which rotates



the  $S_2$  foliation in the Kinusi and Wazaganza domains into a generally moderately SE dipping foliation ( $S_3$ ) with a well developed lineation ( $L_3$ ) (figure 4.6 a & b).

In the Chogola domain a near vertical NNE dipping cleavage is seen.

In the Kikuyu domain the foliation developed in weakly deformed granite is inconsistent with the  $D_2$  foliation seen to either side. A moderate NE dipping foliation ( $S_3$ ) and lineation ( $L_3$ ) formed and stacked feldspar phenocrysts in a small shear indicate top to NE kinematics.

#### 4.4.2.4 $D_4$ deformation

$D_4$  deformation, as described by Reddy et al. (2003), involves an extensional event seen in the Ngerengengere gorge outcrops of the the Isimani suite with greenschist facies metamorphic assemblages. These structures and assemblages were not seen in this section, however nowhere through the 60 km traverse was outcrop exposure so expansive as that seen within the gorge section.

#### 4.4.2.5 $D_5$ deformation

The  $D_5$  event described by Reddy et al (2003) involved a compression event which thrust the Konse Group metasediments over the Tanzanian craton and Isimani suite, with associated greenschist facies metamorphic assemblages. Thrusting is dated by Ar-Ar thermochronology at ~640 Ma (Reddy et al 2004) based on shear zones between the Konse Group, Tanzanian craton and Isimani suites.

Within the traverse mapped within this study no contact was observed between the Konse Group, Tanzanian craton and Isimani suites, however top-to-W kinematics were observed within the Luhomero lithodeme and Jede domains, indicating thrusting towards the west, with actinolite shears in the eclogitic rocks and C' structures preserved in muscovite and biotite in the Jede domains. In the eastern end of the traverse, thrusting of the Wazaganza domain over the Kinusi domain produced greenschist facies (actinolite) shears in amphibolites.

#### 4.4.4 Distribution of bulk strain and strain type

Strain distribution through the section was highly variable. Within the eclogite body (Luhomero domain) non co-axial strain produced small scale top to W actinolite shears. In the Jede domain change from top to west kinematics in the west to isoclinal folding in the east is indicative of a change from non-coaxial strain and top to west movement in the west through to co-axial strain with shortening but no movement in the east. In the Chogola domain non co-axial dextral strain resulted in a wide (~10km) dextral shear zone, the timing of which is uncertain. In the Kikuyu domain strain was coaxial producing large scale folding, while non-coaxial strain resulted in thrusting of the Kinusi domain over the Kikuyu, and the Wazaganza over the Kinusi domain.

#### U-Pb Geochronology

Seven samples were selected for U-Pb zircon geochronology from widely spaced locations along the structural traverse. One sample came from the Konse Group, two from the Isimani Suite in the Gengeregengere gorge from adjacent to the tail of the eclogite body on the

path of the structural traverse of Reddy et al. (Reddy et al., 2003), one from the Ma'angalisa plateau, two from south of the village of Kinusi, and one from the bed of the Great Ruaha river at the most south-easterly point of the traverse. All location co-ordinates are given in longitude and latitude using the WGS 1984 datum.

#### 4.5.1 Analytical methods – LA-ICPMS geochronology

Zircons were separated from crushed rocks samples by magnetic and heavy liquid separation, then grains were handpicked and mounted in epoxy discs. The mounts were carbon coated then imaged using a CL detector fitted to a Phillips XL20 scanning electron microscope at a working distance of 13.5mm and using an accelerating voltage of 10kV (Figure 4.8). Zircon U-Th-Pb analyses for all samples were undertaken by LA-ICPMS at Adelaide Microscopy, University of Adelaide on an Agilent 7500cs ICPMS fitted with a New Wave 213 nm neodymium-yttrium-aluminium-garnet (Nd-YAG) laser. Beam diameter was set at 30  $\mu$ m using a repetition rate of 15 Hz. U-Pb fractionation was corrected using the GEMOC GJ-1 zircon (TIMS normalization data  $^{207}\text{Pb}/^{206}\text{Pb} = 608.3$  Ma,  $^{206}\text{Pb}/^{238}\text{U} = 600.7$  Ma,  $^{207}\text{Pb}/^{235}\text{U} = 602.2$  Ma (Jackson et al., 2004)). Standard GJ-1 was run 4 times at the beginning and end of a run, interspersed by two analyses of the in-house Sri Lankan zircon standard (BJWP-1,  $^{207}\text{Pb}/^{206}\text{Pb} = 720.9$  Ma (Wade et al., 2008)) and ten analyses of unknowns. Total acquisition time per analysis was 90 seconds; 50 seconds background measurement followed by 40 seconds of sample ablation. Data was processed using GLITTER software (Van Achterbergh et al., 2001). Age calculations and data manipulation were conducted using the computer program ISOPLOT

Th/U ratios are plotted against  $^{207}\text{Pb}/^{206}\text{Pb}$  age for all >90% concordant analyses in each sample (figure 4.9), corrected for fractionation using the formula listed in the caption to Figure 4.8, where  $F_{\text{GJ B1}}$  and  $F_{\text{GJ B2}}$  are the fractionation factors for GJ's in the blocks at the start and end of the unknown analyses,  $n$  is the number of unknowns since the last standard analyses,  $N$  is the total number of unknowns between GJ standards,  $\text{Th}/\text{U}_{\text{unk}}$  is the calculated Th/U ratio for the unknown and  $\text{Th}/\text{U}_{\text{unk raw}}$  is the uncorrected ratio calculated for the unknown analyses.

#### 4.5.2 Sample details

A quartzite sample from the Konse Group (sample T01-37) was taken from the Gengeregengere Gorge (E 176009, N 9209884). Sample T06-37 is a felsic gneiss from the Gengeregengere Gorge section (E 36°09'03.258, N 7°8'46.537) and is part of the Isimani Suite. The sample comprised quartz with minor biotite and accessory plagioclase, muscovite and arfvedsonnite. Also from the gorge section, sample T06-27 is a metapelite from the Isimani Group (E 36°9'33.750, N 7°8'55.179). The peak assemblage is plagioclase, kyanite, garnet and ilmenite with minor retrograde biotite and chloritoid.

Sample T07-35 come from the Mang'alisa Plateau (E 36°23'51.487, N 7°3'15.605) and comprises around 75% large anhedral quartz with randomly oriented subhedral biotite and cleavage. There is some chlorite alteration of biotite. Samples T07-59 and T07-71 come from the

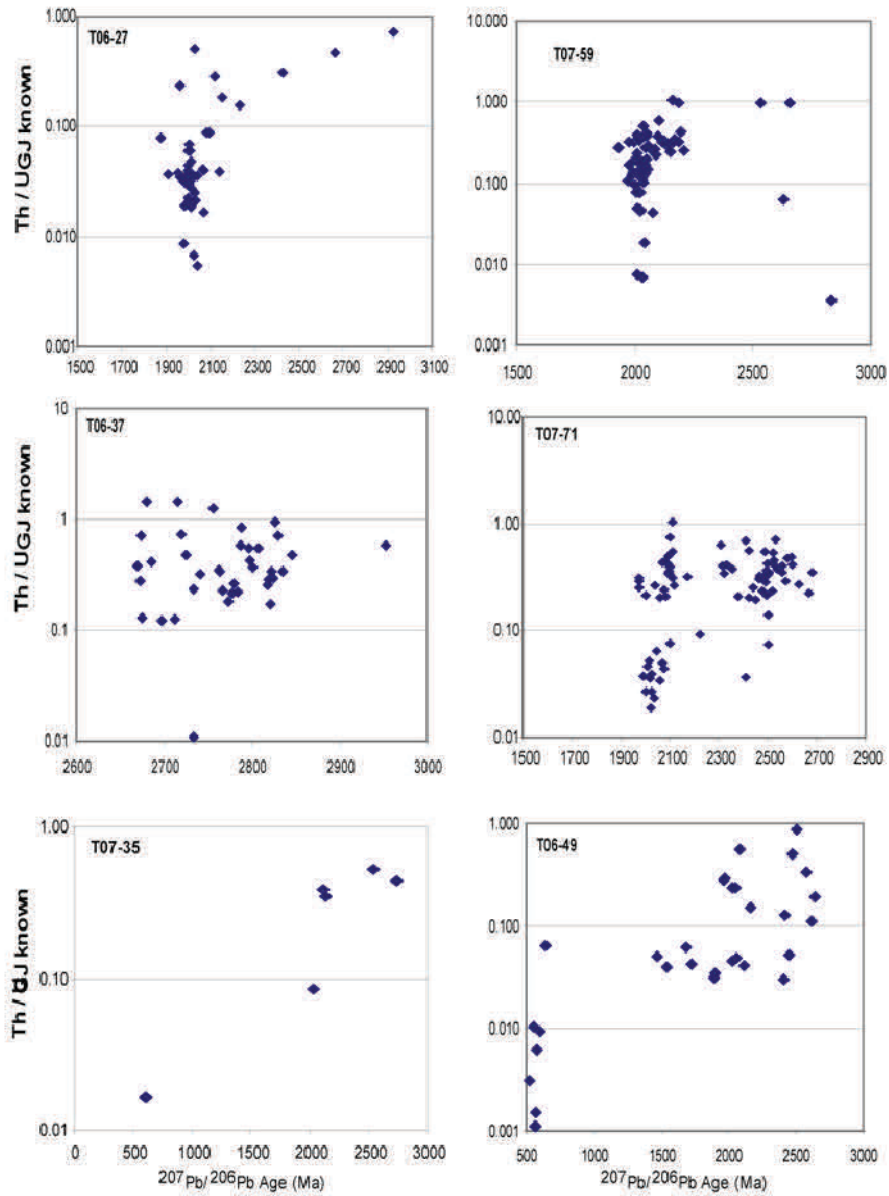


Figure 4. 8 Corrected Th/U plotted against  $^{207}\text{Pb}/^{206}\text{Pb}$  age. Correction performed using the formula:

$$Th / U_{unk} = \left( \frac{1}{Mean (F_{GJ B1}) + \left(\frac{n}{N}\right)[Mean (F_{GJ B2}) - Mean (F_{GJ B1})]} \right) * \frac{Th}{U_{Unk raw}}$$

Kinusi-Ruaha Mbuyuni Road and are both biotite-plagioclase-garnet pelites (E 36°29'19.245, N 7°9'19.038 and E 36°29'48.147, N 7°9'28.632 respectively). T07-59 contains abundant large quartz and rare plagioclase. A fabric is defined by aligned biotite and kyanite. Around 5% garnet is present with grains of up to 0.7 cm in diameter. Garnet is poikiloblastic with inclusions of quartz, biotite and ilmenite. Sample T07-71 contains approximately 50% euhedral biotite which, along with kyanite, defines the foliation. Anhedral quartz is abundant. Garnet is up to 0.5 cm, poikiloblastic with quartz inclusions and is fractured with biotite occurring in the fractures. Fine grained plagioclase and ilmenite make up <5% of the rock.

Sample T06-49 comes from the bed of Great Ruaha River about 10km southeast of Ruaha-Mbuyuni next to the Morogoro Road (E 36°39'33.583, N 7°31'28.086). It is

a pelitic rock with 0.5 – 1 cm garnets and kyanite. A strong foliation is defined by biotite, muscovite and kyanite in a matrix of quartz, plagioclase and ilmenite.

#### 4.5.3 Geochronology results

Zircon U-Pb-Th data for all samples are reported in table 4.1 and plotted as concordia and probability density plots in figure 4.10. All errors are reported at 2σ confidence. Ages reported are  $^{207}\text{Pb}/^{206}\text{Pb}$  ages unless otherwise stated. Concordance reported is obtained by the percentage difference between  $^{206}\text{Pb}/^{238}\text{U}$  and  $^{207}\text{Pb}/^{206}\text{Pb}$  ages. It should be noted that for robust statistical treatment a sample population of at least 117 zircons is ideal (Anderson, 2004; Versmeech, 2004). From each sample as much zircon as possible was extracted from a 1-2 kg sample, stopping only when at least 120 grains were obtained. Only two samples (T07-71 & T01-37) contained over 120 grains of zircon. This means that the



Figure 4.9 Cathodoluminescence images of zircons

remaining samples may contain populations which were not sampled in this study.

Sample T01-37, a quartzite, contains abundant prismatic zircon which was largely unfractured. Grains preserve aspect ratios between 3:1 and 5:1. CL imaging reveals oscillatory growth zoning in all grains. LA-ICPMS U-Pb analysis was conducted at 14 spots on 14 grains. Previous SHRIMP U-Pb analysis of zircon from this sample (Collins, unpublished) provided similar data, however that data was unavailable for inclusion in this thesis. Of the 14 LA-ICPMS analyses, 10 yielded ages with greater than 90% concordance. On a concordia diagram all analysis plot along a single discordia (figure 4.9a) with an upper intercept at  $2718 \pm 24$  Ma (MSWD=1.4). A weighted average of the 8 analyses with greater than 95% concordance yields an age of  $2723 \pm 44$  Ma (MSWD=5.0,  $p=0.00$ ).

Sample T06-37, a felsic gneiss, yielded abundant zircon. CL imaging revealed well developed oscillatory growth zoning. U-Pb-Th analysis was conducted on 107 spots on 100 zircon grains. 48 of these analyses were greater than 90% concordant. All analysed points demonstrated Th/U ratios greater than 0.1, and generally low CL responses. Grains on which multiple spots were targeted had high CL response rims and in all cases the rim yielded an age within error of the grain core. This suggests that all ages obtained represented crystallisation ages. Five main peaks were observed in the data (Figure 4.10b), with 3 additional ages represented by one grain each ( $2374 \pm 18$  Ma,  $2568 \pm 17$  Ma,  $2457 \pm 17$  and  $2953 \pm 16$  Ma). The spread of ages between 2600 and 2900 Ma, representing 71 concordant grains, can be separated into four peaks in the age

spectra. These occur at  $2679 \pm 4$  Ma (16 grains, MSWD=1.4,  $p=0.12$ ),  $2727 \pm 5$  Ma ( $n=15$ , MSWD=1.6,  $p=0.085$ ),  $2778 \pm 5$  Ma ( $n=20$ , MSWD=3.8,  $p=0.00$ ) and  $2821 \pm 5$  Ma ( $n=20$ , MSWD=3.0,  $p=0.00$ ). Based on the statistics none of these peaks is likely to represent a single aged rock source.

Sample T06-27, a metapelite, yielded a small number of largely fractured zircons. Some unfractured prismatic zircon remained with aspect ratios of 3:1. Numerous small euhedral zircons were also present. CL imaging revealed growth zoning in prismatic zircon, with low CL response rims common. Euhedral zircon was unzoned and generally had low CL response. U-Pb analyses were conducted on 56 spots on 53 grains. A group of analyses (Figure 4.10b) coming from both small grains and rims with low Th/U and low CL response is interpreted to indicate the age of metamorphism  $2007 \pm 4$  Ma ( $n=33$ , MSWD=2.5,  $p=0$ ). A second population with similar Th/U ratios and CL response yielded a slightly younger age of  $1970 \pm 10$  Ma ( $n=9$ , MSWD=1.4,  $p=0.21$ ). A third peak in the ages spectra is comprised of analyses from grain cores and yields an age of  $2087 \pm 8$  Ma ( $n=8$ , MSWD=4.0,  $p=0$ ). Additional concordant data yielded ages represented by single grains at  $2231 \pm 19$  Ma,  $2425 \pm 20$  Ma,  $2660 \pm 19$  Ma and  $2927 \pm 30$  Ma.

Sample T07-35, a kyanite biotite schist, yielded little zircon and grains were frequently broken. Aspect ratios ranged from 1:1 to 3:1. CL imaging revealed oscillatory zoning in most grains. 4 grains had low CL response rims. U-Pb analysis of 26 spots on 22 grains yielded only 6 grains with greater than 90% concordance (Figure 4.10a). Analyses of rims yielded only one concordant  $^{206}\text{Pb}/^{238}\text{U}$  age of  $569 \pm 10$  Ma, however two of the





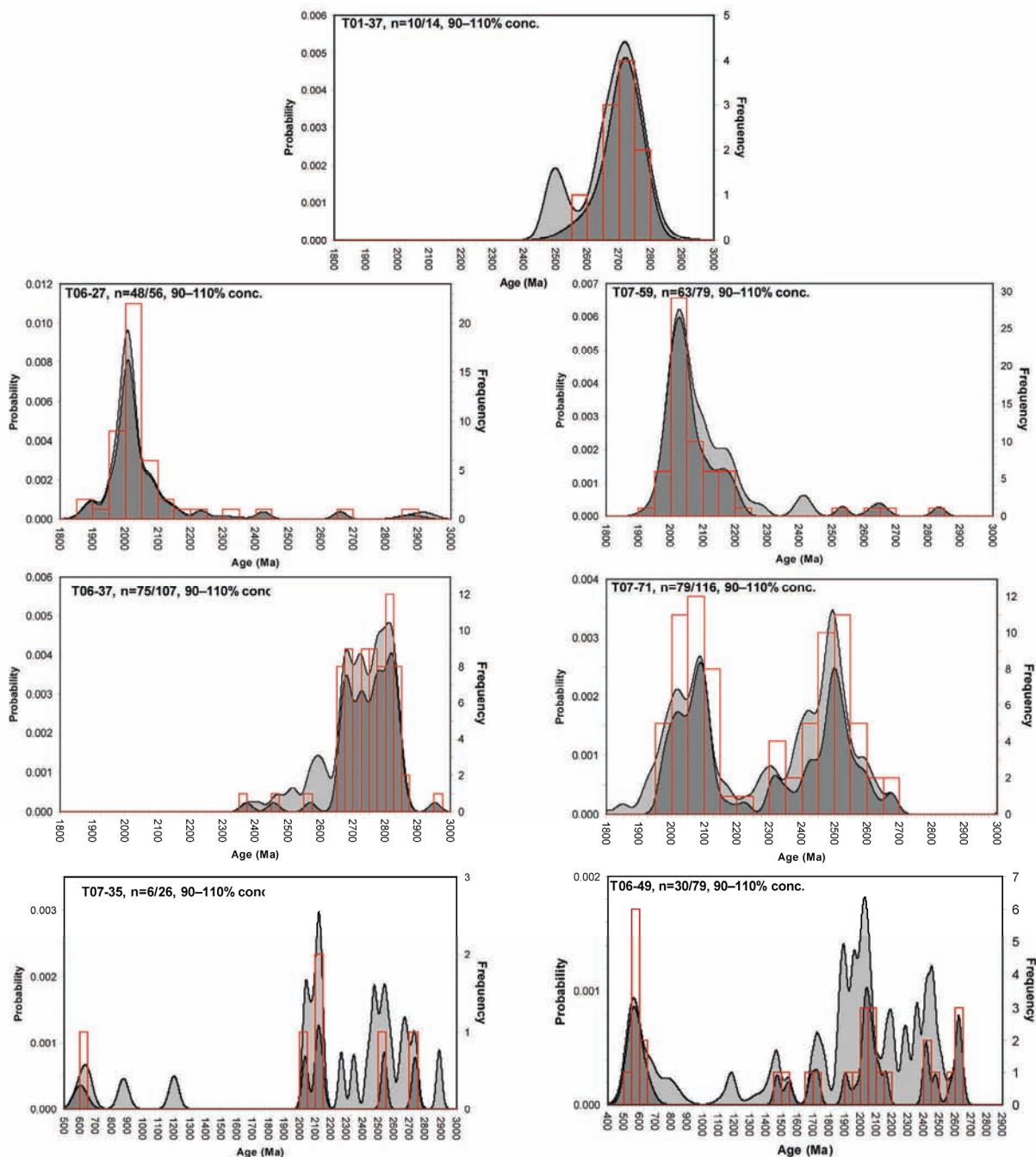


Figure 4.10 (continued) b) Probability density plots. . Histograms and dark grey spectra show >90% concordant data, light grey spectra includes all data.

concordance (30 with greater than 95%). The youngest yielded an age of  $1931 \pm 29$  Ma and was statistically distinct from older populations. Peaks in the age spectra (Figure 4.10b) for these rims formed three Palaeoproterozoic populations at  $1980 \pm 18$  Ma ( $n=5$ ,  $MSWD=0.69$ ,  $p=0.6$ ),  $2016 \pm 8$  Ma ( $n=22$ ,  $MSWD=0.81$ ,  $p=0.71$ ) and  $2055 \pm 17$  Ma ( $n=3$ ,  $MSWD=0.71$ ,  $p=0.49$ ). Analyses of grain cores yielded 43 data with greater than 90% concordance (32 with greater than 95%). Six grains yielded ages greater than 2400 Ma. Two of these for a peak in the age spectra at  $2646 \pm 17$  Ma ( $MSWD=2.1$ ,  $p=0.15$ ). The remaining ages, between 2000 and 2220 Ma, form three peaks in the spectra at  $2040 \pm 7$  Ma ( $n=12$ ,  $MSWD=1.5$ ,  $p=0.13$ ),  $2102 \pm 7$  Ma ( $n=13$ ,  $MSWD=2.4$ ,  $p=0.004$ ) and  $2178 \pm 6$  Ma ( $n=12$ ,  $MSWD=4.5$ ,  $p=0$ ).

Sample T07-71, a metapelite, yielded abundant zircon.

Grains were mostly prismatic and unfractured with aspect ratios between 2:1 and 4:1. CL imaging revealed oscillatory zoning with some grains showing clear regrowth on rims with high CL response. U-Pb analysis was performed on 117 spots on 80 grains. Of the 27 rim analyses 22 yielded ages >90% concordant (18 < 95% concordant). One of these rim spots yielded a concordant age of  $2511 \pm 18$  Ma and another gave  $1941 \pm 24$  Ma, all remaining ages fell within two populations, one at  $2013 \pm 7$  Ma ( $n=12$ ,  $MSWD=2.0$ ,  $p=0.029$ ) and another at  $2065 \pm 9$  Ma ( $n=8$ ,  $MSWD=1.3$ ,  $p=0.24$ ). Of the 80 analyses conducted on grain cores 63 were <90% concordant. One single grain aged  $3040 \pm 18$  Ma did not fall into any population group. The remaining grains fell into two groups of populations (Figure 4.10b), one between 2300 and 2700 Ma, and one between 2230 and 1950 Ma. The older group can be broken into six smaller peaks in the



age spectra at  $2326 \pm 9$  Ma ( $n=5$ ,  $MSWD=4.2$ ,  $p=0.002$ ),  $2407 \pm 6$  Ma ( $n=11$ ,  $MSWD=4.8$ ,  $p=0.00$ ),  $2489 \pm 5$  Ma ( $n=18$ ,  $MSWD=2.2$ ,  $p=0.002$ ),  $2535 \pm 7$  Ma ( $n=10$ ,  $MSWD=2.4$ ,  $p=0.01$ ),  $2596 \pm 8$  Ma ( $n=6$ ,  $MSWD=3.7$ ,  $p=0.03$ ) and  $2675 \pm 13$  Ma ( $n=2$ ,  $MSWD=0.82$ ,  $p=0.36$ ). The younger group breaks into 2 peaks in the age spectra at  $1976 \pm 11$  Ma ( $n=3$ ,  $MSWD=0.0018$ ,  $p=0.998$ ) and  $2099 \pm 6$  Ma ( $n=14$ ,  $MSWD=0.79$ ,  $p=0.67$ ) and with 3 isolated grains aged  $2070 \pm 20$  Ma,  $2174 \pm 22$  Ma and  $2225 \pm 19$  Ma.

Sample T06-49 yielded sparse small zircons with aspect ratios between 1:1 and 1:2. CL imaging revealed sector zoning in all grains. U-Pb analysis was conducted on 81 spot on 80 grains. Concordant (<90%) ages were obtained for 34 spots with 17 <95% concordant. Neoproterozoic ages were obtained for 9 grains with low U/Th and CL responses, 7 of which form a population at  $569 \pm 17$  Ma ( $MSWD=0.27$ ,  $p=0.93$ ) giving an age for metamorphism in this sample. Five grains aged between 1470 and 1899 Ma do not form multiple-grain population peaks in the age spectra (Figure 4.10b). Small peaks in the spectra occurred at  $1969 \pm 19$  Ma ( $n=2$ ,  $MSWD=0.17$ ,  $p=0.68$ ),  $2027 \pm 13$  Ma ( $n=2$ ,  $MSWD=0$ ,  $p=1$ ),  $2053 \pm 12$  Ma ( $n=3$ ,  $MSWD=0.42$ ,  $p=0.66$ ),  $2417 \pm 12$  Ma ( $n=2$ ,  $MSWD=0.91$ ,  $p=0.34$ ),  $2464 \pm 13$  Ma ( $n=2$ ,  $MSWD=2.8$ ,  $p=0.093$ ) and  $2629 \pm 10$  Ma ( $n=3$ ,  $MSWD=2.5$ ,  $p=0.08$ ).

## 4.6 Discussion

### 4.6.1 Geochronology

#### 4.6.1.1 Timing of sediment deposition

Samples from this study come from at least two suites of metasedimentary rocks, the Konse and Isimani Suites (Figure 4.4). Determination of the maximum age of deposition for a sediment can be constrained using detrital zircon dating, or by dating structures which post-date the sediments. Fabrics which are seen in sample T06-37 and T06-27 for instance are cut by unfoliated pegmatites, one of which is dated in Collins et al. (2004) at  $1991 \pm 2$  Ma, providing a lower limit for sediment deposition and development of the D<sub>2</sub> fabric. In sample T06-37 the upper limit on the age of sedimentation is defined by the youngest zircons considered to have an igneous source. In this case a statistically robust population of igneous zircons has been dated at  $2679 \pm 4$  Ma providing a definite upper limit. A less robust upper limit on sedimentation is suggested by the presence of a handful of early Palaeoproterozoic grains, the youngest of which is 2370 Ma, however as this age is represented by only a single grain it may represent sample contamination or instrument error. Thus only ages represented by multiple zircons will be considered valid in this discussion although any individual zircons which would narrow the depositional window will be mentioned.

Of the Isimani Suite samples T06-37 has already been discussed. Sample T06-27 contains a population of zircon with metamorphic characteristics with an average age of  $2007 \pm 4$  Ma, providing an older lower limit on sediment deposition. The upper limit on deposition of this sediment is provided by a population of igneous zircon with an age of  $2087 \pm 8$  Ma. T07-59 is very similar to T06-27 in that it contains a metamorphic population at  $2016 \pm 8$  Ma defining a lower limit on sediment deposition

while the youngest igneous population defines a upper limit at 2040 Ma. In sample T07-35 the youngest igneous population is aged at  $2123 \pm 26$  Ma and the oldest metamorphic population at  $2037 \pm 13$  Ma give a window for sediment deposition between these ages.

Sample T07-71 has the most complex zircon age spectra. Grains with apparently metamorphic signatures form peaks at  $2013 \pm 7$  Ma and  $2065 \pm 9$  Ma would appear to indicate metamorphism of the sediment at this time. An igneous population aged  $2099 \pm 6$  Ma would provide an upper limit on sedimentation, however the presence of a  $1976 \pm 11$  Ma igneous population makes this timing for sedimentation and metamorphism impossible. When the igneous data are considered using a concordia plot anchored at 577 Ma (the age of East African metamorphism) rather than probability density, the ages obtained, while having unacceptably high deviations, are indicative of slightly older ages for these populations ( $2122 \pm 23$  Ma,  $MSWD = 79$  and  $2005 \pm 33$  Ma,  $MSWD = 43$ ). The wide errors on these ages would provide a narrow window for sedimentation between 2038 Ma (oldest possible age for the youngest igneous population) and the younger metamorphic event at  $2013 \pm 7$  Ma, but would require the older (~2065 Ma) metamorphic grains to be detrital. However if the metamorphic population is treated the same way as the igneous (using an anchored concordia) the younger age increases to  $2032 \pm 9$  Ma ( $MSWD = 2.3$ ,  $p = 0.027$ ), which narrows this sedimentation window to a maximum of 15 My. Alternatively the sediment could have been deposited at any time after this, with all metamorphic grains being detrital, however this option is considered to be less likely. This sample records the complex nature of metamorphism in the Usagaran with multiple metamorphic peaks and rapid exhumation and burial.

Sample T01-37 from the Konse group provides little constraint on the timing of sedimentation. The single zircon population is aged  $2718 \pm 24$  Ma so sedimentation must have occurred after this time, however with no metamorphic zircon growth or resetting the only lower limit on sedimentation comes from <sup>40</sup>Ar/<sup>39</sup>Ar dating of biotite and muscovite from the shear zone which separates the Konse and Isimani suite blocks. Cooling in this shear zone was dated at ~640 Ma (Reddy et al., 2004), which allows for sedimentation to have occurred at any time in the preceding ~2.0 Gy. The generally accepted minimum age of sedimentation in the Konse Group, 1.8 Ga, is provided by correlation with the Ndembera volcanic unit (Wendt et al., 1972).

The last sample, T06-49, comes from the south-eastern most point on the traverse in an area considered to be well within the Mozambique Orogen which experienced East African metamorphism in the Neoproterozoic. A population of metamorphic zircons with an age of  $569 \pm 17$  Ma provides a lower limit on sedimentation. The upper limit is weakly constrained by the youngest concordant igneous zircon, aged 1470 Ma, or more strongly constrained by the youngest igneous population aged 1899 Ma.

To summarise, deposition of the Konse group is constrained only as being sometime during the Proterozoic (between 2700 and 640 Ma). Sedimentary rocks in the west of the Usagaran were deposited

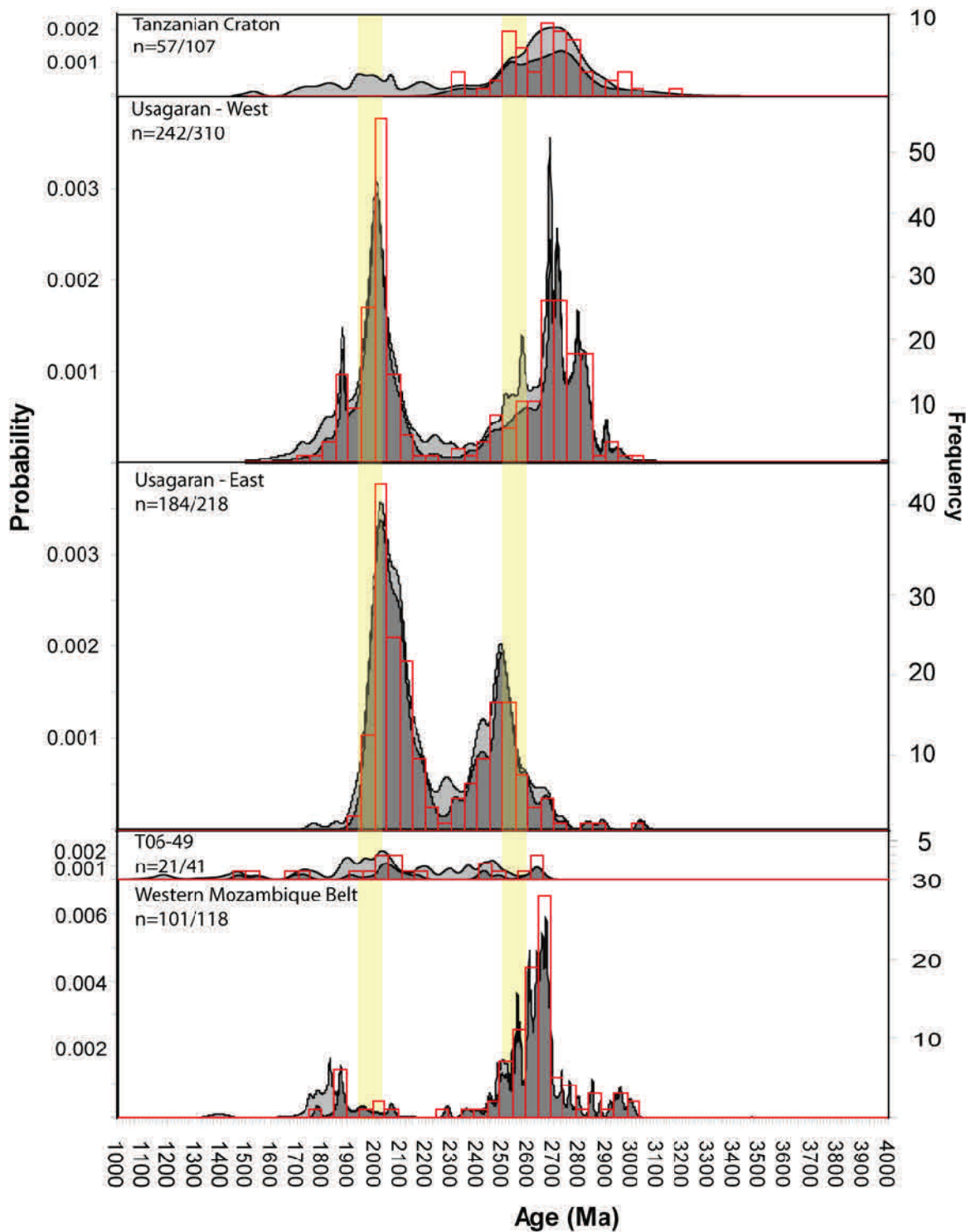


Figure 4.11 Probability density age spectra for the Tanzanian Craton, Usagaran Belt, and western granulites of the Mozambique Belt. Histograms and dark grey spectra show >90% concordant data, light grey spectra includes all data. Ages from this study and published

between  $2087 \pm 8$  Ma and  $2007 \pm 4$  Ma. Sediments in the east of the Usagaran were deposited between ~ 2040 and 2030 Ma, and the Mozambique Orogen sample was definitely deposited between 1980 Ma and  $569 \pm 17$  Ma, and probably after 1470 Ma.

#### 4.6.1.2 Provenance of sediments

The samples selected in this provenance study were pelitic metasedimentary rocks. These rocks are the most common in this part of the Usagaran, although compositions clearly vary between different locations. For the purpose of this discussion these samples have been

grouped, based on similar age spectra and location, into two groups and age spectra for these groups, the Tanzanian Craton and western granulites of the Mozambique Orogen are plotted in figure 4.11. The Western Usagaran group includes samples T06-27 and T06-37 as well as samples T01-05 and T01-19 from Collins et al (2004) which were collected from nearby. These samples preserve a strong 2.7 – 2.85 Ga population and a slightly smaller population at ~2.6 Ga. These Archaean populations are consistent with the Tanzanian Craton as a source region. A Palaeoproterozoic population contains zircon with

igneous characteristics aged between 2050 and 2100 Ma. This is consistent with the expected age of igneous activity that would be associated with subduction under the Tanzanian Craton in the early stages of the Usagaran Orogen, however no igneous rocks of this age have yet been dated. This is likely due to a lack of study rather than the absence of such rocks as there are significant mafic and felsic igneous rocks in the region which have not been dated. The main ~2.0 Ga peak is dominated by zircon with metamorphic characteristics.

The Eastern Usagaran samples include T07-35, T07-59 and T07-71 from this study. This group includes rare > 2.7 Ga grains, though not as many as are seen in the western samples. A ~2.6 Ga peak is seen which is consistent with the western group, however the dominant Archaean population at ~2.5 Ga is not seen in the west. The Palaeoproterozoic peak in this group of samples is stronger than in the west, and contains older zircon aged mainly between 2050 and 2200 Ma. As with the western grouping the ~2.0 Ga peak is dominated by metamorphic zircon, however unlike the western group the eastern contains igneous grains as young as 2.01 Ga. This may indicate that significant igneous activity, as yet unidentified, is associated with the earliest stages of the Usagaran, however the presence of a ~2.5 Ga peak does suggest that these sediments may be derived from multiple sources, involving both the Tanzanian craton and an unidentified terrane with ~2.5 Ga and 2.05 – 2.2 Ga rocks, or potentially not involving the Tanzanian Craton as a source at all.

Zircon crystallisation ages between 2.05 – 2.2 Ga are common in the West African and Amazonia cratons, and also seen in the South China, Central Africa and São Francisco cratons (Figure 4.12 ) (Condie, 2009). Of these cratons both the South China and Central African contain ~2.5 Ga peaks in the zircon age spectra, and the São Francisco contains a slightly older 2.55 Ga peak. Neither of the South China or São Francisco cratons is an ideal candidate as source region for these sediments. The São Francisco craton records a number of older peaks which are not evident in the Eastern Usagaran samples, while the South China block has only the two narrow peaks at ~2.1 and 2.5 Ga, and does not account for the wider spread of ages seen in the Eastern Usagaran. The Central African craton, sometimes referred to as the Congo craton, is made up of a number of smaller Archaean cratonic blocks, including the Tanzanian craton, and the younger orogenic Orogens which suture those blocks together. Most reconstructions show that during the Palaeoproterozoic the Tanzanian craton collided with the Central African craton, with the ~1.85 Ga Ubende Orogen as the suture. Under the constraints of these models the Central African craton would have to rotate over 90° in the 150 My between the Usagaran and Ubende orogens, making it an unlikely source region for Usagaran sediments. However the geochronological and thermochronological data presented in chapter three of this thesis raises the possibility that the Ubende orogeny occurred at ~1050 Ma, not 1850 Ma as previously thought. This frees the Tanzanian craton from the Central African craton during the Usagaran orogeny, and allows for the Central African craton to have been the previously unidentified impacting block in the ~2.0 Ga Usagaran orogeny.

Sample T06-49 is treated individually as it does not fit with either of the other groupings. Although relatively few concordant zircon were found in this sample it does contain a scattering of Archaean and Palaeoproterozoic grains consistent with the eastern Usagaran grouping. However the presence of several Mesoproterozoic igneous grains, the absence of significant ~2.0 Ga metamorphic zircon growth, and the dominant ~0.6 Ga metamorphic peak in this sample are more consistent with samples from the western granulite terrane of the Mozambique Orogen (Cutten, 2006; Vogt et al., 2006). This is consistent with the available geochronological data from the Western Granulite terrane of the Mozambique Orogen. The Archaean signature is similar to that seen from the Tanzanian Craton, and the Palaeoproterozoic zircons could be sourced from post-Usagaran granitoids (Wendt et al., 1972; (Maboko and Nakamura, 1996); Reddy et al., 2003; Sommer et al., 2005b). The source of ~1.4 Ga grains is more enigmatic as the only reports of this age from eastern Tanzania are inherited cores in Taita Hills orthogneiss (Hauzenberger et al., 2007).

#### *4.6.1.3 Timing of Usagaran deformation and metamorphism across the orogen*

The timing of eclogites facies metamorphism within the Usagaran has been constrained by SHRIMP U-Pb zircon dating to 1991.1 Ma; however the timing of amphibolite facies metamorphism in the surrounding gneisses is less well constrained. <sup>40</sup>Ar/<sup>39</sup>Ar thermochronology which aimed to date post-metamorphic cooling of the western Usagaran rocks instead identified heterogeneous excess argon, with a strong Pan African overprint in the few samples which produced usable ages (Reddy et al., 2004). Based on the U-Pb zircon data in this study the timing of peak metamorphism is different on either side of the orogen. In the gneisses closest to the eclogites body metamorphism occurred at 2007 ± 4 Ma. In the east of the orogen a more complex metamorphic history is recorded, with peak metamorphism occurring slightly earlier than in the west. Two samples record ~2060 Ma metamorphic zircon growth in the Kinusi domain, while all three samples record ~2030 Ma growth in both Kikuyu and Kinusi domains. The earlier metamorphic age obtained in the east of the orogen may be indicative of either these domains experiencing metamorphism earlier than the western Usagaran or of later exhumation of the western domains, possibly relating to exhumation from deeper within the orogen.

#### *4.6.1.4 Timing of "East-African" metamorphism*

The generally accepted age for East African metamorphism in the Mozambique Orogen is ~640 Ma, based on samples from the Eastern Granulites of the Mozambique Orogen (Maboko et al., 1985; Möller et al., 2000) and metamorphism is suggested to have occurred prior to the final collision of East and West Gondwana (Möller et al., 2000). The metamorphic age of 569 ± 17 Ma obtained from sample T06-49 in this study is more consistent with the metamorphic ages obtained from the Western Granulite terrane, as could be expected based on the proximity of parts of the western granulite terranes (Cutten et al., 2006; (Sommer et al., 2005b)). An almost identical age (569 ± 10 Ma) was obtained from one zircon in sample T07-35 from the Kikuyu domain,

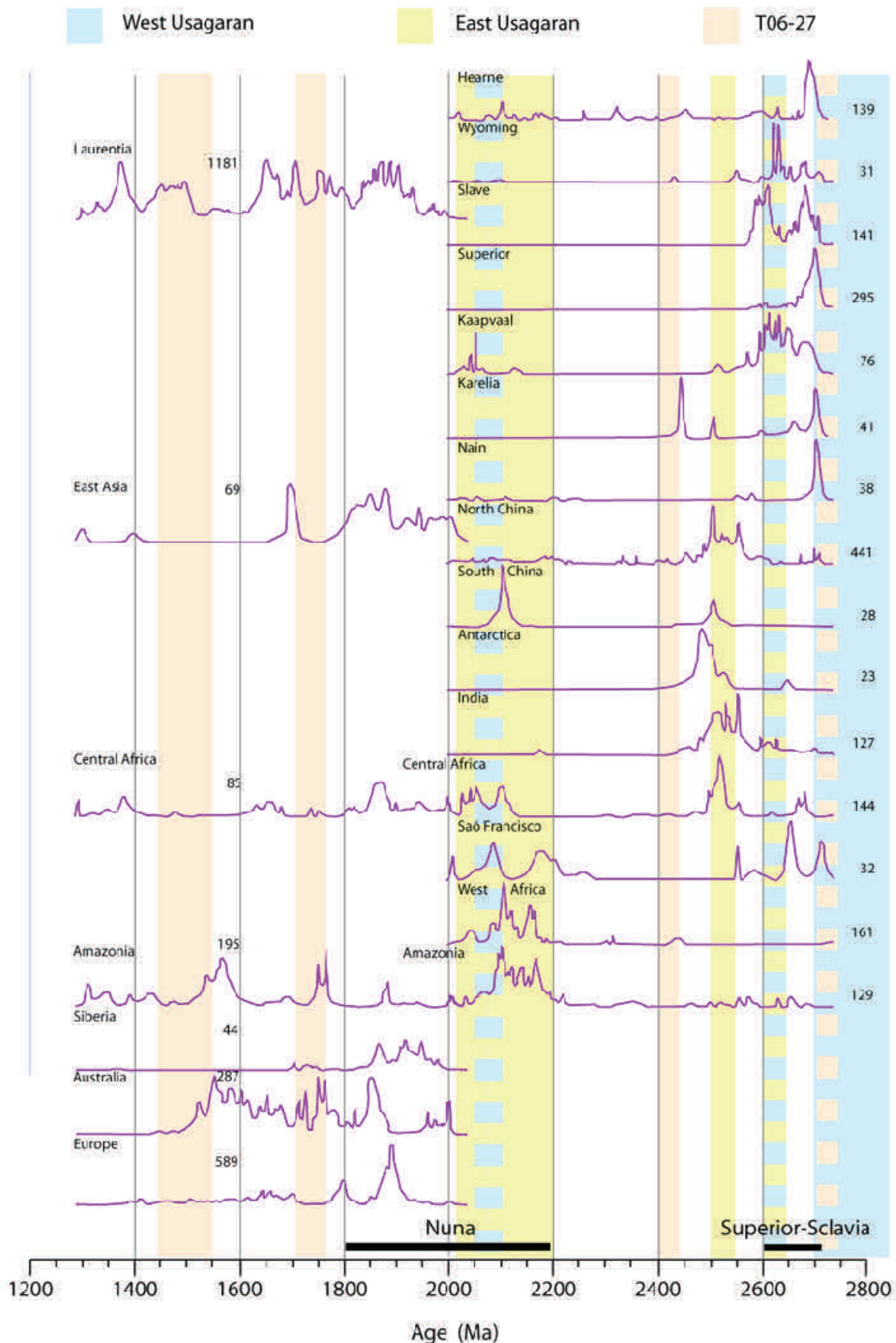


Figure 4. 12 Global zircon age spectra showing main cratonic blocks through time. Highlighting indicates timing of age peaks in Usagaran Orogen with colours indicating which terrane.

indicating that late East African metamorphism impacted at least the eastern Usagaran Orogen.

#### 4.6.2 Structural evolution of the Usagaran Orogen

The structural history recorded in rocks of the Usagaran is complex, and has here been divided into 5

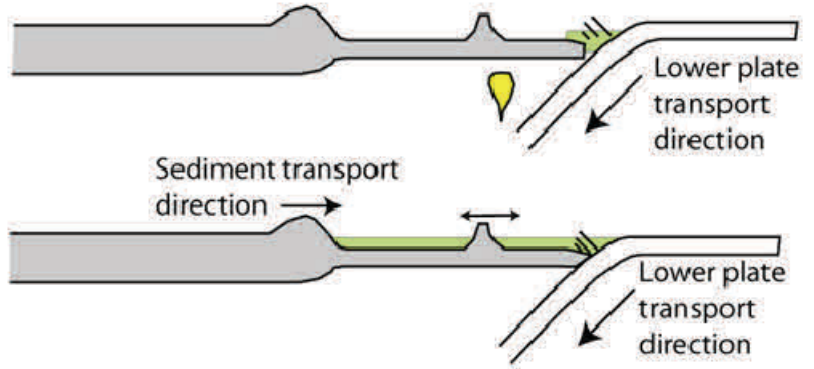
“events”. Reddy et al. (2003) use the orientation of  $S_2$ ,  $L_2$  and shear direction inferred from kinematic indicators to evaluate the formation of differing structural domains using models involving general shear, reworking during a single progressive deformation and reworking. These models are briefly described below: a more detailed



2100 Ma - Igneous activity

2065 ± 9 Ma - Metamorphism

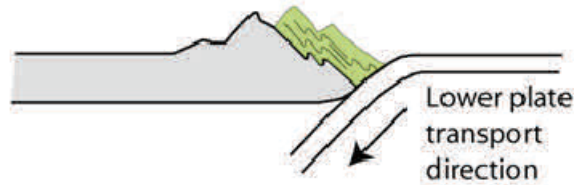
2038 Ma - Igneous activity



2038 - 2013 Ma - Isimani suite sediment deposition

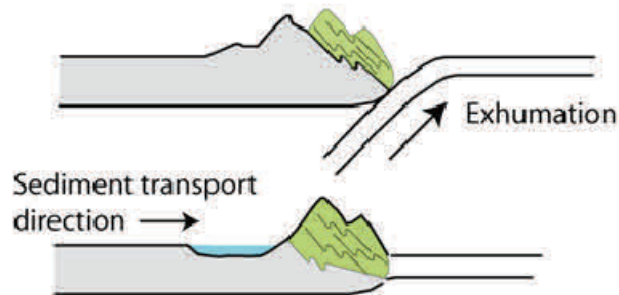


2007 Ma - Metasediments at Amphibolite facies



1999 Ma - Eclogite facies

1991.1 Ma - Amphibolite facies pegmatite formation



1850 - Konse deposition

Figure 4.13 Model for the tectonic development of the Usagaran orogeny

discussion can be found in Reddy et al. (2003).

The general shear (transpression) model explains the complexity of the  $S_2/L_2$  orientations by partitioning, with respect to space and time, the pure and simple shear components (Dewey et al., 1998; Harland, 1971). This can result on the development of zones with different  $S_2/L_2$  orientations developing at the same time. In high-strain zones where blocks converge at angles of  $<20^\circ$  and there is no strain localisation accommodation of pure and simple shear components  $L_2$  variation (through  $90^\circ$ ) can form (Fossen and Tikoff, 1998; Tikoff and Greene, 1997). With strain localised into discrete domains some zones will accommodate pure shear deformation, stretching parallel to the high-strain zone margins, while other

zones will accommodate varying levels of pure and simple shear (Dewey et al., 1998).

The model of reworking during a single progressive deformation is based on the idea of an extended event, with the earliest high-strain  $D_2$  structures overprinted by later stages of the same event during which strain is localised producing varied orientation of structures. Some  $D_2$  structures preserve strain shadows around mafic bodies indicating that this deformation developed progressively, however no evidence of changing metamorphic grade in  $D_2$  foliations was observed. This model is not discounted by Reddy et al (2003) however there was insufficient geochronological data to critically assess the model.



The third model proposed by Reddy et al. (2003) involves post-D<sub>2</sub> reworking of tectonic blocks, with rotation of blocks accounting for differences in the orientation of D<sub>2</sub> structures. Although contacts between some of the domains of Reddy et al. (2003) are clearly tectonic and post-date the amphibolites facies D<sub>2</sub> event (ie. greenschist facies extensional shear between domains 4 and 5: tectonic contact between domains 1 and 2 (Mruma, 1989) which cuts the 1877 ± 7 Ma Kidete granite (Reddy et al., 2003)) this model is discounted by Reddy et al (2003) as it would require rotations of up to 90° around axis which would be perpendicular to all later structures.

Discussion of these models in relation to the structural mapping in this study needs to evaluate all three models. Although model 3 was discounted by Reddy et al. (2003) for the section they studied as there was no evidence of reworking of blocks it may be appropriate to the core of the orogen.

#### 4.6.3 Tectonic models

Based on the U-Pb zircon dating in this study, metamorphism within the Usagaran orogen occurred over a period of ~60 My. Metamorphism occurred earliest in the eastern part of the orogen, with a metamorphic event at ~2060 Ma and sediment deposition between 2038 and 2013 Ma. In the western orogen peak amphibolite-facies metamorphism occurred in the metasediments between 2007 ± 4 Ma (sample T06-27) and 1991 ± 2 Ma, with eclogite-facies metamorphism at 1999.1 ± 1.1 Ma (Sample T01-40, Collins et al., 2004).

This pattern of two-stage metamorphism is similar to that seen in the Mozambique Orogen, in which the metamorphic peak in the west of the Orogen has been dated at ~570 Ma (Cutten, 2006; Sommer et al., 2005a), while in the east of the Orogen it has been dated at ~640 Ma (Maboko et al., 1985; Möller et al., 2000). The structures within the orogenic Orogen, paired with the geochronological data within this part of the Usagaran Orogen are consistent with early volcanism (~2100 Ma) associated with the onset of subduction under the Tanzanian Craton (figure 4.11). The first metamorphic peak occurred at 2060 Ma, is preserved within the eastern part of the Orogen, and is likely to be associated with accretionary wedging. Deposition of the Isimani Suite sediments occurred between 2060 – 2013 Ma in a back-arc basin, with sediments derived from the Tanzanian Craton deposited in the west of the basin, and derived from an island arc and from an unidentified continental block in the east of the basin. Isimani suite sediments were buried during ongoing accretion, reaching peak amphibolite facies conditions at 2007 ± 4 Ma. Eclogite facies rocks reached peak metamorphic conditions at 1999.1 ± 1.1 Ma, and were exhumed to amphibolite facies conditions by 1991 ± 2 Ma (Collins et al., 2004)

No island arc remnants have been identified within the Usagaran terrane, however it is possible that such remnants could be situated further south within the Usagaran Orogen, have been reworked during the East African orogen, or even rifted away from the remaining terrane.

## 4.7 Conclusions

Structures in the Usagaran Orogen as mapped between the villages of Rudi and Ruaha-Mbuyuni are consistent with sinistral transpression associated with collision between the Tanzanian craton and an unknown continent.

Geochronological work on the Usagaran is, thus far, inconclusive on the provenance of sedimentary rocks. The metasedimentary rocks of the eastern Usagaran rocks are inconsistent with being derived from the Tanzanian Craton, indicating the existence of an as yet unidentified continental block as part of the collisional event. Rocks from the western Usagaran are more consistent with being derived from the craton, with some input of sediment derived from local igneous activity, possibly a volcanic arc.

Two metamorphic events were recognised in the Usagaran Orogen. Usagaran metamorphism occurred over ~20 My between 2007 and 1991 Ma. The East African orogen affected these rocks during the Neoproterozoic, and is recorded in zircon growth in the east of the orogen at 577 ± 17 Ma.

Figure 4.1 LA-ICPMS U-Th-Pb geochronology data

Spot No.	Isotope Ratios						Ages (Ma)						Conc <sup>1</sup> %
	<sup>207</sup> Pb/ <sup>206</sup> Pb	1σ	<sup>207</sup> Pb/ <sup>235</sup> U	1σ	<sup>206</sup> Pb/ <sup>238</sup> U	1σ	<sup>207</sup> Pb/ <sup>206</sup> Pb	1σ	<sup>207</sup> Pb/ <sup>235</sup> U	1σ	<sup>206</sup> Pb/ <sup>238</sup> U	1σ	
<b>Sample T01-37</b>													
	n = 14												
KONSE_01	0.19234	0.00445	14.99761	0.3484	0.56593	0.0103	2762.3	38	2815.1	22	2891.1	42	105
KONSE_02	0.18498	0.0044	14.18218	0.3365	0.5565	0.0102	2698	39	2762	23	2852.1	42	106
KONSE_03	0.16537	0.00308	6.92203	0.1327	0.30384	0.00472	2511.3	31	2101.5	17	1710.3	23	68
KONSE_04	0.17992	0.00341	10.30441	0.20037	0.41573	0.00662	2652.2	31	2462.5	18	2241.1	30	84
KONSE_05	0.18323	0.00594	13.52792	0.42105	0.53595	0.01188	2682.3	53	2717.2	29	2766.5	50	103
KONSE_06	0.186	0.00586	12.65767	0.38258	0.49402	0.01059	2707.1	51	2654.5	28	2588.1	46	96
KONSE_07	0.1928	0.00458	14.79712	0.34716	0.55717	0.01013	2766.2	39	2802.3	22	2854.9	42	103
KONSE_08	0.18366	0.0059	13.83329	0.42668	0.54681	0.01193	2686.2	52	2738.4	29	2811.9	50	105
KONSE_09	0.18851	0.00586	13.97439	0.41575	0.53816	0.01167	2729.2	50	2748	28	2775.7	49	102
KONSE_10	0.16289	0.00275	6.42668	0.11158	0.28643	0.00414	2485.9	28	2035.9	15	1623.7	21	65
KONSE_11	0.18692	0.00329	12.42135	0.223	0.48242	0.00724	2715.3	29	2636.8	17	2537.8	32	93
KONSE_12	0.19252	0.00892	16.44705	0.71775	0.62018	0.01929	2763.8	74	2903.2	42	3110.7	77	113
KONSE_13	0.17316	0.00646	11.94347	0.4221	0.50073	0.01184	2588.4	61	2600	33	2616.9	51	101
KONSE_14	0.19071	0.0056	13.96529	0.39238	0.53159	0.01077	2748.3	47	2747.4	27	2748.2	45	100
<b>Sample T06-27 – Metapelite</b>													
	n=57												
27_38	0.14642	0.0046	0.27071	0.0054	5.46414	0.16202	2304.5	53	1544.4	27	1895	25	82.2
27Z4	0.12597	0.00645	0.25753	0.00675	4.47077	0.21592	2042.4	88	1477.2	35	1725.6	40	84.5
27_36	0.2063	0.00496	0.38315	0.00705	10.89613	0.25099	2876.7	39	2091	33	2514.3	21	87.4
27_19	0.11988	0.00138	0.27804	0.00388	4.53484	0.06284	1954.4	20	1581.5	20	1737.4	12	88.9
27_30	0.11481	0.00151	0.36045	0.00488	5.70509	0.08283	1876.8	23	1984.3	23	1932.1	13	102.9
27_4	0.11566	0.00123	0.30462	0.00386	4.84475	0.06184	1890.2	19	1714.2	19	1792.7	11	94.8
27_14	0.11688	0.00119	0.37841	0.00506	6.04025	0.07755	1909.1	18	2068.9	24	1981.7	11	103.8
27_29	0.11979	0.00124	0.36475	0.00472	6.02395	0.07508	1953.1	18	2004.7	22	1979.3	11	101.3
27_35	0.12037	0.00137	0.33166	0.00417	5.50301	0.07253	1961.6	20	1846.4	20	1901.1	11	96.9
27_6	0.12038	0.00126	0.36937	0.00472	6.1094	0.07746	1961.8	18	2026.4	22	1991.6	11	101.5
27_3	0.12101	0.00123	0.37717	0.00473	6.27826	0.07784	1971.1	18	2063	22	2015.4	11	102.2
27_1	0.12162	0.00133	0.37517	0.00472	6.28089	0.08085	1980.1	19	2053.7	22	2015.8	11	101.8
27_11	0.12181	0.00121	0.36587	0.00481	6.09827	0.07672	1982.9	18	2010	23	1990	11	100.4
27_2	0.12193	0.00165	0.33436	0.00443	5.60983	0.08327	1984.6	24	1859.5	21	1917.6	13	96.6
27Z8	0.122	0.00683	0.31617	0.00944	5.31678	0.27885	1985.6	96	1771	46	1871.6	45	94.3
27_15	0.12255	0.00136	0.36775	0.00501	6.1503	0.0827	1993.6	20	2018.8	24	1997.4	12	100.2
27Z5	0.12293	0.00125	0.36641	0.00465	6.20691	0.0783	1999.1	18	2012.5	22	2005.4	11	100.3
27Z6	0.12297	0.00126	0.36541	0.00463	6.19271	0.07838	1999.8	18	2007.7	22	2003.4	11	100.2
27_37	0.12298	0.00138	0.33906	0.00427	5.74793	0.07541	1999.9	20	1882.1	21	1938.6	11	96.9
27_45	0.12302	0.00135	0.35265	0.00446	5.98146	0.07804	2000.5	19	1947.3	21	1973.2	11	98.6
27_47	0.12302	0.00128	0.36345	0.00456	6.16496	0.07791	2000.5	18	1998.5	22	1999.5	11	100.0
27_25	0.12313	0.00142	0.34175	0.00455	5.80138	0.07789	2002.1	20	1895.1	22	1946.6	12	97.2
27Z7	0.12318	0.00125	0.35749	0.00452	6.069	0.07619	2002.8	18	1970.2	21	1985.8	11	99.2
27Z3	0.12323	0.00133	0.38141	0.00515	6.47639	0.08854	2003.5	19	2082.9	24	2042.7	12	102.0
27_33	0.12333	0.0013	0.36553	0.00452	6.21418	0.07783	2004.9	19	2008.3	21	2006.4	11	100.1
27_43	0.12338	0.00127	0.36335	0.00454	6.18077	0.0776	2005.6	18	1998	21	2001.7	11	99.8
27_46	0.12339	0.00135	0.36417	0.00461	6.1956	0.08071	2005.9	19	2001.9	22	2003.8	11	99.9
27Z1	0.12355	0.00126	0.3687	0.00472	6.27915	0.08024	2008	18	2023.3	22	2015.6	11	100.4
27_34	0.12367	0.00136	0.35497	0.00444	6.05154	0.07809	2009.8	19	1958.3	21	1983.3	11	98.7
27Z2	0.12368	0.00136	0.36641	0.00485	6.24581	0.08444	2009.9	19	2012.5	23	2010.9	12	100.0
27_39	0.12383	0.00137	0.33298	0.00419	5.68399	0.07397	2012.1	20	1852.8	20	1928.9	11	95.9
27_49	0.12383	0.00133	0.3505	0.00443	5.98459	0.07733	2012.2	19	1937	21	1973.6	11	98.1
27Z9	0.12384	0.00132	0.36825	0.00462	6.28478	0.08037	2012.2	19	2021.2	22	2016.3	11	100.2
27_42	0.12386	0.00136	0.36598	0.00462	6.24965	0.08136	2012.5	19	2010.5	22	2011.4	11	99.9
27_28	0.12396	0.00131	0.36891	0.0048	6.30467	0.07976	2014	19	2024.3	23	2019.1	11	100.3
27_21	0.12428	0.00121	0.3465	0.00452	5.9368	0.07273	2018.6	17	1917.9	22	1966.6	11	97.4
27_20	0.1243	0.00125	0.34993	0.00481	5.91295	0.07626	2018.8	18	1934.3	23	1963.1	11	97.2
27_26	0.12462	0.00135	0.34736	0.00456	5.96775	0.07695	2023.4	19	1922	22	1971.2	11	97.4
27_23	0.12493	0.0014	0.34334	0.00456	5.9132	0.07818	2027.8	20	1902.7	22	1963.2	11	96.8
27_27	0.12508	0.00138	0.33239	0.00437	5.73174	0.07455	2030	19	1849.9	21	1936.2	11	95.4
27_44	0.12539	0.00149	0.37291	0.00479	6.44713	0.08836	2034.4	21	2043.1	23	2038.7	12	100.2
27_18	0.12578	0.00125	0.38112	0.00517	6.52729	0.08314	2039.8	17	2081.5	24	2049.6	11	100.5
27	0.12579	0.00183	0.34913	0.00467	6.05406	0.09429	2040	26	1930.4	22	1983.7	14	97.2
27_13	0.1276	0.00159	0.34466	0.00477	6.00986	0.08645	2065.1	22	1909.1	23	1977.3	13	95.7
27_9	0.12791	0.00137	0.36033	0.00469	6.32422	0.08178	2069.5	19	1983.8	22	2021.8	11	97.7
27_5	0.12802	0.00151	0.34984	0.00456	6.15647	0.08381	2071	21	1933.9	22	1998.3	12	96.5
27_10	0.12833	0.00179	0.30866	0.00427	5.4324	0.08332	2075.2	24	1734.1	21	1890	13	91.1
27_8	0.12883	0.00135	0.35584	0.00459	6.29302	0.08019	2082	18	1962.4	22	2017.5	11	96.9
27_7	0.12984	0.00134	0.37013	0.00474	6.60051	0.08331	2095.8	18	2030	22	2059.4	11	98.3
27_16	0.13166	0.00156	0.35732	0.00496	6.41558	0.08993	2120.2	21	1969.5	24	2034.4	12	96.0
27_22	0.13317	0.00217	0.35246	0.00521	6.47065	0.11075	2140.2	28	1946.3	25	2041.9	15	95.4
27_24	0.13414	0.00197	0.42642	0.0061	7.88582	0.12506	2152.9	25	2289.6	28	2218.1	14	103.0
27_17	0.14038	0.00157	0.43319	0.00599	8.28669	0.11261	2231.9	19	2320.1	27	2262.9	12	101.4
27_12	0.15713	0.00188	0.46817	0.00645	10.05993	0.1407	2425.1	20	2475.5	28	2440.3	13	100.6
27_32	0.18082	0.00208	0.48161	0.00614	12.00456	0.15876	2660.4	19	2534.3	27	2604.8	12	97.9
27_40	0.21281	0.0039	0.62583	0.01015	18.35942	0.34467	2927	29	3133.1	40	3008.8	18	102.8
27_41	0.44075	0.01886	0.62389	0.02315	37.91076	1.45762	4054.3	62	3125.4	92	3717.6	38	91.7

Table 4.1 Usagaran Isotope chemistry (cont)

Spot No.	Isotope Ratios				Ages (Ma)						Conc <sup>1</sup>		
	<sup>207</sup> Pb/ <sup>206</sup> Pb	1 $\sigma$	<sup>207</sup> Pb/ <sup>235</sup> U	1 $\sigma$	<sup>206</sup> Pb/ <sup>238</sup> U	1 $\sigma$	<sup>207</sup> Pb/ <sup>206</sup> Pb	1 $\sigma$	<sup>207</sup> Pb/ <sup>235</sup> U	1 $\sigma$	<sup>206</sup> Pb/ <sup>238</sup> U	1 $\sigma$	%
Sample T06-37 - Felsic gneiss													
	n=52												
37 z001	0.19253	0.00192	0.5491	0.007	14.57485	0.18261	2763.9	16	2821.4	29	2787.9	12	100.9
37 z002	0.19369	0.00194	0.54234	0.00687	14.48079	0.18068	2773.7	16	2793.2	29	2781.7	12	100.3
37 z003	0.19638	0.00202	0.54994	0.00714	14.88797	0.19142	2796.3	17	2824.9	30	2808.1	12	100.4
37 z004	0.19164	0.00252	0.52053	0.00728	13.75354	0.20469	2756.3	21	2701.4	31	2732.9	14	99.2
37 z005	0.18356	0.00184	0.48442	0.00621	12.25791	0.15454	2685.3	16	2546.5	27	2624.4	12	97.7
37 z006	0.18239	0.00183	0.48007	0.00606	12.06916	0.14998	2674.7	17	2527.6	26	2609.8	12	97.6
37 z007	0.1965	0.002	0.55251	0.00701	14.96408	0.1877	2797.4	17	2835.6	29	2813	12	100.6
37 z008	0.19493	0.00196	0.50001	0.00645	13.43434	0.17025	2784.2	16	2613.8	28	2710.7	12	97.4
37 z009	0.19534	0.00206	0.54597	0.00709	14.70012	0.19028	2787.6	17	2808.4	30	2796	12	100.3
37 z010	0.19287	0.00191	0.54309	0.00692	14.4397	0.18014	2766.8	16	2796.4	29	2779	12	100.4
37 z011	0.19791	0.00201	0.42003	0.00522	11.44595	0.1416	2809	17	2260.6	24	2560.2	12	91.1
37 z012	0.18663	0.00186	0.52883	0.00662	13.60428	0.16827	2712.7	16	2736.5	28	2722.6	12	100.4
37 z013	0.19699	0.002	0.50533	0.00593	13.72333	0.16018	2801.4	16	2636.7	25	2730.8	11	97.5
37 z014	0.19919	0.00202	0.54531	0.00693	14.97144	0.18862	2819.5	16	2805.6	29	2813.4	12	99.8
37 z015	0.21626	0.0022	0.57101	0.00697	17.02603	0.20711	2953.1	16	2911.9	29	2936.3	12	99.4
37 z016	0.19937	0.00203	0.53058	0.00618	14.58503	0.16984	2821.1	16	2743.9	26	2788.6	11	98.8
37 z017	0.18232	0.00186	0.49398	0.00615	12.41717	0.15459	2674.1	17	2587.9	27	2636.5	12	98.6
37 z018	0.15245	0.00159	0.41519	0.00548	8.7259	0.11542	2373.6	18	2238.6	25	2309.8	12	97.3
37 z019	0.16623	0.00169	0.33867	0.00414	7.75922	0.09507	2520.1	17	1880.3	20	2203.5	11	87.4
37 z020	0.17103	0.00172	0.29885	0.00365	7.04534	0.08593	2567.8	17	1685.6	18	2117.2	11	82.5
37 z021	0.18786	0.00199	0.33989	0.00444	8.80243	0.11567	2723.6	17	1886.1	21	2317.7	12	85.1
37 z022	0.18222	0.00184	0.30071	0.00355	7.55511	0.08942	2673.2	17	1694.9	18	2179.5	11	81.5
37 z023	0.19773	0.00207	0.52673	0.00598	14.3596	0.16556	2807.5	17	2727.7	25	2773.8	11	98.8
37 z024	0.18665	0.00191	0.42821	0.00481	11.01819	0.1251	2712.8	17	2297.7	22	2524.7	11	93.1
37 z025	0.19784	0.00211	0.6234	0.00774	17.00335	0.21493	2808.5	17	3123.4	31	2935	12	104.5
37 z026	0.20111	0.00208	0.54704	0.00628	15.16805	0.17625	2835.2	17	2812.8	26	2825.8	11	99.7
37 z027	0.20048	0.00204	0.54645	0.00668	15.10259	0.18568	2830.1	17	2810.4	28	2821.7	12	99.7
37 z028	0.18698	0.00225	0.49154	0.006	12.67167	0.16498	2715.8	20	2577.3	26	2655.6	12	97.8
37 z029	0.18987	0.00191	0.51144	0.0065	13.38855	0.1695	2741	16	2662.8	28	2707.5	12	98.8
37 z030	0.1878	0.0019	0.43651	0.0049	11.30196	0.1278	2723	17	2335	22	2548.4	11	93.6
37 z031	0.18038	0.00187	0.3301	0.00339	8.21041	0.08572	2656.3	17	1838.9	16	2254.5	9	84.9
37 z101	0.19437	0.00203	0.53222	0.00689	14.25627	0.18466	2779.5	17	2750.8	29	2766.9	12	99.5
37 z102	0.19898	0.00205	0.53284	0.00688	14.61234	0.18802	2817.9	17	2753.4	29	2790.3	12	99.0
37 z103	0.18803	0.00194	0.47016	0.00607	12.18423	0.15696	2725	17	2484.3	27	2618.7	12	96.1
37 z104	0.2024	0.00212	0.57079	0.00742	15.92247	0.20695	2845.6	17	2911.1	30	2872.2	12	100.9
37 z105	0.1728	0.00179	0.2408	0.00311	5.73509	0.07423	2585	17	1390.8	16	1936.7	11	74.9
37 z106	0.18905	0.00194	0.52928	0.00685	13.79187	0.17774	2733.9	17	2738.4	29	2735.5	12	100.1
37 z107	0.19978	0.00211	0.58059	0.00758	15.98811	0.20962	2824.4	17	2951.2	31	2876.1	13	101.8
37 z108	0.19954	0.00228	0.5433	0.00726	14.94307	0.20477	2822.4	19	2797.2	30	2811.6	13	99.6
37 z109	0.18739	0.00317	0.24775	0.00373	6.39968	0.11214	2719.4	28	1426.9	19	2032.2	15	74.7
37 z110	0.19411	0.00203	0.55637	0.00725	14.88759	0.19418	2777.3	17	2851.6	30	2808.1	12	101.1
37 z111	0.19239	0.00203	0.55775	0.00732	14.79337	0.19442	2762.7	17	2857.3	30	2802	13	101.4
37 z112	0.18491	0.00188	0.50658	0.00658	12.91442	0.16634	2697.4	17	2642	28	2673.4	12	99.1
37 z113	0.18746	0.00206	0.53773	0.00712	13.89757	0.18662	2720	18	2773.9	30	2742.8	13	100.8
37 z114	0.18902	0.00215	0.46545	0.00621	12.12947	0.16595	2733.7	19	2463.6	27	2614.5	13	95.6
37 z115	0.18214	0.00182	0.51032	0.00659	12.81464	0.16334	2672.4	16	2658	28	2666.1	12	99.8
37 z116	0.2001	0.00206	0.57736	0.00751	15.92814	0.20583	2827	17	2938	31	2872.5	12	101.6
37 z117	0.18363	0.0019	0.19037	0.00247	4.81973	0.06239	2686	17	1123.4	13	1788.3	11	66.6
37 z118	0.17635	0.00182	0.1379	0.00179	3.3528	0.04326	2618.9	17	832.7	10	1493.4	10	57.0
37 z119	0.19538	0.00211	0.6117	0.00804	16.47789	0.21834	2788	18	3076.8	32	2904.9	13	104.2
37 z120	0.18181	0.00182	0.53717	0.00692	13.46539	0.17136	2669.5	17	2771.6	29	2712.9	12	101.6
37 z121	0.18303	0.00226	0.50199	0.00683	12.66757	0.18119	2680.5	20	2622.3	29	2655.3	13	99.1

Table 4.1 Usagaran Isotope chemistry (cont)

Spot No.	Isotope Ratios						Ages (Ma)						Conc <sup>1</sup> %
	<sup>207</sup> Pb/ <sup>206</sup> Pb	1σ	<sup>207</sup> Pb/ <sup>235</sup> U	1σ	<sup>206</sup> Pb/ <sup>238</sup> U	1σ	<sup>207</sup> Pb/ <sup>206</sup> Pb	1σ	<sup>207</sup> Pb/ <sup>235</sup> U	1σ	<sup>206</sup> Pb/ <sup>238</sup> U	1σ	
T07-35 – Kikuyu Pelite													
			n=29										
35_001	0.12565	0.00129	0.32122	0.0046	5.56446	0.08048	2038	18	1795.7	22	1910.6	12	93.7
35_002	0.16187	0.00167	0.3613	0.00524	8.06224	0.11767	2475.3	17	1988.3	25	2238	13	90.4
35_003	0.16576	0.00173	0.37119	0.00536	8.48152	0.12412	2515.3	17	2035	25	2283.9	13	90.8
35_004	0.12823	0.0015	0.19908	0.00304	3.51863	0.05587	2073.9	21	1170.4	16	1531.4	13	73.8
35_005	0.13257	0.00184	0.36953	0.00565	6.75336	0.11459	2132.3	24	2027.2	27	2079.6	15	97.5
35_006	0.15832	0.00182	0.37734	0.00557	8.23576	0.12606	2437.8	19	2063.9	26	2257.3	14	92.6
35_007	0.20808	0.00223	0.48704	0.00706	13.971	0.20603	2890.6	17	2557.8	31	2747.7	14	95.1
35_008	0.17274	0.00188	0.41627	0.00588	9.91556	0.14348	2584.3	18	2243.5	27	2427	13	93.9
35_009	0.16817	0.0018	0.4572	0.00668	10.59911	0.15723	2539.5	18	2427.2	30	2488.6	14	98.0
35_010	0.06127	0.00103	0.08913	0.0014	0.7527	0.01482	648.9	36	550.4	8	569.8	9	87.8
35_011	0.13188	0.00146	0.31127	0.00454	5.65517	0.08472	2123.2	19	1747	22	1924.6	13	90.6
35_012c	0.1255	0.00138	0.33048	0.00478	5.71511	0.08485	2035.8	19	1840.7	23	1933.7	13	95.0
35_012r	0.06831	0.00112	0.08458	0.00131	0.79606	0.01521	878	33	523.4	8	594.6	9	67.7
35_013	0.12935	0.00214	0.2308	0.00357	4.11302	0.07603	2089.1	29	1338.7	19	1656.9	15	79.3
35_015	0.64204	0.00798	1.25395	0.01982	110.98364	1.74641	4606.1	18	5238.9	57	4790.9	16	104.0
35_016	0.16959	0.00183	0.35088	0.00508	8.20303	0.12096	2553.6	18	1938.8	24	2253.7	13	88.3
35_017	0.17947	0.00219	0.16998	0.0025	4.20863	0.06526	2648	20	1012	14	1675.7	13	63.3
35_018	0.18659	0.00346	0.22384	0.00389	5.74625	0.11647	2712.3	30	1302.1	21	1938.4	18	71.5
35_020	0.1432	0.00149	0.36362	0.00538	7.17794	0.10614	2266.3	18	1999.3	25	2133.8	13	94.2
35_021	0.14997	0.00166	0.25485	0.00377	5.26838	0.07954	2345.6	19	1463.4	19	1863.8	13	79.5
35_022	0.13131	0.00162	0.3677	0.00533	6.65531	0.10343	2115.5	21	2018.6	25	2066.7	14	97.7
35_023c	0.18257	0.0021	0.44736	0.00646	11.25367	0.16876	2676.4	19	2383.5	29	2544.4	14	95.1
35_023r	0.13287	0.00157	0.10932	0.00177	2.00209	0.0327	2136.3	20	668.8	10	1116.2	11	52.2
35_024c	0.16234	0.00184	0.4129	0.00603	9.2373	0.13903	2480.2	19	2228.2	28	2361.8	14	95.2
35_024r	0.05998	0.00122	0.09086	0.00145	0.7513	0.01675	603	43	560.6	9	569	10	94.4
35_025c	0.18937	0.0023	0.50238	0.00747	13.10961	0.20341	2736.7	20	2624	32	2687.6	15	98.2
35_025r	0.08011	0.00127	0.07819	0.00125	0.86361	0.01634	1199.7	31	485.3	8	632.1	9	52.7

Table 4.1 Usagaran Isotope chemistry (cont)

Spot No.	Isotope Ratios				Ages (Ma)				Conc <sup>1</sup> %				
	<sup>207</sup> Pb/ <sup>206</sup> Pb	1σ	<sup>207</sup> Pb/ <sup>235</sup> U	1σ	<sup>206</sup> Pb/ <sup>238</sup> U	1σ	<sup>207</sup> Pb/ <sup>206</sup> Pb	1σ		<sup>207</sup> Pb/ <sup>235</sup> U	1σ	<sup>206</sup> Pb/ <sup>238</sup> U	1σ
Sample T07-59 – Kinusi Pelite													
n=79													
59_001c	0.15552	0.0018	0.25384	0.00371	5.44337	0.08141	2407.6	20	1458.2	19	1891.7	13	78.6
59_001r	0.12451	0.00196	0.35784	0.00564	6.14281	0.11106	2021.9	28	1971.9	27	1996.4	16	98.7
59_002	0.12851	0.00164	0.37191	0.00562	6.5892	0.10513	2077.7	22	2038.4	26	2057.9	14	99.0
59_003c	0.1549	0.00204	0.38324	0.00589	8.1846	0.13233	2400.8	22	2091.4	27	2251.6	15	93.8
59_003r	0.12601	0.00198	0.3569	0.00561	6.20062	0.11186	2043.1	28	1967.5	27	2004.5	16	98.1
59_004c	0.13943	0.0021	0.33469	0.00487	6.43099	0.1051	2220.1	26	1861.1	24	2036.5	14	91.7
59_004r	0.12359	0.00178	0.33969	0.00524	5.78772	0.09889	2008.6	25	1885.2	25	1944.6	15	96.8
59_005	0.17779	0.00271	0.49212	0.00781	12.06411	0.21171	2632.4	25	2579.8	34	2609.4	16	99.1
59_006c	0.20094	0.00236	0.51001	0.00763	14.12906	0.21541	2833.8	19	2656.7	33	2758.4	14	97.3
59_006r	0.12532	0.00197	0.36093	0.00567	6.23625	0.11271	2033.4	28	1986.6	27	2009.5	16	98.8
59_007	0.12928	0.00237	0.35578	0.00575	6.33559	0.126	2088.2	32	1962.1	27	2023.4	17	96.9
59_008	0.12653	0.00197	0.35379	0.00551	6.17094	0.11102	2050.3	27	1952.7	26	2000.3	16	97.6
59_008r	0.127	0.00201	0.35752	0.00576	6.25862	0.11542	2056.9	28	1970.4	27	2012.7	16	97.9
59_009	0.12621	0.00157	0.3583	0.00546	6.23326	0.09985	2045.8	22	1974.1	26	2009.1	14	98.2
59_010	0.1373	0.00226	0.38609	0.00618	7.30773	0.13602	2193.4	28	2104.7	29	2149.8	17	98.0
59_011	0.13166	0.00173	0.32643	0.00497	5.92444	0.09712	2120.2	23	1821	24	1964.8	14	92.7
59_012	0.12529	0.00167	0.33982	0.00573	5.84369	0.09843	2032.9	23	1885.8	28	1952.9	15	96.1
59_013	0.13688	0.00169	0.37793	0.00568	7.13092	0.11266	2188.1	21	2066.6	27	2127.9	14	97.2
59_013r	0.12538	0.00179	0.36059	0.00561	6.23207	0.10729	2034.2	25	1985	27	2009	15	98.8
59_014	0.13527	0.00153	0.38786	0.00579	7.23218	0.11003	2167.5	20	2112.9	27	2140.5	14	98.8
59_014r	0.12131	0.00201	0.33055	0.00528	5.52796	0.10422	1975.6	29	1841.1	26	1905	16	96.4
59_015	0.13065	0.00265	0.27002	0.00482	4.85938	0.10657	2106.7	35	1540.9	24	1795.2	18	85.2
59_015r	0.12426	0.00192	0.35387	0.00559	6.0614	0.10952	2018.2	27	1953.1	27	1984.7	16	98.3
59_016	0.15763	0.00181	0.35652	0.0053	7.74692	0.11792	2430.4	19	1965.6	25	2202.1	14	90.6
59_016r	0.12254	0.00174	0.35436	0.00549	5.9861	0.10276	1993.5	25	1955.4	26	1973.8	15	99.0
59_017	0.13144	0.00143	0.38321	0.00554	6.94248	0.10174	2117.3	19	2091.3	26	2104.1	13	99.4
59_018	0.12473	0.00161	0.35365	0.00538	6.08058	0.09875	2024.9	23	1952	26	1987.5	14	98.2
59_018r	0.12478	0.00176	0.36159	0.00561	6.21972	0.1065	2025.7	25	1989.7	27	2007.2	15	99.1
59_019	0.12662	0.00144	0.35989	0.00542	6.28138	0.09632	2051.6	20	1981.7	26	2015.9	13	98.3
59_019r	0.12462	0.0017	0.37084	0.00573	6.3709	0.10712	2023.4	24	2033.4	27	2028.3	15	100.2
59_020	0.13667	0.00142	0.38367	0.00573	7.22793	0.10641	2185.4	18	2093.4	27	2140	13	97.9
59_021	0.1804	0.00242	0.50653	0.00798	12.59739	0.20948	2656.6	22	2641.8	34	2650	16	99.8
59_022	0.12626	0.00163	0.35925	0.00542	6.25301	0.10096	2046.5	23	1978.6	26	2011.9	14	98.3
59_023	0.13582	0.00193	0.31656	0.00479	5.92529	0.09921	2174.5	25	1772.9	23	1964.9	15	90.4
59_023r	0.12302	0.00189	0.35547	0.00561	6.02827	0.10835	2000.4	27	1960.7	27	1979.9	16	99.0
59_024	0.13381	0.0018	0.31164	0.00468	5.74675	0.09386	2148.5	23	1748.8	23	1938.4	14	90.2
59_025	0.14472	0.00165	0.29269	0.00427	5.83854	0.08737	2284.5	19	1655	21	1952.2	13	85.5
59_025r	0.12365	0.00177	0.34962	0.00543	5.95953	0.10277	2009.6	25	1932.8	26	1970	15	98.0
59_025r2	0.1242	0.00174	0.35038	0.00539	5.99921	0.10186	2017.4	25	1936.4	26	1975.7	15	97.9
59_026c	0.13017	0.00155	0.37421	0.00563	6.71484	0.10463	2100.2	21	2049.2	26	2074.6	14	98.8
59_026r1	0.12399	0.00224	0.35663	0.00585	6.09567	0.1217	2014.5	32	1966.2	28	1989.6	17	98.8
59_026r2	0.12457	0.00192	0.35049	0.00553	6.01913	0.10816	2022.7	27	1936.9	26	1978.6	16	97.8
59_027c	0.13016	0.00131	0.33936	0.00504	6.08832	0.08853	2100.1	18	1883.6	24	1988.6	13	94.7
59_027r	0.12619	0.00186	0.35977	0.0057	6.2581	0.11029	2045.5	26	1981.1	27	2012.6	15	98.4
59_028	0.13389	0.00152	0.3745	0.00552	6.91264	0.10412	2149.6	20	2050.5	26	2100.3	13	97.7
59_029c	0.13407	0.00185	0.38572	0.00589	7.12988	0.11898	2152	24	2103	27	2127.8	15	98.9
59_029r	0.1236	0.0022	0.3616	0.00588	6.16142	0.1213	2008.8	31	1989.7	28	1999	17	99.5
59_030c	0.13045	0.00147	0.37036	0.00553	6.66072	0.10122	2104.1	20	2031.1	26	2067.4	13	98.3
59_030r	0.12761	0.00154	0.36673	0.0055	6.45174	0.10079	2065.3	21	2014	26	2039.3	14	98.7
59_031c	0.13272	0.00192	0.36559	0.00566	6.68933	0.11463	2134.3	25	2008.6	27	2071.2	15	97.0
59_031r	0.1237	0.00201	0.34742	0.00552	5.9243	0.1097	2010.2	29	1922.3	26	1964.8	16	97.7
59_032c	0.13082	0.00298	0.31851	0.00568	5.74358	0.13534	2108.9	39	1782.4	28	1938	20	91.9
59_032r	0.12458	0.00166	0.35254	0.00538	6.05414	0.09948	2022.9	23	1946.7	26	1983.7	14	98.1
59_033	0.12569	0.00155	0.36729	0.00553	6.36369	0.1004	2038.6	22	2016.6	26	2027.3	14	99.4
59_034c	0.12857	0.00163	0.3272	0.00495	5.79901	0.09269	2078.5	22	1824.8	24	1946.3	14	93.6
59_034r	0.12216	0.00167	0.36097	0.00555	6.07822	0.10158	1988	24	1986.8	26	1987.1	15	100.0
59_035	0.12659	0.00147	0.37651	0.0056	6.57002	0.10021	2051.1	20	2059.9	26	2055.3	13	100.2
59_036c	0.12375	0.00166	0.33515	0.00515	5.7167	0.09483	2011	24	1863.3	25	1933.9	14	96.2
59_036r	0.12325	0.00162	0.35276	0.00537	5.99349	0.09763	2003.9	23	1947.8	26	1974.9	14	98.6
59_037	0.14172	0.00181	0.20447	0.00309	3.99447	0.06385	2248.4	22	1199.3	17	1633.1	13	72.6
59_038D	0.13192	0.00191	0.37502	0.00581	6.81985	0.11707	2123.7	25	2053	27	2088.3	15	98.3
59_039c	0.12929	0.00159	0.36456	0.00553	6.49708	0.10271	2088.3	21	2003.7	26	2045.5	14	98.0
59_039r	0.11828	0.00187	0.31119	0.0049	5.07401	0.09223	1930.4	28	1746.6	24	1831.8	15	94.9
59_040c	0.12918	0.00136	0.24661	0.00366	4.39169	0.06464	2086.9	18	1421	19	1710.8	12	82.0
59_040r	0.12406	0.00195	0.34861	0.00551	5.96137	0.10823	2015.4	28	1928	26	1970.2	16	97.8
59_041c	0.12541	0.00159	0.36264	0.00545	6.26967	0.09958	2034.6	22	1994.7	26	2014.2	14	99.0
59_041r	0.12136	0.00179	0.36554	0.00569	6.11568	0.10657	1976.4	26	2008.4	27	1992.5	15	100.8
59_042c	0.13864	0.00156	0.39748	0.00597	7.59604	0.11535	2210.2	19	2157.4	28	2184.4	14	98.8
59_042r	0.1249	0.002	0.3563	0.00565	6.13485	0.11226	2027.4	28	1964.6	27	1995.2	16	98.4
59_043	0.12459	0.00171	0.31804	0.00484	5.46241	0.09074	2023	24	1780.1	24	1894.7	14	93.7
59_044c	0.1346	0.00173	0.38687	0.00584	7.17895	0.11485	2158.8	22	2108.3	27	2133.9	14	98.8
59_044r	0.12309	0.00161	0.35619	0.00542	6.04359	0.09816	2001.5	23	1964.1	26	1982.1	14	99.0
59_045c	0.129	0.00178	0.38844	0.00593	6.90795	0.11505	2084.4	24	2115.6	28	2099.7	15	100.7
59_045r	0.1239	0.00169	0.3642	0.00564	6.2203	0.10447	2013.1	24	2002	27	2007.3	15	99.7
59_046c	0.16753	0.00179	0.43754	0.0064	10.10466	0.14702	2533.1	18	2339.6	29	2444.4	13	96.5
59_046r	0.1209	0.00144	0.3586	0.00539	5.97594	0.09281	1969.5	21	1975.5	26	1972.3	14	100.1
59_047c	0.13691	0.00163	0.33188	0.00499	6.26353	0.097	2188.5	20	1847.5	24	2013.4	14	92.0
59_047r	0.12264	0.00205	0.33889	0.00541	5.72944	0.10768	1995	29	1881.3	26	1935.8	16	9



Table 4.1 Usagaran Isotope chemistry (cont)

Spot No.	Isotope Ratios				Ages (Ma)				Conc <sup>1</sup>				
	<sup>207</sup> Pb/ <sup>235</sup> U	1σ	<sup>207</sup> Pb/ <sup>235</sup> U	1σ	<sup>206</sup> Pb/ <sup>238</sup> U	1σ	<sup>207</sup> Pb/ <sup>206</sup> Pb	1σ	<sup>207</sup> Pb/ <sup>235</sup> U	1σ	<sup>206</sup> Pb/ <sup>238</sup> U	1σ	%
Sample T07-71 - Kinusi Pelite n=117													
71_010	0.16816	0.00179	0.40204	0.00582	9.3175	0.13509	2539.4	18	2178.4	27	2369.7	13	93.3
71_011	0.12132	0.00125	0.33619	0.00484	5.62094	0.08033	1975.7	18	1868.3	23	1919.3	12	97.1
71_012	0.16336	0.00171	0.43003	0.00622	9.68184	0.13931	2490.8	17	2305.9	28	2405	13	96.6
71_013	0.1443	0.00194	0.2555	0.0038	5.08077	0.08389	2279.4	23	1466.8	20	1832.9	14	80.4
71_014	0.16835	0.00179	0.44886	0.00652	10.41417	0.15153	2541.3	18	2390.2	29	2472.3	13	97.3
71_015	0.13024	0.00172	0.36111	0.00536	6.48145	0.10634	2101.2	23	1987.4	25	2043.4	14	97.2
71_016	0.17716	0.002	0.46272	0.00679	11.29785	0.16957	2626.5	19	2451.6	30	2548	14	97.0
71_017	0.1288	0.00152	0.3674	0.00539	6.52155	0.10029	2081.6	21	2017.2	25	2048.8	14	98.4
71_017b	0.12378	0.00132	0.28367	0.00411	4.83909	0.07059	2011.4	19	1609.8	21	1791.7	12	89.1
71_018	0.16402	0.00176	0.4412	0.00643	9.9732	0.146	2497.5	18	2356	29	2432.3	14	97.4
71_019	0.15718	0.00176	0.42279	0.00622	9.15837	0.13804	2425.5	19	2273.1	28	2354	14	97.1
71_019r	0.12776	0.0014	0.30129	0.00441	5.30502	0.07891	2067.4	19	1697.7	22	1869.7	13	90.4
71_020	0.16094	0.00167	0.30114	0.00442	6.67908	0.09709	2465.6	17	1697	22	2069.9	13	84.0
71_021	0.12974	0.00164	0.39885	0.00601	7.13101	0.11598	2094.5	22	2163.7	28	2127.9	14	101.6
71_021r	0.12855	0.00136	0.36429	0.00535	6.45367	0.09503	2078.3	19	2002.5	25	2039.6	13	98.1
71_022	0.1297	0.0016	0.38465	0.00573	6.87558	0.10961	2093.9	22	2098	27	2095.5	14	100.1
71_023	0.16114	0.00204	0.43775	0.00659	9.72118	0.15735	2467.6	21	2340.6	30	2408.7	15	97.6
71_023r	0.12559	0.00153	0.35811	0.00532	6.19817	0.09791	2037.1	21	1973.2	25	2004.2	14	98.4
71_024	0.17417	0.0019	0.48327	0.00714	11.60005	0.1733	2598.1	18	2541.5	31	2572.7	14	99.0
71_025	0.11306	0.00133	0.16998	0.00251	2.64846	0.04104	1849.1	21	1012	14	1314.2	11	71.1
71_026	0.12996	0.00138	0.38793	0.00574	6.94793	0.10302	2097.4	18	2113.2	27	2104.8	13	100.4
71_026r	0.12417	0.00144	0.34036	0.00507	5.82445	0.09043	2016.9	21	1888.4	24	1950.1	13	96.7
71_027	0.16653	0.00188	0.4733	0.00707	10.86249	0.16638	2523.1	19	2498	31	2511.4	14	99.5
71_028	0.14787	0.00188	0.39606	0.00599	8.07189	0.13167	2321.5	22	2150.9	28	2239.1	15	96.5
71_029	0.16309	0.00177	0.43107	0.00641	9.68962	0.1456	2488	18	2310.5	29	2405.7	14	96.7
71_029r	0.12455	0.00149	0.35903	0.00537	6.16284	0.09724	2022.3	21	1977.6	25	1999.2	14	98.9
71_030	0.16454	0.0017	0.46575	0.0069	10.56195	0.15533	2502.9	17	2464.9	30	2485.4	14	99.3
71_030r	0.12725	0.00145	0.35298	0.00526	6.19097	0.09535	2060.4	20	1948.8	25	2003.2	13	97.2
71_031	0.15582	0.00211	0.44499	0.00685	9.55647	0.16257	2410.8	23	2372.9	31	2393	16	99.3
71_032	0.16211	0.00173	0.42981	0.0064	9.60326	0.14361	2477.8	18	2304.8	29	2397.5	14	96.8
71_032r	0.12294	0.00154	0.35436	0.00541	6.00542	0.09851	1999.4	22	1955.4	26	1976.6	14	98.9
71_033	0.22834	0.00254	0.45325	0.00682	14.26729	0.21774	3040.4	18	2409.7	30	2767.6	14	91.0
71_033r	0.12488	0.00154	0.3705	0.0056	6.37844	0.10324	2027.1	22	2031.8	26	2029.3	14	100.1
71_034	0.1338	0.00139	0.21461	0.00319	3.95863	0.05866	2148.4	18	1253.3	17	1625.8	12	75.7
71_034r	0.11852	0.00154	0.25283	0.00382	4.1311	0.06852	1934.1	23	1453.1	20	1660.5	14	85.9
71_035	0.1776	0.00184	0.29519	0.00439	7.2275	0.10697	2630.6	17	1667.4	22	2139.9	13	81.3
71_036	0.16268	0.00181	0.37855	0.00568	8.4896	0.13008	2483.7	19	2069.5	27	2284.8	14	92.0
71_036r	0.16541	0.00175	0.41418	0.00618	9.44463	0.14143	2511.7	18	2234	28	2382.2	14	94.8
71_036r2	0.12478	0.00147	0.35951	0.00542	6.18438	0.09795	2025.7	21	1979.9	26	2002.2	14	98.8
71_037	0.15971	0.00166	0.33098	0.00493	7.28757	0.10815	2452.6	17	1843.2	24	2147.3	13	87.6
71_037r	0.12731	0.00161	0.34472	0.00524	6.05052	0.09947	2061.2	22	1909.3	25	1983.1	14	96.2
71_038	0.16468	0.00194	0.46392	0.00705	10.53286	0.16747	2504.3	20	2456.9	31	2482.8	15	99.1
71_039	0.15691	0.00161	0.33615	0.00504	7.27167	0.10827	2422.7	17	1868.1	24	2145.3	13	88.5
71_040	0.17438	0.00188	0.47241	0.0071	11.3574	0.17243	2600.1	18	2494.1	31	2552.9	14	98.2
71_040r	0.12858	0.00162	0.37222	0.00567	6.59843	0.10853	2078.6	22	2039.9	27	2059.1	15	99.1
71_041	0.16614	0.00195	0.45976	0.00699	10.53109	0.16726	2519.2	20	2438.5	31	2482.7	15	98.6
71_042	0.15861	0.00179	0.41251	0.00623	9.02072	0.14032	2440.9	19	2226.4	28	2340.1	14	95.9
71_042r	0.12642	0.00158	0.3656	0.00556	6.37222	0.10442	2048.7	22	2008.7	26	2028.4	14	99.0
71_043	0.14665	0.00155	0.40181	0.00602	8.12432	0.12255	2307.2	18	2177.4	28	2245	14	97.3
71_043r	0.12443	0.00165	0.36408	0.00558	6.2458	0.10606	2020.6	23	2001.5	26	2010.9	15	99.5
71_044	0.16298	0.00174	0.39871	0.00598	8.9601	0.13483	2486.8	18	2163.1	28	2333.9	14	93.9
71_044r	0.12792	0.00151	0.34726	0.00524	6.12528	0.09684	2069.6	21	1921.5	25	1993.9	14	96.3
71_045c	0.12952	0.00154	0.36059	0.00545	6.43971	0.10229	2091.5	21	1985	26	2037.7	14	97.4
71_046c	0.17015	0.00237	0.45378	0.00709	10.64588	0.18499	2559.1	23	2412	31	2492.7	16	97.4
71_047c	0.16678	0.00183	0.44577	0.00671	10.25098	0.15634	2525.6	18	2376.4	30	2457.7	14	97.3
71_048c	0.13586	0.00145	0.1741	0.0026	3.26138	0.04904	2175.1	19	1034.7	14	1471.9	12	67.7
71_048r	0.12207	0.00153	0.29071	0.00441	4.89269	0.07999	1986.6	22	1645.1	22	1801	14	90.7
71_049c	0.12912	0.00181	0.36407	0.00562	6.48136	0.11319	2086	25	2001.5	27	2043.4	15	98.0
71_050c	0.17217	0.00197	0.47868	0.00725	11.36264	0.17684	2578.9	19	2521.5	32	2553.4	15	99.0
71_051c	0.15675	0.00167	0.38824	0.00582	8.39025	0.12596	2420.9	18	2114.7	27	2274.1	14	93.9
71_052c	0.16391	0.00187	0.43788	0.00663	9.8929	0.15407	2496.4	19	2341.2	30	2424.8	14	97.1
71_052r	0.15462	0.00168	0.30602	0.00459	6.52189	0.09893	2397.7	18	1721.1	23	2048.9	13	85.5
71_053c	0.161	0.00177	0.43072	0.00648	9.55782	0.14593	2466.1	18	2309	29	2393.1	14	97.0
71_054c	0.14727	0.00162	0.40477	0.00609	8.21606	0.12545	2314.4	19	2191	28	2255.1	14	97.4
71_055c	0.14504	0.00152	0.32833	0.00491	6.56336	0.09792	2288.2	18	1830.3	24	2054.4	13	89.8
71_056c	0.13105	0.00184	0.37178	0.00575	6.71515	0.11737	2112.1	24	2037.8	27	2074.6	15	98.2
71_057c	0.15328	0.00168	0.38635	0.00581	8.16199	0.12436	2382.9	19	2105.9	27	2249.1	14	94.4
71_058c	0.14345	0.00152	0.20807	0.00311	4.11364	0.06166	2269.3	18	1218.5	17	1657	12	73.0
71_058r	0.11812	0.00173	0.23575	0.00364	3.83787	0.06867	1928	26	1364.6	19	1600.7	14	83.0
71_059c	0.16312	0.00183	0.44442	0.00671	9.9907	0.15432	2488.3	19	2370.4	30	2433.9	14	97.8
71_059r	0.12308	0.00174	0.3596	0.00555	6.10144	0.10339	2001.3	25	1980.3	26	1990.5	15	99.5
71_060c	0.12133	0.0013	0.35813	0.00523	5.99028	0.08757	1975.9	19	1973.3	25	1974.4	13	99.9
71_061c	0.13978	0.00152	0.38876	0.00569	7.49154	0.11006	2224.5	19	2117.1	26	2172	13	97.6
71_062c	0.16137	0.00189	0.31356	0.00505	6.96558	0.11026	2470	20	1758.2	25	2107.1	14	85.3
71_062r	0.11901	0.00163	0.29143	0.0046	4.7796	0.08136	1941.5	24	1648.7	23	1781.3	14	91.7
71_063	0.16372	0.00168	0.36121	0.00526	8.15288	0.11691	2494.5	17	1987.9	25	2248.1	13	90.1
71_065	0.15719	0.0016	0.43846	0.0064	9.50208	0.13622	2425.6	17	2343.7	29	2387.7	13	98.4

Table 4.1 Usagaran Isotope chemistry (cont)

Spot No.	Isotope Ratios				Ages (Ma)								Conc <sup>1</sup>
	<sup>207</sup> Pb/ <sup>206</sup> Pb		<sup>207</sup> Pb/ <sup>235</sup> U		<sup>206</sup> Pb/ <sup>238</sup> U		<sup>207</sup> Pb/ <sup>206</sup> Pb		<sup>207</sup> Pb/ <sup>235</sup> U		<sup>206</sup> Pb/ <sup>238</sup> U		
		1 $\sigma$		1 $\sigma$		1 $\sigma$		1 $\sigma$		1 $\sigma$		1 $\sigma$	%
71_066c	0.16108	0.00181	0.34521	0.00501	7.6631	0.11243	2467	19	1911.7	24	2192.3	13	88.9
71_066r	0.12327	0.00151	0.33905	0.00507	5.76231	0.0902	2004	22	1882.1	24	1940.8	14	96.8
71_067	0.11948	0.00228	0.25817	0.00423	4.25392	0.08723	1948.5	34	1480.5	22	1684.5	17	86.5
71_068c	0.16445	0.00171	0.45096	0.0066	10.22547	0.14796	2502	17	2399.5	29	2455.4	13	98.1
71_069c	0.12794	0.00146	0.37605	0.00556	6.63341	0.10021	2069.8	20	2057.8	26	2063.8	13	99.7
71_070c	0.13101	0.00179	0.38119	0.0058	6.885	0.11393	2111.5	24	2081.8	27	2096.7	15	99.3
71_071c	0.13105	0.00223	0.37963	0.00608	6.85848	0.13022	2112.1	30	2074.6	28	2093.3	17	99.1
71_072c	0.13022	0.00139	0.36027	0.00518	6.46724	0.09354	2101	19	1983.5	25	2041.5	13	97.2
71_073c	0.10808	0.00145	0.20934	0.00314	3.11932	0.05119	1767.2	24	1225.3	17	1437.5	13	81.3
71_074c	0.15424	0.00177	0.39083	0.00564	8.30558	0.12313	2393.4	19	2126.7	26	2264.9	13	94.6
71_075c	0.15351	0.00171	0.34535	0.00515	7.30962	0.10931	2385.4	19	1912.4	25	2150	13	90.1
71_076c	0.16371	0.00191	0.46005	0.00678	10.38278	0.15695	2494.4	20	2439.8	30	2469.5	14	99.0
71_077c	0.1488	0.00192	0.42088	0.00627	8.63292	0.1372	2332.1	22	2264.5	28	2300	14	98.6
71_081	0.13018	0.00156	0.37479	0.00551	6.72704	0.10381	2100.4	21	2051.9	26	2076.2	14	98.8
71_082	0.17369	0.00183	0.39021	0.00573	9.34442	0.13809	2593.6	17	2123.8	27	2372.4	14	91.5
71_083	0.12137	0.00138	0.32017	0.00468	5.35795	0.0809	1976.5	20	1790.6	23	1878.2	13	95.0
71_084	0.15295	0.00204	0.41066	0.00613	8.65997	0.13986	2379.2	23	2218	28	2302.9	15	96.8
71_085c	0.1702	0.00184	0.43974	0.00643	10.31694	0.15213	2559.6	18	2349.5	29	2463.6	14	96.2
71_085r	0.12258	0.00152	0.33362	0.00502	5.63664	0.08988	1994.1	22	1855.9	24	1921.7	14	96.4
71_086	0.16759	0.00188	0.46232	0.00683	10.67956	0.16097	2533.7	19	2449.8	30	2495.6	14	98.5
71_087	0.18309	0.00206	0.50492	0.00761	12.74096	0.19443	2681.1	18	2634.9	33	2660.7	14	99.2
71_088	0.13149	0.00196	0.38359	0.00597	6.95225	0.12232	2118	26	2093	28	2105.4	16	99.4
71_089	0.18176	0.00213	0.48348	0.00732	12.11246	0.18804	2669	19	2542.4	32	2613.2	15	97.9
71_090	0.12517	0.00129	0.24121	0.00358	4.16125	0.06149	2031.3	18	1393	19	1666.4	12	82.0
71_091c	0.15966	0.00187	0.43938	0.00667	9.66701	0.15098	2452	20	2347.9	30	2403.6	14	98.0
71_091r	0.12358	0.00168	0.36157	0.00556	6.15831	0.10354	2008.6	24	1989.6	26	1998.6	15	99.5
71_092	0.15363	0.00187	0.37364	0.00567	7.91139	0.12534	2386.7	21	2046.5	27	2221	14	93.1
71_093	0.1508	0.00158	0.43045	0.00622	8.94923	0.13087	2355	18	2307.8	28	2332.8	13	99.1
71_094	0.17161	0.00233	0.47488	0.0073	11.23602	0.18699	2573.4	22	2504.9	32	2542.9	16	98.8
71_095	0.14214	0.00252	0.29244	0.00476	5.731	0.11244	2253.5	30	1653.7	24	1936.1	17	85.9
71_096	0.16459	0.00184	0.43891	0.0065	9.95901	0.15111	2503.3	19	2345.8	29	2431	14	97.1
71_097	0.16323	0.0019	0.41234	0.00609	9.27927	0.14253	2489.4	20	2225.6	28	2366	14	95.0
71_098	0.13025	0.00155	0.34902	0.00539	6.26165	0.10075	2101.3	21	1929.9	26	2013.1	14	95.8
71_099	0.1557	0.00171	0.43576	0.00643	9.35385	0.14106	2409.5	19	2331.6	29	2373.3	14	98.5
71_100c	0.16662	0.00199	0.45884	0.00686	10.54046	0.16362	2524	20	2434.4	30	2483.5	14	98.4
71_100r	0.12581	0.00213	0.34537	0.00542	5.99034	0.11267	2040.2	30	1912.5	26	1974.4	16	96.8
71_101c	0.15742	0.00173	0.23217	0.00337	5.03884	0.07435	2428.1	18	1345.8	18	1825.9	13	75.2
71_101r	0.11889	0.00167	0.2732	0.00415	4.47816	0.07604	1939.6	25	1557	21	1726.9	14	89.0
71_78	0.16595	0.00217	0.45465	0.0069	10.4021	0.16856	2517.2	22	2415.9	31	2471.2	15	98.2
71_80	0.13579	0.00174	0.35657	0.00535	6.67541	0.1075	2174.2	22	1965.9	25	2069.4	14	95.2

Table 4.1 Usagaran Isotope chemistry (cont)

Spot No.	Isotope Ratios				Ages (Ma)						Conc <sup>1</sup>		
	<sup>207</sup> Pb/ <sup>206</sup> Pb	1σ	<sup>207</sup> Pb/ <sup>235</sup> U	1σ	<sup>206</sup> Pb/ <sup>238</sup> U	1σ	<sup>207</sup> Pb/ <sup>206</sup> Pb	1σ	<sup>207</sup> Pb/ <sup>235</sup> U	1σ		<sup>206</sup> Pb/ <sup>238</sup> U	1σ
Sample T06-49		n= 80											
49-Z1	0.17922	0.00199	0.48571	0.00625	12.0025	0.15797	2645.7	18	2552.1	27	2604.6	12	98.4
49-Z2	0.17645	0.00175	0.47162	0.00608	11.47306	0.14501	2619.8	16	2490.7	27	2562.4	12	97.8
49-Z3	0.15092	0.00155	0.33061	0.00432	6.87888	0.08926	2356.4	17	1841.4	21	2095.9	12	88.9
49-Z4	0.12351	0.00123	0.30626	0.00398	5.21451	0.06674	2007.5	18	1722.3	20	1855	11	92.4
49-Z5	0.06206	0.00098	0.0838	0.00112	0.71699	0.01218	676.1	33	518.8	7	548.9	7	81.2
49-Z6	0.11903	0.01181	0.07639	0.00364	1.25605	0.11283	1941.7	168	474.6	22	826.1	51	42.5
49-Z7	0.12719	0.00139	0.35087	0.00447	6.15259	0.08029	2059.6	19	1938.8	21	1997.7	11	97.0
49-Z8	0.1599	0.00164	0.40737	0.00527	8.98148	0.11494	2454.6	17	2202.9	24	2336.1	12	95.2
49-Z9	0.15121	0.0017	0.34711	0.00449	7.23541	0.09651	2359.7	19	1920.8	21	2140.9	12	90.7
49-Z10	0.05792	0.00082	0.09262	0.00127	0.73958	0.01199	526.5	31	571	7	562.2	7	106.8
49-Z11	0.05788	0.00133	0.09452	0.00145	0.75362	0.01787	524.8	50	582.2	9	570.3	10	108.7
49-Z12	0.05911	0.00151	0.09128	0.00142	0.74352	0.01923	571.2	55	563.1	8	564.5	11	98.8
49-Z13	0.1606	0.00165	0.38175	0.00489	8.45058	0.10748	2461.9	17	2084.4	23	2280.6	12	92.6
49-Z14	0.10503	0.00123	0.1963	0.00255	2.84203	0.03897	1714.9	21	1155.4	14	1366.7	10	79.7
49-Z15	0.13142	0.00134	0.38551	0.00494	6.98375	0.08875	2117	18	2102	23	2109.4	11	99.6
49-Z16	0.05902	0.00121	0.0893	0.00132	0.72654	0.0156	567.8	44	551.4	8	554.5	9	97.7
49-Z17	0.15577	0.00167	0.40063	0.00513	8.60061	0.11124	2410.3	18	2171.9	24	2296.6	12	95.3
49-Z19	0.05932	0.00089	0.09523	0.00129	0.77867	0.013	578.7	32	586.4	8	584.7	7	101.0
49-Z20	0.05884	0.00092	0.09954	0.00133	0.80738	0.01369	561.2	33	611.7	8	601	8	107.1
49-z22	0.12391	0.00153	0.30923	0.00413	5.28129	0.07583	2013.2	22	1736.9	20	1865.8	12	92.7
49-z23	0.09063	0.00137	0.16994	0.00233	2.12284	0.03513	1438.8	29	1011.8	13	1156.3	11	80.4
49-z25	0.11637	0.00123	0.26772	0.00346	4.29403	0.05604	1901.2	19	1529.2	18	1692.2	11	89.0
49-z26	0.12626	0.0016	0.35655	0.00478	6.20436	0.09031	2046.5	22	1965.8	23	2005.1	13	98.0
49-z27	0.11912	0.00284	0.30128	0.00502	4.9463	0.11713	1943.1	42	1697.6	25	1810.2	20	93.2
49-z29	0.05954	0.00162	0.09361	0.00144	0.7682	0.02091	586.9	58	576.9	9	578.7	12	98.6
49-z30	0.17683	0.00176	0.56161	0.00719	13.68666	0.17306	2623.3	16	2873.3	30	2728.3	12	104.0
49-z31	0.14414	0.00166	0.34917	0.00459	6.93613	0.09486	2277.5	20	1930.6	22	2103.3	12	92.4
49_101	0.10775	0.00131	3.62891	0.05289	0.24433	0.00333	1761.7	22	1555.9	12	1409.2	17	80.0
49_102	0.12068	0.00164	4.88189	0.07619	0.29348	0.00411	1966.3	24	1799.1	13	1658.9	20	84.4
49_103	0.06424	0.00171	0.71881	0.01926	0.08118	0.00128	749.6	55	550	11	503.1	8	67.1
49_104	0.14834	0.00282	4.34605	0.0852	0.21256	0.00334	2326.9	32	1702.1	16	1242.4	18	53.4
49_105	0.05868	0.00123	0.73521	0.01615	0.0909	0.00133	555.3	45	559.6	9	560.9	8	101.0
49_106	0.06118	0.00131	0.80484	0.01797	0.09545	0.00142	645.5	46	599.6	10	587.7	8	91.0
49_107	0.12698	0.00156	5.76092	0.08496	0.32919	0.00455	2056.5	22	1940.6	13	1834.5	22	89.2
49_108	0.11549	0.00139	3.89492	0.05665	0.24471	0.00336	1887.5	21	1612.6	12	1411.1	17	74.8
49_109	0.1385	0.00144	6.84098	0.09218	0.3584	0.00482	2208.5	18	2091	12	1974.6	23	89.4
49_110	0.08691	0.00248	1.40542	0.03959	0.11734	0.00201	1358.5	54	891.2	17	715.2	12	52.6
49_111	0.05998	0.00153	0.81026	0.02103	0.09802	0.00153	603	54	602.6	12	602.8	9	100.0
49_112	0.1212	0.00218	5.91612	0.11319	0.35421	0.00543	1974	32	1963.6	17	1954.7	26	99.0
49_113	0.16475	0.00194	9.4629	0.13621	0.4168	0.00578	2505	20	2384	13	2245.9	26	89.7
49_114	0.06642	0.00204	0.86911	0.02646	0.09496	0.00161	819.6	63	635.1	14	584.8	9	71.4
49_115	0.13694	0.0015	9.51569	0.13393	0.50423	0.00699	2188.9	19	2389.1	13	2631.9	30	120.2
49_116	0.09225	0.00097	3.21207	0.04421	0.25267	0.00345	1472.3	20	1460.1	11	1452.2	18	98.6
49_117	0.15686	0.00158	10.15132	0.13638	0.4696	0.00639	2422.1	17	2448.7	12	2481.8	28	102.5
49_118	0.12028	0.00125	7.81044	0.10647	0.47116	0.00642	1960.4	18	2209.4	12	2488.7	28	126.9
49_119	0.14316	0.00224	4.62147	0.07945	0.23425	0.00348	2265.7	27	1753.2	14	1356.7	18	59.9
49_120	0.1058	0.0011	4.02818	0.05477	0.27626	0.00374	1728.2	19	1639.9	11	1572.5	19	91.0
49_121	0.1594	0.00165	15.31489	0.20772	0.69712	0.00947	2449.3	17	2835	13	3409.7	36	139.2
49_122	0.07948	0.00105	1.81595	0.02819	0.16578	0.00229	1184.1	26	1051.2	10	988.8	13	83.5
49_123	0.13486	0.00142	7.65585	0.10399	0.41191	0.00556	2162.2	18	2191.4	12	2223.6	25	102.8
49_124	0.10347	0.00116	4.46058	0.06267	0.31279	0.00424	1687.3	21	1723.7	12	1754.4	21	104.0
49_125	0.09583	0.00131	3.86542	0.06118	0.29268	0.00407	1544.4	26	1606.5	13	1654.9	20	107.2
49_126	0.1566	0.00175	5.46144	0.07573	0.25306	0.00342	2419.2	19	1894.6	12	1454.2	18	60.1
49_127	0.15713	0.00307	5.49246	0.10984	0.25364	0.00406	2425	33	1899.4	17	1457.2	21	60.1
49_128	0.06529	0.00183	0.7682	0.02153	0.08537	0.00137	783.8	58	578.7	12	528.1	8	67.4
49_129	0.12331	0.00134	5.01417	0.06847	0.29506	0.00394	2004.7	19	1821.7	12	1666.7	20	83.1
49_130	0.16196	0.00185	9.30396	0.12995	0.41685	0.00563	2476.2	19	2368.4	13	2246.2	26	90.7
49_131	0.12064	0.00168	5.23821	0.08263	0.31508	0.00439	1965.7	25	1858.9	13	1765.7	22	89.8
49_132	0.10824	0.00154	3.17663	0.05079	0.21297	0.00295	1769.9	26	1451.5	12	1244.6	16	70.3

Spot No.	Isotope Ratios			Ages (Ma)						Conc <sup>1</sup>			
	<sup>207</sup> Pb/ <sup>206</sup> Pb	1σ	<sup>207</sup> Pb/ <sup>235</sup> U	1σ	<sup>206</sup> Pb/ <sup>238</sup> U	1σ	<sup>207</sup> Pb/ <sup>206</sup> Pb	1σ	<sup>207</sup> Pb/ <sup>235</sup> U	1σ	<sup>206</sup> Pb/ <sup>238</sup> U	1σ	%
49_133	0.12661	0.00172	5.96344	0.09251	0.34181	0.00474	2051.4	24	1970.5	13	1895.4	23	92.4
49_134	0.16645	0.00295	9.43618	0.17547	0.4114	0.00638	2522.3	30	2381.4	17	2221.3	29	88.1
49_135	0.11587	0.00136	4.8117	0.06754	0.30128	0.00399	1893.5	21	1786.9	12	1697.6	20	89.7
49_136	0.1211	0.00298	3.24047	0.07849	0.19414	0.00324	1972.5	43	1466.9	19	1143.7	17	58.0
49_137	0.11655	0.00125	5.5957	0.07441	0.3483	0.00452	1904	19	1915.4	11	1926.5	22	101.2
49_138	0.17246	0.00246	10.33894	0.16296	0.4349	0.00614	2581.7	24	2465.6	15	2327.8	28	90.2
49_139	0.11534	0.00299	4.65473	0.11881	0.29275	0.00503	1885.2	46	1759.1	21	1655.2	25	87.8
49_140	0.13474	0.00192	4.31447	0.06775	0.23227	0.00319	2160.7	25	1696.1	13	1346.4	17	62.3
49_141	0.0785	0.00216	1.04461	0.02838	0.09652	0.00155	1159.6	54	726.2	14	594	9	51.2
49_142	0.13777	0.00186	4.26278	0.06437	0.22443	0.00303	2199.4	23	1686.2	12	1305.2	16	59.3
49_143	0.09243	0.00221	1.12408	0.02668	0.08821	0.00136	1476.1	45	764.9	13	545	8	36.9
49_144	0.11942	0.00144	4.50305	0.06319	0.2735	0.00356	1947.6	21	1731.5	12	1558.5	18	80.0
49_145	0.06453	0.00134	0.82192	0.0176	0.09244	0.00133	759.2	43	609.1	10	570	8	75.1
49_146	0.12487	0.00128	6.85007	0.08868	0.39818	0.00516	2026.9	18	2092.2	11	2160.6	24	106.6
49_147	0.11443	0.00125	4.3822	0.05866	0.27796	0.00363	1871	20	1709	11	1581.1	18	84.5
49_148	0.12579	0.0014	5.01047	0.06766	0.28911	0.0038	2040	19	1821.1	11	1637.1	19	80.3
49_149	0.15168	0.00197	6.02359	0.08916	0.28826	0.00394	2364.9	22	1979.3	13	1632.8	20	69.0
49_150	0.11402	0.00127	4.04676	0.05482	0.25763	0.00338	1864.4	20	1643.6	11	1477.7	17	79.3
49_151	0.12893	0.00139	6.04077	0.08017	0.34009	0.00445	2083.4	19	1981.7	12	1887.1	21	90.6
49_152	0.12487	0.00137	6.07983	0.08155	0.35343	0.00464	2026.9	19	1987.4	12	1950.9	22	96.3
49_153	0.14554	0.00155	5.77184	0.07618	0.28788	0.00377	2294.1	18	1942.2	11	1630.9	19	71.1



## Chapter 5—P-T-t evolution of the 2.0 Ga eclogite-hosting Usagaran orogenic belt, Tanzania

### 5.1 Introduction

Eclogites commonly occur as lenses or boudins within metapelites and felsic gneisses in subduction related convergent orogens. Examples of eclogite-hosting terranes include the Bohemian Massif and Dora-Maira Massifs in the European Alps, the Western Gneiss Region in Norway and the Dabie-Su-Lu in China (see review of Chopin (Chopin, 2003). Metamorphism of the eclogites and surrounding gneisses in the Usagaran Orogen of central Tanzania has been dated by U-Pb zircon and monazite as ~2.0 Ga (Collins et al., 2004b; Möller et al., 1995). Because eclogites are often considered to be indicative of the occurrence of deep subduction, and because the Usagaran Orogen hosts one of the oldest recorded well preserved eclogite-hosting terrains, it is important to our understanding of the geodynamic evolution of the Earth that we understand how this terrain formed. Does the presence of eclogite in the Usagaran Orogen prove the existence of Palaeoproterozoic deep subduction, or not? By better constraining the burial and exhumation histories recorded in these rocks we hope to begin to answer this question.

The question of when Earth first developed a modern style plate tectonic system has been the subject of debate over the last decade or more (eg. Maruyama & Liou, 1998; Stern, 2005; Brown 2007a, b; (Sizova et al., 2010)). Metamorphic, structural and geochronological studies have identified fundamental changes in the styles of metamorphism through time. Differences in tectonic processes are discussed in chapter 1 of this thesis, and the reasons for these differences (i.e. changes in mantle temperatures, geothermal gradients, plate sizes, etc) are discussed in detail in Brown 2007a.

A common question in studying eclogite-hosting terrains is whether the surrounding rocks have experienced the same burial and exhumation history as the eclogites themselves, or have been juxtaposed at mid-crustal levels during the exhumation process. Previous such studies have demonstrated shared P-T paths in some terrains such as Adula Nappe, (Chopin, 2003; Meyre et al., 1999; Wei and Powell, 2006), however separate P-T paths have been postulated or proven in others (Okay, 1989; Štípska et al., 2006a). Štípska & Powell (2006) used P-T pseudosections to constrain pro-, peak-, and retrograde metamorphism, showing clearly separate paths in eclogites and surrounding gneisses in the Bohemian Massif. The same approach was applied to glaucophane-phengite schists associated with eclogites and blueschists in the southern Tianshan high-pressure Orogen in northwest China (Wei and Powell, 2006). This study showed that peak metamorphic conditions were the same in all three rock-types. Calculations based on garnet-omphacite-phengite thermobarometry and THERMOCALC average P-T calculations were applied to Franciscan eclogites by Tsujimori *et al.* (2006) to assess the relationship between the eclogite-facies metamorphism and a blueschist-facies retrogression.

The best way to evaluate metamorphic histories of a

complex association of metamorphic rocks is to examine the geothermobarometry of each rock unit, evaluating the P-T conditions experienced during prograde, peak and retrograde metamorphism to determine whether each rock unit shared a similar P-T history, or whether different P-T trajectories are tractable from the preserved assemblages. It has been theorized that in some instances where the gneisses surrounding eclogites preserve lower pressure mineral assemblages that this is an issue of preservation. Metapelitic and felsic rocks are more likely to have experienced the combined effects of fluid, plasticity and kinetics leading to greater recrystallisation (Rubie, 1990; Schmädicke, 1994) and have mineral assemblages which are more readily affected by retrograde metamorphism than eclogites, meaning that it is possible higher pressure minerals have been overprinted during the decompression process (Proyer, 2003). The mineral assemblages in eclogites and other mafic rocks are less affected by retrogression, particularly where dehydrated, and are thus more likely to preserve their high pressure mineral chemistry (Štípska and Powell, 2005).

If the different rocks in a terrane have experienced different metamorphic histories it suggests that exhumation of the eclogites involved emplacement of high-pressure rocks into a lower pressure rock suite. Exhumation can occur during a variety of processes including slab roll-back (Froitzheim et al., 2003), extrusion in the subduction trench (Cloos, 1983), buoyancy caused by density differences in surrounding gneisses (England and Holland, 1979a), reverse thrusting during accretionary orogenesis (Collins and Robertson, 1997), or a combination of these processes.

In this study we apply thermobarometry to a large eclogite lens and the surrounding metapelites that occurs amongst felsic gneisses and metavolcanics in the Rubeho Mountains of central Tanzania (Figure 5.1 ). Three approaches are used in this study:

- Conventional thermobarometry using THERMOCALC to obtain P-T conditions during metamorphism.
- Modeling the diffusive properties of garnet to study the rate of metamorphic cooling.

Trace element thermometry (Ti in zircon and Zr in rutile) to constrain maximum temperatures experienced by these samples.

All three approaches are based on mineral chemistry, from individual points (for thermobarometry) and from traverses across individual garnets for the diffusion study.

### 5.2 Geological setting

The evolution of the Rubeho and Usagara mountain ranges in Tanzania was driven by three orogenic events, the Palaeoproterozoic Usagaran Orogeny, the Cryogenian-Ediacaran East African Orogeny and the Ediacaran-Cambrian Malagasy Orogeny (as defined by Collins and Pisarevsky (2005)). The region affected by the Neoproterozoic-Cambrian orogenies is known as the East

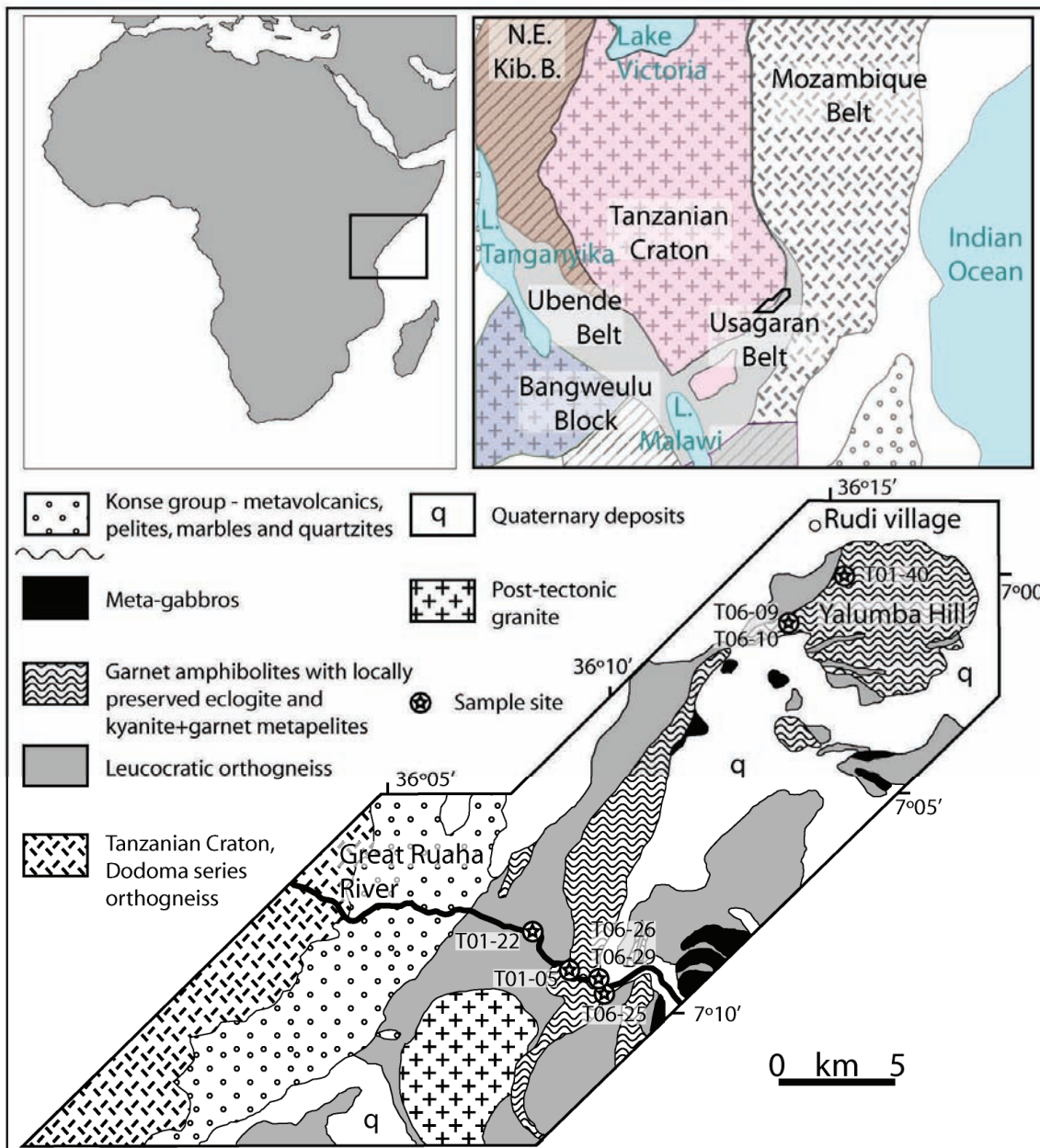


Figure 5.1 Map showing the location of the Usagaran Orogen in Tanzania. The box indicates the location of the study area. Blow-up shows basic geology and location of samples discussed in this study.

African Orogen (Stern, 1994b). The East African Orogen is associated with the assembly of Gondwana and affects much of the Mozambique Orogen of eastern Tanzania, Kenya, northern Mozambique, and Malawi. The Usagaran Orogen is bounded on the northwest by the Tanzanian Craton, and on the south and eastern sides by the Mozambique Orogen (figure 5.1).

The Usagaran Orogen is a generally SW-NE trending orogenic belts which, in the north, is made up of the metasedimentary Konse Group and the Isimani Suite that has previously been divided into the Luhomero, Mbunga River and Iguruba Lithodemes (Mruma, 1989a). The Luhomero lithodeme is composed of eclogite & associated garnetiferous gneisses of Yalumba Hill (sometimes referred to as Nyalumba Hill on some maps). These gneisses are surrounded by the Mbunga River Lithodeme which contains porphyroblastic microcline gneiss, muscovite-biotite gneiss, leucocratic muscovite-feldspar gneiss, garnet amphibolite, epidote- and garnet-amphibolites with pyroxene bearing pockets, kyanite-garnet-biotite gneiss,

and grunerite-magnetite-quartzite (Mruma, 1989). The gneisses proximal to the Luhomero lithodeme are muscovite-biotite gneiss, leucocratic muscovite-feldspar gneiss, garnet amphibolite and kyanite-garnet-biotite gneiss.

Both the Luhomero and Mbunga River lithodemes are characterized by generally south-east-dipping structures and foliations (Reddy et al., 2003). Kinematics indicate mostly top-to-north-west shear with some sinistral (top-to-north-east) shearing.

### 5.2.1 Previous metamorphic studies

The overall metamorphic evolution of the Usagaran Orogen has not been studied in detail, however *P-T* calculations have been done for individual some rock suites. The formation of the eclogites was assessed by Möller et al. (1995), using multi-mineral Fe-Mg exchange thermobarometry on eclogite and metapelites, as occurring at ~18 kbar and 700°C.

The Usagaran Orogen is characterized by generally east-

Table 5.1. Summary of petrological observation of metamorphic assemblages.

P = peak assemblage, fol = minerals which define the foliation, R(x) = retrograde assemblage associated with mineral(s) x, I(x) = inclusions in mineral x

Sample	T01-05	T01-22a	T06-25	T06-27	T06-26	T06-29	T01-40	T06-09	T06-10
Rock type	metapelite				mafic gneiss		eclogite		
Location – E	186053	184029	186315		186225	186225	199072	195240	195240
– N	9208698	9210254	9208486		9208532	9208532	9227224	9225768	9225768
Quartz	P	P	P	P	P	P	R <sub>(g)</sub>		R <sub>(v)</sub>
Amphiboles	R <sub>(ky)</sub> I <sub>(g)</sub>	P	P	P	P <sub>fol</sub>	R <sub>(g-cpx) (g-pl)</sub>	R <sub>(g)</sub>	R <sub>(v) (g-cpx)</sub>	R <sub>(v) (g-cpx)</sub>
K-feldspar					P				
Plagioclase	P	R <sub>(g)</sub>	P	P	P	P	I <sub>(g)</sub> R <sub>(g)</sub>	R <sub>(g-cpx)</sub>	R <sub>(g-cpx)</sub>
Garnet	P	P	P	P	P	P	P	P	P
Orthopyroxene						P <sub>fol</sub>			R <sub>(v)</sub>
Clinopyroxene							P	P	P R <sub>(v)</sub>
Biotite	P <sub>(fol)</sub>		P <sub>(fol)</sub>	P <sub>(fol)</sub>	P <sub>fol</sub>				
Muscovite		R <sub>(g)</sub>	P <sub>fol</sub> R <sub>g/ky</sub>						
Sillimanite	R <sub>(ky)</sub>		R <sub>(ky)</sub>	R <sub>(ky)</sub>					
Kyanite	P P <sub>(g)</sub>	P <sub>(fol)</sub> I <sub>(g)</sub>	P R <sub>fol</sub>	P P <sub>(g)</sub>					
Ilmenite	P <sub>(ky g)</sub>	P <sub>(fol)</sub>	P <sub>(fol)</sub>	P <sub>(ky g)</sub>					
Rutile (?)	P	P	P	P			P		
Zircon		I <sub>(g)</sub>					I <sub>(g)</sub>		
Sericite		R <sub>(ky)(g)</sub>							
Apatite	I <sub>(bi)</sub>	I <sub>(g)</sub>	Pa	I <sub>(bi)</sub>			I <sub>(g)</sub>		
Staurolite		I <sub>(pl)(g)</sub>							
Ilmenite		P <sub>(ky)</sub>	limonite		P		P R <sub>(amp+pl)</sub>	R <sub>(g-cpx)</sub>	R <sub>(g-cpx)</sub>

dipping structures and foliations. Metamorphism at the northern end of the belt is at amphibolite facies (Mruma, 1989a), with greenschist facies mineral assemblages seen in late faults and shears (Reddy et al., 2003) and eclogite facies (700-750 °C and 18 kbar) in the Luhomero lithodeme (Möller et al., 1995). In the southern end of the Usagaran Orogen, south of the Malawi border, granulite facies metamorphism (850-880°C and 9-11 kbar) is recorded in enderbitic gneisses (Ring et al., 1997). Sillimanite-cordierite gneisses are recorded in the Isimani suite around 100km SW of the eclogites at Nyalumba Hill (Meinhold and Venzlaff, 1965; Mruma, 1989a) indicating that some units have seen granulite facies metamorphism.

### 5.3 Metamorphic petrology

Sample locations are shown in figure 5.1. Representative samples were chosen from the pelitic gneisses surrounding the eclogite body, from eclogitic rocks at Yalumba Hill, and from retrogressed eclogitic rocks in the tail of the eclogite body. The metapelites and retrogressed eclogitic sample were selected from the south of the study where a detailed structural section by Reddy et al. (2003) reveals the structural relationship between the sheets of eclogitic and other mafic rocks and the surrounding felsic gneisses and metapelite rocks (Reddy et al., 2003). From this section two pelitic samples were selected from

structurally "above" the eclogite body and one from "below". From the main eclogite body both highly strained and unstrained samples were chosen. The petrology of all samples is summarized in table 5.1.

#### 5.3.2 Eclogites and mafic rocks

Three samples were taken from two locations at Yalumba Hill and a fourth sample was taken from an extension of the Yalumba Hill lithology that forms a 40 km 'tail' (Figure 5.1) and crops out in the Great Ruaha River. T01-40 comes from partway up the hill in the core of an area with outcropping eclogitic rocks. Samples T06-09 and T06-10 come from further west, and were targeted to investigate how P-T vary with differing strain gradients in these rocks. T06-09 is an unstrained sample while T06-10 records higher strain. All samples presented by Möller *et al.* (Möller et al., 1995) come from this vicinity. While omphacite is typically the clinopyroxene end-member found in eclogite the samples in this study do not contain omphacite. The samples described by Möller *et al.* (1995) contain very minor omphacite.

Sample T01-40 has a primary mineralogy of coarse garnet, clinopyroxene (diopside), fine grained ilmenite and rare primary plagioclase. The presence of primary plagioclase within the sample indicates that it is not an eclogite *sensu strictu*. A secondary assemblage of amphibole (grunerite), ilmenite and plagioclase between primary



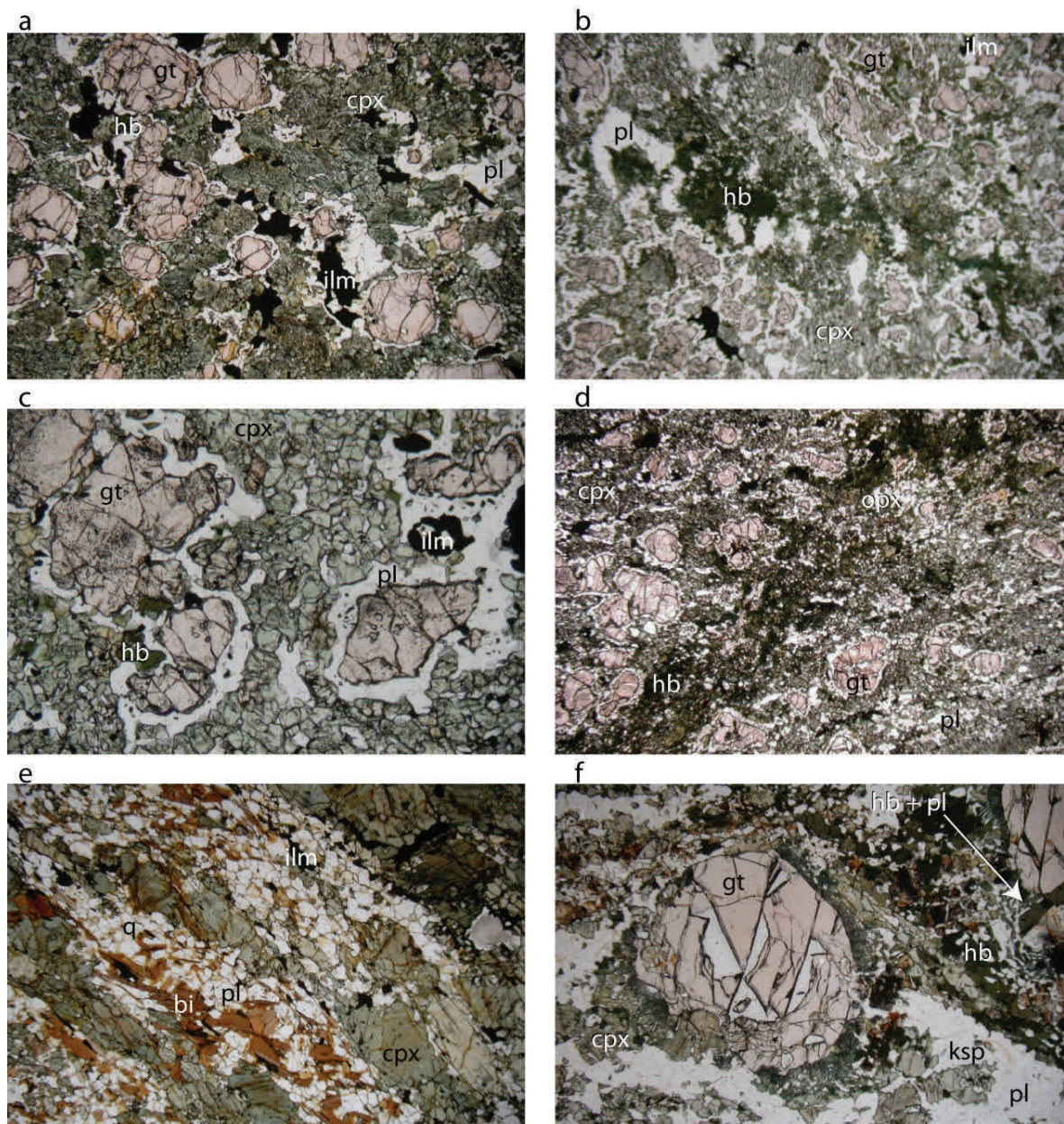


Figure 5.2. Photomicrographs of metamorphic textures/assemblages in each sample.

garnet and clinopyroxene is interpreted to have formed during retrograde metamorphism (Figure 5.2 a). Most clinopyroxene is diopside; however it commonly contains augite exsolution lamellae. This sample was dated using the U-Pb zircon Sensitive High Resolution Ion Microprobe (SHRIMP) technique and yielded an age of  $1999 \pm 1.1$  Ma (Collins et al., 2004b).

Sample T06-09 is an eclogitic sample with no visible foliation. The primary mineralogy is garnet, clinopyroxene (aegirine-augite) and ilmenite. Grain size ranges from 1-5 mm garnet surrounded by < 1mm clinopyroxene (Figure 5.2 b). Clinopyroxene has a sieve-like appearance with small late growths of wollastonite, ilmenite and plagioclase. Fine grained ilmenite is evenly distributed through the sample with rare larger ilmenite (0.2-0.3 mm) sometimes associated with garnet. Garnet contains abundant negative inclusions, indicating that it has undergone partial-melting at some stage in its history. Coronas of plagioclase and ilmenite separate garnet and clinopyroxene (figure 5.2 c), suggesting garnet resorption during which Ti from garnet was unable to be accommodated in plagioclase, thus forming very fine grained ilmenite. A 2mm

wide vein of amphibole (grunerite and ferrogredite), plagioclase and ilmenite runs across the sample.

Sample T06-10 is a foliated eclogitic sample with the foliation cut by distinct veins. The primary mineralogy is coarse grained garnet, clinopyroxene (diopside and augite) and fine grained ilmenite with grain sizes up to 1 mm diameter. Foliation is defined by plagioclase ribbons, non-euhedral garnet and clinopyroxene. Although there are larger (1 mm) crystals, most clinopyroxene is fine-grained (< 0.1 mm) and interspersed with plagioclase and ilmenite. Most garnet is separated from clinopyroxene by coronas of retrograde plagioclase and hornblende with rare plagioclase-ilmenite symplectites. Veins cutting the sample cut the foliation at obtuse angles, and are comprised of amphibole (ferrogredite) and wollastonite replacing clinopyroxene and plagioclase (figure 5.2 d).

Sample T06-26 is a mafic gneiss from within the 'tail' of the eclogite boudin where it crosses the Great Ruaha River, between the metapelitic samples T01-05 and T06-26. It is compositionally banded on a mm-cm scale. Mafic bands are coarse grained (up to 1 cm) amphibole, or-



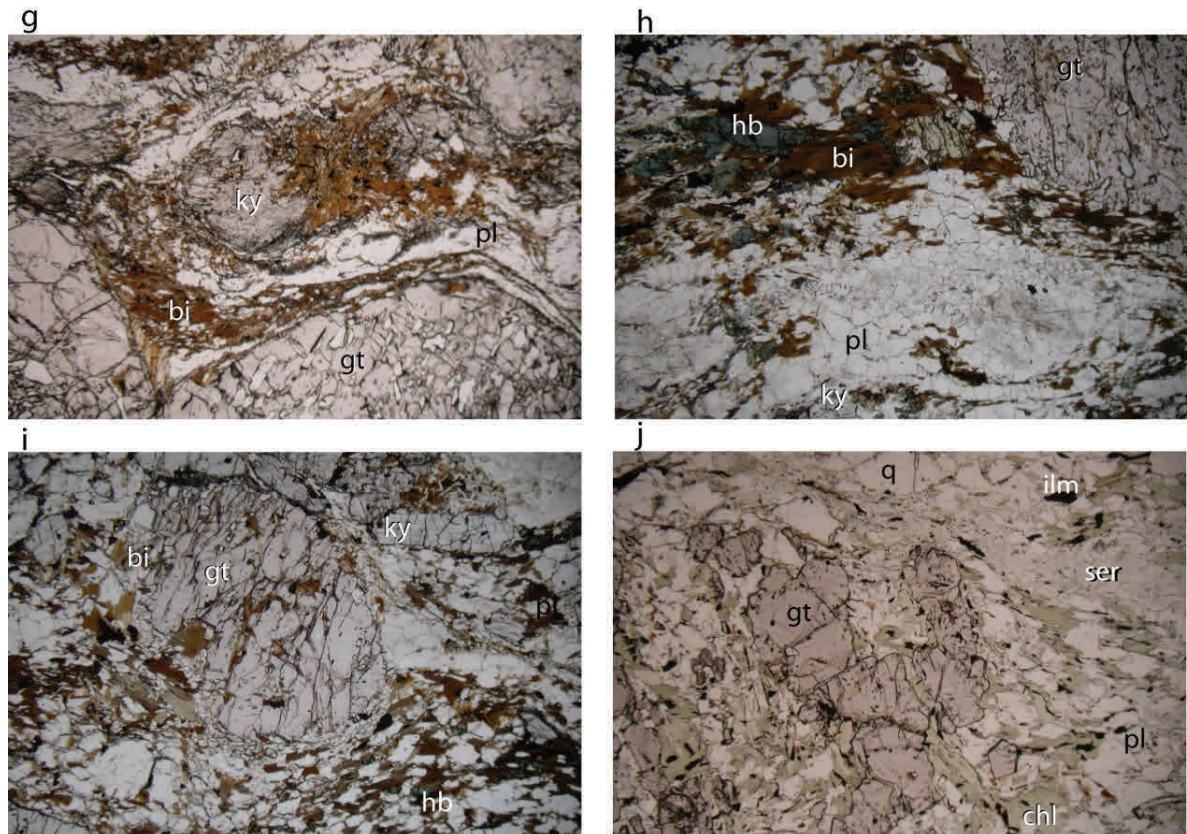


Figure 5.2. (cont.) Photomicrographs of metamorphic textures/assemblages in each sample.

thopyroxene and clinopyroxene with fine-grains of minor biotite at the margins (Figure 5.2 e). Felsic bands contain fine-grained (up to 0.2 mm) quartz, plagioclase and coarser garnet (up to 0.8 cm). Ilmenite and rare rutile occur throughout the sample.

Sample T06-29 is a mafic gneiss from the same area as T06-26. The primary assemblage is garnet, clinopyroxene (aegirine with some diopside exsolution), plagioclase, K-feldspar and quartz (Figure 5.2 f). A late symplectitic corona texture of plagioclase and grunerite developed between garnet and clinopyroxene.

### 5.3.3 Metapelites

Four metapelitic samples were chosen from different structural zones and exhibit differing strain gradients. Each comes from alongside the Great Ruaha River where outcrop exposure is excellent. Sample T01-22 was collected furthest from the eclogite boudin, it is situated structurally lower than that boudin, and mineral fabrics indicate it has been subjected to moderate strain. T01-05 was collected adjacent to, and structurally below, the eclogite boudin and the well developed foliation and highly rotated garnet porphyroclasts suggest this sample has experienced the highest strain of these samples. T06-25 and T06-27 are from adjacent to and structurally above the eclogite boudin.

Samples T01-05, T06-25 and T06-27 have very similar mineral assemblages, comprising peak assemblages of garnet, biotite, kyanite, plagioclase, quartz, ilmenite, rutile and minor amphibole (ferro-gedrite) and retrograde assemblages of biotite, sillimanite, plagioclase and muscovite. Garnet size and strain fabrics are inversely related, with the largest garnets in the lower strained samples,

T06-25 and T06-27 (figure 5.2 g & h), and the smallest garnet in T01-05, the most strained sample (Figure 5.2 i).

In contrast sample T01-22 contains only minor biotite, with chlorite as the dominant mafic mineral, suggesting that this assemblage may be linked to greenschist thrust-zone formation during the Neoproterozoic East-African orogen. Fragmented garnet remains along with ilmenite, quartz, and plagioclase. Cracks in garnets are filled with chlorite, muscovite, quartz and plagioclase (figure 5.2 j). Biotite has been almost completely replaced by chlorite and muscovite with only small remnants in garnet pressure shadows. Kyanite is completely replaced by sericite masses. Rare staurolite also occurs as inclusions in garnet.

## 5.4 Analytical procedures

### 5.4.1 Electron Microprobe

Analyses were done at Adelaide Microscopy at the University of Adelaide on a Cameca SX51 electron microprobe (EMP). Elements were calibrated against synthetic Astimex standards. Operating conditions for quantitative analyses were a 15kV accelerating voltage, 20nA beam current and 2-3  $\mu\text{m}$  beam diameter. For selected garnet grains compositional maps were also run (figure 5.3). These were conducted by setting the four spectrometers to measure the peaks of Mg, Ca, Fe and Mn. Operating conditions for mapping were an accelerating voltage of 15kV and a beam current of 100 nA. Trace element data for Ti-in-quartz, Ti-in-zircon and Zr-in-rutile were collected using the same beam and current with extended count times to lower detection limits. Representative electron microprobe analyses (EPMA) are shown in table 4.2.



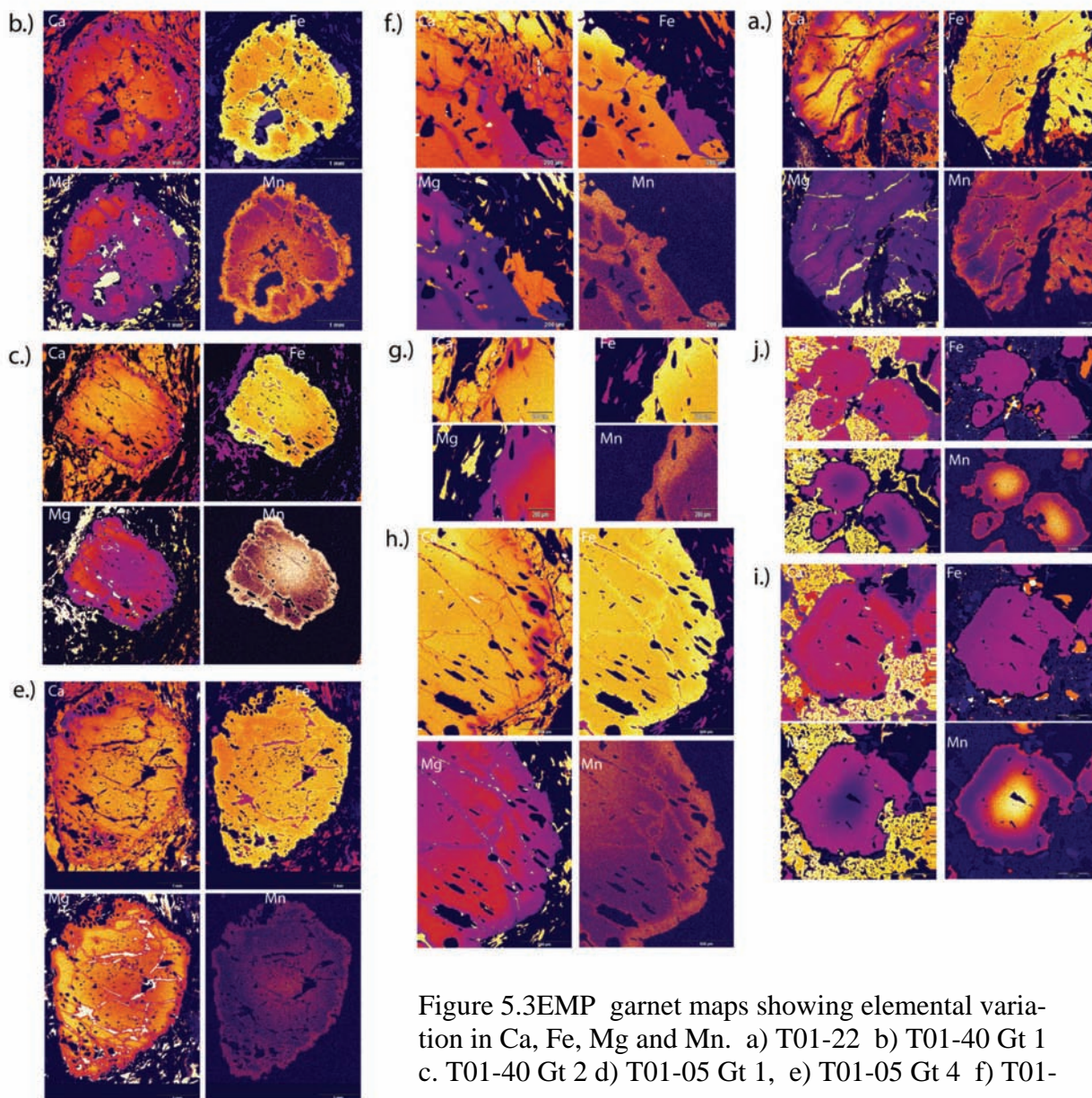


Figure 5.3 EMP garnet maps showing elemental variation in Ca, Fe, Mg and Mn. a) T01-22 b) T01-40 Gt 1 c. T01-40 Gt 2 d) T01-05 Gt 1, e) T01-05 Gt 4 f) T01-

#### 5.4.1.1 Garnet profiles

Garnet samples were selected from thin sections, and from whole garnets extracted from metapelites. Extracted garnets were cut in half then mounted in epoxy before polishing and carbon coating. By extracting the garnets the section can be well constrained to pass through the centre of the mineral. In thin sections the largest garnet was selected and assumed to be cut through the centre. Garnets were analysed on the electron microprobe, and either elemental maps, a quantitative profile or both were obtained for each garnet.

Garnet zoning in eclogitic samples (figure 5.3 i & j, figure 5.4) show samples from the tail and edges of the eclogite boudin (T06-26, T06-10 and T06-09) with relatively flat centers curving towards the margins contrast with garnets in T01-40 which have a more M-shaped curve in almandine and pyrope and W-shaped curve in spessartine compositions, although grossular content is relatively even across the grain. A central bell shaped curve in the spessartine zonation suggests that the central zone preserves part of the prograde garnet zonation (Spear, 1991;

Yardley, 1977). Samples T06-09 and T06-10 have distinct rim zones with compositions lower in grossular and pyrope, and higher in almandine.

Garnets in the metapelitic samples show variable chemical zonation profiles (figure 5.3 a-h, figure 5.4). These metapelites generally show slightly flatter W-shaped spessartine zoning curves than the eclogites, with a central peak and a slight increase in the spessartine component at the margins. Almandine-pyrope zoning in most garnets shows little discernable zoning in the centre of smaller (< 0.5 cm) garnets. Larger garnets (ie ~1cm garnets in T01-5 and T06-25) display distinct central zonation with peaks in spessartine, almandine and grossular and a depression in the pyrope curve. The rim compositions of these garnets show distinct zoning in almandine and pyrope compositions, and in some grains also have small peaks in the spessartine composition.

#### 5.4.2 Thermobarometry

##### 5.4.2.1 THERMOCALC overview

Pressure and temperatures for the formation of metamor-

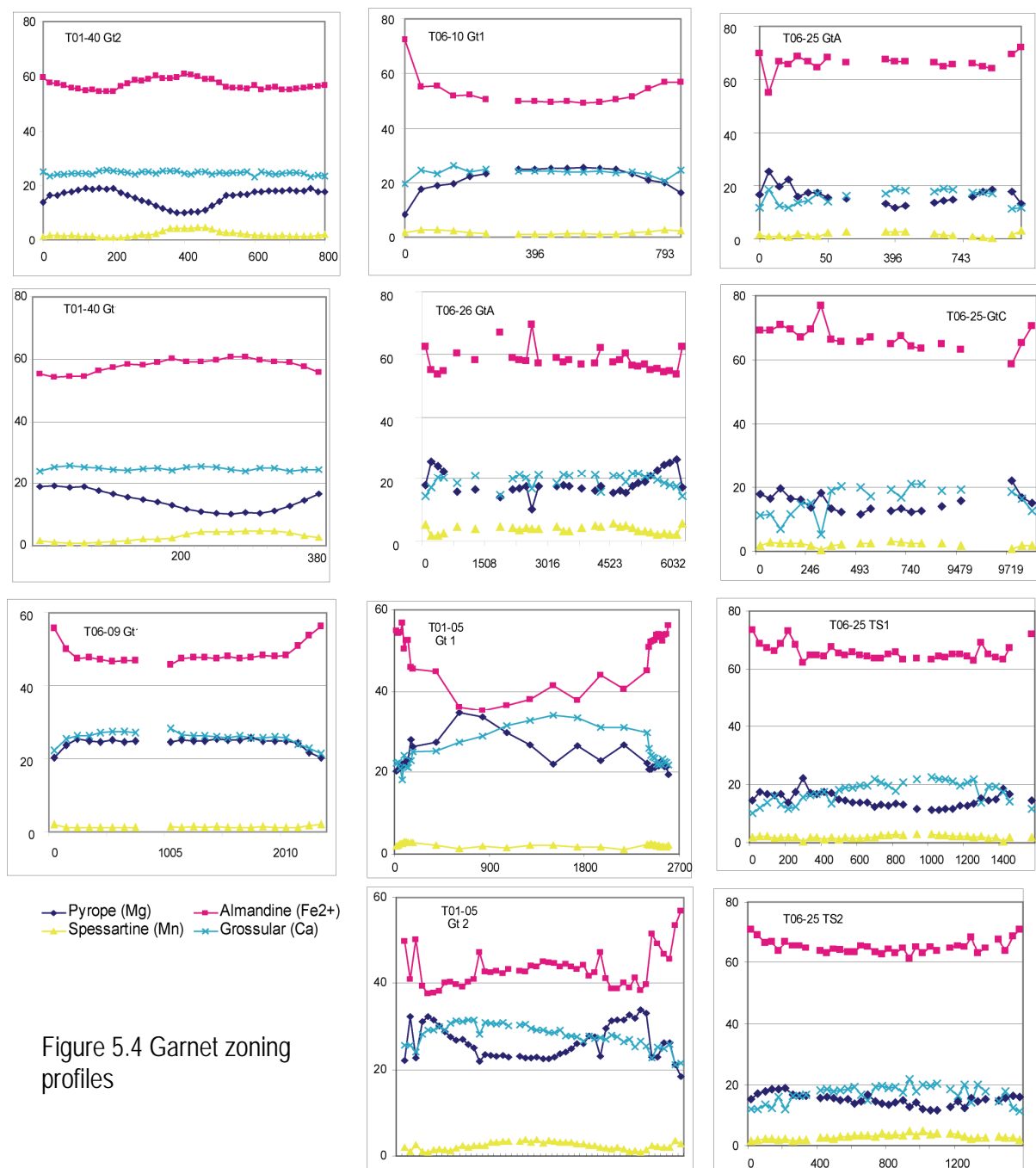


Figure 5.4 Garnet zoning profiles

phic minerals were calculated using EPMA mineral chemistry analyses (table 5.2) processed using the AX software of Holland and Powell (2005) to calculate end-member activities. A representative output file from AX is provided in Appendix 2.

Pressures and temperatures for the formation of metamorphic mineral assemblages were calculated using THERMOCALC v3.21 in the average- $P$ , average- $T$  and average- $PT$  mode with the updated internally consistent datasets of Holland and Powell (Holland and Powell, 1998). This technique was chosen because it uses multiple mineral equilibria, statistically tests the result using a  $\chi^2$  test to check the assumption that the minerals being used are in equilibria, and preserves the uncertainties in activities and enthalpies of mineral end-members and thermodynamic equations in calculating  $P$ - $T$  results with errors. The average- $P$  approach allows the calculation of pressure for a chosen temperature, while the average- $T$  approach calculates the temperature for a given pressure. The average- $PT$  approach calculates pressure and

temperature simultaneously, however this approach cannot always be used as some assemblages or assemblage compositions may not allow an average  $PT$  calculation due to insensitivity to either pressure or temperature.

All samples processed using THERMOCALC produced an independent set of reactions, and  $P$ - $T$  intersections defined using these equilibria were able to pass the  $\chi^2$  test at the 95% confidence level. End-members were occasionally omitted from calculations due to their poor fit within the equilibria generated. This improved the statistical fit of the calculation but did not significantly alter the determined  $P$ - $T$  estimates. The existence of end-member outliers in otherwise well constrained dataset may reflect either inadequacies in activity models for certain ranges of mineral compositions, or analytical issues relating to electron microprobe analysis (e.g. (Mawby, 2000)).

#### 5.4.2.2 $P$ - $T$ calculations

To broaden the pool of data available for this location  $P$ - $T$

Table 5.3 Summary of P-T calculations

Sample	Stage	Mineral assemblage	Average $P$ (kbar, $\pm 1\sigma$ )	Average $T$ ( $^{\circ}\text{C} \pm 1\sigma$ )
<b>Pelite</b>				
T06-25	Peak	g bi pl ky q	$12.5 \pm 1.6$	$610 \pm 83$
	Peak	g bi pl ky q	$11.7 \pm 2.4$	$670 \pm 101$
	Retro	g bi pl q ky	$9.4 \pm 2.1$	$630 \pm 107$
T01-22	Peak	gt <sub>81</sub> pl <sub>45</sub> ilm <sub>53</sub> bi <sub>84</sub>	$9.9 \pm 1.6$	$622 \pm 78$
	greenschist	gt <sub>293</sub> chl <sub>295</sub> pl <sub>63</sub> ilm <sub>294</sub>	$9.4 \pm 0.7$	$574 \pm 9$
T01-05	Peak	gt <sub>6</sub> pl <sub>87</sub> bi <sub>111</sub> mu <sub>55</sub>	$11.4 \pm 4.6$	$840 \pm 258$
<b>Eclogite</b>				
T06-09	Retro	g <sub>82</sub> amph <sub>1062</sub> pl <sub>1039</sub>	$7.5 \pm 1.5$	$596 \pm 106$
T06-10	Peak	pl <sub>82</sub> g <sub>20</sub> px <sub>92</sub> ( $\downarrow$ Mg)	$15.2 \pm 1.6$	$1042 \pm 113$
	Peak	pl <sub>82</sub> g <sub>20</sub> amph <sub>95</sub> px <sub>91</sub> ( $\uparrow$ Mg)	$14.5 \pm 1.7$	$1005 \pm 122$
	Retro Vein	gt <sub>12</sub> pl <sub>27</sub> ( $\downarrow$ Ca) px <sub>39</sub> ( $\uparrow$ Ca)	$13.4 \pm 2$	$923 \pm 137$
<b>Mafic gneiss</b>				
T06-26	Retro	gt cpx opx gt-bi-pl	$11.5 \pm 1.5$	$840 \pm 90$
Recalculated mineral assemblages from (Möller et al., 1995)				
T68-6	Peak	cpx <sub>105</sub> , g <sub>13</sub> , pl <sub>60</sub>	$17.2 \pm 3.6$	$839 \pm 173$
	Retro	cpx <sub>115</sub> , g <sub>15</sub>	n.e.a.*	
T69-12	Peak	gt <sub>(22)19</sub> pl <sub>102</sub> cpx <sub>150</sub> hbl <sub>145</sub>	n.e.a.*	
	Retro	gt <sub>78</sub> cpx <sub>148</sub> pl <sub>120</sub> hbl <sub>145</sub>	n.e.a.*	
T68-7	Peak	gt <sub>48</sub> cpx <sub>55</sub> , opx <sub>47</sub>		
	Retro	gt <sub>98</sub> pl <sub>80</sub> opx <sub>69</sub> Hbl <sub>12</sub>	$10.5 \pm 1.1$	$899 \pm 55$
T69-6	Peak	gt <sub>82</sub> , pl <sub>2</sub> , bt <sub>77</sub> ky q	$8.4 \pm 2.1$	$514 \pm 101$
	Retro	gt <sub>67</sub> pl <sub>59</sub> bt <sub>61</sub> sill q	$11.2 \pm 1.5$	$831 \pm 83$
T69-4	Peak	gt <sub>84</sub> pl <sub>7</sub> bt <sub>95</sub> ky q	$13.4 \pm 3.7$	$917 \pm 218$
	Retro	gt <sub>20</sub> pl <sub>99</sub> sill q	n.e.a.*	

\* n.e.a. indicates that given assemblage did not yield a statistically valid result when used to generate P-T conditions in THERMOCALC, and is thus unlikely to represent an equilibrium mineral assemblage.

conditions for the samples from Möller et al. (1995) have been recalculated where possible (table 5.3) using the internally consistent dataset of Holland and Powell (1998). Some samples could not be recalculated as not all analyses of minerals in the assemblages were included, and because in some instances the calculations of Möller et al. (1995) were based on assemblages which based on the statistics given by THERMOCALC were not at equilibrium.

P-T calculations for eclogite and mafic samples (table 5.3) indicate peak conditions in the core of the eclogite complex at  $17.2 \pm 3.6$  kbar at  $839 \pm 173$  °C with subsequent higher temperature, lower pressure conditions of  $10.5 \pm 1.1$  kbar and  $899 \pm 55$  °C recorded in the core. Sample T06-10 from the margins of the main eclogite body records conditions of  $14.9 \pm 2.3$  kbar at  $1023 \pm 122$  °C. The sample in the tail of the eclogite boudin (T06-26) does not retain the high-pressure mineral chemistry, recording peak conditions at  $11.5 \pm 1.5$  kbar and  $840 \pm 90$  °C, which places metamorphism in the granulite-facies.

The metamorphic conditions recorded by metapelites indicate peak pressures of  $10.7 \pm 3.9$  kbar, and peak temperatures at around  $609 \pm 182$  °C. Cores of garnet and plagioclase from sample T69-6 of Möller *et al.* (1995) were reported to preserve conditions of  $8.4 \pm 2.1$  kbar and  $514 \pm 101$  °C while the rims of grains record  $11.2 \pm 1.5$  kbar and  $831 \pm 83$  °C. Recalculation of these conditions in this study gives peak conditions of  $13.4 \pm 3.7$  kbar and  $917 \pm 218$  °C. There are no garnet inclusions or textural evidence in these samples that suggest that they have reached higher pressures. A later metamorphic event is recorded in sample T01-22, where an assemblage of chl-pl-ilm in equilibrium with outermost garnet records P-T condition of upper amphibolite facies  $9.4 \pm 0.7$  kbar,  $574 \pm 9$  °C.

#### 5.4.3 Trace element thermometry

In this study, temperatures estimated from trace element concentrations in accessory minerals utilise the Zr in rutile thermometer of Ferry and Watson (2007) and the Ti in quartz thermometer of Wark and Watson (Wark and Watson, 2006). The application of these thermometers



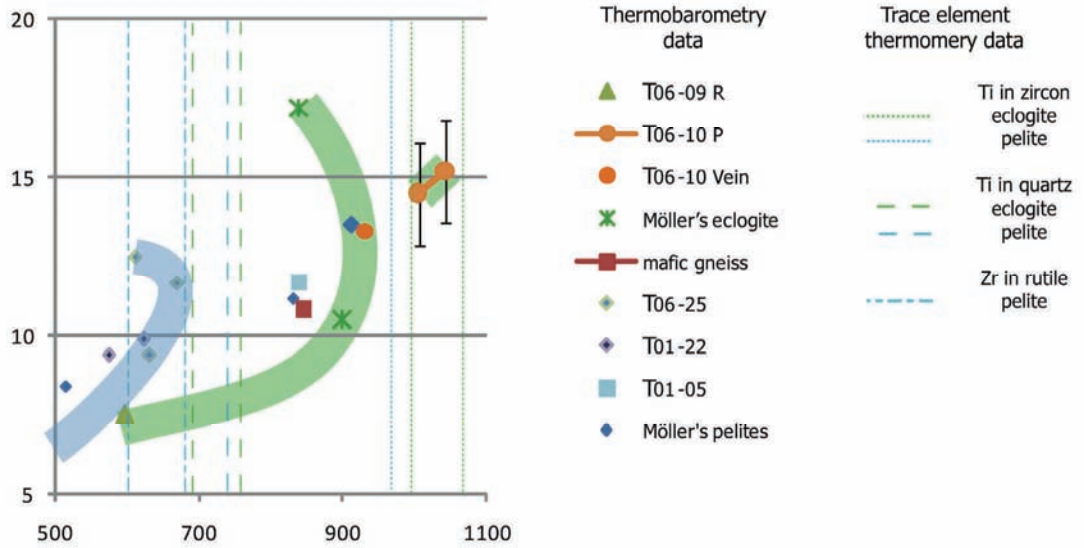


Figure 5.6. PT diagrams.

provides independent verification of the temperature of zircon and rutile formation, allowing comparison with additional temperature estimates obtained via alternative methods (e.g. mineral equilibria thermometry). The agreement or disagreement between trace element thermometry and mineral equilibria thermometry estimates assists in placing zircon and rutile paragenesis within a specific thermal context, and in establishing links between accessory minerals and the specific metamorphic assemblages with which they are associated. Both trace element thermometers are based on the limited and temperature dependent exchangeability between the essential structural constituents of rutile and zircon, namely Ti and Zr. They are calibrated using the combined results of trace element analysis completed on natural and synthetic examples of these accessory minerals whose crystallisation conditions are independently constrained. The log-linear relationships between equilibrium Ti and Zr content (expressed in ppm by weight) and reciprocal absolute temperature (K) are presented below:

$$\left[ \log(Zr_{\text{rutile}}) + \log \alpha_{\text{SiO}_2} \right] = (7.42 \pm 0.105) - \frac{4530 \pm 111}{T} \quad (1)$$

$$\log(Ti_{\text{quartz}}) = (5.96 \pm 0.02) - \frac{3765 \pm 24}{T(K)} \quad (2)$$

$$\log(Ti_{\text{zircon}}) = (6.01 \pm 0.03) - \frac{5080 \pm 30}{T(K)} \quad (3)$$

Both the Zr in rutile and Ti in quartz thermometers are completely independent of pressure. REE and F-Al substitutions also have negligible impact on Zr and Ti concentration, implying that analytical uncertainties present the only limitation to temperature resolution (Hayden et al., 2006; Watson et al., 2006b). Preliminary data indicate that these elements have relatively sluggish diffusivities, implying that quartz and rutile will generally record high

closure temperatures and be relatively robust to later thermal disturbances (Watson et al., 2006a). Ti diffusion in zircon is predicted to be practically negligible at all crustal conditions, making it slower than both Pb and REE (Cherniak et al., 1997; Cherniak and Watson, 2003, 2007). This implies that temperature estimates generated using these thermometers may, in zircons recording metamorphic zircon growth or later lead loss, be decoupled from age estimates determined from U-Th-Pb geochronology.

The application of these thermometers is based on average Ti (or Zr) content. The quoted error is partly based on the range in Ti concentration measured across each sample, which provides a maximum and minimum temperature range. EPMA analytical uncertainties for Ti and Zr are higher than ideal for trace element thermometry, with errors of up to 200 ppm. Because of the log-linear relationship between Ti and Zr concentrations and absolute temperature these errors make a larger contribution to the uncertainties for lower concentrations, and all errors are increased more in the negative than the positive direction. As an example, sample T06-25 has Ti in quartz concentrations ranging from 142 to 323 ppm. The smallest concentrations are above the detection limit of ~100 ppm. Analytical uncertainty contributes to temperature of  $716^\circ\text{C} + 110^\circ\text{C}$ ,  $- 323^\circ\text{C}$  for 142 ppm, whereas at 323 ppm the temperature calculated is  $818^\circ\text{C} + 70^\circ\text{C}$ ,  $- 118^\circ\text{C}$ . These errors are included in the final column of Table 5.4.

#### 5.4.3.1 Quartz temperature estimates

Quartz from three metapelitic and two eclogitic samples was analysed for Ti content. Average temperatures were calculated from these analyses using the equation of Wark & Watson (2006). Both metapelitic and eclogitic samples yielded similar temperatures with the results mostly within error between samples. These results are summarized in table 5.4. Of the metapelitic samples, T01-05 yielded an average temperature of  $740^\circ\text{C} \pm 12^\circ\text{C}$ , T01-22 yielded an average temperature of  $733^\circ\text{C} \pm 13^\circ\text{C}$  and sample T06-25 yielded an average temperature of



Table 5.4. Summary of thermometry parameters.						
Zr in rutile thermometer (Watson et al., 2006)						
Sample no.	No. of analyses	Zr conc. range (ppm)	Calculated $T$ range ( $^{\circ}\text{C}$ )	Average Zr conc. (ppm)	Calculated average $T$ ( $^{\circ}\text{C}$ , $\pm 1\sigma$ )	Calculated average $T$ range incorporating analytical uncertainties ( $^{\circ}\text{C}$ )
T01-05	3	159-557	570-767	371	$609 \pm 75$	507 – 725
T01-22	1	498	686	498	$686 \pm 44$	617 – 766
T06-25	3	257 -466	680-788	332	$648 \pm 33$	591 – 712
Ti in quartz thermometer (Wark & Watson, 2006)						
Sample no.	No. of analyses	Ti conc. range (ppm)	Calculated $T$ range ( $^{\circ}\text{C}$ )	Average Ti conc. (ppm)	Calculated average $T$ ( $^{\circ}\text{C}$ , $\pm 1\sigma$ )	Calculated average $T$ range incorporating analytical uncertainties ( $^{\circ}\text{C}$ )
<b>Pelites</b>						
T01-05	2	161-192	729-752	177	$740 \pm 17$	584 – 840
T01-22	5	103-323	681-818	219	$760 \pm 27$	611 – 855
T06-25	9	142-323	716-818	199	$752 \pm 38$	609 – 848
<b>Eclogites</b>						
T01-40	2	180-882	743-976	531	$860 \pm 20$	779 - 1014
T06-09	2	89-154	695-725	122	$695 \pm 17$	463 - 818
Ti in zircon thermometer (Cherniak and Watson, 2007)						
Sample no.	No. of analyses	Ti conc. range (ppm)	Calculated $T$ range ( $^{\circ}\text{C}$ )	Average Ti conc. (ppm)	Calculated average $T$ ( $^{\circ}\text{C}$ , $\pm 1\sigma$ )	Calculated average $T$ range (inc. analytical uncertainties) ( $^{\circ}\text{C}$ )
<b>Pelites</b>						
T06-27	7	123-204	1013-1089	166	$1054 \pm 49$	860 – 1188
<b>Eclogites</b>						
T06-09	3	106-244	992-1118	160	$1043 \pm 48$	844 – 1185
T06-19	20	106-646	992-1300	451	$1142 \pm 154$	692 - 1302

$722^{\circ}\text{C} \pm 13^{\circ}\text{C}$ . Of the eclogitic samples, T01-40 yielded an average temperature of  $746^{\circ}\text{C} \pm 140^{\circ}\text{C}$  and T06-09 yielded an average temperature of  $695^{\circ}\text{C} \pm 12^{\circ}\text{C}$ .

#### 5.4.3.2 Rutile temperature estimates

Rutile in two pelitic samples was analysed for Zr content. Calculated average temperatures from these results, using the equation of Wark & Watson (2006) were within error of each other. These results are summarized in table 5.4. Sample T01-05 yielded an average temperature of  $670^{\circ}\text{C} \pm 100^{\circ}\text{C}$ . Only one analysis was performed on sample T01-22, which yielded a temperature of  $707^{\circ}\text{C} \pm 49^{\circ}\text{C}$ .

#### 5.4.3.3 Zircon temperature estimates

Zircon from three samples was analysed for Ti content. Seven zircons from the metapelitic sample T06-27, all dated at  $\sim 2000$  Ma and interpreted in chapter 4 to record the peak Usagaran metamorphic event, yielded an average temperature of  $1054 \pm 49^{\circ}\text{C}$ . Two eclogitic samples were also analysed. Three zircons from sample T06-09 yielded an average temperature of  $1043 \pm 48^{\circ}\text{C}$ , and

twenty zircons from T06-19 yielded an average temperature of  $1142 \pm 154^{\circ}\text{C}$ . These temperatures are considerably higher than estimates reached using conventional thermobarometry.

These high temperature results are discussed in section 5.5.1.

#### 5.4.3.4 U-Pb-Th LA-ICPMS analyses

Zircon from two eclogite samples, T06-09 and T06-19, was separated and analysed according to the method outlined in chapters 2-4 of this thesis. Five zircons were separated and analysed from sample T06-09 and 30 analyses conducted on 27 zircons from T06-19. Results are given in Table 5.5.  $^{207}\text{Pb}/^{206}\text{Pb}$  ages obtained were mostly  $>90\%$  concordant but did not occur along a concordia or in tight population clusters. The U-Pb-Th data is presented in table 5.5 and results have been plotted on concordia and probability density plots (Figure 5.7). Sample T06-09 yielded 4 concordant Palaeoproterozoic ages spread between  $2065.8 \pm 44$  Ma and  $2166.1 \pm 46$  Ma. Sample T06-19 yielded 25 concordant Archaean ages, spread between  $2487 \pm 18$  Ma and  $2934 \pm 25$ , with one

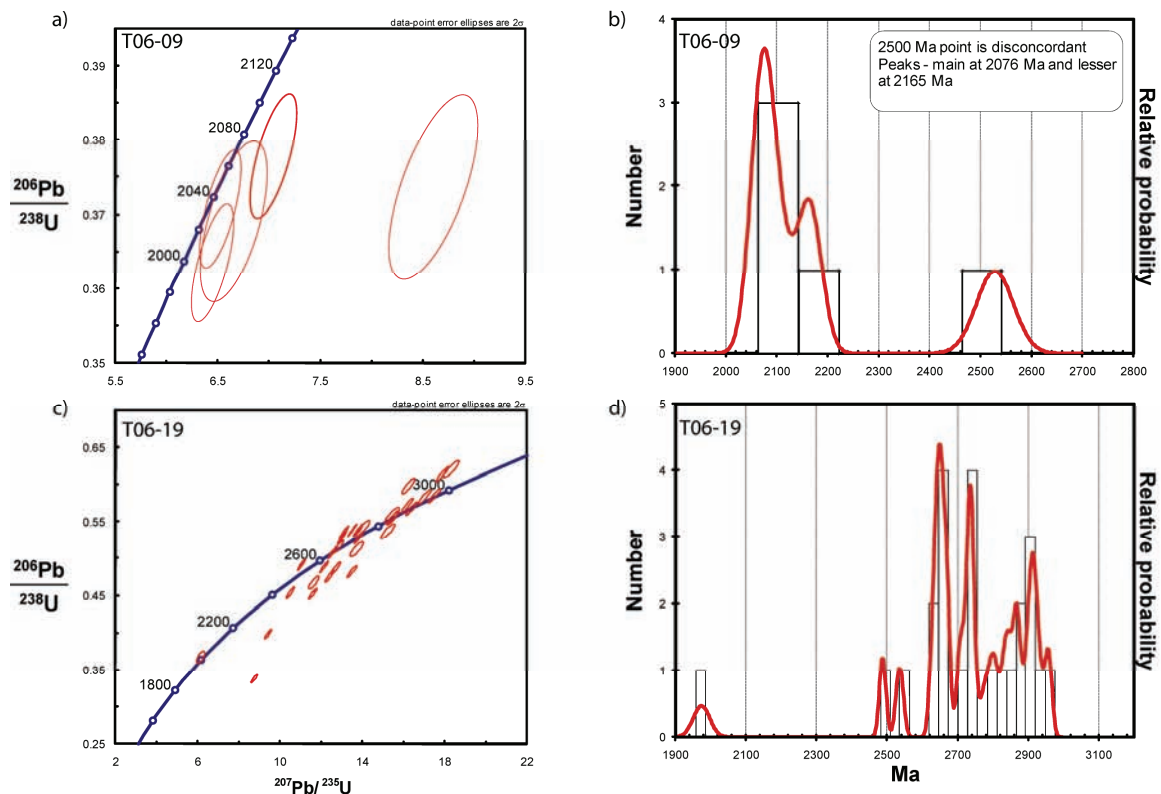


Figure 5.7 U-Pb zircon geochronology results for eclogitic samples.

concordant Palaeoproterozoic grain  $^{207}\text{Pb}/^{206}\text{Pb}$  dated at  $2019 \pm 31$  Ma.

## 5.5 Discussion

The aim of this work was to investigate the burial, and exhumation history of the eclogites and surrounding gneisses to determine whether they have a shared metamorphic history, or have been juxtaposed after peak metamorphism, and thus to make inferences about the relationship between protoliths of the metamorphic rocks. Analyses have been used to make inferences about P-T-t histories of the different suites, as discussed below.

### 5.5.1 Ti in zircon thermometry

Use of the Ti in zircon thermometer on these samples has yielded T in the UHT range (900 – 1200 °C) in rocks which preserve no evidence of UHT metamorphism. In the eclogitic samples subsequent dating of these zircons using the LA-ICPMS procedure outlined in chapter 4 yielded ages between  $2065.8 \pm 44$  Ma and  $2166.1 \pm 46$  Ma for T06-09 and between  $2487 \pm 18$  Ma and  $2934 \pm 25$  Ma for sample T06-19. These ages do not reflect the well constrained ~2000 Ma Usagaran metamorphic event evidenced in other eclogite samples (Möller *et al.*, 1995; Collins *et al.*, 2004), and are interpreted to represent zircon inheritance rather than the eclogite facies event.

In contrast only zircons recording ~2.0 Ga metamorphism from sample T06-27 were analysed for Ti, and these also gave UHT temperatures. Uncertainty in Ti analytical results is introduced by the possibility of higher Ti levels resulting from contamination (ie. from double sided tape (Hiess *et al.*, 2008)), however analyses were conducted on mounts in which the part of the zircon which had contact with the tape was ground off then polished, and the centre of the grain analysed, so no tape residue should

have been present.

In a study of zircon from 45 different igneous rocks Fu *et al.* (2008) observed that some mafic zircons have higher Ti content, and thus record higher temperatures, and also suggested that some factors other than  $a_{\text{TiO}_2}$  and temperature appear to control the Ti content of zircon in mafic rocks.

### 5.5.2 Eclogites and intercalated rocks

U-Pb zircon study of a number of the eclogites in this study has shown that there are differences between different units within the intercalated eclogite body. Zircon from sample T01-40 yielded a metamorphic age of  $1991.1 \pm 1.1$  Ma (Collins *et al.*, 2004), an age supported by dating of other metamorphic minerals within the eclogite body (Möller *et al.*, 1995). Zircon dated from samples T06-09 and T06-19 in this study, however, yielded a wide range of older ages with no indication of any concordant age cluster. Consistently high Th/U ratios in these zircons are inconsistent with post-crystallisation isotope remobilization (Ashwal *et al.*, 1999; Collins, 2003; Hoskin and Black, 2000; Maas *et al.*, 1992; Pidgeon, 1992; Pidgeon *et al.*, 1998; Rubatto, 2002; Vavra *et al.*, 1999; Williams *et al.*, 1996), suggesting that these zircons were not disturbed during the ~2.0 Ga metamorphic event.

Geochemical investigation of eclogitic rocks from the Usagaran has revealed that while the majority of eclogitic rock from this location have mid-ocean ridge basalt (MORB) chemical signatures some have island-arc basalt (IAB) signatures (Lau, 2009a). This, when considered in combination with IAB geochemical signatures of the ultramafic rocks intercalated with eclogitic and felsic rocks within the eclogite body, suggests that not all rocks in the ~35km long eclogite body are MORB-derived rocks which have been metamorphosed at eclogite-facies. Some of

Location	Age	Peak P-T condition	Exhumation rates	Garnet zoning	Reference
<b>Eclogite</b>					
Franciscan eclogites, California, USA		22-25 kbar, 550-620 °C		Mn cores	(Tsujiyori et al., 2006)
Bohemian Massif	340 Ma	18-20 kbar, 835-935 °C	100-150 °C/My	Eclogite - significant Mn-Fe-Mg zoning, less defined in Ca but still present Spačice eclogite, retains high Mn core	(Stipska and Powell, 2005) (Medaris et al., 2006)
Dora Maira Massif	340		3.4 cm/yr (110 - 35 km) then 1.6 cm/yr (35 - 18 km)	Eclogite zoned in all but Mn Metabasite relatively flat. pelites v. zoned, esp in Mn.	(Stipska et al., 2006b) (Rubatto and Hermann, 2001)
Rhodope metamorphic complex, N-Greece		700 °C, 17.5 kbar then 820 °C and 15.5-17.5 kbar		Eclogite - flat Mn zoning, subtle zoning in Fe, Mg and Ca Pelite - ~4mm garnet. 1mm pelitic garnet totally reset	(Bauer et al., 2007)
Western Gneiss Region, Norway	402 Ma	>10.8 kbar, 486 ± 50 °C 11 kbar, 650-750 °C	59 °C/My 15 °C/My		(Walsh and Hacker, 2004) (Carswell et al., 2003; Hacker et al., 2003)
Quinglongshan, southern-Sulu, China		30-40 kbar, 650 - 830 °C		Eclogite -1650 um garnet retains high Mn core Gt-bearing granitic gneiss, 250um, retains high Mn core	(Zhang et al., 2005b)
East Athabasca Region, Snowbird Tectonic Zone, Canada	1.9 Ga	16 kbar, 750 °C			(Baldwin et al., 2007)
Western Dabieshan Terrane, Central China	210 - 240 Ma	28-32 kbar, 605-613 °C		High Mn core in 2-4 mm gt Flat Mn core in 0.32 mm gt Sulu	(Wei et al., 2010) (Zhang et al., 2009)
North Quidam HP/UHP terrane, west China	430 Ma	Sulu 50 kbar 816 °C 23-38 kbar, 600-630 °C	17mm/yr Yuka -13-19 °C/My Xitieshan 3-4°C/My	Yuka Eclogite -- Mn core, sharp rims Xitieshan Eclogite -- no prograde zoning is preserved	(Zhang et al., 2005a)
<b>High-pressure granulites</b>					
Sierras de la Huerta and Valle Fértil, NW Argentina		6-7 kbar, 800 °C	3-6 °C/My	Gt-Cpx - no zoning	(Gallien et al., 2010)
North Dabie-Sulu, China	244 ± 11 Ma	>18 kbar, 730 °C 7 kbar, 920 °C		Gt-Cpx - garnet is relatively unzoned Px zoned, cpx core, opx rim	(Xiao et al., 2001)
Bohemian Massif, south Bohemia	340 Ma	>15 kbar, >900 °C 18 kbar, 800°C 10-17 kbar, 650-800 °C		Gt-Cpx - only rim zoning Matrix cpx is slightly zoned Cpx granulite - gt has no Mn zoning, retains growth Fe-Mg	(O'Brien, 2008) (Racek et al., 2008) (Schulmann et al., 2005; Stipska et al., 2008)
Moldanubian Zone, Austria	340 Ma	1090°C, 15.6 kbar 900 °C, >20 kbar		Gt-Cpx - High-Mn core, Gt-Cpx - Weak Mn rise in core	(Cooke et al., 2000) (Faryad et al., 2010)
Gagnon terrane, eastern Grenville Province	~1000 Ma	13-16 kbar, 700-800 °C		Metapelites retain strong prograde zoning in XFe	(Indares, 1995)
Lurio Orogen, NE Mozambique	557 ± 16 Ma	15.7 ± 1.4 kbar, 949 ± 92 °C		Gt-Cpx - Flat Mn profile, typical cooling zoning in Mg and Fe	(Engvik et al., 2007)
Mozambique Orogen, SE-Kenya		11.5 kbar, 820 °C	1-3 °C/My	Metapelites, no preserved prograde zoning in Mn, Fe, Mg	(Hauzenberger et al., 2005)
North China Craton - central zone	1.8 Ga	Peak 13.4-15.5 kbar, cooling through 8.2-10.7 kbar,		Mn centre in 5.5 mm garnet, (cpx-opx-pl corona rims), matrix cpx relatively unzoned in Ca mg, minor Al/Fe zoning	(Zhao et al., 2000; Zhao et al., 2001)
Snowbird Tectonic Zone	1.9 Ga	~18-20 kbar, 920-1000 °C	27-70 °C / My	garnets show only cooling curving	(Baldwin et al., 2004) (Baldwin et al., 2003)

**Table 5.6 summary of garnet zoning in eclogites and surrounding gneisses.**

the ultramafic and eclogitic rocks were likely intercalated with the rest of the body during the exhumation process, and have thus experienced a different prograde metamorphic history.

Both trace element thermometry and conventional thermobarometry yield unexpectedly high temperatures for some some samples. There are differences in the temperatures yielded by different methods. For samples T06-09 and T06-10, taken from within a small area, Ti in quartz yielded  $695 \pm 17$  °C while thermobarometry calculated peak temperatures of  $1005 \pm 122$  °C. High temperatures obtained using thermobarometry could be due

to assumptions of  $Fe^{2+}/Fe^{3+}$  content of minerals. Overestimating  $Fe^{2+}$  relative to  $Fe^{3+}$  in garnet produces incorrectly high temperatures (Stipska and Powell, 2005). THERMOCALC propagates the errors associated with these assumptions, so this should not be a major contributor to these high temperatures.

Peak conditions experienced by eclogitic rocks were  $17.2 \pm 3.6$  kbar,  $839 \pm 173$  °C. Metapelitic and ultramafic lithologies intercalated with eclogite in the eclogite body experienced conditions of at least  $13.4 \pm 2$  kbar,  $920 \pm 130$  °C (figure 5.6). The P-T conditions for these intercalated eclogite/pelite/ultramafic lithologies overlap at the

1 $\sigma$  level, but do not overlap with the peak P-T conditions recorded in the non-intercalated peltilites.

### 5.5.3 Garnet zoning

Garnet is an important mineral in metamorphic studies as it is stable at a wide range of temperatures, pressures and bulk compositions. Zoning within garnet is significant as changing compositions in terms of Fe, Mg, Ca and Mn record variations in the P-T conditions through which the rock has passed. Growth zoning in garnets, developed with increasing temperatures, has been well quantified (Chakraborti and Ganguly, 1990) (Spear et al., 1990).

The garnet profiles seen in these samples include both simple and more complex profiles. In terms of  $X_{Fe}$  (Fe/Fe+Mg) compositions the simplest garnets have relatively flat core compositions with decreasing  $X_{Fe}$  at the rims. More complex grains have a lower  $X_{Fe}$  values in the centre, rising to a peak then lowering again at the rims. In some instances the transition from rising to falling  $X_{Fe}$  values is sharp while in others the transition is gradual (i.e. Figure 5.4 T06-25 Gt B compared to T01-40 Gt2). Garnets with lower  $X_{Fe}$  in the core and composition higher in Mn are generally considered to preserve growth zoning (Chakraborti and Ganguly, 1990) (Spear et al., 1990), while those zircons without a central high-Mn low  $X_{Fe}$  core are considered to have homogenized growth zoning.

Some of the temperature estimates obtained with thermobarometry and trace element thermometry for the mafic samples indicate that metamorphism occurred at high-pressure granulite conditions rather than eclogite facies. The increased rate of intra-crystalline diffusion at high temperatures (>750°C) generally produces homogeneous garnet cores (Tracey et al., 1976; Wordsworth, 1977; Yardley, 1977). However garnets in rocks which have experienced only short residence at peak temperatures and the absence of an intergranular fluid phase may retain some interior growth zoning. A review of the literature on metamorphic rocks, focusing on garnet zoning in garnet-clinopyroxene rocks, is summarized in table 5.6. Numerous examples were found of both homogenized core compositions and of garnet with remnant growth zoning. No systematic variation was seen when comparing garnet zoning patterns with peak P-T conditions (Figure 5.8 a). When cooling rates for these were taken into account a correlation between the time spent above ~750°C appears (figure 5.8 b), with samples which spent more than ~5 million years at higher temperatures showing homogenized core compositions.

The Usagaran eclogitic rocks are varied in their retention of growth related core Mn zoning. Sample T01-40 preserves beautiful growth zoning, while samples T06-09 and T06-10 have un-zoned cores. This is consistent with the interpretation of P-T data as indicating that not all eclogitic rocks within the Yalumba Hill eclogite body have experienced the same metamorphic history, with rocks in the core of the body experiencing deeper burial and faster exhumation than other intercalated rocks within the body. Those rocks retaining growth zoning must have experienced rapid burial and exhumation, with no more than ~5 My spent at peak temperatures.

#### 5.5.3.1 Garnet-biotite diffusion modeling

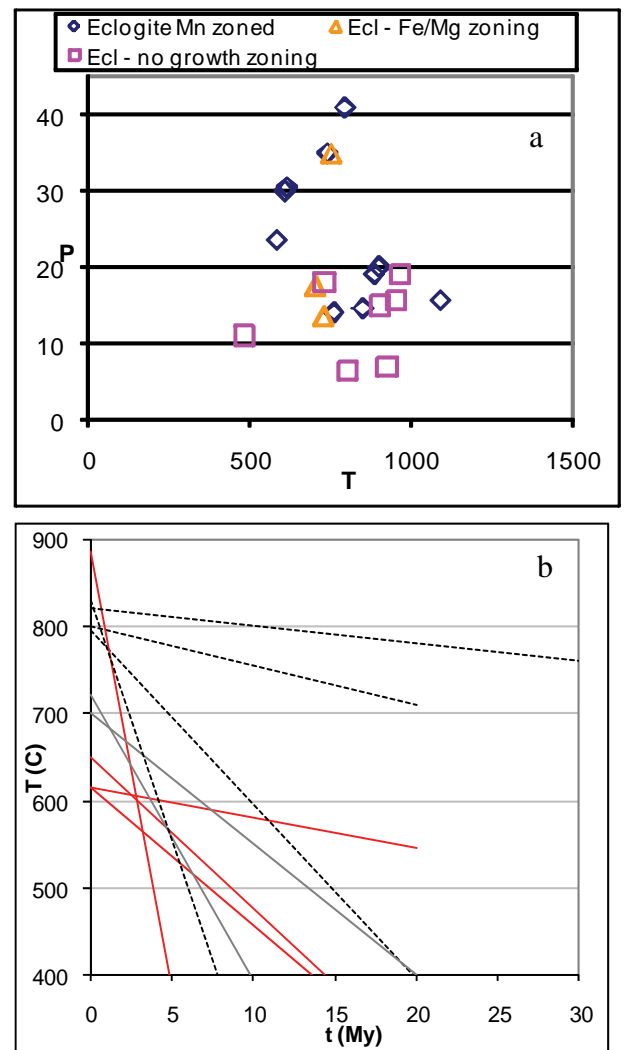


Figure 5.8 P-T-t conditions and garnet zoning in eclogites and surrounding gneisses (data in table 5.6). a) P-T conditions for zoned and un-zoned eclogitic garnet and peltilites. b) T-t conditions. Red lines indicate eclogitic garnet with preserved zoning, grey indicates pelitic garnet with zoning, dashed line indicates eclogite with no preserved garnet zonation

Garnet-biotite Fe-Mg diffusion zoning and cooling is modeled using the THERMAL HISTORY software (Robl et al., 2007). The approach is that used by many authors (Florence and Spear 1995; Spear, 1995; Hauzenberger et al., 2005) in which the diffusion equation in spherical coordinates is coupled with a thermometer equation and a Kd (kinetic diffusion) expression to formulate the boundary conditions. The Arrhenius relationship is used to describe the temperature dependence of diffusivity. The diffusion coefficients used are those of Ganguly et al. (1998). Fe-Mg diffusion in biotite is assumed to be significantly higher than in garnet and can thus be neglected in modeling. Starting conditions of biotite  $X_{Mg}$  are taken from EPMA analyses and starting temperatures are taken from P-T calculations.

Chemical zoning within minerals due to diffusion has been well studied in many minerals, especially in garnet (Chakraborti and Ganguly, 1990; Crowley, 1991; Florence and Spear, 1995; Ganguly and Chakraborti, 1991; Ganguly et al., 1998). Chemical diffusion is discussed in depth by Spear (Spear, 1995) and a hierarchy of diffusivities has been approximated:



Sample	Garnet	Radius (µm)	X <sub>Mg</sub> Bi	Start T (K)	Start T (°C)	Best fit cooling rate (°C/My)
T01-05	Gt 1	1309	0.584	1023	750	-
T01-05	Gt 2 081108	1688	0.589	1023	750	-
T01-22	TS 081108	6200	0.48	1006	733	1-2
T01-22	Bl Gt N	3426	0.46	1006	733	1-2
T01-22	Bl Gt S	3950	0.517	1006	733	-
T01-22	Bl Gt 2	5659	0.48	1006	733	1.0
T01-22	Bl Gt1	3402	0.53	1006	733	0.5
T06-25	Gt A	5250	0.594	1023	750	-
T06-25	Gt B	4691	0.594	1023	750	-
T06-25	Gt C	4941	0.594	1023	750	-
T06-25	TS 1	780	0.47	1023	750	2-5
T06-25	TS 2	780	0.47	1023	750	1-2

Diffusion Constants: (Ganguly *et al.*, 1998)  
D Fe (m<sup>2</sup>/s) = 3.50E-09, Q Fe (J/mol) = 274186, D Mg (m<sup>2</sup>/s) = 4.66E-09, Q Mg (J/mol) = 254220

**Table 5.7** Parameters used for garnet profile modelling

$$D_{KN\alpha_1}^{Micas} > D_{KN\alpha_1}^{Feldspars} \gg D_{FeMg_1}^{Chlorite} \approx D_{FeMg_1}^{Biotite} > D_{FeMg_1}^{Staurolite} \approx D_{FeMg_1}^{Chloritoid} \approx D_{FeMg_1}^{Cordierite} > D_{Mn}^{Garnet} > D_{FeMg_1}^{Garnet} > D_{Ca}^{Biotite} \gg D_{AlAlMg_1SL_1}^{Micas} \approx D_{AlAlMg_1SL_1}^{Pyroxene} \approx D_{AlAlMg_1SL_1}^{Amphibole} \gg D_{CaAlN\alpha_1SL_1}^{Plagioclase}$$

The calculation of cooling rates from garnet profiles is based upon the diffusive properties of Fe and Mg in garnet in equilibrium with another mineral which has diffusive rates significantly higher than garnet. From the above hierarchy it can be seen that biotite and chlorite have the highest diffusivity of Fe and Mg, with staurolite, chloritoid and cordierite having slightly lower diffusivities, but still higher than garnet. Thus any of these minerals can be paired with garnet to study cooling rates so long as suitable diffusion coefficients have been calculated.

### 5.5.3.2 Thermal History software

In the THERMAL HISTORY software package the relationship between temperature and time is quantified by the expression:  $T_t = T_s - ts$

where  $t$  is time,  $T_t$  is the temperature at time  $t$ ,  $T_s$  is the starting temperature and  $s$  is the cooling rate. The relationship between temperature and diffusivity is quantified using the Arrhenius relationship:

$$D = D_0 e^{\frac{Q}{RT}}$$

where  $D$  is the diffusivity,  $R$  is the gas constant,  $T$  is the absolute temperature,  $D_0$  is the pre-exponent diffusivity and  $Q$  is the activation energy. Because chlorite and biotite have approximately equivalent Fe-Mg diffusion rates, both several orders of magnitude higher than that of garnet, and because the rate of diffusion between these minerals is rate-limited by the diffusivity of garnet rather than the micas, the garnet-biotite diffusion rates of Ganguly *et al.* (1998) can be effectively used to model chlorite-garnet diffusion as well as garnet-biotite. The inter-relationship between diffusion of Fe and Mg is de-

tailed in Florence & Spear (1991) and Ganguly *et al.* (1998) using the expression:

$$D_{Fe-Mg} = \frac{D_{Mg} D_{Fe}}{X_{Mg} D_{Mg} + X_{Fe} D_{Fe}}$$

where  $D_{Fe-Mg}$  is the inter-diffusion rate of Fe & Mg,  $D_{Fe}$  and  $D_{Mg}$  are the  $T$  dependent diffusivities and  $X_{Fe}$  and  $X_{Mg}$  are the concentration ratios described in Hauzenberger *et al.* (2005). This expression is only applicable where the outermost point of the modelled garnet is in equilibrium with adjacent biotite at  $T_t$  and controlled by  $Kd$ .

Temperature calculations can be performed using the thermometer equation of Ferry & Spear (1978):

$$Kd = \exp\left(\frac{-\Delta H + T\Delta S}{3Rt}\right)$$

where  $\Delta H$  is the enthalpy change (52107.536 J) and  $\Delta S$  is the entropy change (19.506 JK<sup>-1</sup>). The diffusion of elements within the garnet is modelled using the spherical form of the one-dimensional diffusion equation:

$$\frac{\partial C}{\partial t} = \left( D \frac{\partial^2 C}{\partial r^2} + \frac{2}{r} \cdot \frac{\partial C}{\partial r} \right)$$

where  $C$  is a given chemical species,  $D$  is the diffusion rate and  $r$  is the radius of the modeled garnet.

### 5.5.3.3 Cooling rates of pelites

Fe-Mg zoning in garnets, expressed in terms of their  $X_{Mg}$  value across a calculated profile, were calculated for garnets with the radius of analysed garnets using the  $X_{Mg}$  value of adjacent biotite grains, the peak temperatures calculated using Thermocalc or trace element thermometry, and a range of cooling rates. These calculated profiles were then compared with the measured profiles (Figure 5.9), and the closest match between calculated and analysed profiles taken to indicate the rate of cooling

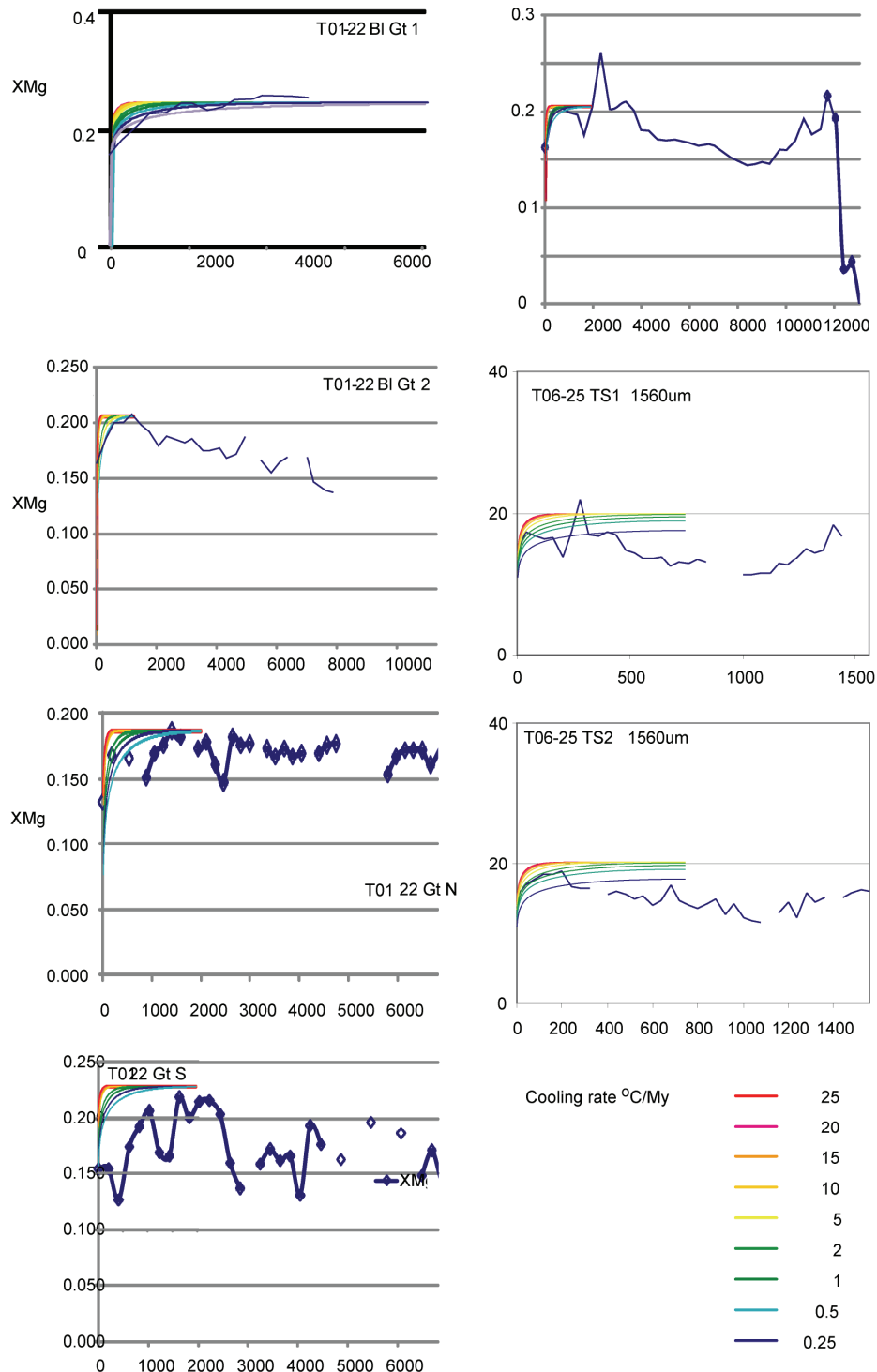


Figure 5.9 Garnet profiles, analysed  $X_{Mg}$  with overlay of THERMAL HISTORY modeled profiles.

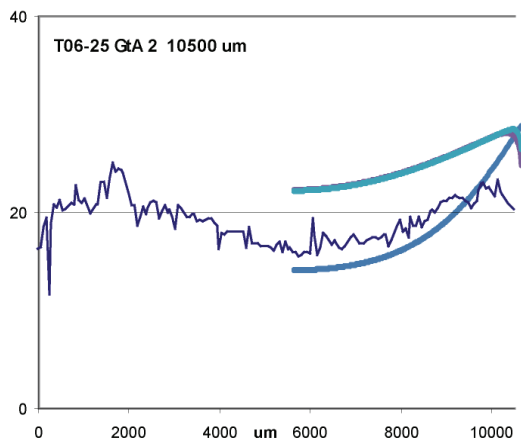
experienced by that garnet. The obtained cooling rates, and the parameters used to obtain them, are summarized in Table 5.7.

For sample T01-05 the garnets were commonly cracked, leading to complex Fe-Mg zoning profiles which could not be easily modeled. Treating the cracked sections as individual grains is not valid using this type of modeling as the non-spherical shape of the sections will invalidate the assumptions inherent in using a spherical diffusion model. Thus no acceptable cooling rate could be obtained from this sample.

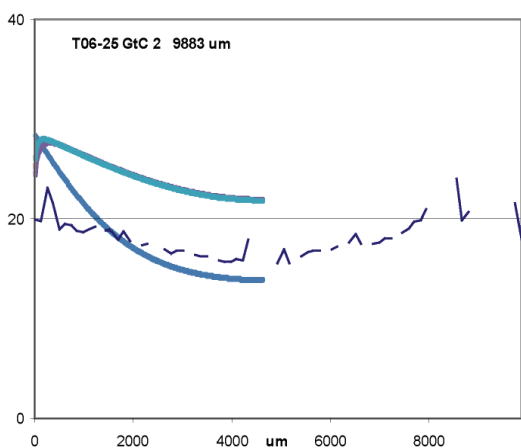
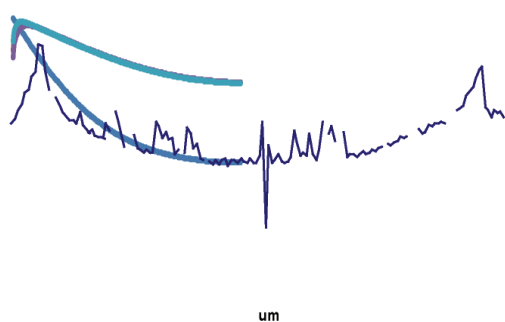
The two smaller garnets from thin sections of T06-25 yielded rates of 1-2 and 2-5 °C/My. Sample T01-22 contained one ~1.5 cm garnet which was analysed in thin section, but the zoning of the garnet was disrupted by cracks as seen in figure 5.3 (a). One other garnet in thin section and four garnets mounted in epoxy discs were analysed, and these yielded cooling rates of 0.5-2 °C/My.

#### 5.5.4 Cooling rates

Sample T06-25 contained a number of large (~1cm) garnets which were across which profiles were taken. These garnets (T06-25 Gt A, B, and C) retain a distinct prograde



T06-25 GtB 2 9381um



- 7500 My heating path
- Heating then 4 °C/My cooling
- Heating then 2 °C/My cooling
- Heating then 10°C/My cooling

Figure 5.9 Garnet profiles for large T06-25 garnet, analysed  $X_{Mg}$  with overlay of unsuccessfully modeled THERMAL HISTORY prograde and retrograde profiles.

zoning pattern with a sharp change in the edge  $\sim 500 \mu m$ .

Attempts to introduce this prograde pattern into the software by inserting a heating T-t path were successful utilizing a 7500 My prograde path. This timeframe has no validity in terms of constraining the heating path of the sample, but is used solely to help constrain the cooling path. Attempts to then use the created zoned profile as a basis to calculate the effect of cooling at different rates on a growth zoned garnet failed, as seen in figure 5.10 in which the results of these attempts are shown overlain on the actual zoning profile. This method also failed to give any indication of the time at high temperatures required to overprint a growth zoned garnet as the garnet core remained the same regardless of rapid or slow cooling.

The cooling rates obtained from the garnets which displayed less pronounced growth zoning yielded rates of 1-2 °C/My for pelites situated, structurally speaking, both above and below the eclogite body. Cooling rates calculated are considerably slower than the exhumation rate of Usagaran eclogites previously constrained at 25°C/My (0.6 - 2.2 kbar/My, 0.17-0.33 km/My) using geochronology of  $1999.1 \pm 1.1$  Ma eclogite and of a pegmatite dated at  $1991 \pm 2$  Ma which cross-cuts amphibolite-facies fabrics (Collins *et al.*, 2004b). Subsequent exhumation is constrained by  $1895 \pm 27$  Ma deposition of the Konse group (Mruma, 1989). This deposition requires surface exposure of the Isimani Suite as a conformable contact between the two is seen further south (Mruma, 1989). This requires exhumation from  $\sim 40$ km depth in  $\sim 100$  My, indicating an exhumation rate of  $\sim 40$  m/My.

#### 5.5.5 P-T evolution

While eclogites record metamorphic conditions of up to  $\sim 17.5$  kbars and 840 °C, with slight temperature increases during decompression the maximum pressure recorded by the metapelitic rocks from around the eclogite body is  $\sim 12.5$  kbar. With no evidence in mineral textures, or inclusions in garnet in metapelites to suggest that they have reached higher pressures it seems apparent that only the later decompression part of the P-T path is shared with the eclogites.

Also of note is the disparity in P-T histories recorded within the eclogite boudin. The eclogite samples collected do not all have similar compositions, with the highest Na clinopyroxenes seen only in the samples from Möller *et al.* (1995). The higher P-T conditions are recorded in those samples with higher Na content, and only those samples display the "true" eclogite mineral assemblage of omphacite and garnet with no primary plagioclase.

The temperatures experienced by the Usagaran eclogites are higher than those seen in modern subduction settings, verging on the high-pressure granulite facies as opposed to eclogite-facies *sensu strictu*. This could be due to a slower burial-exhumation process, however the exhumation rates described by Collins *et al.* (2004) are very similar to modern subduction systems (Reddy *et al.*, 1999). The slower exhumation rates obtained from modeling Fe-Mg diffusion in garnet apply only to the surrounding gneisses, not to the eclogite body itself. Thus the higher temperatures are likely the predictable result of higher geothermal gradients during the Palaeoproterozoic. Geothermal gradients calculated for the eclogite body range from 488°C/GPa for the true-eclogite samples to  $\sim 690$ °C/GPa for the eclogitic samples which re-

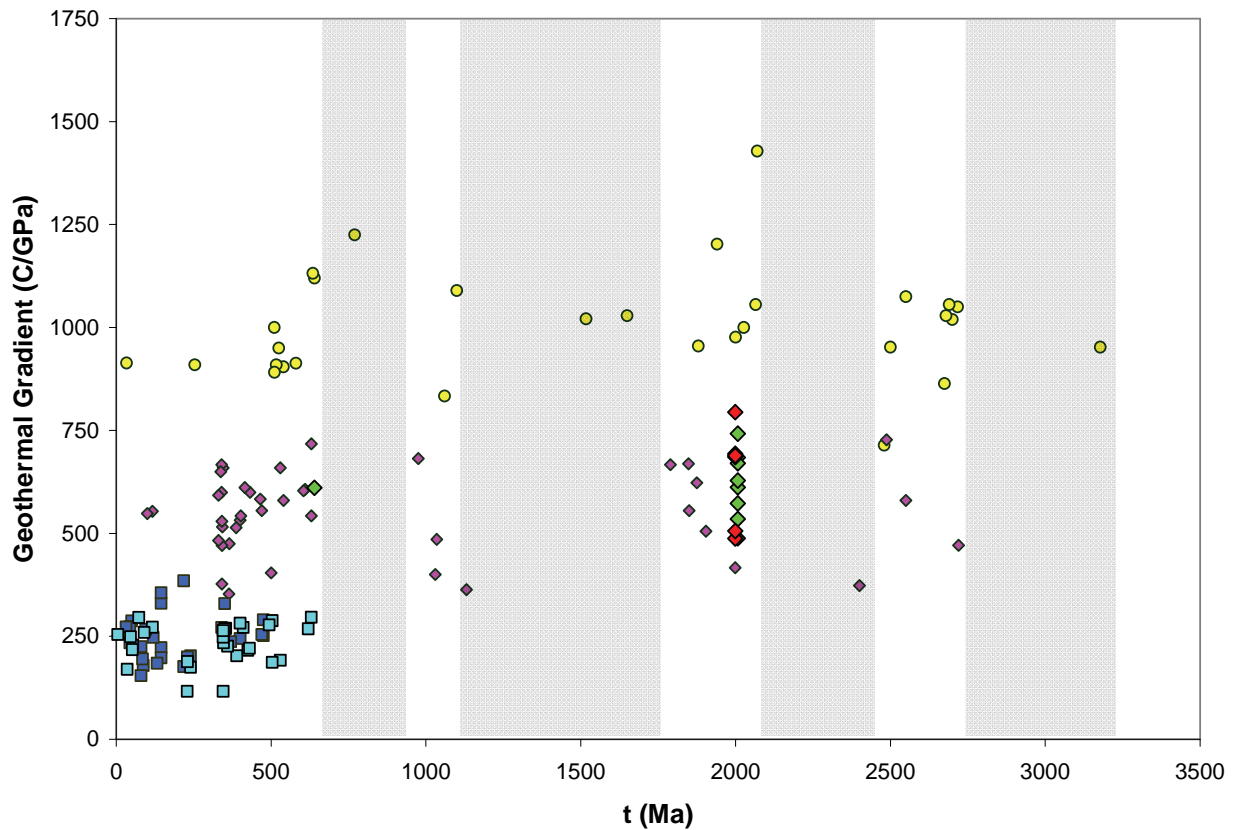


**Figure 5.10** Plot of geothermal gradients versus time for the main types of extreme metamorphic belt (modified after Brown, 2007). **Symbols:** circles = granulite – ultra-high-temperature metamorphism; diamonds = eclogite – high-pressure-granulite metamorphism; dark squares = blueschist – lawsonite-eclogite metamorphism; light squares = ultra-high-pressure; red diamonds = eclogites (this study); green diamonds = pelites (this study).

cord higher temperatures. Pelitic samples record geothermal gradients between 540 - 680° C/GPa. Figure 5.10 shows these gradients plotted against time with gradients from other metamorphic events for comparison (data from Brown, 2007 tables 1-5), and shows that these geothermal gradients are not uncommon for Palaeoproterozoic metamorphic Orogens (Brown, 2007a, 2007b)

### 5.6 Conclusions

The metamorphic conditions experienced during burial and exhumation of eclogites and the surrounding country-rock have been constrained using thermobarometry and trace element thermometry, and the cooling rates of country-rock metapelites constrained using garnet-biotite Fe-Mg exchange modeling. The main conclusions of this study are:

- that peak eclogite facies metamorphic conditions ( $17.2 \pm 3.6$  kbar,  $839 \pm 173$  °C) are slightly higher temperature than previously published for the Usagaran.
- that metapelitic and ultramafic lithologies intercalated with eclogite in the eclogite body experienced conditions of at least  $13.4 \pm 2$  kbar,  $920 \pm 130$  °C, however there is no evidence of pelitic rocks having experienced the 17 kbar which the eclogites saw.
- that the eclogite body comprises varied lithologies with differences in protolith, chemistry and prograde and

peak P-T paths.

- that country-rock pelites cooled at  $\sim 1\text{-}2$  °C/My, compared to 25°C/My for eclogites between 1999 and 1991 Ma.

All of these facts are consistent with the eclogite body having formed during subduction of Palaeoproterozoic sea-floor which became intercalated with metasediments and other metaigneous rocks during exhumation. The surrounding blocks of the Isimani suite did not experience eclogite-facies metamorphism but were tectonically juxtaposed during exhumation.



Spot No.	Core/ Rim	Isotope Ratios						Ages (Ma)				Conc <sup>1</sup> %		
		<sup>207</sup> Pb/ <sup>206</sup> Pb	1 $\sigma$	<sup>207</sup> Pb/ <sup>235</sup> U	1 $\sigma$	<sup>206</sup> Pb/ <sup>238</sup> U	1 $\sigma$	<sup>207</sup> Pb/ <sup>235</sup> U	1 $\sigma$	<sup>206</sup> Pb/ <sup>238</sup> U	1 $\sigma$			
Sample T06-09 n = 5														
T06-09_01	c	0.13516	0.00363	7.04077	0.18558	0.37789	0.00687	2166.1	46.02	2116.6	23.43	2066.4	32.16	95
T06-09_02	c	0.12864	0.00337	6.44537	0.16698	0.36348	0.00645	2079.4	45.47	2038.5	22.77	1998.7	30.5	96
T06-09_03	c	0.16698	0.00736	8.60143	0.35436	0.3737	0.01014	2527.6	72.18	2296.7	37.47	2046.8	47.57	81
T06-09_04	c	0.12764	0.00323	6.5239	0.16424	0.37078	0.00646	2065.8	43.99	2049.1	22.16	2033.1	30.39	98
T06-09_05	c	0.13078	0.00545	6.65196	0.26447	0.36899	0.00883	2108.4	71.37	2066.3	35.09	2024.7	41.59	96
Sample T06-19 n = 30														
T06-19_01	r	0.18927	0.00242	12.71189	0.18877	0.48721	0.00665	2735.8	20.91	2658.5	13.98	2558.6	28.83	94
T06-19_02	c	0.21693	0.00253	17.50077	0.2462	0.58524	0.00781	2958	18.72	2962.7	13.51	2970.1	31.78	100
T06-19_03	c	0.1898	0.00214	13.83636	0.19084	0.52888	0.00697	2740.4	18.43	2738.6	13.06	2736.7	29.4	100
T06-19_04	c	0.18573	0.00224	11.59666	0.16618	0.45299	0.00609	2704.7	19.79	2572.4	13.4	2408.5	27.01	89
T06-19_05	c	0.163	0.00179	11.04752	0.15025	0.49173	0.00644	2487.1	18.4	2527.1	12.66	2578.2	27.84	104
T06-19_06	c	0.17147	0.00214	9.42088	0.13766	0.39865	0.0054	2572	20.7	2379.9	13.41	2162.8	24.9	84
T06-19_07	c	0.18778	0.0024	8.74936	0.12946	0.33809	0.00463	2722.9	20.94	2312.2	13.48	1877.5	22.29	69
T06-19_08	r	0.18812	0.00316	14.03833	0.25168	0.54152	0.00831	2725.8	27.43	2752.3	16.99	2789.8	34.76	102
T06-19_09	c	0.19701	0.0028	16.24135	0.25883	0.59827	0.00862	2801.6	23.06	2891.1	15.24	3022.9	34.76	108
T06-19_10	r	0.18908	0.00234	12.40171	0.18025	0.47603	0.00649	2734.2	20.2	2635.3	13.66	2509.9	28.36	92
T06-19_11	c	0.20282	0.00244	13.48946	0.19185	0.4823	0.00647	2849	19.46	2714.5	13.44	2537.3	28.14	89
T06-19_12	c	0.20921	0.00245	16.38219	0.22953	0.56782	0.00758	2899.4	18.86	2899.4	13.41	2898.9	31.16	100
T06-19_13	c	0.18063	0.00234	12.86109	0.19191	0.51627	0.0071	2658.7	21.34	2669.5	14.06	2683.4	30.2	101
T06-19_14	c	0.21374	0.00336	18.31109	0.31163	0.62121	0.00939	2934.1	25.21	3006.2	16.39	3114.7	37.34	106
T06-19_15	c	0.21131	0.00275	17.02074	0.25449	0.58406	0.00814	2915.6	20.93	2936	14.34	2965.3	33.13	102
T06-19_16	c	0.17739	0.00199	13.10039	0.17917	0.5355	0.0071	2628.6	18.52	2686.9	12.9	2764.6	29.79	105
T06-19_17	c	0.18004	0.00207	12.13603	0.16817	0.4888	0.00653	2653.2	18.91	2615	13	2565.5	28.27	97
T06-19_18	c	0.20503	0.00252	16.18457	0.23342	0.5724	0.00785	2866.7	19.83	2887.8	13.79	2917.7	32.17	102
T06-19_19	c	0.1804	0.00302	11.62894	0.20634	0.46745	0.00713	2656.6	27.48	2575	16.59	2472.4	31.34	93
T06-19_20	c	0.21113	0.00257	17.87168	0.25673	0.61386	0.00844	2914.3	19.61	2982.9	13.81	3085.4	33.7	106
T06-19_21	c	0.18194	0.00195	13.50615	0.17885	0.53849	0.00708	2670.7	17.62	2715.7	12.52	2777.1	29.68	104
T06-19_22	c	0.17915	0.00206	12.54815	0.17304	0.50806	0.0068	2645.1	18.99	2646.3	12.97	2648.4	29.07	100
T06-19_23	c	0.20047	0.00352	15.44203	0.28303	0.55873	0.00886	2830.1	28.32	2842.9	17.48	2861.4	36.65	101
T06-19_24	c	0.20573	0.00347	15.23197	0.27056	0.53705	0.00835	2872.2	27.17	2829.9	16.92	2771.1	35.04	96
T06-19_25	c	0.17863	0.00195	13.02243	0.17371	0.52879	0.00694	2640.2	17.98	2681.3	12.58	2736.3	29.27	104
T06-19_26	c	0.20216	0.00288	15.48462	0.2438	0.55557	0.00799	2843.7	23.02	2845.5	15.02	2848.3	33.11	100
T06-19_27	c	0.12115	0.00325	6.14398	0.16205	0.36783	0.00654	1973.3	46.96	1996.5	23.03	2019.2	30.81	102
T06-19_28	c	0.16776	0.00213	10.5033	0.15318	0.45412	0.00618	2535.4	21.14	2480.2	13.52	2413.5	27.38	95
T06-19_29	c	0.19418	0.00352	13.72274	0.25732	0.51258	0.00814	2777.9	29.42	2730.8	17.75	2667.6	34.69	96
T06-19_30	c	0.18596	0.00218	13.79878	0.19132	0.5382	0.00715	2706.8	19.19	2736	13.13	2775.9	29.98	102

Table 5.5 U–Pb zircon geochronology results for eclogitic samples.

**Table 5.2** Representative EPMA mineral chemistry analyses

<b>Mineral</b>	Feldspar	ilmenite	Garnet	Biotite	Garnet	ilmenite	chlorite	Feldspar
Sample	T01-22	T01-22	T01-22	T01-22	T01-22	T01-22	T01-22	T01-22
ID number	_L2_3	T01-22_P7	2-GTI-P9	2-GTI-P12	15-gt	_16-ilm	_17-chl	-P2
SiO2	62.5891	0.1173	36.9692	34.3285	37.9845	0.0771	26.2086	59.9751
TiO2	0.0002	51.3855	0.0115	1.663	0.0109	52.0971	0.2023	0.0059
Al2O3	22.6363	0.0003	20.8595	17.1735	21.3111	0.0003	22.0056	21.6471
Cr2O3	0.0001	0.073	0.0422	0.065	0.0525	0.0481	0.1559	0.0263
FeO	0.0226	44.4552	32.9608	17.6071	34.4072	46.1574	22.651	0.0098
MnO	0.0001	0.8789	1.7816	0.0002	1.6761	0.7928	0.0856	0.0002
MgO	0.0097	0.1804	3.5884	11.8547	3.211	0.0821	17.388	0.0003
ZnO	0.0001	0.0001	0.0002	0.1867				0.0002
CaO	4.0967	0.0432	3.7213	0.0727	3.2133	0.0643	0.0002	4.0673
Na2O	9.2494	0.0003	0.057	0.1595	0.0002	0.0003	0.0002	8.72
K2O	0.0524	0.0001	0.017	8.6552	0.0001	0.0001	0.0001	0.0397
Zr (ppm)					293	139	2	
<b>Mineral</b>	Garnet	Biotite	Muscovite	Feldspar	Garnet	Biotite	Rutile	Rutile
Sample	T01-05	T01-05	T01-05	T01-05	T01-05	T01-05	T01-05	T01-05
ID number	gt1_inc_6	gt1_inc_7	gt1_1_1	plagline1_1	2_traverse5	Pl_line2_14	gt1_inc_3	7_rut
SiO2	37.7915	37.1076	54.7468	61.8719	36.9115	43.7313	0.0479	0.0349
TiO2	0.0802	1.6665	0.0196	0.009	0.0311	1.0893	96.1607	99.0256
Al2O3	21.2043	17.5197	26.6199	24.8044	21.3297	19.5723	0.0003	0.0003
Cr2O3	0.0088	0.0586	0.0002	0.0234	0.0002	0.1313	0.1428	0.2756
FeO	30.3459	13.2231	1.8347	0.4764	24.8435	10.5212	0.7156	0.1853
MnO	0.5227	0.0639	0.0002	0.0002	0.2673	0.0345	0.0002	0.0002
MgO	3.2054	14.5357	0.5888	0.0152	5.9438	8.3561	0.0003	0.0003
ZnO								
CaO	5.1832	0.0192	1.5211	5.5867	6.4644	1.5173	0.1624	0.0478
Na2O	0.0361	0.2109	0.8081	7.9317	0.0118	2.915	0.0135	0.0003
K2O	0.0729	8.8388	3.2267	0.0925	0.0001	5.9723	0.0087	0.0001
<b>Mineral</b>	Garnet	Biotite	Feldspar	Feldspar	Garnet	Biotite		
Sample	T06-25	T06-25	T06-25	T06-25	T06-25	T06-25		
ID number	g Gt1_line	bi biotite	fsp	Gt1_l_23	Gt1_l_24	Gt1_l_25		
SiO2	37.22	35.35	57.42	61.70	37.70	46.79		
TiO2	0	1.72	0.03	0.00	0.03	0.41		
Al2O3	21.06	16.79	24.47	24.02	20.88	34.79		
Cr2O3	0.04	0.07	0	0.00	0.03	0.02		
FeO	1.4	1.96	0.1	0.74	29.29	1.66		
MnO	29.89	15.36	0	0.05	1.27	0.02		
MgO	0.83	0.03	0	0.00	2.97	1.01		
ZnO	4.18	12.32	0	0.00	0.00	0.00		
CaO	4.91	0.04	7.67	5.87	7.66	0.00		
Na2O	0	0.21	7.2	8.19	0.00	1.22		
K2O	0.01	8.54	0.09	0.05	0.00	9.07		

Mineral	Feldspar	Garnet	Pyroxene	Amphibole	Pyroxene	Garnet	Feldspar	Pyroxene
Sample	T06-10	T06-10	T06-10	T06-10	T06-10	T06-10	T06-10	T06-10
ID number	pr_pl_10	VZn-Gt_12	pr_px_9	pr_px_12	pr_px_8	VeinZn-Gt_4	VZnPlamp1	VeinZn-7
SiO2	57.5485	38.2375	51.8726	41.5153	50.8652	34.5634	55.6337	51.1937
TiO2	0.0002	0.0555	0.0725	1.3634	0.1308	0.0524	0.0096	0.1814
Al2O3	25.3577	21.1389	1.4901	11.3311	1.949	19.035	27.1588	2.2051
Cr2O3	0.0001	0.0346	0.0001	0.0001	0.0001	0.0242	0.0001	0.0001
FeO	0.0796	22.5084	7.6577	16.1988	8.3507	23.5516	0.1657	8.5371
MnO	0.0001	0.5369	0.0001	0.0001	0.0001	0.9972	0.0001	0.0001
MgO	0.0003	6.5452	12.5944	9.0944	12.248	4.5279	0.0003	12.1172
ZnO	0.0001	0.0001	0.0001	0.0001	0.0001	0.0001	0.0001	0.0001
CaO	7.9848	8.5969	22.8417	11.0578	22.1895	8.505	9.2616	22.012
Na2O	7.0384	0.0002	0.6123	2.0414	0.5872	0.0002	6.1708	0.5805
K2O	0.0826	0.0001	0.0173	0.5629	0.0282	0.0001	0.0521	0.0174

Mineral	Garnet	Feldspar	Biotite
Sample	T06-26	T06-26	T06-26
ID number	Gt1_42	Pl_fm_gt_3	2
SiO2	35.764	58.5405	35.3481
TiO2	0.024	0.0002	1.5915
Al2O3	20.694	23.2674	16.2626
Cr2O3	0.014	0.0001	0.1195
FeO	28.808	0.1163	14.039
MnO	2.341	0.0001	0.0934
MgO	4.185	0.0003	14.3234
ZnO	0.000	0.0001	0.1436
CaO	4.893	5.7137	0.0245
Na2O	0.000	8.176	0.3052
K2O	0.000	0.0363	8.4762

## Chapter 6—Archaean to Proterozoic crustal evolution of the orogenic belts surrounding the Tanzanian Craton

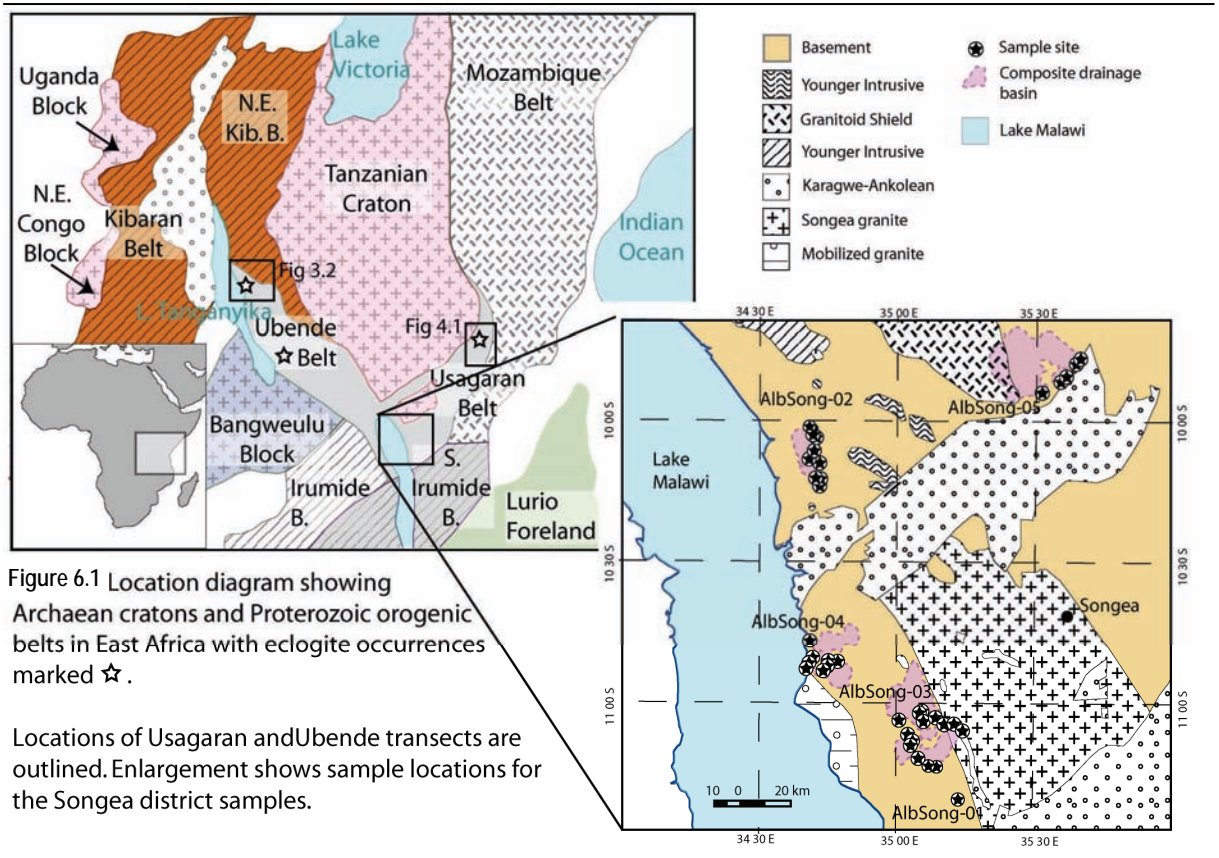


Figure 6.1 Location diagram showing Archaean cratons and Proterozoic orogenic belts in East Africa with eclogite occurrences marked ☆.

Locations of Usagaran and Ubende transects are outlined. Enlargement shows sample locations for the Songea district samples.

### 6.1 Introduction

Zircon in high-grade metasedimentary rocks retains isotopic signatures which can be used to investigate the source of sediments, crystallization history of the source rocks, timing of separation of the source magmas from the mantle, and metamorphic zircon growth within the metasediment (Chen et al., 2010; Davis et al., 2005; Griffin et al., 2006; Zeh et al., 2008). The application of U-Pb and Lu-Hf isotope analysis in detrital zircons to provide information about the formation of continental crust is discussed in chapter 2 of this thesis. Chapters 3 & 4 discuss the application of U-Pb geochronology to investigate the provenance of sedimentary rocks. This chapter presents *in situ* laser ablation multicollector inductively coupled plasma mass spectrometry (LA-MC-ICPMS) Lu-Hf zircon analyses from metasedimentary samples obtained from the Ubende and Usagaran Orogens, coupled with the laser ablation inductively coupled plasma mass spectrometry (LA-ICPMS) U-Pb zircon data presented in chapters 3 & 4 in order to investigate the crustal evolution of the source region for metasedimentary rocks in the Usagaran and Ubendian orogenic Orogens, and what this means for the evolution of Precambrian Tanzania.

In addition four stream sediment samples from the south of Tanzania are included in the discussion section of this chapter. These samples are from the Songea district, and were collected by Albidon Limited to assist in mineral exploration. Data was collected and processed by Belousova and Griffin (unpublished data) and is

presented in Appendix 3. These samples are from directly south of the Tanzanian Craton, in a zone which may be the transition or intersection between the Ubende and Usagaran Orogens, or may be related to the Mesoproterozoic Irumide orogeny.

#### 6.1.1 Regional geology

The geology of the Tanzanian Craton is discussed in chapter 2, the Usagaran Orogen is discussed in chapters 4 & 5 and the Ubende, Kibaran and Irumide orogenic Orogens in chapter 3. The location of these Orogens is shown in figure 6.1.

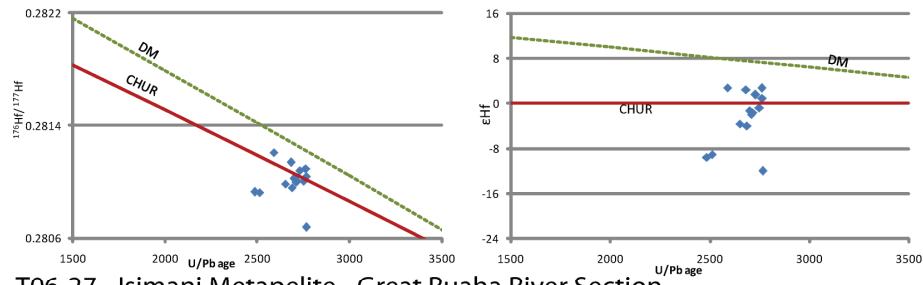
#### 6.2 Sampling strategy and analytical techniques

Sedimentary rocks from the Ubende and Usagaran Orogens, dated in chapters 3 and 4 respectively, were analysed for their Lu-Hf isotopic compositions. The sample locations are shown in figures 3.2 and 4.2.

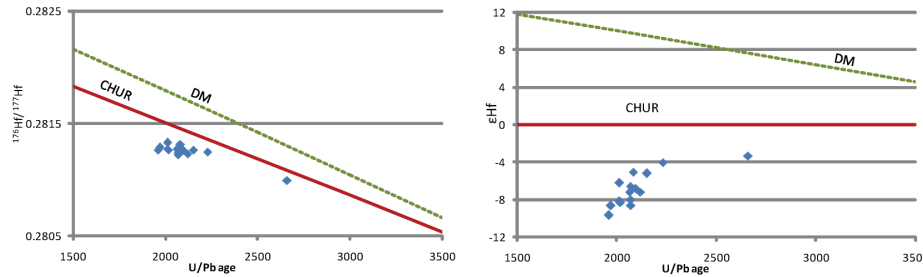
In addition four samples from the Songea district in the south of Tanzania, collected by Albidon Limited and dated and analysed by Elena Belousova, are included for the purpose of discussion. These samples are stream sediments, not rocks, and are assumed to have sampled many of the rock units within the modern drainage catchments of the streams from which they were sampled. Samples 2-5 of the Albidon Ltd Songea samples were composite samples, representing zircon combined from between 5 and 14 streams within the one catchment. The sample sites and combined drainage basins are shown in figure 6.1.



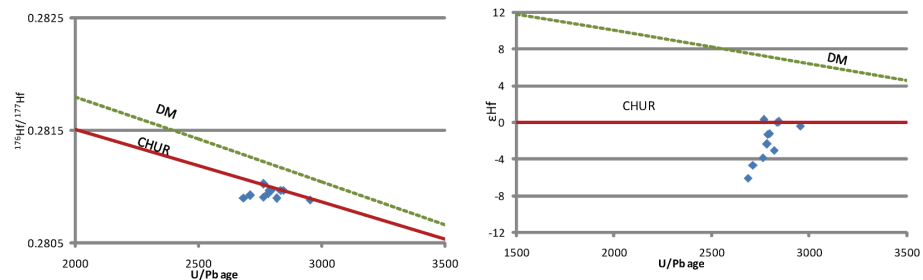
T01-37 - Konse Group Quartzite - Great Ruaha River Section



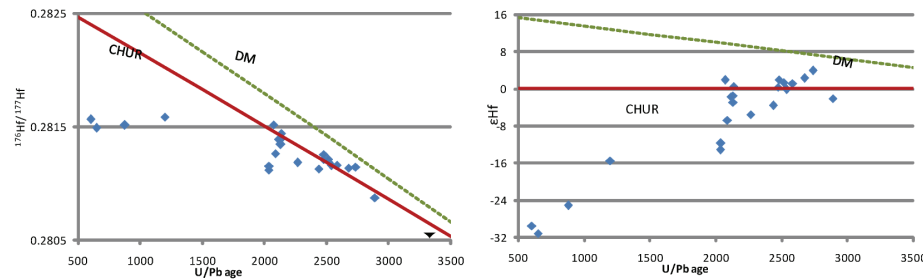
T06-27 - Isimani Metapelite - Great Ruaha River Section



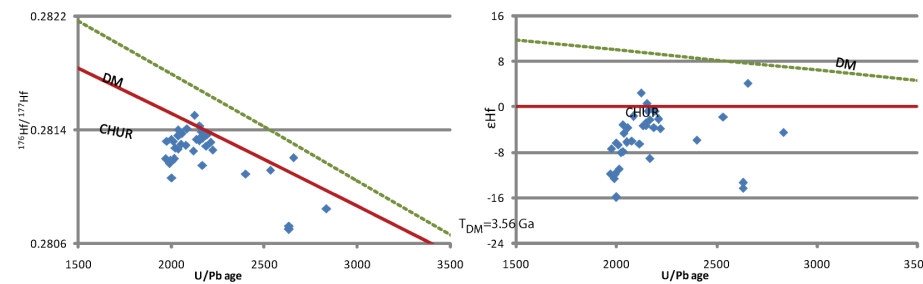
T06-37 - Isimani Metapelite - Great Ruaha River Section



T07-35 - Isimani Metapelite - Mangaliisa Plateau



T07-59 - Isimani Metapelite - Sasimo River Section



T07-71 - Isimani Metapelite - Sasimo River Section

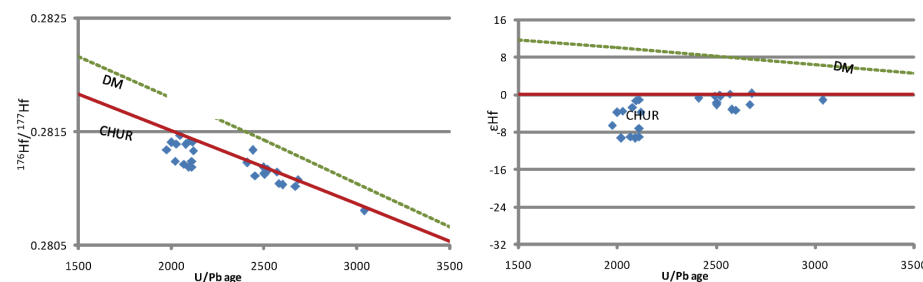


Figure 6.2. Results of combined Lu-Hf and U-Pb zircon spot analyses from the Usagaran Belt presented as  $^{176}\text{Hf}/^{177}\text{Hf}$  (vs  $^{207}\text{Pb}/^{206}\text{Pb}$  age, and  $\epsilon\text{Hf}(t)$  vs  $^{207}\text{Pb}/^{206}\text{Pb}$  age.  $^{176}\text{Hf}/^{177}\text{Hf}(t)$  is initial  $^{176}\text{Hf}/^{177}\text{Hf}$  calculated at the time of crystallisation

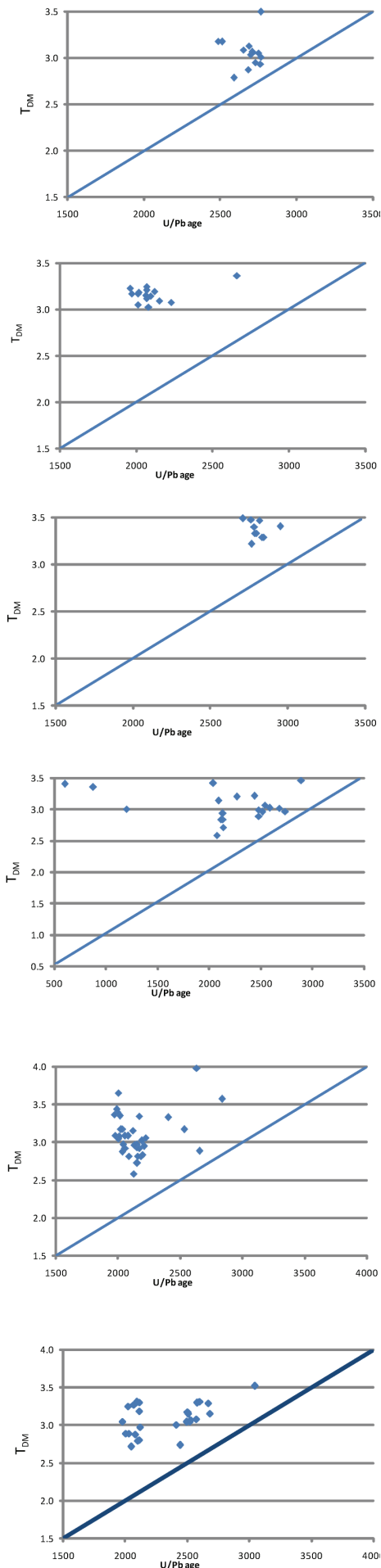


Figure 6.2. (continued)  $T_{DM}$  vs  $^{207}\text{Pb}/^{206}\text{Pb}$  age.  $^{176}\text{Hf}/^{177}\text{Hf}(t)$  is initial  $^{176}\text{Hf}/^{177}\text{Hf}$  calculated at the time of crystallisation

### 6.2.1 LA-ICPMS U-Pb-Th analysis

Zircon U-Th-Pb analyses for all Usagaran and Ubende Orogen samples were undertaken by LA-ICPMS at Adelaide Microscopy, University of Adelaide on an Agilent 7500cs ICPMS fitted with a New Wave 213 nm neodymium–yttrium–aluminium–garnet (Nd-YAG) laser. Beam diameter was set at 30  $\mu\text{m}$  using a repetition rate of 15 Hz. U-Pb fractionation was corrected using the GEMOC GJ-1 zircon (TIMS normalization data  $^{207}\text{Pb}/^{206}\text{Pb} = 608.3$  Ma,  $^{206}\text{Pb}/^{238}\text{U} = 600.7$  Ma,  $^{207}\text{Pb}/^{235}\text{U} = 602.2$  Ma (Jackson et al., 2004)). Standard GJ was run 4 times at the beginning and end of a run, interspersed by two analyses of the in-house Sri Lankan zircon standard (BJWP-1,  $^{207}\text{Pb}/^{206}\text{Pb} = 720.9$  Ma (Wade et al., 2008)) and ten analyses of unknowns. Total acquisition time per analysis was 90 seconds; 50 seconds background measurement followed by 40 seconds of sample ablation. Data was processed using GLITTER software (Van Achterbergh et al., 2001). Standard bracketing was used as described in section 2.3.3.

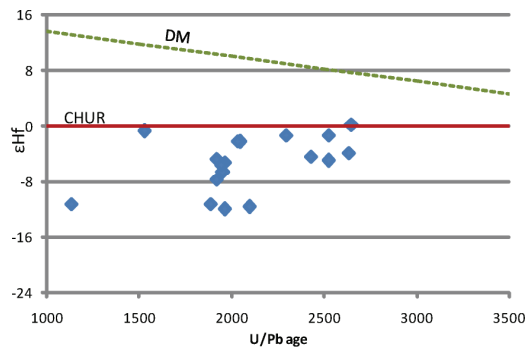
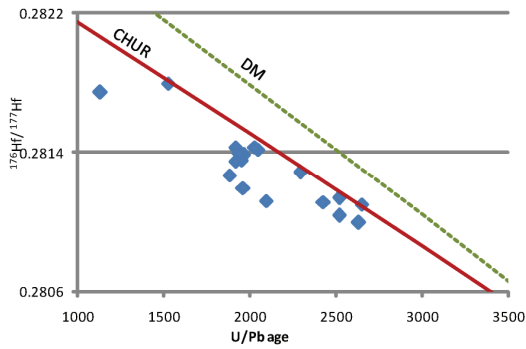
Zircon U-Pb-Th analyses for samples from the Songea district were conducted by Belousova (unpublished data) at Macquarie University at GEMOC on a Nu Plasma MC-ICPMS details coupled with a New Wave 213 nm Nd-YAG laser following the analytical technique outlined in Pearson et al. (2008).

### 6.2.2 LA-ICPMS Lu-Hf analysis

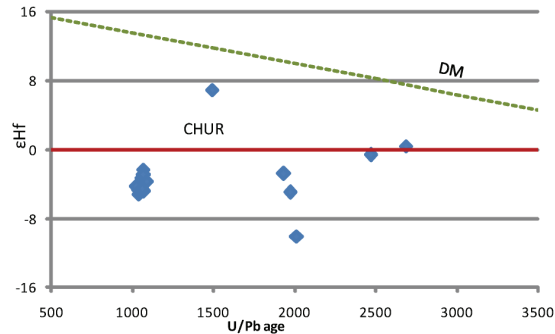
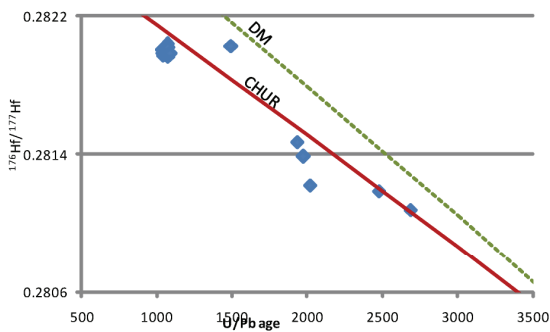
Zircon Lu-Hf analyses were undertaken at Macquarie University at GEMOC on a Nu Plasma multi-collector ICPMS details coupled with a New Wave 213 nm Nd-YAG laser. Beam diameter was set at 40–55  $\mu\text{m}$  using a repetition rate of 5 Hz. Total acquisition time per analysis was 200 seconds, with 30 seconds background measurement. The “Lu-Hf laser spot” was drilled next to the “U-Pb laser spot” within the same domain as constrained by the CL images. The reference zircons Mud Tank ( $^{176}\text{Hf}/^{177}\text{Hf} = 0.282530 \pm 30$ ) (Griffin et al., 2007) and Harvard 91500 ( $^{176}\text{Hf}/^{177}\text{Hf} = 0.282280 \pm 120$ ) (Weidenback et al., 1995; Weidenback et al., 2004) were run at the beginning and end of each session, with the Mud Tank zircon also run between sets of ten analyses for consistency.

Measurement of accurate  $^{176}\text{Hf}/^{177}\text{Hf}$  ratios in zircon requires correction for interferences of  $^{176}\text{Lu}$  and  $^{176}\text{Yb}$  on  $^{176}\text{Hf}$ . Because the Nu Plasma multi-collector ICPMS mass bias instrument is independent of mass over the mass range considered here this correction is relatively straightforward. Interference of  $^{176}\text{Lu}$  on  $^{176}\text{Hf}$  was corrected by measuring the intensity of the interference-free  $^{175}\text{Lu}$  isotope and using  $^{176}\text{Lu}/^{175}\text{Lu} = 0.02669$  to calculate the intensity of  $^{176}\text{Lu}$ . Similarly, the interference of  $^{176}\text{Yb}$  on  $^{176}\text{Hf}$  was corrected by measuring the interference-free  $^{172}\text{Yb}$  isotope and using  $^{176}\text{Yb}/^{172}\text{Yb}$  to calculate the intensity of  $^{176}\text{Yb}$ . The appropriate value of  $^{176}\text{Yb}/^{172}\text{Yb}$  (0.5865) was determined by successively spiking the JMC475 Hf standard (100 ppb solution) with Yb (10–80 ppb), and determining the value of  $^{176}\text{Hf}/^{177}\text{Hf}$  obtained on the pure Hf solution (Griffin et al., 2004; Pearson et al., 2008). More detailed discussions regarding the overlap corrections for  $^{176}\text{Lu}$  and  $^{176}\text{Yb}$  can be found in Griffin et

## T04-07



## T04-12b



## T04-39

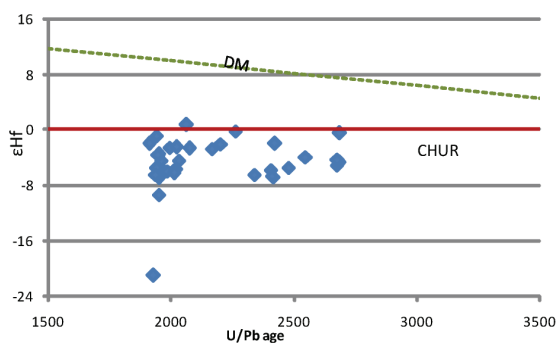
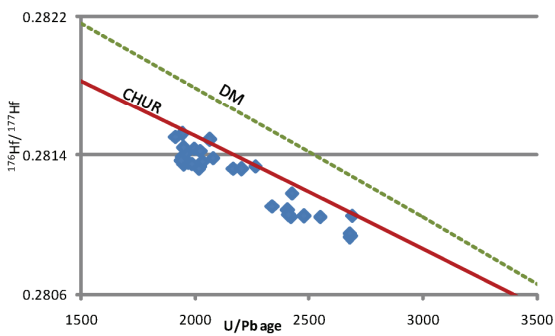


Figure 6.3 Results of combined Lu-Hf and U-Pb zircon spot analyses from the Ubende Belt presented as  $^{176}\text{Hf}/^{177}\text{Hf}(t)$  vs  $^{207}\text{Pb}/^{206}\text{Pb}$  age,  $\epsilon\text{Hf}(t)$  vs  $^{207}\text{Pb}/^{206}\text{Pb}$  age and  $T_{\text{DM}}$  vs  $^{207}\text{Pb}/^{206}\text{Pb}$  age.  $^{176}\text{Hf}/^{177}\text{Hf}(t)$  is initial  $^{176}\text{Hf}/^{177}\text{Hf}$  calculated at the time of crystallisation

al. (2007) and Pearson et al. (2008).

The measured  $^{176}\text{Lu}/^{177}\text{Hf}$  ratios of the zircons have been used to calculate initial  $^{176}\text{Hf}/^{177}\text{Hf}$  ratios. These age corrections are very small, and the typical uncertainty on a single analysis of  $^{176}\text{Lu}/^{177}\text{Hf}$  (+1%) contributes an uncertainty of <0.05  $\epsilon\text{Hf}$  unit. For the calculation of  $\epsilon\text{Hf}$  values, representing the per mil difference between the sample and the chondritic reservoir (CHUR) at the time of intrusion, we have adopted a decay constant for  $^{176}\text{Lu}$  of  $1.865 \times 10^{-11}$  and the chondritic values of  $^{176}\text{Hf}/^{177}\text{Hf}$  and  $^{176}\text{Lu}/^{177}\text{Hf}$  derived by (Scherer et al., 2001). The accuracy and precision of the method are discussed in further detail by Griffin et al. (2004; 2000).

### 6.3 Results

The U-Pb zircon geochronology results are presented in chapter 3 for the Ubende Orogen and chapter 4 for the

Usagaran Orogen samples. Lu-Hf isotope analyses are summarised below. Full results are presented in table 6.1.

#### 6.3.1 Usagaran Orogenic Belt

Figure 6.2 shows all Lu-Hf isotope analyses from the Usagaran Orogen, plotted against U-Pb ages for each zircon.

Sample T01-37 is a quartzite from the Konse group, deposited in a peripheral foreland basin formed at the margin of the Tanzanian Craton during the main phase of the Usagaran orogen (Mruma, 1995). The  $^{207}\text{Pb}/^{206}\text{Pb}$  data indicated a single source for this quartzite, most likely being granitoid from the Tanzanian Craton with a crystallisation age of  $2718 \pm 24$  Ma. Lu-Hf analysis of 14 grains yielded  $T_{\text{DM}}$  ages of  $\sim 3.16$  Ga for the majority of grains. A few grains with younger discordant  $^{207}\text{Pb}/^{206}\text{Pb}$

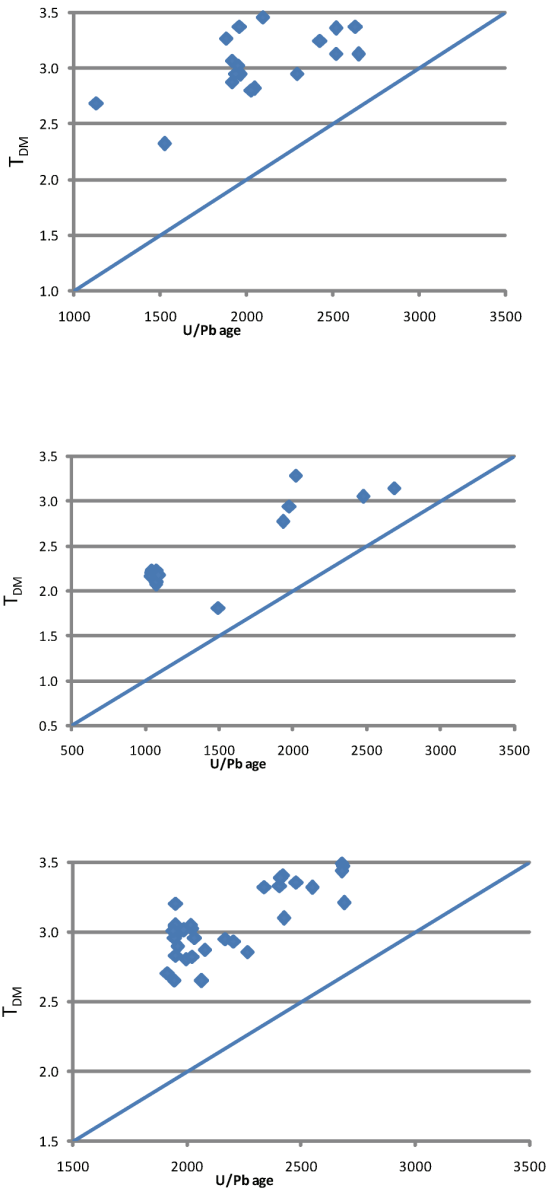


Figure 6.3 (continued)

ages yielded apparently older  $T_{DM}$  ages of  $\sim 3.56$  Ga, however this is a direct result of the younger U-Pb ages as the  $^{176}\text{Hf}/^{177}\text{Hf}$  values are within error of main population.

Sample T06-37, a quartzite from the west of the Usagaran Orogen, yielded only zircon with Archaean  $^{207}\text{Pb}/^{206}\text{Pb}$  ages, with peaks in the age spectra at  $2679 \pm 4$  Ma,  $2727 \pm 5$  Ma,  $2778 \pm 5$  Ma, and  $2821 \pm 5$  Ma. The  $^{176}\text{Hf}/^{177}\text{Hf}$  signatures of these populations were indistinguishable ( $^{176}\text{Hf}/^{177}\text{Hf} = 0.2809 - 0.2810$ ,  $\epsilon_{\text{Hf}} = 0.2 - -6.1$ ) and yielded  $T_{DM}$  ages of  $\sim 3.36$  Ga.

Sample T06-27, a pelitic sample also from the western Usagaran Orogen, yielded zircon crystallised at  $\sim 2.6$  Ga and between 2.1 – 2.0 Ga. A population of zircon dated at  $2087 \pm 8$  Ma is interpreted to have an igneous origin while populations aged  $2007 \pm 4$  Ma and  $1970 \pm 10$  Ma represent metamorphic zircon recrystallisation. Lu-Hf analysis of the Archaean grain ( $2660 \pm 19$  Ma) yielded a  $^{176}\text{Hf}/^{177}\text{Hf}$  value of 0.2809 with a  $T_{DM}$  age of 3.32 and  $\epsilon_{\text{Hf}}$  value of -3.4. The igneous Palaeoproterozoic grains yielded  $T_{DM}$  ages of 3.0 – 3.2 Ga ( $^{176}\text{Hf}/^{177}\text{Hf} = 0.2812 - 0.2813$ ,  $\epsilon_{\text{Hf}} = -5.1 - -8.6$ ) and the metamorphic Palaeoproterozoic grains yielded indistinguishable  $T_{DM}$  ages of  $\sim 3.2$  Ga ( $^{176}\text{Hf}/^{177}\text{Hf} = 0.2813$ ,  $\epsilon_{\text{Hf}} = -6.3 - -9.7$ ).

Sample T07-35, a kyanite-biotite pelite from the eastern Usagaran Orogen contains both igneous and metamorphic zircon, with peaks in the  $^{207}\text{Pb}/^{206}\text{Pb}$  age spectra at  $\sim 2520$ , 2480 and 2123 Ma interpreted as having an igneous origin while peaks at  $2037 \pm 13$  Ma and  $\sim 630$  Ma are interpreted to be of metamorphic origin. The  $\sim 2520$  Ma population yielded  $T_{DM}$  ages of 3.0 Ga ( $^{176}\text{Hf}/^{177}\text{Hf} = 0.2812$ ,  $\epsilon_{\text{Hf}} = 1.3 - -0.2$ ). The  $\sim 2480$  Ma population yielded  $T_{DM}$  ages of 2.9 Ga ( $^{176}\text{Hf}/^{177}\text{Hf} = 0.2812 - 0.2813$ ,  $\epsilon_{\text{Hf}} = 2.0 - 0.3$ ). The 2123  $\pm 16$  Ma population yielded  $T_{DM}$  ages of  $\sim 2.8$  Ga ( $^{176}\text{Hf}/^{177}\text{Hf} = 0.2813 - 0.2814$ ,  $\epsilon_{\text{Hf}} = 0.6 - -3.0$ ). Individual older grains ( $2584 \pm 18$  Ma,  $2676 \pm 19$  Ma,  $2737 \pm 20$  Ma and  $2890 \pm 17$  Ma) yielded  $T_{DM}$  ages of 3.02 Ga ( $^{176}\text{Hf}/^{177}\text{Hf} = 0.2812$ ,  $\epsilon_{\text{Hf}} = 1.1$ ), 3.02 Ga ( $^{176}\text{Hf}/^{177}\text{Hf} = 0.2811$ ,  $\epsilon_{\text{Hf}} = 2.3$ ), 2.96 Ga ( $^{176}\text{Hf}/^{177}\text{Hf} = 0.2811$ ,  $\epsilon_{\text{Hf}} = 3.8$ ) and 3.46 Ga ( $^{176}\text{Hf}/^{177}\text{Hf} =$

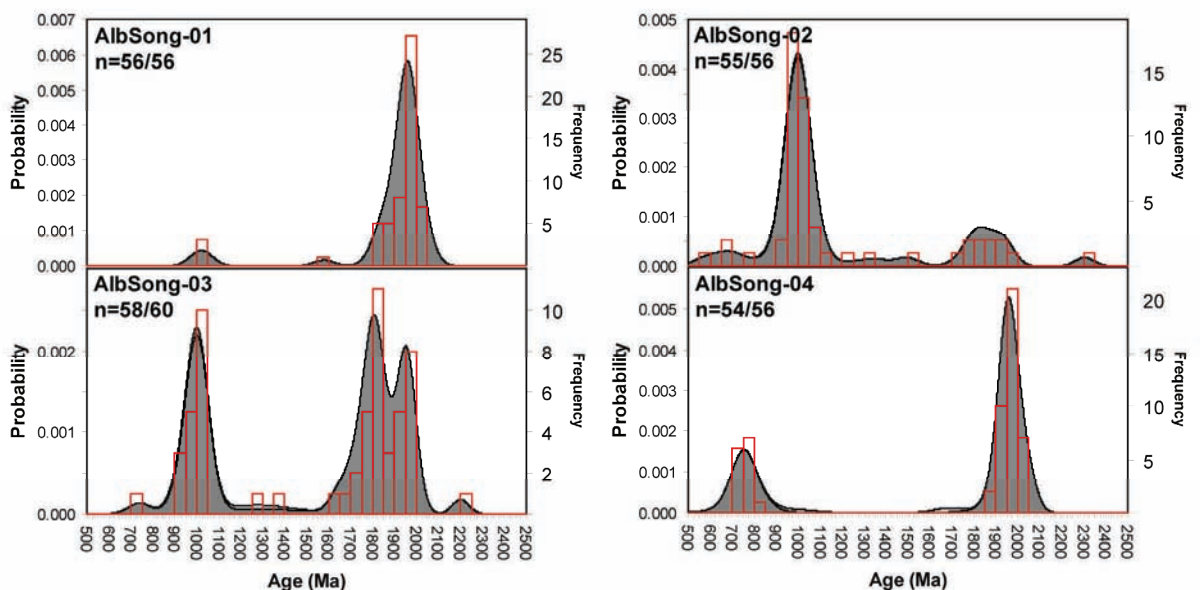
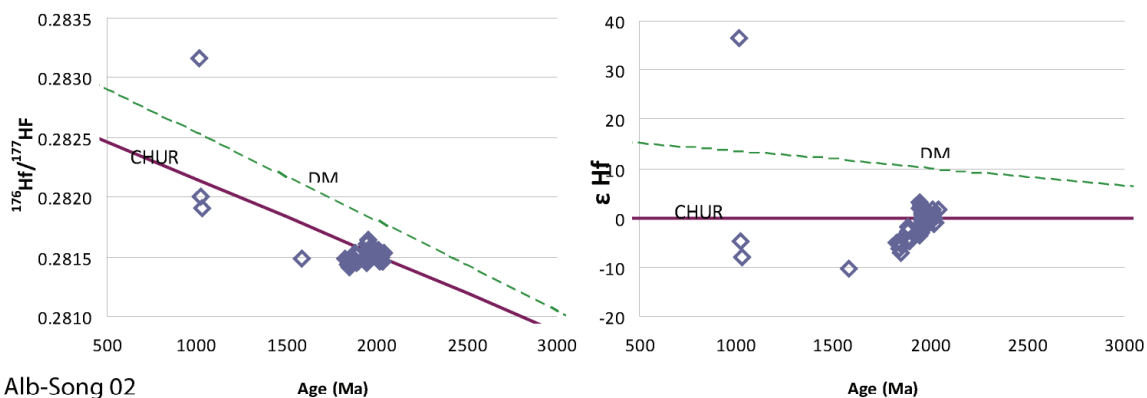


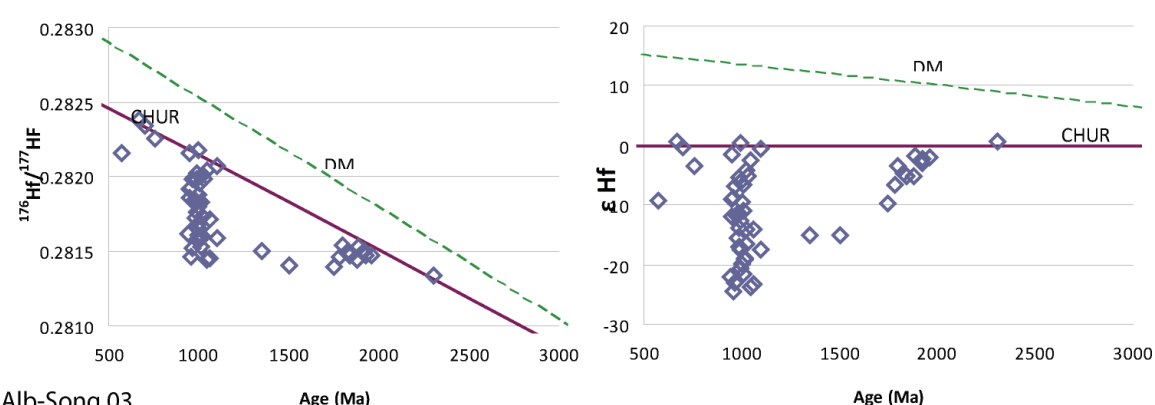
Figure 6.4 Concordant U-Pb zircon ages from Songea District samples presented as probability density plots.



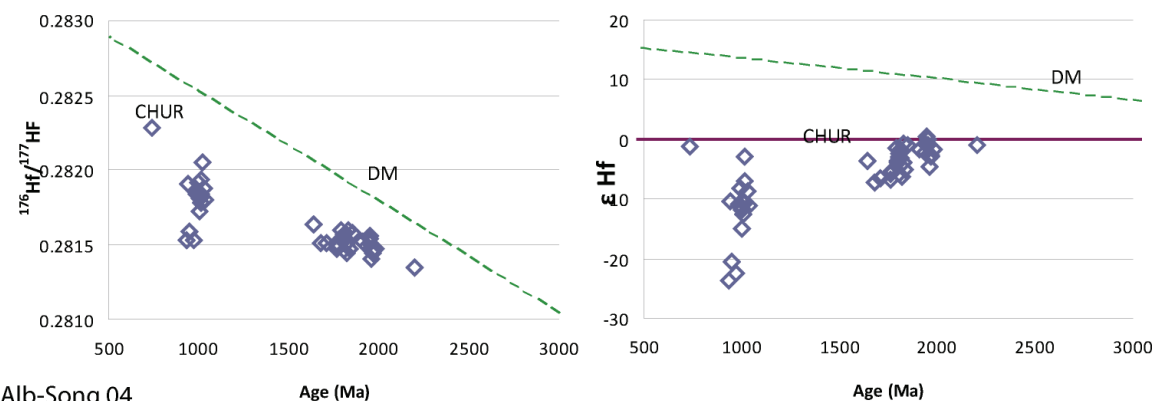
### Alb-Song 01



### Alb-Song 02



### Alb-Song 03



### Alb-Song 04

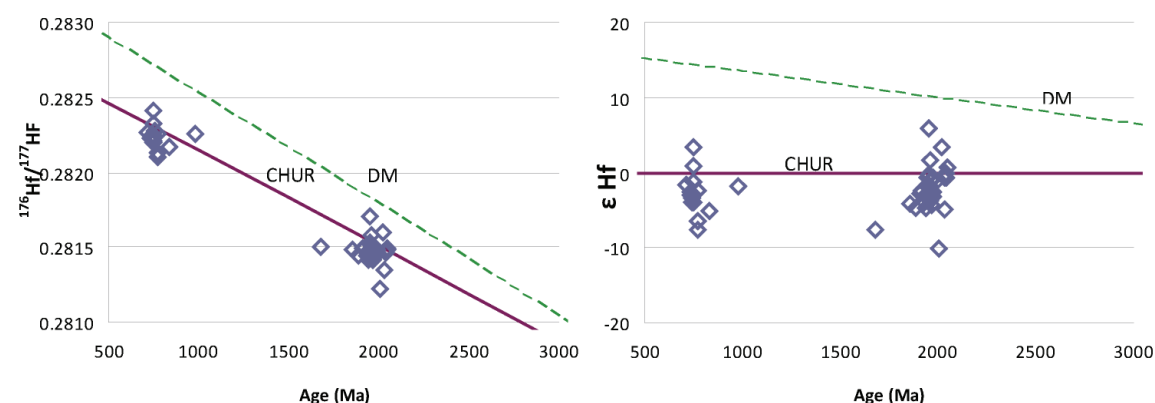


Figure 6.5 Results of combined Lu-Hf and U-Pb zircon spot analyses from the Songea District presented as  $^{176}\text{Hf}/^{177}\text{Hf}(t)$  vs  $^{207}\text{Pb}/^{206}\text{Pb}$  age,  $\epsilon_{\text{Hf}}(t)$  vs  $^{207}\text{Pb}/^{206}\text{Pb}$  age and  $T_{\text{DM}}$  vs  $^{207}\text{Pb}/^{206}\text{Pb}$  age.  $^{176}\text{Hf}/^{177}\text{Hf}(t)$  is initial  $^{176}\text{Hf}/^{177}\text{Hf}$  calculated at the time of crystallisation

0.2809,  $\epsilon_{\text{Hf}} = -2.1$ ) respectively. The  $2037 \pm 13$  Ma population yielded  $T_{\text{DM}}$  ages of  $\sim 3.45$  Ga ( $^{176}\text{Hf}/^{177}\text{Hf} = 0.2811 - 0.2812$ ,  $\epsilon_{\text{Hf}} = -11.8 - -13.2$ ) and the  $\sim 620$  Ma grains yielded similar  $T_{\text{DM}}$  ages of  $\sim 3.45$  Ga ( $^{176}\text{Hf}/^{177}\text{Hf} = 0.2815 - 0.2816$ ,  $\epsilon_{\text{Hf}} = -29.5 - -31.2$ ).

Sample T07-59, also from the eastern Usagaran Orogen, contains zircons with peaks in the  $^{207}\text{Pb}/^{206}\text{Pb}$  age spectra at  $2646 \pm 17$  Ma,  $2102 \pm 7$  Ma,  $2178 \pm 6$  Ma, and  $2040 \pm 7$  Ma, which are interpreted to be igneous in origin. Peaks interpreted to be of metamorphic origin

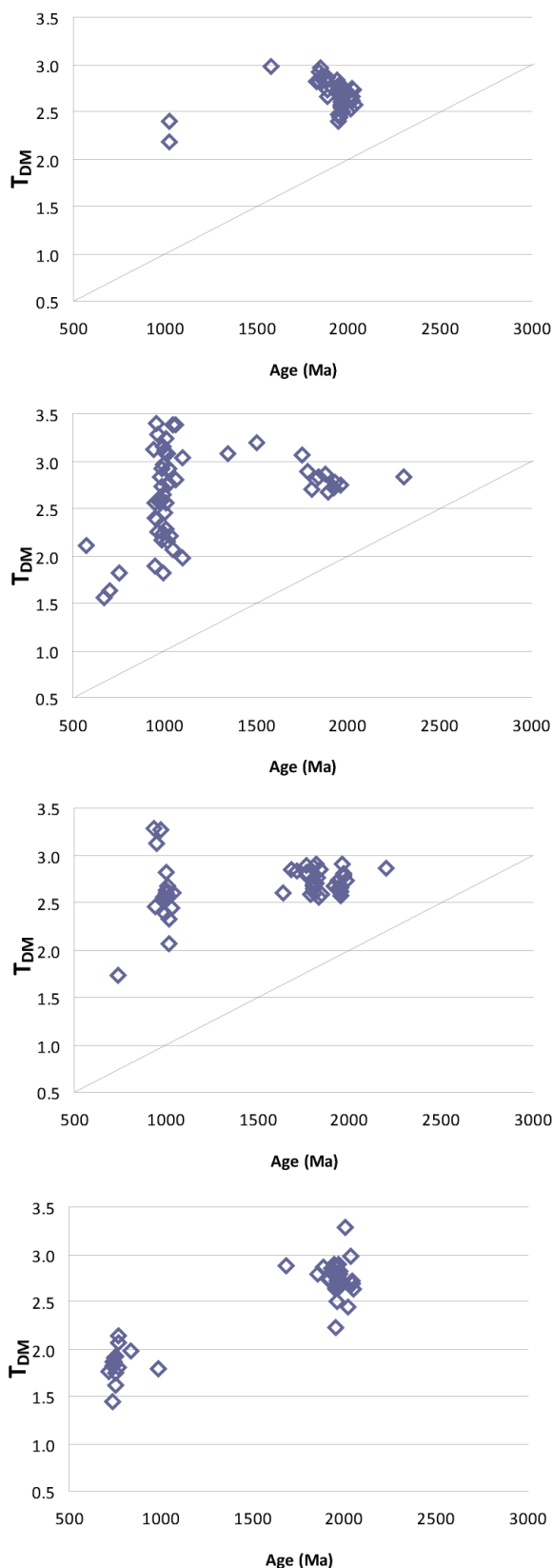


Figure 6.5 (continued)

occur at  $2055 \pm 17$  Ma,  $2016 \pm 8$  Ma and  $1980 \pm 18$  Ma. The  $2646 \pm 17$  Ma zircons yielded  $T_{DM}$  ages of  $\sim 4.0$  Ga ( $^{176}\text{Hf}/^{177}\text{Hf} = 0.2807$ ,  $\epsilon_{\text{Hf}} = -13.4 - -14.4$ ) with one grain yielded a younger crustal age of  $2.88$  Ga ( $^{176}\text{Hf}/^{177}\text{Hf} = 0.2812$ ,  $\epsilon_{\text{Hf}} = 4.1$ ). The  $2178 \pm 6$  Ma zircons yielded  $T_{DM}$  ages between  $2.72$  and  $3.06$  Ga ( $^{176}\text{Hf}/^{177}\text{Hf} = 0.2811 -$

$0.2814$ ,  $\epsilon_{\text{Hf}} = 0.5 - -9.0$ ). The  $2102 \pm 7$  Ma zircons yielded  $T_{DM}$  ages of between  $2.58$  and  $3.15$  Ga ( $^{176}\text{Hf}/^{177}\text{Hf} = 0.2812 - 0.2815$ ,  $\epsilon_{\text{Hf}} = 2.5 - -6.6$ ). The  $2040 \pm 7$  Ma zircons yielded  $T_{DM}$  ages of  $\sim 2.95$  Ga ( $^{176}\text{Hf}/^{177}\text{Hf} = 0.2813 - 0.2814$ ,  $\epsilon_{\text{Hf}} = -3.2 - -6.3$ ). The metamorphic zircon populations ( $2055 \pm 17$  Ma,  $2016 \pm 8$  Ma and  $1980 \pm 18$  Ma) yielded  $T_{DM}$  ages of between  $3.43$  and  $2.82$  Ga ( $^{176}\text{Hf}/^{177}\text{Hf} = 0.2812 - 0.2813$ ,  $\epsilon_{\text{Hf}} = -1.7 - -12.6$ ),  $3.04$  to  $3.65$  Ga ( $^{176}\text{Hf}/^{177}\text{Hf} = 0.2811 - 0.2813$ ,  $\epsilon_{\text{Hf}} = -6.3 - -15.9$ ) and  $3.09$  to  $3.39$  Ga ( $^{176}\text{Hf}/^{177}\text{Hf} = 0.2811 - 0.2813$ ,  $\epsilon_{\text{Hf}} = -1.8 - -11.9$ ) respectively.

The final sample from the Usagaran Orogen, T07-71, is also from the eastern Usagaran Orogen and contains zircons with complex  $^{207}\text{Pb}/^{206}\text{Pb}$  age spectra. Igneous peaks in the spectra occur in two clusters, the elder between  $2300$  and  $2700$  Ma (peaks at  $2675 \pm 13$  Ma,  $2596 \pm 8$  Ma,  $2535 \pm 7$  Ma,  $2489 \pm 5$  Ma,  $2407 \pm 6$  Ma and  $2326 \pm 9$  Ma) and the younger with peaks at  $2099 \pm 6$  Ma and  $1976 \pm 11$  Ma. These groups of peaks are not easily distinguishable in the Lu/Hf data. The elder populations yielded  $T_{DM}$  ages of between  $2.63$  and  $3.29$  Ga ( $^{176}\text{Hf}/^{177}\text{Hf} = 0.2810 - 0.2814$ ,  $\epsilon_{\text{Hf}} = 4.1 - -3.3$ ). The younger group yield  $T_{DM}$  ages between  $2.79$  and  $3.31$  Ga ( $^{176}\text{Hf}/^{177}\text{Hf} = 0.2812 - 0.2814$ ,  $\epsilon_{\text{Hf}} = -1.2 - -9.1$ ). Metamorphic zircon populations at  $2013 \pm 7$  Ma and  $2065 \pm 9$  Ma yield  $T_{DM}$  ages of between  $2.71$  and  $3.26$  Ga ( $^{176}\text{Hf}/^{177}\text{Hf} = 0.2812 - 0.2814$ ,  $\epsilon_{\text{Hf}} = -0.5 - -9.3$ ).

### 6.3.2 Ubende Orogen

Figure 6.3 shows all Lu-Hf isotope analyses from the Ubende Orogen plotted against U-Pb ages for each zircon.

The zircon  $^{207}\text{Pb}/^{206}\text{Pb}$  age spectra for sample T04-07 contains multiple zircon peaks at  $1947 \pm 24$  Ma,  $2045 \pm 37$  Ma,  $2416 \pm 14$  Ma, and  $2622 \pm 42$  Ma. Each of these populations was targeted for Lu-Hf analysis. Individual grains aged  $1131 \pm 27$  Ma,  $1525 \pm 34$  Ma and  $2291 \pm 21$  Ma were also analysed. Each of these populations is considered to be igneous in origin. The Archaean peak yielded a  $T_{DM}$  age of  $\sim 3.2$  Ga ( $^{176}\text{Hf}/^{177}\text{Hf} = 0.2811 - 0.28125$ ,  $\epsilon_{\text{Hf}} = -4.9 - 0.2$ ). The single targeted  $\sim 2420$  Ma grain yielded a  $T_{DM}$  age of  $\sim 2.9$  Ga ( $^{176}\text{Hf}/^{177}\text{Hf} = 0.281174$ ,  $\epsilon_{\text{Hf}} = -4.3$ ). The  $2045 \pm 37$  Ma zircons yielded  $T_{DM}$  age of  $\sim 2.5$  Ga ( $^{176}\text{Hf}/^{177}\text{Hf} = 0.2812 - 0.2815$ ,  $\epsilon_{\text{Hf}} = -2.2 - -11.7$ ). The  $1947 \pm 24$  Ma grains yielded a  $T_{DM}$  age of  $\sim 2.6$  Ga ( $^{176}\text{Hf}/^{177}\text{Hf} = 0.2813 - 0.2814$ ,  $\epsilon_{\text{Hf}} = -5.2 - -12.1$ ). The two Mesoproterozoic grains ( $1131$  &  $1525$  Ma) yielded  $T_{DM}$  ages of  $2.7$  Ga ( $^{176}\text{Hf}/^{177}\text{Hf} = 0.2818$ ,  $\epsilon_{\text{Hf}} = -11.3$ ) and  $2.4$  Ga ( $^{176}\text{Hf}/^{177}\text{Hf} = 0.28185$ ,  $\epsilon_{\text{Hf}} = -0.7$ ) respectively.

In sample T04-12b the major peak at  $1973 \pm 100$  Ma in the  $^{207}\text{Pb}/^{206}\text{Pb}$  age spectra is interpreted to be igneous in origin, as are individual grains aged  $2685 \pm 19$  Ma,  $2473 \pm 21$  Ma and  $1494 \pm 32$  Ma. A strong peak in the data at  $1068 \pm 11$  Ma is interpreted to represent metamorphic zircon recrystallisation. The  $1973 \pm 100$  Ma grains yielded a range  $T_{DM}$  ages between  $2.8$  and  $2.43$  Ga ( $^{176}\text{Hf}/^{177}\text{Hf} = 0.2813 - 0.2815$ ,  $\epsilon_{\text{Hf}} = -2.8 - -10.0$ ). The individual grains at The  $2658 \pm 19$  Ma,  $2473 \pm 21$  and  $1494 \pm 32$  Ma yield  $T_{DM}$  ages of  $\sim 3.14$  Ga ( $^{176}\text{Hf}/^{177}\text{Hf} = 0.2811$ ,  $\epsilon_{\text{Hf}} = 0.4$ ),  $3.05$  Ga ( $^{176}\text{Hf}/^{177}\text{Hf} = 0.2812$ ,  $\epsilon_{\text{Hf}} = -$

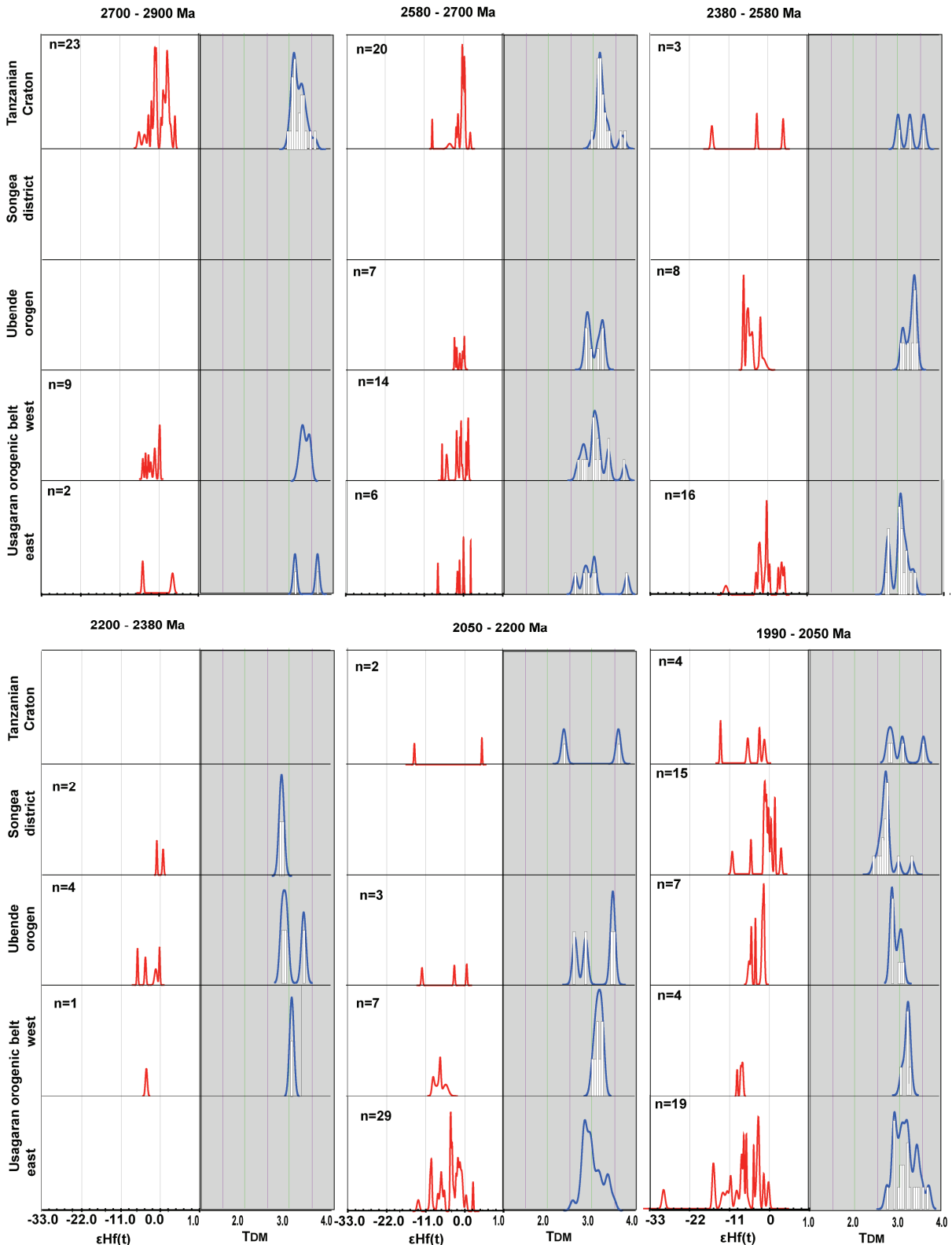


**Figure 6.6** Time slices of combined data for all Tanzanian terranes, presented as probability density plots of  $\epsilon\text{Hf}(t)$  and  $T_{\text{DM}}$  results. Time slices represent  $^{207}\text{Pb}/^{206}\text{Pb}$  age populations.  $n=\#$  gives the number of zircon analyses in those age populations.

0.6), and 1.81 Ga ( $^{176}\text{Hf}/^{177}\text{Hf} = 0.2820$ ,  $\epsilon_{\text{Hf}} = 6.9$ ) respectively. The metamorphic grains aged  $1068 \pm 11$  Ma yielded a  $T_{\text{DM}}$  age of  $\sim 1.7$  Ga ( $^{176}\text{Hf}/^{177}\text{Hf} = 0.2820$ ,  $\epsilon_{\text{Hf}} = 2.3 - 5.2$ ).

In sample T04-39 all zircon is considered to be of igneous origin. Peaks in the  $^{207}\text{Pb}/^{206}\text{Pb}$  age spectra occurred at  $1975 \pm 9$  Ma,  $2059 \pm 8$  Ma,  $2334 \pm 12$  Ma,  $2436 \pm 22$  Ma,  $2538 \pm 39$  Ma,  $2631 \pm 29$  Ma,  $2691 \pm 17$  Ma. All age peaks were targeted for Lu-Hf analysis. The

$2691 \pm 17$  Ma grains yielded a  $T_{\text{DM}}$  age of  $\sim 2.9 - 3.5$  Ga ( $^{176}\text{Hf}/^{177}\text{Hf} = 0.281 - 0.2813$ ,  $\epsilon_{\text{Hf}} = -0.5 - 5.2$ ). The  $2538 \pm 39$  Ma grains yielded a  $T_{\text{DM}}$  age of  $\sim 3.32$  Ga ( $^{176}\text{Hf}/^{177}\text{Hf} = 0.2810$ ,  $\epsilon_{\text{Hf}} = -4.0$ ). The  $2436 \pm 22$  Ma grains yielded a  $T_{\text{DM}}$  age of  $\sim 3.1 - 3.4$  Ga ( $^{176}\text{Hf}/^{177}\text{Hf} = 0.2811 - 0.2831$ ,  $\epsilon_{\text{Hf}} = -2.0 - -6.9$ ). The  $2334 \pm 12$  Ma grains yielded a  $T_{\text{DM}}$  age of  $\sim 3.32$  Ga ( $^{176}\text{Hf}/^{177}\text{Hf} = 0.2816$ ,  $\epsilon_{\text{Hf}} = -6.6$ ). The  $2059 \pm 8$  Ma grains yielded a  $T_{\text{DM}}$  age of  $\sim 2.8 - 3.0$  Ga ( $^{176}\text{Hf}/^{177}\text{Hf} = 0.2814 - 0.2815$ ,  $\epsilon_{\text{Hf}} = 0.7 - -7.0$ ). The  $1975 \pm 9$  Ma grains yielded a similar  $T_{\text{DM}}$  age of  $\sim 2.6 - 3.0$  Ga

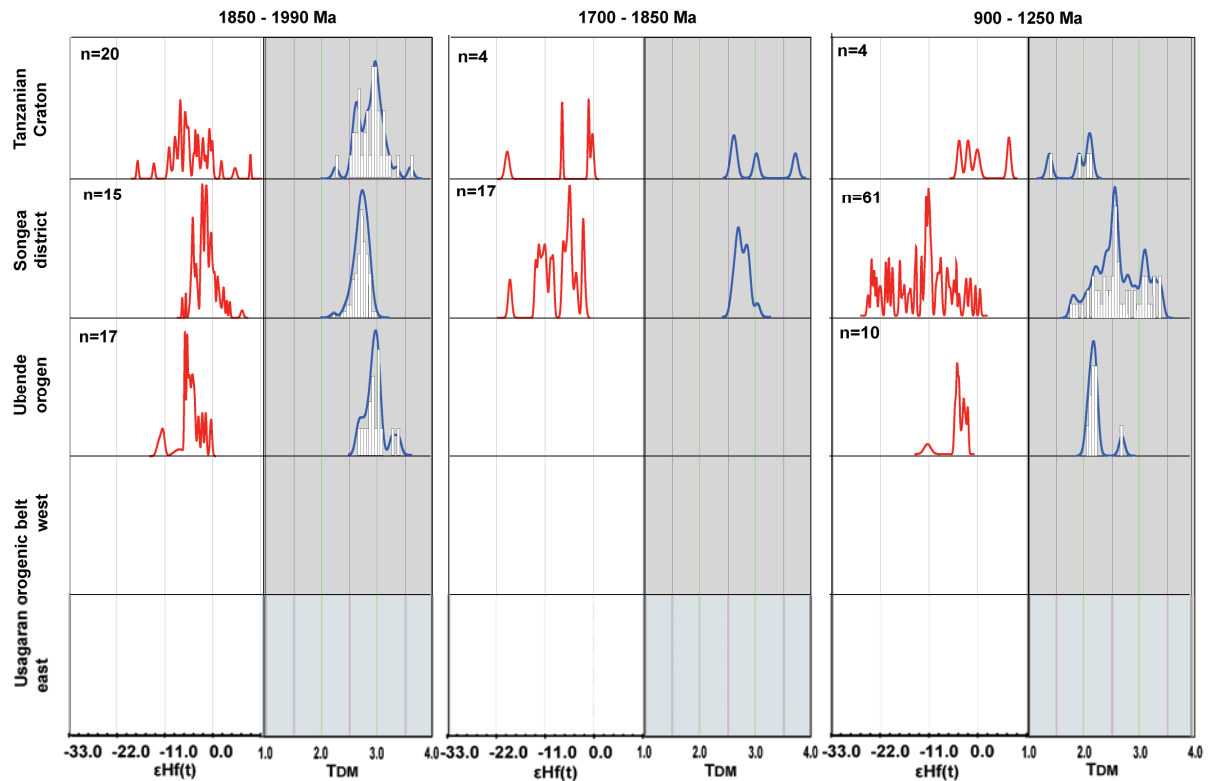


Figure 6.6 (continued)

( $^{176}\text{Hf}/^{177}\text{Hf} = 0.2814 - 0.2816$ ,  $\epsilon_{\text{Hf}} = -0.9 - -6.1$ ).

### 6.3.3 Songea District – stream sediment samples

Figure 6.4 shows probability density plots of U-Pb age data for samples from the Songea district, and figure 6.5 shows all Lu-Hf isotope analyses from this district plotted against U-Pb ages for each zircon. All data for these samples is presented in Appendix 3.

In sample Albsong-01 U-Pb analysis of 56 spots was carried out on 56 grains and Lu-Hf analysis performed on 46 grains with concordant U-Pb ages. U-Pb data yielded populations at  $1859 \pm 15$ ,  $1964 \pm 7$  and  $2021 \pm 16$  Ma with a minor population at  $1021 \pm 28$  Ma. The 2021 Ma population shows an injection of relatively juvenile crust ( $T_{\text{DM}} = 2.6$  Ga) while the 1964 and 1859 Ma populations have lower  $^{176}\text{Hf}/^{177}\text{Hf}$  indicating reworking of a mixture of juvenile crust and more evolved materials ( $T_{\text{DM}} = 3.0$  Ga). The Mesoproterozoic (Stenian) population has higher  $^{176}\text{Hf}/^{177}\text{Hf}$ , and indicates reworking of a  $T_{\text{DM}} = 2.6$  Ga source.

U-Pb analysis of 56 spots was carried out on 56 grains in Albsong-02 and Lu-Hf analysis performed on 55 grains with concordant U-Pb ages. The U-Pb age data yielded dominant Neo- to Mesoproterozoic populations  $983 \pm 5$  Ma and  $1022 \pm 8$  Ma and a minor Palaeoproterozoic population at  $\sim 1850$  Ma. The minor Palaeoproterozoic population had U-Pb ages between 1.8 – 1.9 Ga with Lu-Hf data indicating juvenile crust ( $T_{\text{DM}} = 2.6$  Ga). The Mesoproterozoic population had a wide range of  $^{176}\text{Hf}/^{177}\text{Hf}$  values with a mixture of juvenile ( $T_{\text{DM}} = 2.0$  Ga) and reworked ( $T_{\text{DM}} = 3.0$  Ga) crust.

In sample Albsong-03 U-Pb analysis of 60 spots was carried out on 60 grains and Lu-Hf analysis was

performed on 53 grains with concordant U-Pb ages. U-Pb ages data yielded a Mesoproterozoic population  $980 \pm 8$  Ma and two Palaeoproterozoic populations at  $1968 \pm 24$  Ma and  $1813 \pm 20$  Ma. The Palaeoproterozoic populations indicate a mixture of juvenile ( $T_{\text{DM}} \approx 2.6$  Ga) and reworked crust. The Mesoproterozoic population had a wide range of  $^{176}\text{Hf}/^{177}\text{Hf}$  values indicating a mixture of juvenile and reworked crust ( $T_{\text{DM}} \approx 2.6$  Ga to 3 Ga).

In the fourth sediment sample, Albsong-04, U-Pb analysis of 56 spots was carried out on 55 grains and Lu-Hf analysis was performed on 47 spots on 46 grains with concordant U-Pb ages. U-Pb age data yielded a predominant population at  $1969 \pm 9$  Ma and a minor  $732 \pm 5$  Ma population. The Lu-Hf data for the Palaeoproterozoic population indicates mainly reworked crust ( $T_{\text{DM}} \approx 2.6$  Ga). The Neoproterozoic population has a  $T_{\text{DM}} \approx 1.8$  Ga indicating a more evolved crustal source. Many of these grains are reported to look magmatic (Belousova and Griffin, 2006) and had high Th/U ratios.

## 6.4 Discussion

### 6.4.1 Crustal evolution studies of other East African orogenic Orogens

A crustal evolution study of the Mozambique Orogen by Möller *et al.* (1998b) using Rb-Sr and Sm-Nd found that the Tanzanian craton formed from material which separated from the mantle at  $\sim 3.1$  Ga, consistent with the Lu-Hf data from chapter 3 of this thesis. The Usagaran samples in Möller *et al.*'s (1998a) study include three metasediments from the Yalumba Hill district and two from the Mautia Hill region. Four of these samples record 2.7 – 3.1 Ga Nd  $T_{\text{DM}}$  model ages. Sr  $T_{\text{DM}}$  model ages in these samples are reset by subsequent high-grade metamorphic events during the Usagaran and East



African orogenies (Möller et al., 1998a). Metasediments from the adjacent Mozambique Orogen display a range of isotopic compositions with Nd  $T_{DM}$  model ages ranging from fairly uniform 1.1 Ga ages in the east to 1.2 - 2.4 Ga ages in the west of the orogen near the Usagaran Orogen. This indicates a mixture of evolved and juvenile material in the west as distinct from purely juvenile material in the east of the orogen. This trend is mirrored by the igneous rocks from these regions.

The Sm-Nd composition of mafic rocks and metasediments from the western Usagaran orogen has been investigated in two additional studies (Möller et al., 1995; Lau, 2009), both of which found that the rocks had consistently less evolved  $\epsilon Nd$  signatures than the Tanzanian Craton ( $\epsilon Nd = -14 - -15$ ), although Lau (2009a) determined more juvenile values ( $\epsilon Nd = 2.4 - -4.1$ ) than the values ( $\epsilon Nd = -7 - -14$ ) of Möller et al. (1995). These  $\epsilon Nd$  ages are uniformly higher than those of (Möller et al., 1998a) which range from -23 - -29 for the Usagaran samples and -26 - -36 for the Tanzanian Craton.

The only East African zircon U-Pb Lu-Hf study investigates igneous rocks in the Irumide Orogen, and shows a relative juvenile crust ( $T_{DM} \sim 2.0$  Ga) which was reworked to produce granites in three events aged 2047 - 1940 Ma, 1665 - 1545 Ma and ~1030 Ma, with only a minor evolved crustal contribution from an Archaean basement seen in a single Palaeoproterozoic granitic gneiss (DeWaele et al., 2009).

#### 6.4.2 Crustal evolution of Ubende and Usagaran Orogens

The combined U-Pb and Lu-Hf data from all samples is shown in Figure 6.6. The Ubendian samples indicate a major contribution of Archaean material (2.7 - 2.5 Ga) with Hf  $T_{DM}$  model ages between 3.2 - 3.0 Ga, which is consistent with material derived from the Tanzanian Craton. In the Palaeoproterozoic there is an input of new material between 2050 - 1950 Ma with an isotopic signature consistent with combined reworking of the older crustal material and input from a new, less evolved source ( $T_{DM} \sim 2.7$  Ga). There is a minor contribution of even younger material at ~1500 Ma  $T_{DM}$  model ages of 1.8 - 2.2 Ga. The population of ~1050 Ma zircon represents metamorphic rims to igneous zircon, and these retain the Lu/Hf isotopic signature of their original crystallization.

The Usagaran samples show a similar contribution of Archaean material which may also be derived from the Tanzanian craton. However, in addition there are a few older grains, mostly from the east of the Orogen, with similar Hf  $T_{DM}$  model ages of ~3.2 Ga. A subtle trend of slightly older model ages in the east of the orogen compared with the west is observed. Palaeoproterozoic material in the east of the Orogen is slightly older than that seen in the Ubende with crystallisation ages between 2200 - 2000 Ma, while in the west of the Orogen ages of 2050 - 2000 Ma are more comparable to the Ubende Orogen though they do not include the Ubende Orogen (figure 6.6). Variation between the eastern and western parts of the Usagaran Orogen may indicate ongoing accretion during the origin of an island arc system, with slightly younger metamorphism and a more complex zircon U-Pb age spectra on the hinterland, while the proximal (western) sediments preserve slightly older metamorphism and a more unimodal zircon source. This model is consistent with tectonic models based on structural mapping and traverses through the

orogen (Mruma, 1989b; Reddy et al., 2003) indicating that the orientation of subduction was under the Tanzanian Craton, and with a magnetotelluric traverse from the Tanzanian Craton into the western Usagaran Orogen which shows a high resistivity-boundary structure dipping westwards under the Tanzanian Craton (Selway et al., unpub).

The Ubende Orogen is bounded by the Kibaran Orogen in the north, the Bangweulu Block to the west and the Irumide Orogen to the south. There are some similarities between zircon crystallisation ages within the Ubende and Irumide Orogens. As with the Ubende Orogen, the Irumide Orogen comprises a Palaeoproterozoic basement ( $2049 \pm 6$  to  $1927 \pm 10$  Ma) (DeWaele, 2005; DeWaele et al., 2006a; DeWaele et al., 2006b; Rainaud, 2003, 2002; Rainaud et al., 1999) and minor Archaean granite gneiss ( $2726 \pm 36$  Ma) (DeWaele, 2005; DeWaele et al., 2006a; DeWaele et al., 2006b), overlain by a Palaeoproterozoic sedimentary package (DeWaele, 2005; DeWaele and Fitzsimons, 2007; DeWaele and Fitzsimons, 2004; Rainaud, 2003) intruded by granitoids aged between  $1664 \pm 4$  and  $1532 \pm 32$  (DeWaele, 2005; DeWaele et al., 2006b) and metamorphosed between 1080 - 1020 Ma (DeWaele et al., 2009). Figure 6.7, however, shows that the Lu-Hf composition of igneous rocks from the Irumide Orogen indicates a much more juvenile source ( $T_{DM}$  model ages between 2.2 - 1.7 Ga) than the source of metasediments from the northern Ubende Orogen.

#### 6.4.3 Do the Usagaran and Ubende Orogens form one contiguous orogenic belt?

Most models of the tectonic evolution of the eastern-Congo craton include the Usagaran-Ubendian system as a single Palaeoproterozoic orogenic Orogen which is wrapped around the southern end of the Tanzanian craton between ~2.0 - 1.85 Ga (Boven et al., 1999; DeWaele et al., 2008; Lenoir et al., 1994a). Work in this study has identified a new metamorphic age within the Ubende Orogen of ~1050 Ma, significantly later than the accepted ~1850 Ma metamorphic age, which raises the possibility that the Ubende Orogen may be younger than previously considered.

Significant granitic rocks have been dated from within the Ubende Orogen with Palaeoproterozoic ages between 2085 - 1840 Ma, and a few granites with Neoproterozoic ages between 850 - 720 Ma (Lenoir et al., 1994a). The Palaeoproterozoic granite intrusions are likely to be related to active subduction under the craton during the Usagaran orogeny. The question is whether the main deformation and metamorphism in this terrane occurred at this time. The ~1.5 Ga zircons in Ubendian metapelitic rocks are consistent with the Hf isotopic signature of the ~1.5 Ga granites and gneisses in the Irumide Orogen which yield  $\epsilon_{Hf}(t)$  values between 0.0 and 5.7 (DeWaele et al., 2009). The presence of 1.5 Ga material in these sediments supports the argument that the main orogenesis in the Ubende Orogen post-dated the Usagaran orogeny.

The Songea district samples come from a region where the Usagaran and Ubendian Orogens intersect. The exact distribution of Usagaran vs Ubendian structures in this Orogen is unclear and has not been addressed in the literature. Although samples from the Ubende and Usagaran Orogens in this study are Palaeoproterozoic metasedimentary rocks while samples from Songea are modern stream sediments, some comparison can be made so long as the assumption that modern streams sediments are locally derived is accepted. To test this hypothesis the crustal residence times for samples from the Songean samples are compared to those from the

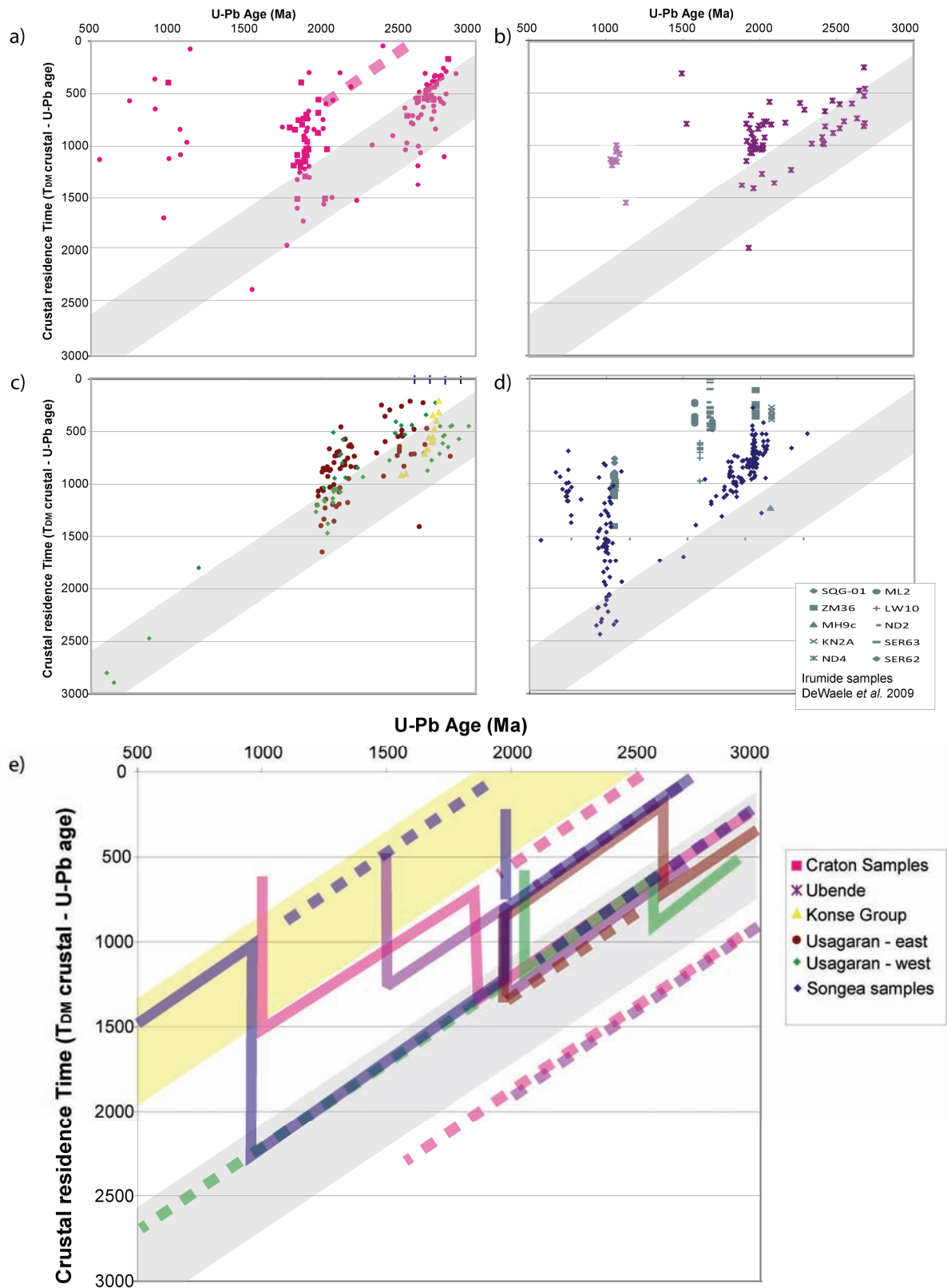


Figure 6.7 Crustal residence plots for all terranes. Crustal residence is calculated as  $T_{DM}$  crustal - U-Pb zircon age.

nearby Irumide Orogen to see if there are indications of an Irumide contribution to the stream sediments. Although some overlap occurs in the crustal residence times and  $\epsilon_{HF}(t)$  values of the ~1.0 Ga grains in the Irumide igneous rocks and the Songea stream sediments there is little indication of the dominant 1.6 Ga granites seen in the Irumide Orogen, suggesting that they are at least partially derived from the local rocks. Since this

discussion focuses on whether the Songea district is the link between the east and west parts of an extensive Palaeoproterozoic orogenic Orogen, and since there is a clear difference between the Palaeoproterozoic signatures of the Irumide samples and those analysed in this study, it is reasonable to assume that the Palaeoproterozoic grains are locally derived, especially when that isotopic signature overlaps the signature of

similar aged grains from the Ubende and Usagaran Orogens. The samples from the Songea district are more similar to the Ubende than the Usagaran samples in terms of crystallization ages, however there is a notable absence of any Archaean material in the Songea district samples. This absence is enigmatic since an Archaean cratonic block is located within 40km of some sample sites. Although there is some overlap in the more evolved Palaeoproterozoic grains from the Songea region when compared to the Ubende and Usagaran Orogens there is also a significant more juvenile source ( $T_{DM} \sim 2.2 - 2.4$  Ga) which has contributed to these samples. This, in combination with the absence of any Archaean signature, indicates that the evolution of this domain different from the evolution of the Usagaran and Ubende Orogens, and supports the notion, proposed in chapter 3 based on U-Pb geochronology and  $^{40}\text{Ar}$ - $^{39}\text{Ar}$  thermochronology, that

the Songea district is not the link between a single continuous Usagaran-Ubendian system.

## 6.5 Conclusions

The Ubende and Usagaran Orogens have similar but not identical crustal evolution histories through the Archaean and Palaeoproterozoic, but the Mesoproterozoic evolution of the Ubende diverges from the Usagaran. The Songea district, situated at the junction of these orogenic Orogens, has a separate crustal evolution and does not form the link between the two orogens. Thus the Orogens, sometimes referred to as a continuous orogenic system, are in fact distinguishable by their crustal evolution and the timing of sedimentation and metamorphism.

**Table 6.1** MC-LA-ICPMS Lu-Hf data for all Usagaran and Ubende belt samples. U-Th-Pb and age data given in chapters 3 and 4.

	$\frac{^{176}\text{Yb}}{^{177}\text{Hf}}$	$\pm 1\sigma$	$\frac{^{176}\text{Lu}}{^{177}\text{Hf}}$	$\pm 1\sigma$	$\frac{^{178}\text{Hf}}{^{177}\text{Hf}}$	$\frac{^{180}\text{Hf}}{^{177}\text{Hf}}$	VHf	$\frac{^{176}\text{Hf}}{^{177}\text{Hf}}$	$\pm 1\sigma$	$\frac{^{176}\text{Hf}}{^{177}\text{Hf}}$	$\epsilon\text{Hf}^1$	$\pm 1\sigma$	$T_{\text{DM}}$ (Ga) <sup>1</sup>	$T_{\text{DM}}$ (Crustal) <sup>1</sup>
T01-37-01	0.0186031	0.00027	0.0005083	0.0000047	1.46716	1.88663	3.07	0.281119	11	0.281092126	2.7	385000	2.93	3.06
T01-37-02	0.0217536	0.0001E	0.000646	0.0000078	1.46707	1.88649	4.69	0.281055	6.9	0.281021663	-1.3	241500	3.03	3.26
T01-37-03	0.038479	0.0012	0.0010918	0.000037	1.46697	1.88662	2.15	0.280977	19	0.280924647	-9.1	665000	3.17	3.61
T01-37-04	0.0218117	0.00037	0.0007973	0.000015	1.46705	1.88676	1.89	0.281025	14	0.280984573	-3.7	490000	3.08	3.38
T01-37-05	0.0177914	0.0002E	0.0006096	0.0000064	1.46706	1.88669	1.58	0.281169	18	0.281137729	2.4	630000	2.87	
T01-37-06	0.0140346	0.0003E	0.0004286	0.0000064	1.46711	1.88685	3.93	0.281019	8.3	0.280996807	-2.0	290500	3.06	3.31
T01-37-07	0.027728	0.0005E	0.0007817	0.000021	1.46707	1.88669	3.88	0.280717	8.9	0.280675614	-12.1	311500	3.49	3.99
T01-37-08	0.0395617	0.00017	0.0010699	0.000016	1.46708	1.88661	3.17	0.28101	12	0.280955036	-4.0	420000	3.12	3.42
T01-37-09	0.0247774	0.0014	0.0006436	0.00003	1.46707	1.88657	3.63	0.281114	8.5	0.281080391	1.5	297500	2.95	3.11
T01-37-10	0.0488157	0.0021	0.0012909	0.000047	1.46706	1.88651	4.57	0.280987	16	0.280925743	-9.6	560000	3.17	3.63
T01-37-11	0.0218751	0.0001E	0.0006025	0.0000047	1.46712	1.88667	4.09	0.281033	9.8	0.281001702	-1.6	343000	3.06	3.30
T01-37-12	0.0241775	0.0006E	0.0007752	0.000048	1.46725	1.88681	2.40	0.281081	17	0.281039993	0.9	595000	3.00	3.17
T01-37-13	0.0166274	0.0003E	0.0003523	0.0000039	1.46709	1.88663	2.02	0.281224	17	0.281206577	2.7	595000	2.78	2.92
T01-37-14	0.0183267	0.0002E	0.0004487	0.0000078	1.46717	1.88671	1.94	0.281027	20	0.2810034	-0.8	700000	3.05	3.27
T06-27-03	0.00107501	0.0001E	2.40474E-05	0.000003	1.46706	1.88657	4.35	0.281285	11	0.281284	-8.7	385000	2.68	3.17
T06-27-05	0.000664338	0.0000E	2.20708E-05	0.000002	1.46715	1.88714	1.68	0.281239	37	0.281238	-8.0	1295000	2.74	3.21
T06-27-05	0.000492379	0.0000E	1.49538E-05	0.000001	1.46715	1.88679	3.23	0.281222	17	0.281221	-8.6	595000	2.76	3.24
T06-27-06	0.00136801	0.0001E	4.66663E-05	0.000007	1.46707	1.88667	3.01	0.281264	9.2	0.281262	-9.7	322000	2.71	3.23
T06-27-07	0.00078868	0.00004	2.54769E-05	0.000001	1.46709	1.88669	1.25	0.281259	18	0.281258	-6.8	630000	2.71	3.15
T06-27-08	0.00155846	0.0000E	5.10575E-05	0.000001	1.4671	1.88651	0.77	0.281317	37	0.281315	-5.1	1295000	2.64	3.03
T06-27-09	0.000896993	0.0000E	2.31847E-05	0.000001	1.46707	1.88674	3.69	0.28128	11	0.281279	-6.6	385000	2.68	3.12
T06-27-10	0.00144499	0.0000E	4.82528E-05	0.000003	1.46713	1.88659	3.76	0.281268	10	0.281266	-7.2	350000	2.70	3.15
T06-27-16	0.0104255	0.00094	0.000470519	0.000051	1.46717	1.8862	1.20	0.281248	45	0.281229	-7.2	1575000	2.76	3.19
T06-27-17	0.00304206	0.0003E	0.00017399	0.000021	1.46709	1.88677	2.55	0.281255	16	0.281248	-4.0	560000	2.73	3.08
T06-27-21	0.000670791	0.00001	1.98387E-05	0.000002	1.46709	1.88667	3.77	0.281265	16	0.281264	-8.3	560000	2.70	3.18
T06-27-24	0.000403692	0.0000E	1.87015E-05	0.000001	1.46707	1.8874	0.81	0.281266	46	0.281265	-5.2	1610000	2.70	3.09
T06-27-28	0.000848514	0.0000E	2.67641E-05	0.000002	1.46706	1.88634	2.36	0.281326	24	0.281325	-6.3	840000	2.62	3.05
T06-27-28	0.000743383	0.00001	2.04477E-05	0	1.46706	1.88651	4.77	0.281273	12	0.281272	-8.1	420000	2.69	3.17
T06-27-32	0.0261334	0.0005E	0.00118193	0.000021	1.46707	1.88689	0.99	0.281049	30	0.280989	-3.4	1050000	3.08	3.36
T06-37-01	0.0649842	0.0009E	0.00165101	0.000042	1.46708	1.88658	3.10	0.280995	7.9	0.280908	-3.9	276500	3.19	3.47
T06-37-03	0.0531657	0.0016	0.00134794	0.000041	1.46705	1.88662	2.45	0.281033	12	0.280961	-1.2	420000	3.12	3.33
T06-37-05	0.0769213	0.0079	0.00181251	0.00018	1.4671	1.88649	5.46	0.280989	9.3	0.280896	-6.1	325500	3.22	3.56
T06-37-08	0.0503373	0.0012	0.00136014	0.000041	1.46709	1.88659	3.05	0.281008	12	0.280936	-2.4	420000	3.15	3.40
T06-37-09	0.0518676	0.0028	0.00126697	0.000073	1.46709	1.88659	2.80	0.281031	14	0.280963	-1.3	490000	3.11	3.33
T06-37-10	0.0161461	0.0003E	0.000446316	0.000013	1.4671	1.88657	3.62	0.281045	6.9	0.281021	0.2	241500	3.03	3.21
T06-37-104	0.0465697	0.001	0.0011106	0.000026	1.46706	1.88665	3.46	0.281025	9.4	0.280964	0.1	329000	3.11	3.29
T06-37-12	0.0777938	0.0022	0.00190892	0.000056	1.46711	1.88655	3.52	0.281018	10	0.280919	-4.6	350000	3.18	3.49
T06-37-14	0.0465689	0.0018	0.00153347	0.000066	1.46705	1.88656	4.87	0.280977	8.5	0.280894	-3.0	297500	3.21	3.47
T06-37-15	0.0240913	0.0025	0.000730386	0.000069	1.46706	1.88656	4.19	0.280922	6.1	0.280881	-0.4	213500	3.22	3.40
T06-37-26	0.0108652	0.0009E	0.000311853	0.000027	1.46711	1.88669	3.68	0.280986	9.9	0.280969	0.0	346500	3.10	3.28



	$\frac{^{176}\text{Yb}}{^{177}\text{Hf}}$	$\pm 1\sigma$	$\frac{^{176}\text{Lu}}{^{177}\text{Hf}}$	$\pm 1\sigma$	$\frac{^{178}\text{Hf}}{^{177}\text{Hf}}$	$\frac{^{180}\text{Hf}}{^{177}\text{Hf}}$	VHf	$\frac{^{176}\text{Hf}}{^{177}\text{Hf}}$	$\pm 1\sigma$	$\frac{^{176}\text{Hf}}{^{177}\text{Hf}_1}$	$\epsilon\text{Hf}_1$	$\pm 1\sigma$	$T_{\text{DM}}$ (Ga) <sup>1</sup>	$T_{\text{DM}}$ (Crustal) <sup>1</sup>
T07-35_001	0.0355386	0.0013	0.00101041	0.000035	1.46708	1.88657	4.10	0.281194	14	0.281155	-11.8	490000	2.87	3.41
T07-35_002	0.0630454	0.0038	0.00191932	0.00009	1.46704	1.88671	3.43	0.281302	30	0.281211	0.3	1050000	2.79	2.99
T07-35_003	0.0544863	0.0026	0.00184482	0.00011	1.46708	1.88667	3.88	0.281302	17	0.281213	1.3	595000	2.78	2.96
T07-35_004	0.0295045	0.0026	0.00085089	0.000066	1.46716	1.88696	2.61	0.281548	12	0.281514	1.8	420000	2.38	2.58
T07-35_005	0.0459056	0.0004	0.00122931	0.000034	1.46708	1.88661	3.57	0.281392	14	0.281342	-3.0	490000	2.62	2.93
T07-35_006	0.0376942	0.0016	0.00124052	0.000073	1.46711	1.88646	2.66	0.281183	15	0.281125	-3.7	525000	2.90	3.21
T07-35_007	0.0539893	0.0046	0.00142696	0.000098	1.46705	1.88664	4.06	0.280953	15	0.280874	-2.1	525000	3.23	3.46
T07-35_008	0.0753777	0.001	0.00230934	0.000055	1.46712	1.88669	4.09	0.281277	15	0.281163	1.1	525000	2.85	3.02
T07-35_009	0.0436859	0.0014	0.0012256	0.000034	1.46706	1.88648	4.79	0.281216	14	0.281157	-0.2	490000	2.86	3.07
T07-35_010	0.0747594	0.0059	0.00203065	0.00012	1.4671	1.88685	2.18	0.281512	51	0.281487	-31.2	1785000	2.50	3.54
T07-35_011	0.0281615	0.0009	0.000960735	0.000042	1.46706	1.88677	3.97	0.281423	13	0.281384	-1.5	455000	2.55	2.84
T07-35_012c	0.0825192	0.001	0.00310578	0.00011	1.46711	1.88673	4.03	0.281237	29	0.281117	-13.2	1015000	2.97	3.50
T07-35_012r	0.0500379	0.0005	0.00183942	0.000025	1.46714	1.88684	2.07	0.281543	27	0.281513	-25.2	945000	2.45	3.35
T07-35_013	0.0493408	0.0019	0.00139462	0.000044	1.46713	1.88664	3.46	0.281319	13	0.281264	-6.7	455000	2.73	3.14
T07-35_020	0.0425109	0.0013	0.00124818	0.000035	1.46706	1.8867	3.44	0.281237	15	0.281183	-5.5	525000	2.83	3.20
T07-35_022	0.0269174	0.0007	0.000779831	0.000005	1.46708	1.88676	4.48	0.281419	15	0.281388	-1.7	525000	2.55	2.84
T07-35_023c	0.0313992	0.0003	0.000878002	0.000018	1.4671	1.88662	3.57	0.281182	11	0.281137	2.3	385000	2.88	3.02
T07-35_023r	0.0364145	0.0007	0.000998335	0.000017	1.46709	1.88652	2.28	0.281479	23	0.281438	0.6	805000	2.48	2.71
T07-35_024c	0.0288443	0.0008	0.000762035	0.000019	1.46707	1.88651	4.58	0.281292	17	0.281256	2.0	595000	2.72	2.88
T07-35_024r	0.0290244	0.0009	0.000962528	0.000025	1.46712	1.88664	1.98	0.281573	24	0.281562	-29.5	840000	2.35	3.40
T07-35_025c	0.0245416	0.0007	0.000786089	0.000018	1.46703	1.88663	2.68	0.281183	21	0.281142	3.8	735000	2.87	2.96
T07-35_025r	0.0491893	0.0012	0.00155126	0.000032	1.46701	1.88681	2.33	0.281617	17	0.281582	-15.6	595000	2.33	3.00
T07-59-46c	0.0483214	0.0016	0.0014217	0.000058	1.46708	1.8866	4.57	0.281183	13	0.281114	-1.8	455000	2.92	3.17
T07-59-41r	0.060157	0.0009	0.0019153	0.000022	1.46714	1.88667	5.09	0.28139	7.2	0.281318	-7.4	252000	2.67	3.09
T07-59-16r	0.061998	0.0037	0.002327	0.00013	1.46714	1.88678	1.71	0.281268	27	0.281180	-11.9	945000	2.87	3.39
T07-59-23c	0.0588922	0.0008	0.0017328	0.000016	1.46711	1.88667	5.33	0.281398	14	0.281332	-6.3	490000	2.64	3.04
T07-59-44r	0.0912223	0.0014	0.0034086	0.00005	1.46707	1.88672	3.27	0.281191	16	0.281061	-15.9	560000	3.07	3.65
T07-59-29r	0.0478674	0.0017	0.0014387	0.000036	1.4671	1.88664	6.49	0.281372	7.4	0.281317	-6.7	259000	2.66	3.07
T07-59-45r	0.062469	0.0012	0.0023336	0.000038	1.46714	1.88671	2.52	0.281282	15	0.281193	-11.0	525000	2.85	3.35
T07-59-19r	0.0568435	0.0005	0.0019252	0.000042	1.46706	1.88659	5.60	0.281343	18	0.281269	-8.0	630000	2.73	3.17
T07-59-18r	0.0424999	0.0008	0.0015214	0.000029	1.46709	1.88675	4.04	0.281324	15	0.281265	-7.9	525000	2.73	3.17
T07-59-41c	0.048575	0.0036	0.0014016	0.00011	1.46708	1.88666	3.56	0.281453	14	0.281399	-3.2	490000	2.54	2.87
T07-59-33c	0.0356316	0.0022	0.0011003	0.000075	1.46709	1.88655	4.84	0.281398	7.4	0.281355	-4.6	259000	2.60	2.96
T07-59-35c	0.0383927	0.0006	0.0012184	0.000049	1.46706	1.88662	5.28	0.281418	9.7	0.281370	-3.8	339500	2.58	2.92
T07-59-19c	0.0281395	0.0007	0.0009033	0.000042	1.46708	1.88684	3.77	0.281335	8.7	0.281300	-6.3	304500	2.67	3.08
T07-59-48c	0.0668735	0.0011	0.0019548	0.00001	1.46713	1.88666	4.55	0.281448	9	0.281372	-3.6	315000	2.59	2.92
T07-59-02	0.0475302	0.0028	0.0016682	0.00013	1.46708	1.88662	4.34	0.281357	12	0.281291	-6.0	420000	2.69	3.08
T07-59-34r	0.0696311	0.0015	0.0026152	0.000057	1.4671	1.88667	3.30	0.281261	20	0.281162	-12.6	700000	2.90	3.43
T07-59-45r	0.0669954	0.0016	0.0018802	0.000027	1.46707	1.88653	3.81	0.281482	12	0.281407	-1.7	420000	2.53	2.82
T07-59-17	0.0533299	0.0015	0.001685	0.0001	1.46712	1.88657	4.67	0.281317	12	0.281249	-6.6	420000	2.75	3.15
T07-59-38c	0.0229969	0.0007	0.0007089	0.000022	1.46709	1.88662	3.63	0.281529	7.7	0.281500	2.5	269500	2.39	2.58
T07-59-31c	0.0372997	0.0024	0.0011479	0.000069	1.46706	1.88665	4.82	0.281377	7.9	0.281330	-3.3	276500	2.63	2.96
T07-59-24	0.0484051	0.0011	0.0012238	0.00005	1.46707	1.8867	6.01	0.281387	9.4	0.281337	-2.8	329000	2.62	2.93
T07-59-28	0.0327672	0.0015	0.0011252	0.000047	1.46709	1.88662	6.12	0.281367	8	0.281321	-3.3	280000	2.64	2.97
T07-59-29c	0.047274	0.0014	0.0014219	0.000038	1.46708	1.88652	4.32	0.281486	14	0.281428	0.5	490000	2.50	2.72
T07-59-14c	0.0762415	0.0029	0.0028989	0.00011	1.46715	1.88712	1.63	0.281268	39	0.281148	-9.0	1365000	2.91	3.34
T07-59-23r	0.0391895	0.0002	0.0012548	0.000014	1.467	1.88623	6.22	0.281438	15	0.281386	-0.8	525000	2.55	2.81
T07-59-20c	0.0567375	0.0015	0.0016936	0.000048	1.46711	1.88666	6.74	0.28145	13	0.281380	-0.4	455000	2.57	2.81
T07-59-47c	0.0316144	0.0007	0.0008519	0.000011	1.46709	1.88656	4.86	0.281321	6.9	0.281286	-3.7	241500	2.69	3.02
T07-59-10	0.0408027	0.0013	0.0013151	0.000068	1.46712	1.88666	4.66	0.28142	13	0.281365	-0.7	455000	2.58	2.84
T07-59-42c	0.0578268	0.0005	0.0016478	0.000031	1.46709	1.88655	4.74	0.281382	8.3	0.281313	-2.2	290500	2.66	2.94
T07-59-04c	0.0628598	0.0011	0.0020074	0.000049	1.4671	1.88656	5.39	0.281344	8.9	0.281259	-3.9	311500	2.74	3.06
T07-59-03c	0.029834	0.0011	0.0009588	0.000035	1.46706	1.88658	4.15	0.28113	16	0.281086	-5.9	560000	2.95	3.32
T07-59-46r	0.12346	0.0033	0.0039923	0.000084	1.46707	1.88667	4.22	0.281348	30	0.281199	-11.8	1050000	2.88	3.36
T07-59-05c	0.0111521	0.0006	0.0003297	0.000024	1.46706	1.88662	5.25	0.280741	12	0.280724	-13.4	420000	3.42	3.98
T07-59-05c	0.0098307	0.0001	0.0002731	0.0000025	1.46704	1.88671	3.95	0.280712	11	0.280698	-14.4	385000	3.46	4.04
T07-59-21c	0.0550038	0.0005	0.0015294	0.000026	1.46713	1.88664	6.03	0.28128	6.4	0.281202	4.1	224000	2.79	2.88
T07-59-06c	0.0277115	0.0006	0.0009157	0.000027	1.46721	1.88681	3.92	0.280894	13	0.280844	-4.5	455000	3.27	3.57

	$^{176}\text{Yb}/$ $^{177}\text{Hf}$	$\pm 1\sigma$	$^{176}\text{Lu}/$ $^{177}\text{Hf}$	$\pm 1\sigma$	$^{178}\text{Hf}/$ $^{177}\text{Hf}$	$^{180}\text{Hf}/$ $^{177}\text{Hf}$	VHf	$^{176}\text{Hf}/$ $^{177}\text{Hf}$	$\pm 1\sigma$	$^{176}\text{Hf}/$ $^{177}\text{Hf}_1$	$\epsilon\text{Hf}_1^1$	$\pm 1\sigma$	$T_{\text{DM}}$ (Ga) <sup>1</sup>	$T_{\text{DM}}$ (Crustal) <sup>1</sup>
T07-71-22	0.0356924	0.0013	0.000752433	0.000027	1.46706	1.88651	2.52	0.281217	9.7	0.281187	-9.4	339500	2.82	3.31
T07-71-24	0.0291049	0.00051	0.000617169	0.000018	1.46712	1.88667	2.42	0.281175	9.2	0.281145	0.1	322000	2.87	3.08
T07-71-26c	0.0822497	0.00082	0.00175725	0.000015	1.46704	1.88645	3.38	0.281483	12	0.281413	-1.2	420000	2.53	2.79
T07-71-27	0.0400943	0.0018	0.000866264	0.000035	1.46708	1.88663	3.09	0.281204	11	0.281162	-0.4	385000	2.85	3.07
T07-71-30c	0.0469207	0.0038	0.000934631	0.000057	1.46706	1.88644	3.10	0.281168	11	0.281123	-2.2	385000	2.90	3.17
T07-71-31	0.0451752	0.0021	0.00119552	0.000052	1.46712	1.88659	3.39	0.281279	14	0.281224	-0.8	490000	2.77	3.01
T07-71-33c	0.0461325	0.00086	0.00100261	0.000011	1.46711	1.8865	2.56	0.28086	12	0.280802	-1.2	420000	3.32	3.52
T07-71-33r	0.0638778	0.00065	0.0021863	0.000025	1.46712	1.88649	4.00	0.281476	13	0.281392	-3.6	455000	2.56	2.89
T07-71-38	0.040259	0.00072	0.000819553	0.000021	1.46705	1.88667	2.49	0.281173	11	0.281134	-1.8	385000	2.88	3.14
T07-71-40c	0.0297172	0.001	0.000665765	0.000023	1.46713	1.88662	3.24	0.281063	15	0.281030	-3.3	525000	3.02	3.31
T07-71-40r	0.0599298	0.0031	0.00197334	0.00011	1.46714	1.88695	2.88	0.281462	28	0.281384	-2.7	980000	2.57	2.87
T07-71-41	0.0303573	0.00034	0.000710157	0.000007	1.4671	1.88667	3.42	0.281206	11	0.281172	-0.1	385000	2.83	3.05
T07-71-41r	0.296961	0.0002	0.0000069	0.000007	1.46709	1.88672	4.60	0.281191	8.9	0.281191	0.5	0.3115	2.80	3.01
T07-71-42c	0.0491775	0.0018	0.00114901	0.000036	1.46707	1.8865	3.82	0.281388	13	0.281335	3.8	455000	2.62	2.73
T07-71-42r	0.0676883	0.00092	0.00182243	0.000022	1.46703	1.88652	5.08	0.281535	17	0.281464	-0.5	595000	2.47	2.71
T07-71-43r	0.0680445	0.0018	0.00234409	0.000067	1.46711	1.88667	3.27	0.281325	25	0.281235	-9.3	875000	2.79	3.25
T07-71-50	0.0231695	0.0014	0.000607807	0.000043	1.46709	1.88667	3.79	0.281075	12	0.281045	-3.3	420000	3.00	3.29
T07-71-59r	0.0283216	0.00057	0.00089813	0.00002	1.46715	1.88655	0.96	0.281436	24	0.281402	-3.8	840000	2.53	2.89
T07-71-60	0.0391197	0.0021	0.00131846	0.0001	1.46708	1.88669	0.78	0.281389	30	0.281340	-6.6	1050000	2.63	3.04
T07-71-69	0.0483461	0.0028	0.00130612	0.000081	1.46712	1.88676	3.83	0.281264	8.4	0.281213	-9.0	294000	80	3.26
T07-71-70	0.0389228	0.0013	0.00115096	0.000067	1.46699	1.88654	3.05	0.28123	13	0.281184	-9.1	455000	2.83	3.30
T07-71-70	0.0372444	0.0015	0.000867233	0.000016	1.46706	1.88664	3.95	0.28127	13	0.281235	-7.2	455000	2.76	3.19
T07-71-71	0.015054	0.00026	0.000381532	0.000009	1.46712	1.88673	3.53	0.281421	11	0.281406	-1.2	385000	2.522	2.80
T07-71-76	0.0177189	0.00034	0.000427456	0.000011	1.4671	1.88659	3.54	0.281203	7.7	0.281183	-0.3	269500	2.82	3.04
T07-71-78	0.322393	0.00035	0.000044	0.000044	1.46708	1.88664	5.13	0.281294	17	0.281292	4.1	0.595	2.67	2.78
T07-71-80	0.31431	0.0013	0.000025	0.000025	1.46706	1.88653	3.36	0.281246	11	0.281245	-5.4	0.385	2.73	3.12
T07-71-87	0.0200034	0.00085	0.000503694	0.000025	1.4671	1.88659	2.57	0.281102	14	0.281076	0.2	490000	2.96	3.15
T07-71-88	0.0438032	0.00072	0.000959014	0.000009	1.46714	1.88653	3.00	0.281367	9.2	0.281328	-3.8	322000	2.63	2.97
T07-71-89	0.0161021	0.00036	0.000395423	0.000009	1.46711	1.88661	2.87	0.281038	10	0.281018	-2.1	350000	3.03	3.29
T07-71-91r	0.336027	0.0023	0.000043	0.00012	1.46427	1.88879	3.33	0.281413	12	0.281411	-3.3	0.42	2.51	2.86
T07-71-92	0.326132	0.0016	0.000068	0.000068	1.46707	1.88664	3.19	0.281398	17	0.281395	4.8	0.595	2.53	2.63
T07-71-93	0.332915	0.001	0.000026	0.000026	1.46701	1.88649	2.74	0.281219	11	0.281218	-2.3	0.385	2.76	3.06
T07-71-94	0.340829	0.00095	0.000017	0.000017	1.46706	1.88664	3.10	0.281272	11	0.281271	4.7	0.385	2.69	2.78
T07-71-96	0.320775	0.0013	0.000034	0.000034	1.46714	1.88675	3.22	0.281115	7.6	0.281113	-2.6	0.266	2.90	3.19
T07-71-97	0.348387	0.0024	0.000042	0.000042	1.46704	1.88662	3.79	0.281108	11	0.281106	-3.1	0.385	2.91	3.22
T07-71-98	0.347434	0.0037	0.000065	0.000065	1.46702	1.88665	3.20	0.2814	13	0.281397	-1.7	0.455	2.52	2.83
T07-71-99	0.343996	0.0013	0.000041	0.000041	1.46708	1.88671	3.72	0.281333	10	0.281331	3.0	0.35	2.61	2.76

	$^{176}\text{Yb}/$ $^{177}\text{Yb}$	$\pm 1\sigma$	$^{176}\text{Lu}/$ $^{177}\text{Hf}$	$\pm 1\sigma$	$^{178}\text{Hf}/$ $^{177}\text{Hf}$	$^{180}\text{Hf}/$ $^{177}\text{Hf}$	VHf	$^{176}\text{Hf}/$ $^{177}\text{Hf}$	$\pm 1\sigma$	$^{176}\text{Hf}/$ $^{177}\text{Hf}_1$	$\epsilon\text{Hf}_1$	$\pm 1\sigma$	$T_{\text{DM}}$ (Ga) <sup>1</sup>	$T_{\text{DM}}$ (Crustal) <sup>1</sup>
<b>Sample T04-07</b>														
-31	0.014153	3	0.000387	7	1.46716	1.88663	3.85	0.281434	9	0.281419	-2.2	318500	2.50	2.82
-30	0.032297	7	0.000925	17	1.46705	1.88661	4.12	0.281157	11	0.281120	-11.7	385000	2.91	3.45
-29	0.040427	11	0.001166	19	1.46713	1.88659	3.29	0.281052	11	0.280993	-3.9	385000	3.08	3.37
-28	0.011685	1	0.000322	2	1.46708	1.88675	3.95	0.281368	8	0.281356	-6.6	266000	2.59	3.02
-25	0.040626	13	0.001287	60	1.46716	1.88670	2.71	0.281174	16	0.281114	-4.3	560000	2.92	3.24
-22	0.037641	23	0.000950	60	1.46710	1.88668	4.88	0.281327	21	0.281286	-1.3	735000	2.68	2.95
-21	0.055301	17	0.001979	110	1.46726	1.88829	3.09	0.281788	43	0.281746	-11.3	1505000	2.11	2.68
-20	0.019213	12	0.000485	33	1.46706	1.88662	5.27	0.281059	17	0.281036	-4.9	595000	3.01	3.36
-18	0.064149	8	0.002222	32	1.46697	1.88606	1.19	0.281244	46	0.281137	-1.3	1610000	2.89	3.13
-17	0.044323	4	0.001413	46	1.46704	1.88689	3.37	0.281318	22	0.281267	-11.3	770000	2.73	3.26
-16	0.046607	24	0.001468	140	1.46701	1.88694	3.15	0.281173	26	0.281099	0.2	910000	2.93	3.12
-15	0.085395	62	0.002058	62	1.46703	1.88677	2.82	0.281273	30	0.281196	-12.1	1050000	2.84	3.37
-12	0.031953	3	0.000676	11	1.46707	1.88652	3.08	0.281457	13	0.281431	-2.2	455000	2.49	2.80
-10	0.031398	9	0.000954	31	1.46705	1.88667	2.65	0.281467	18	0.281432	-4.7	630000	2.49	2.87
-09	0.070023	30	0.001440	60	1.46704	1.88662	4.17	0.281441	22	0.281387	-5.2	770000	2.56	2.94
-08	0.044803	12	0.001738	73	1.46702	1.88683	1.90	0.281845	36	0.281795	-0.7	1260000	2.02	2.32
-07	0.053194	8	0.001080	25	1.46706	1.88655	3.70	0.281433	17	0.281393	-5.5	595000	2.55	2.95
-05	0.052316	16	0.001700	30	1.46736	1.88762	1.05	0.281411	69	0.281349	-7.7	2415000	2.62	3.06
<b>Sample T04-12b</b>														
-01	0.019785	24	0.0005232	2.4	1.46711	1.8868	2.53	0.2819760	17	0.281965	-4.8	595000	1.77	2.23
-02	0.009817	8.6	0.0003311	3.7	1.46713	1.88671	2.96	0.2819810	12	0.281975	-5.2	420000	1.76	2.23
-03	0.006624	6.6	0.0001925	2.3	1.46711	1.88671	3.72	0.2819910	10	0.281987	-4.7	339500	1.74	2.20
-04	0.047146	10	0.0010578	2.4	1.46707	1.88669	2.45	0.2811320	10	0.281078	0.4	350000	2.96	3.14
-05	0.041835	11	0.000841	2.6	1.4671	1.8866	3.33	0.2812270	11	0.281187	-0.6	385000	2.81	3.05
-07	0.047257	14	0.000862	5.1	1.46753	1.88764	0.10	0.2802880	750	0.280213	12.1	2625000	4.07	3.76
-08	0.004689	5.6	0.0001456	2.2	1.46712	1.88666	3.43	0.2820100	10	0.282007	-4.3	332500	1.71	2.16
-11	0.007894	11	0.0002251	3.8	1.46703	1.8866	3.51	0.2820180	11	0.282013	-3.3	385000	1.70	2.12
-12	0.011183	11	0.0003455	4.2	1.46705	1.88706	2.90	0.2819870	18	0.281980	-4.5	630000	1.75	2.20
-13	0.024554	2.6	0.000518	0.65	1.46715	1.88669	2.69	0.2814930	11	0.281474	-2.8	385000	2.43	2.77
-18	0.024178	8.9	0.0005624	2.8	1.46709	1.88678	1.56	0.2814090	12	0.281388	-5.0	420000	2.55	2.94
-19	0.062999	22	0.0021042	7.1	1.46708	1.88667	1.51	0.2813000	21	0.281219	-10.0	735000	2.81	3.29
-20	0.009639	2	0.0003314	2.5	1.46721	1.88671	2.42	0.2820440	10	0.282037	-2.3	339500	1.67	2.07
-21	0.010577	2.8	0.0002565	0.65	1.4671	1.88668	2.30	0.2820260	13	0.282021	-2.8	455000	1.69	2.10
-30	0.008989	3.2	0.0003498	1	1.46707	1.88721	0.71	0.2820030	87	0.281987	24.5	3045000	1.73	1.31
-31	0.017747	8	0.0005514	4.2	1.46697	1.88659	1.88	0.2819980	19	0.281987	-3.7	665000	1.74	2.17
-35	0.009627	5.9	0.0002882	2.7	1.46723	1.88716	2.51	0.2820370	26	0.282029	6.9	910000	1.68	1.81
<b>Sample T04-39</b>														
-102	0.018223	4	0.00046555	9.6	1.46705	1.88665	4.19	0.281294	12	0.281277	-9.4	420000	2.70	3.20
-103	0.032573	24	0.00083994	53	1.46707	1.88662	4.18	0.281369	8.6	0.281337	-5.7	301000	2.62	3.02
-104	0.038347	13	0.000948977	58	1.4671	1.88661	4.34	0.281423	13	0.281388	-5.6	455000	2.55	2.95
-105	0.046567	8.9	0.00154929	79	1.46709	1.88675	3.48	0.281405	21	0.281348	-6.9	735000	2.62	3.04
-106	0.069797	13	0.0016227	45	1.46717	1.8866	2.89	0.2815	18	0.281438	-2.7	630000	2.49	2.81
-107	0.057914	24	0.00136216	28	1.46707	1.8866	4.85	0.281572	13	0.281522	-0.9	455000	2.38	2.65
-108	0.042822	12	0.00144396	70	1.46714	1.88667	4.54	0.281399	17	0.281346	-7.0	595000	2.62	3.05
-109	0.055574	22	0.00122667	49	1.46708	1.88658	4.05	0.281487	7.9	0.281442	-3.6	276500	2.48	2.83
-110	0.069659	26	0.00162736	43	1.46706	1.88661	4.25	0.281567	11	0.281508	-2.1	385000	2.40	2.71
-111	0.047294	6.7	0.00117577	18	1.46712	1.88657	3.31	0.281372	10	0.281324	-2.8	350000	2.64	2.95
-112	0.043517	17	0.00116321	31	1.46706	1.88657	4.99	0.281159	9.1	0.281107	-6.6	318500	2.93	3.32
-113	0.037357	7	0.00105954	17	1.46705	1.88655	4.52	0.281095	10	0.281046	-6.9	350000	3.01	3.40
-114	0.021344	12	0.000582741	33	1.46711	1.88662	5.52	0.28136	8.8	0.281335	-0.2	308000	2.61	2.86
-115	0.057344	29	0.00164547	89	1.46709	1.8866	5.22	0.281425	6.9	0.281361	-4.6	241500	2.60	2.96
-116	0.033566	13	0.000839546	26	1.46711	1.88656	5.56	0.281088	11	0.281048	-5.5	385000	3.00	3.36
-117	0.029062	9.7	0.000873374	25	1.46708	1.88659	5.12	0.281391	7.3	0.281358	-6.1	255500	2.59	3.00
-118	0.055645	3.5	0.00152554	20	1.4671	1.88658	5.52	0.281407	10	0.281349	-6.0	350000	2.62	3.01
-119	0.029664	13	0.000829695	40	1.46711	1.8866	5.06	0.281521	9.1	0.281488	0.7	318500	2.41	2.65
-120	0.058063	11	0.00148181	22	1.46712	1.88659	5.08	0.281421	6.6	0.281366	-6.5	231000	2.59	3.01
-121	0.035240	9.2	0.000968342	57	1.46708	1.88691	5.61	0.281361	20	0.281324	-6.3	700000	2.64	3.05
-122	0.047034	11	0.00106205	26	1.46713	1.88657	4.10	0.28145	13	0.281410	-4.5	455000	2.52	2.89
-123	0.083281	16	0.00182202	11	1.46707	1.88655	5.27	0.281493	11	0.281423	-2.6	385000	2.52	2.82
-124	0.038701	5.6	0.000803026	8.9	1.4671	1.88663	4.09	0.281471	12	0.281441	-3.6	420000	2.48	2.83
-125	0.029121	4.8	0.000610202	15	1.46714	1.88655	3.66	0.281074	6.4	0.281044	-4.0	224000	3.00	3.32
-126	0.028259	5.5	0.000612253	9.2	1.46712	1.88658	2.74	0.280987	10	0.280965	-21.0	350000	3.12	3.91
-127	0.044988	12	0.00129592	43	1.46708	1.88667	3.58	0.280994	8.2	0.280928	-5.2	287000	3.16	3.49
-128	0.0326239	4.1	0.000805908	7.5	1.46711	1.8867	3.78	0.280976	11	0.280935	-4.8	385000	3.15	3.47
-129	0.051712	19	0.00098673	35	1.46713	1.88666	3.30	0.281002	12	0.280951	-4.3	420000	3.13	3.44
-130	0.0318781	18	0.000692128	38	1.46707	1.88645	3.34	0.281349	15	0.281320	-2.1	525000	2.64	2.93
-131	0.0448431	23	0.00115125	47	1.46709	1.88653	5.05	0.28143	9.6	0.281385	-2.8	336000	2.56	2.87
-132	0.0472323	11	0.00125544	47	1.46708	1.88668	4.89	0.281115	15	0.281050	-0.5	525000	3.00	3.21
-133	0.0433064	26	0.000990777	41	1.46706	1.88661	4.62	0.281129	11	0.281084	-5.9	385000	2.96	3.33
-134	0.0166857	13	0.000435241	29	1.46711	1.8866	4.93	0.2812	12	0.281180	-2.0	420000	2.82	3.10
-135	0.0285771	8.3	0.000710586	23	1.46705	1.88659	4.47	0.281089	8.3	0.281056	-6.7	290500	2.99	3.38

# Chapter 7 – Conclusions

## 7.1 Crustal evolution

The Tanzanian Craton formed between 2850 – 2500 Ga with magmas derived from an evolved ( $T_{DM}$  crustal = 3.2 Ga) source. Within the Ubende Orogen and Usagaran Orogens crustal material formed between 1850 – 2050 Ma from a more evolved magma source ( $T_{DM}$  crustal = 2.6 Ga) that also reworked some Archaean material from the Tanzanian Craton. The youngest zircon population (1.0 – 1.2 Ga) seen in the southern samples may be derived from the Irumide Orogen, and have a mixed ( $T_{DM}$  crustal = 2.1 and 1.3 Ga) magma source.

The Ubende and Usagaran Orogens have similar but not identical crustal evolution histories through the Archaean and Palaeoproterozoic, but the Mesoproterozoic evolution of the Ubende diverges from the Usagaran. The Songea district, situated at the junction of these orogenic Orogens, has a separate crustal evolution and does not form the link between the two orogens. Thus the Orogens, sometimes referred to as a continuous orogenic system, are in fact distinguishable by their crustal evolution and the timing of sedimentation and metamorphism.

### 7.2 Ubende Orogen

A new metamorphic age for the Ubende Orogen of ~1070 Ma is preserved in zircon within metasedimentary rocks, with cooling below ~500 °C occurring at ~1020 Ma. Although the Ubende Orogen is currently considered to be a Palaeoproterozoic suture between the the Tanzanian Craton and an unidentified Archaean (~3.3 Ga) basement to the Kibaran and Irumide terranes (DeWaele 2008), but the data presented in this study raises the possibility that this suture is actually of Mesoproterozoic age.

## 7.3 Usagaran Orogen

### 7.3.1 Structure

Structures in the Usagaran Orogen as mapped between the villages of Rudi and Ruaha-Mbuyuni are consistent with sinistral transpression associated with collision between the Tanzanian craton and an unknown continent.

### 7.3.2 Timing of Metamorphism

Two metamorphic events were recognised in the Usagaran Orogen. Usagaran metamorphism occurred over ~20 My between 2007 and 1991 Ma. The East African orogen affected these rocks during the Neoproterozoic, and is recorded in zircon growth in the east of the orogen at  $577 \pm 17$  Ma.

## 7.3.3 Geochronology

Geochronological work on the Usagaran is, thus far, inconclusive on the provenance of sedimentary rocks. The metasedimentary rocks of the eastern Usagaran rocks are inconsistent with being derived from the Tanzanian Craton, indicating the existence of an as yet unidentified continental block as part of the collisional event. Rocks from the western Usagaran are more consistent with being derived from the craton, with some input of sediment derived from local igneous activity, possibly a volcanic arc.

### 7.3.4 Metamorphic Conditions

The metamorphic conditions experienced during burial and exhumation of eclogites and the surrounding country-rock have been constrained using thermobarometry and trace element thermometry, and the cooling rates of country-rock metapelites constrained using garnet-biotite Fe-Mg exchange modeling. The main conclusions of this study are:

- that peak eclogite facies metamorphic conditions ( $17.2 \pm 3.6$  kbar,  $839 \pm 173$  °C) are slightly higher temperature than previously published for the Usagaran.
- that metapelitic and ultramafic lithologies intercalated with eclogite in the eclogite body experienced conditions of at least  $13.4 \pm 2$  kbar,  $920 \pm 130$  °C, however there is no evidence of pelitic rocks having experienced the 17 kbar which the eclogites saw.
- that the eclogite body comprises varied lithologies with differences in protolith, chemistry and prograde and peak P-T paths.
- that country-rock pelites cooled at ~1-2 °C/My, compared to 25°C/My for eclogites between 1999 and 1991 Ma.

All of these facts are consistent with the eclogite body having formed during subduction of Palaeoproterozoic sea-floor which became intercalated with metasediments and other metaigneous rocks during exhumation. The surrounding blocks of the Isimani suite did not experience eclogite-facies metamorphism but were tectonically juxtaposed during exhumation.

## 7.4 Conclusions

The original aim of this project was to investigate whether the eclogites of the Usagaran and Ubende orogenic belts could be proved to have formed during Palaeoproterozoic metamorphic events.



This study found no evidence that eclogite formation in the Ubende Orogen occurred during the Palaeoproterozoic, and in fact suggests a new Mesoproterozoic age for eclogite formation.

The Usagaran Orogen study result, in contrast, strongly support a Palaeoproterozoic subduction origin for the Yalumba Hill eclogites. Differing metamorphic grades experienced by eclogites and surrounding gneisses suggest these rocks were intercalated during extrusion. Structures within the orogen are consistent with an intercontinental collisional orogen, as are differences in sediment provenance between the east and west of the orogen.

## References

- Alderman, A.R., 1936, Eclogites from the vicinity of Glenelg, Inverness-shire: *Quarterly Journal of the Geological Society, London*, v. 92, p. 488-533.
- Amelin, Y., Lee, D.-C., and Halliday, A.N., 2000, Early-middle Archaean crustal evolution deduced from Lu-Hf and U-Pb isotopic studies of single zircon grains: *Geochimica et Cosmochimica Acta*, v. 64, p. 4205-4225.
- Amelin, Y., Lee, D.-C., Halliday, A.N., and Pidgeon, R.T., 1999, Nature of the Earth's earliest crust from hafnium isotopes in single detrital zircons: *Nature*, v. 399, p. 252-255.
- Anczkiewicz, R., Thirlwall, M., and Platt, J., 2002, Influence of inclusions and leaching techniques on Sm-Nd and Lu-Hf garnet chronology: *Geochimica et Cosmochimica Acta*, v. 66, p. A19-A19.
- Anderson, T., 2004, Detrital zircons as tracers of sedimentary provenance: limiting conditions from statistics and numerical simulation: *Chemical Geology*, v. 204, p. 249-270.
- Ashwal, L.D., Tucker, R.D., and Zinner, E.K., 1999, Slow cooling of deep crustal granulites and Pb-loss in zircons: *Geochimica et Cosmochimica Acta*, v. 63, p. 2839-2851.
- Baldwin, J.A., Bowring, S.A., and Williams, M.L., 2003, Petrological and geochronological constraints on high pressure, high temperature metamorphism in the Snowbird tectonic zone, Canada.: *Journal of Metamorphic Geology*, v. 21, p. 81-98.
- Baldwin, J.A., Bowring, S.A., Williams, M.L., and Williams, I.S., 2004, Eclogites of the Snowbird tectonic zone: petrological and U-Pb geochronological evidence for Paleoproterozoic high-pressure metamorphism in the western Canadian Shield.: *Contributions to Mineralogy and Petrology*, v. 147, p. 528-548.
- Baldwin, J.A., Powell, R., Williams, M.L., and Goncalves, P., 2007, Formation of eclogite, and reaction during exhumation to mid-crustal levels, Snowbird tectonic zone, western Canadian Shield: *Journal of Metamorphic Geology*, v. 25, p. 853-974.
- Batumike, J.M., Griffin, W.L., O'Reilly, S.Y., Belousova, E.A., and Pawlitschek, M., 2009, Crustal evolution in the central Congo-Kasai Craton, Luebo, D.R.Congo: insights from zircon U-Pb ages, Hf-isotope and trace-element data: *Precambrian Research*, v. 170, p. 107-115.
- Bauer, C., Rubatto, D., Krenn, K., Proyer, A., and Hoinkes, G., 2007, A zircon study from the Rhodope metamorphic complex, N-Greece: time record of multistage metamorphism: *Lithos*, v. 99, p. 207-228.
- Beard, B.L., Medaris, L.G., Johnson, C.M., Jelinek, E., Tonika, J., and Riciputi, L.R., 1995, Geochronology and geochemistry of eclogites from the Marianke Laze complex, Czech Republic - implications for Variscan orogenesis *Geologische Rundschau*, v. 84, p. 552-567.
- Bell, K., and Dodson, M.H., 1981, The geochronology of the Tanzanian Shield: *Journal of Geology*, v. 89, p. 109-228.
- Belousova, E., and Griffin, W.L., 2006, Report on south-western Tanzania TerraneChron samples for Albidon Ltd, GEMOC, Macquarie University
- Bibikova, E.V., Slabunov, A.I., Volodichev, O.I., and Whitehouse, M., 2005, The Archaean eclogites of the Belomorian Province, the Fennoscandian shield.: *Geophysical Research Abstracts*, v. 7.
- Bickle, M.J., 1984, Variation in tectonic style with time: Alpine & Archean systems, *in* Holland, H.D., and Threndell, A.F., eds., *Patterns of change in earth evolution*: Berlin, Springer-Verlag, p. 357-370.
- Bleeker, W., 2008, The late Archean record - a puzzle in ca. 35 pieces: *Lithos*, v. 71, p. 99-134.
- Boniface, N., and Schenk, V., 2007, Polymetamorphism in the Paleoproterozoic Ubendian Belt, Tanzania: *Geochimica et Cosmochimica Acta*, v. 71, p. A107.
- Borg, G., and Krogh, T., 1999, Isotopic age data of single zircons from the Archaean Sukumaland Greenstone Belt, Tanzania: *Journal of African Earth Sciences*, v. 29, p. 301-312.
- Boven, A., Theunissen, K., Sklyarov, E., Klerkx, J., Melnikov, A., Mruma, A., and Punzalan, L.E., 1999, Timing of exhumation of a high-pressure mafic granulite terrane of the Paleoproterozoic Ubende belt (West Tanzania): *Precambrian Research*, v. 93, p. 119-137.
- Brewer, M.S., Haslam, H.W., Darbyshire, D.P.F., and Davis, A.E., 1979, Rb-Sr age determination in the Bangweulu block, Luapula province, Zambia, Report Institute of Geological Sciences, Volume 79/5: London, England, p. 11.
- Brock, P.W.G., 1963, The Mbozi syenite-gabbro complex [PhD dissertation thesis], University of Leeds.
- Brown, M., 2006, Duality of thermal regimes is the distinctive characteristic of plate tectonics since the Neoproterozoic: *Geology*, v. 34, p. 961-964.
- , 2007a, Characteristic thermal regimes of plate tectonics and their metamorphic imprint throughout Earth history: when did Earth first adopt a plate tectonics mode of behaviour?, *in* Condie, K.C., and Pease, V., eds., *When did plate tectonics begin?*, Volume Special Publication, Geological Society of America
- , 2007b, Metamorphic conditions in orogenic belts: a record of secular change: *International Geology Review*, v. 49, p. 198-234.
- Buchwaldt, R., Toulkeridis, T., Todl, W., and Ucakuwun, E.K., 2007, Crustal age domains in the Kibaran belt of SW-Uganda: Combined zircon geochronology and Sm-Nd isotopic investigation: *Journal of African Earth Sciences*, v. 51, p. 4-20.
- Burton, K.W., Kohn, M.J., Cohen, A.S., and Onions, R.K., 1995, THE RELATIVE DIFFUSION OF PB, ND, SR AND O IN GARNET: *Earth and Planetary Science Letters*, v. 133, p. 199-211.
- Cahen, L., and Snelling, N.J., 1966, *The geochronology of equatorial Africa*: Amsterdam, North Holland.
- Cahen, L., Snelling, N.J., Delhal, J., Vail, J.R., Bonhomme, M., and Ledent, D., 1984, *The geochronology and evolution of Africa*: Oxford, Clarendon Press, 512 p.

- Camacho, A., Lee, J.K.W., Hensen, B.J., and Braun, J., 2005, Short-lived orogenic cycles and the eclogitization of cold crust by spasmodic hot fluids.: *Nature*, v. 432, p. 1191-1195.
- Cao, R., and Zhu, S., 1995, The Dabieshan coesite-bearing eclogite terrane - A Neo Archaean ultra-high pressure metamorphic belt: *Acta Geologica Sinica*, v. 69, p. 232-242.
- Carswell, D.A., Brueckner, H.K., Cuthbert, S.J., Mehta, K., and O'Brien, P.J., 2003, The timing of stabilisation and the exhumation rate for ultra-high pressure rocks in the Western Gneiss Region of Norway: *Journal of Metamorphic Geology*, v. 21, p. 601-612.
- Cawood, P.A., Kröner, A., Collins, W.J., Kusky, T.M., Mooney, W.D., and Windley, B. F., 2009, Accretionary orogens through Earth history: Geological Society, London, Special Publications, v. 318, p. 1-36.
- Cawood, P.A., Kröner, A., and Pisarevsky, S.A., 2006, Precambrian plate tectonics: criteria and evidence: *GSA Today*, v. 16, p. 4-11.
- Cawood, P.A., and Nemchin, A.A., 2001, Source regions for Laurentia margin sediments: constraints from U-Pb dating of detrital zircon in the Newfoundland Appalachians: *Geological Society of America Bulletin*, v. 113, p. 1234-1246.
- Cawood, P.A., Nemchin, A.A., Freeman, M., and Sircombe, K.N., 2003, Linking source and sedimentary basin: detrital zircon record of sediment flux along a modern river system and implications for provenance studies: *Earth and Planetary Science Letters*, v. 213, p. 259-268.
- Chakraborti, S., and Ganguly, J., 1990, Compositional zoning and cation diffusion in garnets, *in* Ganguly, J., ed., *Diffusion, atomic ordering, and mass transport: selected problems in geochemistry*: New York, Springer-Verlag.
- Chemenda, A.I., Mattauer, M., Malavieille, J., and Bokun, A.N., 1995, A mechanism for syn-collisional rock exhumation and associated faulting: Results from physical modelling: *Earth and Planetary Science Letters*, v. 132.
- Chen, R.-X., Zheng, Y.-F., and Xie, L., 2010, Metamorphic growth and recrystallisation of zircon: distinction by simultaneous in-situ analyses of trace elements, U-Th-Pb and Lu-Hf isotopes in zircons from the eclogite-facies rocks in the Sulu orogen: *Lithos*, v. 114, p. 132-154.
- Cherniak, D.J., Hanchar, J.M., and Watson, E.B., 1997, Diffusion of tetravalent cations in zircon: *Contributions to Mineralogy and Petrology*, v. 127, p. 383-390.
- Cherniak, D.J., and Watson, E.B., 2003, Diffusion in zircon, *Zircon, Volume 53: Reviews in mineralogy & geochemistry*, Mineralogical Society of America, p. 113-143.
- , 2007, Ti diffusion in zircon: *Chemical Geology*, v. 242, p. 470-483.
- Chopin, C., 2003, Ultrahigh-pressure metamorphism: tracing continental crust into the mantle.: *Earth and Planetary Science Letters*, v. 212, p. 1-14.
- Cloos, M., 1983, Comparative study of melange matrix and metashales from the Franciscan subduction complex with the basal Great Valley Sequence, California: *Journal of Geology*, v. 91, p. 291-306.
- Cloutier, J., Stevenson, R.K., and Bardoux, M., 2005, Nd isotopic, petrologic and geochemical investigation of the Tulawaka East gold deposit, Tanzanian Craton: *Precambrian Research*, v. 139, p. 147-163.
- Coleman, 1965, *In*: Stern 1996.
- Collins, A.S., 2003, Structure and Age of the Northern Leeuwin Complex, Western Australia: constraints from field mapping and U-Pb isotopic analysis: *Australian Journal of Earth Sciences*, v. 50, p. 585-599.
- Collins, A.S., and Pisarevsky, S.A., 2005, Amalgamating eastern Gondwana: the evolution of the Circum-Indian Orogens.: *Earth-Science Reviews*, v. 71, p. 229-270.
- Collins, A.S., Raddy, S.M., Buchan, C., and Mruma, A.H., 2004a, Temporal constraints on Palaeoproterozoic eclogite formation and exhumation (Usagaran Orogen, Tanzania): *Earth and Planetary Science Letters*, v. 224, p. 175-192.
- Collins, A.S., Reddy, S.M., Buchan, C., and Mruma, A., 2004b, Temporal constraints on Palaeoproterozoic eclogite formation and exhumation (Usagaran Orogen, Tanzania): *Earth and Planetary Science Letters*, v. 224, p. 175-192.
- Collins, A.S., and Robertson, A.H.F., 1997, Lycian Melange, southwestern Turkey: an emplaced Late Cretaceous accretionary complex: *Geology*, v. 25, p. 255-258.
- Compston, W., Williams, I.S., and Meyer, C., 1984, U-Pb geochronology of zircons from lunar breccia 73217 using a sensitive high mass-resolution ion microprobe. : *Journal of Geophysical Research*, v. 89, p. B525-B534.
- Condie, K.C., 2008, Did the character of subduction change at the end of the Archaean? Constraints from convergent-margin granitoids: *Geology*, v. 36, p. 611-614.
- Condie, K.C., Belousova, E., Griffin, W.L., and Sircombe, K.N., 2009a, Granitoid events in space and time: constraints from igneous and detrital age spectra: *Gondwana Research*, v. 15, p. 228-242.
- , 2009b, Granitoid events in space and time: constraints from igneous and detrital zircon age spectra: *Gondwana Research*, v. 15, p. 228-242.
- Condie, K.C., Beyer, E., Belousova, E., Griffin, W.L., and O'Reilly, S.Y., 2005, U-Pb isotopic ages and Hf isotopic composition of single zircons: the search for juvenile Precambrian continental crust: *Precambrian Research*, v. 139, p. 42-100.
- Condie, K.C., O'Neill, C., and Aster, R.C., 2009c, Evidence for a widespread magmatic shutdown for 250 My on Earth: *Earth and Planetary Science Letters*, v. 282, p. 294-298.
- Cooke, R.A., O'Brien, P.J., and Carswell, D.A., 2000, Garnet zoning and the identification of equilibrium mineral compositions in high-pressure-temperature granulites from the Moldanubian Zone, Austria: *Journal of Metamorphic Geology*, v. 18, p. 551-569.
- Coolen, J.J.M.M.M., 1980, Chemical petrology of the Furua granulite complex, southern Tanzania: *GUA Papers of Geology*, v. Series 1 13, p. 1-258.

- Cordani, U.G., Brito-Neves, B.B., and D'Agrella-Filho, M.S., 2003, From Rodinia to Gondwana: a review of the available evidence from South America: *Gondwana Research*, v. 6, p. 275-283.
- Corfu, F., Hanchar, J.M., Hoskin, P.W.D., and Kinny, P.D., 2003, Atlas of zircon textures, in Hanchar, J.M., and Hoskin, P.W.D., eds., *Zircon, Volume 53: Reviews in Mineralogy and Geochemistry*: Washington, Mineralogical Society of America, p. 468-500.
- Crowley, P.D., 1991, Thermal and kinetic constraints on the tectonic applications of thermobarometry: *Mineralogical Magazine*, v. 55, p. 57-69.
- Cutten, H., 2006, Protolith ages and timing of metasomatism related to the formation of whiteschists at Mautia Hill, Tanzania: implications for the assembly of Gondwana: *Journal of Geology*, v. 114, p. 683-698.
- D'Agrella-Filho, M.S., Pacca, I.I.G., Trindade, R.I.F., Teixeira, W., Raposo, M.I.B., and Onstott, T.C., 2004, Palaeomagnetism and Ar-40/Ar-39 ages of mafic dykes from Salvador (Brazil): new constraints on the Sao Francisco craton APW path between 1080 and 1010 Ma.: *Precambrian Research*, v. 132, p. 55-77.
- Davis, D.W., Amelin, Y., Nowell, G.M., and Parrish, R.R., 2005, Hf isotopes from the western Superior province, Canada: implications for Archean crustal development and evolution of the depleted mantle.: *Precambrian Research*, v. 114, p. 295-325.
- DeWaele, B., 2005, The Proterozoic geological history of the Irumide belt, Zambia [PhD Thesis thesis]: Perth, Curtin University of Technology.
- , 2009, The geochronological framework of the Irumide Belt: a prolonged crustal history along the margin of the Bangweulu craton.: *American Journal of Science*, v. 309, p. 132-187.
- DeWaele, B., and Fitzsimons Ian, C.W., 2004, The age and detrital footprint of the Muva Supergroup of Zambia: molassic deposition to the southwest of the Ubendian belt, Abstracts Volume of Geoscience Africa: Johannesburg, South Africa, p. 162-163.
- , 2007, The nature and timing of Palaeoproterozoic sedimentation at the southeastern margin of the Congo Craton: *Precambrian Research*, v. 159, p. 95-116.
- DeWaele, B., and Fitzsimons, I.C.W., 2004, The age and detrital footprint of the Muva Supergroup of Zambia: molassic deposition to the southwest of the Ubendian belt, Abstracts Volume of Geoscience Africa: Johannesburg, South Africa, p. 162-163.
- , 2007, The nature and timing of Palaeoproterozoic sedimentation at the southeastern margin of the Congo Craton: *Precambrian Research*, v. 159, p. 95-116.
- DeWaele, B., Fitzsimons, I.C.W., Wingate, M.T.D., Tembo, F., Mapani, B.S.E., and Belousova, E., 2009, The geochronological framework of the Irumide Belt: a prolonged crustal history along the margin of the Bangweulu craton: *American Journal of Science*, v. 309, p. 132-187.
- DeWaele, B., Johnson, S.P., and Pisarevsky, S.A., 2008, Palaeoproterozoic to Neoproterozoic growth and evolution of the eastern Congo Craton: its role in the Rodinia puzzle: *Precambrian Research*, v. 160, p. 127-141.
- DeWaele, B., Kampunzu, A.B., Mapani, B.S.E., and Tembo, F., 2006a, The Irumide Belt of Zambia: *Journal of African Earth Sciences*, v. 46, p. 36-70.
- DeWaele, B., Liegeois, J.P., Nemchin, A.A., and Tembo, F., 2006b, Isotopic and geochemical evidence of Proterozoic episodic crustal reworking within the Irumide Belt of south-central Africa, the southern metacratonic boundary of an Archaean Bangweulu Craton: *Precambrian Research*, v. 148, p. 225-256.
- DeWaele, B., Wingate, M.T.D., Fitzsimons Ian, C.W., and Mapani, B.S.E., 2003, Untying the Kibaran knot: a reassessment of Mesoproterozoic correlations in southern Africa based on SHRIMP U-Pb data from the Irumide belt: *Geology*, v. 31, p. 509-512.
- Dewey, J.F., Holdsworth, R.E., and Strachan, R.A., 1998, Transpression and transtension zones, in Holdsworth, R.E., Strachan, R.A., and Dewey, J.F., eds., *Continental transpression and transtensional tectonics, Volume 135: Special Publication*: London, Geological Society, London, p. 1-14.
- DeWolf, C.P., Zeissler, C.J., Halliday, A.N., Mezger, K., and Essene, E.J., 1996, The role of inclusions in U-Pb and Sm-Nd garnet geochronology: Stepwise dissolution experiments and trace uranium mapping by fission track analysis: *Geochimica et Cosmochimica Acta*, v. 60, p. 121-134.
- Dodson, M.H., Cavanagh, B.J., Thatcher, E.C., and Aftalion, M., 1975, Age limits for the Ubendian metamorphic episode in northern Malawi: *Geological Magazine*, v. 112, p. 403-410.
- Dziggel, A., Armstrong, R.A., Stevens, G., and Nasdala, L., 2006, Growth of zircon and titanite during metamorphism in the granitoid-gneiss terrain south of the Baberton greenstone belt, South Africa.: *Mineralogical Magazine*, v. 69, p. 1021-1038.
- El-Shazly, A.E.-D., Coleman, R.G., and Liou, J.G., 1990, Eclogites and blueschists from Northeastern Oman: petrology and P-T evolution.: *Journal of Petrology*, v. 31, p. 1990.
- England, and Holland, 1979a, ?? eclogites in carbonates in eastern alps.
- England, P.C., and Holland, T.J.B., 1979b, Archimedes and the Tauern eclogite - role of buoyancy in the preservation of exotic eclogite blocks: *Earth and Planetary Science Letters*, v. 44, p. 287-294.
- Engvik, A.K., Tveten, E., Bingen, B., Viola, G., Erambert, M., Feito, P., and De Azavedo, S., 2007, P-T-t evolution and textural evidence for decompression of Pan-African high-pressure granulites, Lurio Belt, north-eastern Mozambique: *Journal of Metamorphic Geology*, v. 25, p. 935-952.
- Eriksson, K.A., Campbell, I.H., Palin, J.M., Allen, C.M., and Bock, B., 2004, Evidence for multiple recycling in neoproterozoic through Pennsylvanian sedimentary rocks of the central Appalachian basin: *Journal of Geology*, v. 112, p. 261-276.
- Eskola, P., 1929, Om mineralfacies: *Geologiska Föreningens i Stockholm Förhandlingar*, v. 51, p. 157-172.

- Faryad, S.W., 1999, Metamorphic evolution of the Precambrian South Badakhshan block, based on mineral reactions in metapelites and metabasites associated with whiteschists from Sare Sang (Western Hindu Kush Afghanistan). *Precambrian Research*, v. 98, p. 223-241.
- Faryad, S.W., Nahodilova, R., and Dolejš, D., 2010, Incipient eclogite facies metamorphism in the Moldanubian granulites revealed by mineral inclusions in garnet: *Lithos*, v. 114, p. 54-69.
- Faure, M., Lin, W., Schärer, U., Shu, L., Sun, Y., and Arnaud, N., 2003, Continental subduction and exhumation of UHP rocks. Structural and geochronological insights from the Dabieshan (East China). *Lithos*, v. 70, p. 213-241.
- Ferry, J.M., and Spear, F.S., 1978, Experimental calibration of the partitioning of Fe and Mg between biotite and garnet: *Contributions to Mineralogy and Petrology*, v. 66, p. 113-117.
- Ferry, J.M., and Watson, E.B., 2007, New thermodynamic models and revised calibrations for the Ti-in-zircon and Zr-in-rutile thermometers: *Contributions to Mineralogy and Petrology*, v. 154, p. 429-437.
- Florence, F.P., and Spear, F.S., 1991, Effects of diffusional modification of garnet growth zoning on P-T path calculations: *Contributions to Mineralogy and Petrology*, v. 107, p. 487-500.
- , 1995, Integranular diffusion kinetic of Fe and Mg during retrograde metamorphism of a pelitic gneiss from the Adirondack mountains: *Earth and Planetary Science Letters*, v. 134, p. 329-340.
- Forster, M.A., and Lister, G.S., 2004, The interpretation of  $^{40}\text{Ar}/^{39}\text{Ar}$  apparent age spectra produced by mixing: application of the method of asymptotes and limits *Journal of Structural Geology*, v. 26, p. 287-305.
- Fossen, H., and Tikoff, B., 1998, Extended models of transpression and transtension, and application to tectonic settings, in Holdsworth, R.E., Strachan, R.A., and Dewey, J.F., eds., *Continental transpression and transtensional tectonics*, Volume 135: Special Publication: London, Geological Society, London, p. 15-33.
- Fritz, H., Tenczer, V., Hauzenberger, C.A., Wallbrecher, E., Hoinkes, G., Muhongo, S., and Mogessie, A., 2005, Central Tanzanian tectonic map: a step forward to decipher Proterozoic structural events in the East African Orogen: *Tectonics*, v. 24, p. TC6013.
- Froitzheim, N., Pleuger, J., Roller, S., and Nagel, T., 2003, Exhumation of high- and ultrahigh-pressure metamorphic rocks by slab extraction.: *Geology*, v. 31, p. 925-928.
- Fu, B., Page, F.Z., Casovic, A.J., Fournelle, J., Kita, N.T., Lackey, J.S., Wilde, S.A., and Valley, J.W., 2008, Ti-in-zircon thermometry: applications and limitations: *Contributions to Mineralogy and Petrology*, v. 156, p. 197-215.
- Gallien, F., Mogessie, A., Bjerg, E., Delpino, S., de Machuca, B.C., Thoni, M., and Klotzli, U., 2010, Timing and rate of granulite facies metamorphism and cooling from multi-mineral chronology on migmatitic gneisses, Sierras de La Huerta and Valle Fertil, NW Argentina: *Lithos*, v. 114, p. 229-252.
- Ganguly, J., and Chakraborti, S., 1991, Compositional zoning and cation diffusion in garnets, in Ganguly, J., ed., *Diffusion, atomic ordering, and mass transport: selected problems in geochemistry*: New York, Springer-Verlag.
- Ganguly, J., Cheng, W., and Chakraborti, S., 1998, Cation diffusion in aluminosilicate garnets: experimental determination in pyrope almandine diffusion couples: *Contributions to Mineralogy and Petrology*, v. 131, p. 171-180.
- Godard, G., 2001, Eclogites and their geodynamic interpretation: a history.: *Journal of Geodynamics*, v. 32, p. 165-203.
- Grainger, D.J., and Fozzard, P.M.H., 1966, QDS 199 Mikumi, Tanzanian Geology quarter degree sheets: Dodoma, Tanzanian Geological Survey.
- Green, D.H., and Ringwood, A.E., 1972, Comparison of recent experimental-data on gabbro-garnet granulite-eclogite transition: *Journal of Geology*, v. 80, p. 277.
- Griffin, W.L., Belousova, E., Shee, S.R., Pearson, N.J., and O'Reilly, S.Y., 2004, Archean crustal evolution in the northern Yilgarn Craton: U-Pb and Hf-isotope evidence from detrital zircons: *Precambrian Research*, v. 131, p. 231-282.
- Griffin, W.L., Belousova, E., Walters, S.G., and O'Reilly, S.Y., 2006, Archean and Proterozoic crustal evolution in the Eastern Succession of the Mt Isa district, Australia: U - Pb and Hf-isotope studies of detrital zircons: *Australian Journal of Earth Sciences*, v. 53, p. 125-149.
- Griffin, W.L., Pearson, N.J., Belousova, E., Jackson, S.E., O'Reilly, S.Y., van Acherbergh, E., and Shee, S.R., 2000, The Hf isotope composition of cratonic mantle: LAM-MC-ICPMS analysis of zircon megacrysts in kimberlites: *Geochimica et Cosmochimica Acta*, v. 64, p. 133-147.
- Griffin, W.L., Pearson, N.J., Belousova, E.A., and Saeed, A., 2007, Reply to "Comment to short-communication •Comment: Hf-isotope heterogeneity in zircon 91500' by W.L. Griffin, N.J. Pearson, E.A. Belousova and A. Saeed (Chemical Geology 233 (2006) 358–363)" by F. Corfu. : *Chemical Geology*, v. 244, p. 354-356.
- Hacker, B.R., Andersen, T.B., Root, D.B., Mehl, L., Mattinson, J.M., and Wooden, J.L., 2003, Exhumation of high-pressure rocks beneath the Solund Basin, Western Gneiss Region of Norway: *Journal of Metamorphic Geology*, v. 21, p. 613-629.
- Hacker, B.R., Ratschbacher, L., Webb, L.E., Ireland, T.R., Calvert, A., Gans, P.B., and Shuwen, D., 2000, Exhumation of ultrahigh-pressure continental crust in east-central China: Late Triassic-Early Jurassic tectonic unroofing.: *Journal of Geophysical Research*, v. 105, p. 13339-13364.
- Hanmer, S., 1997, Shear zone reactivation at granulite facies: The importance of plutons in the localization of viscous flow: *Journal of the Geological Society*, v. 154, p. 111-116.
- Hanmer, S., Parrish, R., Williams, M., and Kopf, C., 1994, Striding-Athabasca mylonite zone - complex Archean deep-crustal deformation in the East



- Athabasca mylonite triangle, northern Saskatchewan: *Canadian Journal of Earth Sciences*, v. 31, p. 1287-1300.
- Hanmer, S., Williams, M., and Kopf, C., 1995a, Modest movements, spectacular fabrics in an intracontinental deep-crustal strike-slip-fault - Striding-Athabasca mylonite zone, NW Canadian Shield: *Journal of Structural Geology*, v. 17, p. 493-507.
- , 1995b, Striding-Athabasca mylonite zone - implications for the Achean and early Proterozoic tectonics of the Western Canadian Shield: *Canadian Journal of Earth Sciences*, v. 32, p. 178-196.
- Harland, W.B., 1971, Tectonic transpression in Caledonian Spitzbergen: *Geological Magazine*, v. 108, p. 27-42.
- Harrison, T.M., Blichert-Toft, J., Müller, W., Albarède, F., Holden, P., and Mojzsis, S.J., 2005, Heterogeneous Hadean hafnium: evidence of continental crust by 4.4-4.5 Ga: *Science*, v. 310, p. 1947-1950.
- Hauzenberger, C., Robl, J., and Stuwe, K., 2005, Garnet zoning in high pressure granulite-facies metapelites, Mozambique belt, SE-Kenya: constraints on the cooling history: *European Journal of Mineralogy*, v. 17, p. 43-55.
- Hauzenberger, C.A., Sommer, H., Fritz, H., Bauernhofer, A., Kroner, A., Hoinkes, G., Wallbrecher, E., and Thoni, M., 2007, SHRIMP U-Pb zircon and Sm-Nd garnet ages from the granulite-facies basement of SE Kenya: evidence for Neoproterozoic polycyclic assembly of the Mozambique Belt: *Journal of the Geological Society*, v. 164, p. 189-201.
- Hawkesworth, C.J., and Kemp, A.I.S., 2006, Using Hafnium and oxygen isotopes in zircons to unravel the record of early crustal evolution: *Chemical Geology*, v. 226, p. 144-162.
- Hayden, L.A., Watson, E.B., and Wark, D.A., 2006, A thermobarometer for sphene: *Geochimica et Cosmochimica Acta*, v. 70, p. A237.
- Hiess, J., Nutman, A.P., Bennett, V.C., and Holden, P., 2008, Ti-in-zircon thermometry applied to contrasting Archean metamorphic and igneous systems: *Chemical Geology*, v. 247, p. 323-338.
- Hoffman, P.F., 1991, Did the breakout of Laurentia turn Gondwanaland inside out?: *Science*, v. 252, p. 1409-1412.
- Holland, T., and Powell, R., 1998, An internally consistent thermodynamic data set for phases of petrological interest: *Journal of Metamorphic Geology*, v. 13, p. 309-343.
- , 2005, AX software.
- Horeva, B.J., Iskanderova, A.D., and Shergina, J.P., 1971, Age of protoliths from metamorphic series of SW Pamir, according to Pb isotope method: *Geologicheskaya*, v. 8, p. 40-46.
- Hoskin, P.W.D., and Black, L.P., 2000, Metamorphic zircon formation by solid-state recrystallisation of protolith igneous grains: *Journal of Metamorphic Geology*, v. 18, p. 423-439.
- Hou, G., Santosh, M., Qian, X., Lister, G.S., and Li, J., 2008, Configuration of the Late Palaeoproterozoic supercontinent Columbia: insights from radiating mafic dyke swarms: *Gondwana Research*, v. 14, p. 395-409.
- Howard, K.E., Hand, M., Barovich, K.M., Reid, A., Wade, B.P., and Belousova, E., 2009, Detrital zircon ages: improving interpretation via Nd and Hf isotopic data: *Chemical Geology*, v. 262, p. 277-292.
- Indares, A.D., 1995, Metamorphic interpretation of high-pressure-temperature metapelites with preserved growth zoning in garnet, Eastern Grenville Province, Canadian Shield: *Journal of Metamorphic Geology*, v. 13, p. 475-486.
- Jackson, S.E., Pearson, N.J., Griffin, W.L., and Belousova, E., 2004, The application of laser ablation-inductively coupled plasma-mass spectrometry to in situ U-Pb zircon geochronology: *Chemical Geology*, v. 211, p. 47-69.
- Jahn, B.-m., Caby, R., and Monie, P., 2001, The oldest UHP eclogites of the world: age of UHP metamorphism, nature of protoliths and tectonic implications.: *Chemical Geology*, v. 178, p. 143-158.
- Johnson, S.P., and Oliver, G.J.H., 2004, Tectonothermal history of the Kaourera Arc, northern Zimbabwe: implications for the tectonic evolution of the Irumide and Zambezi Belts of south central Africa: *Precambrian Research*, v. 130, p. 71-97.
- Johnson, S.P., Rivers, T., and De Waele, B., 2005, A review of the Mesoproterozoic to early Palaeozoic magmatic and tectonothermal history of south-central Africa: implications for Rodinia and Gondwana: *Journal of the Geological Society London*, v. 162, p. 433-450.
- Jourdan, F., and Renne, P.R., 2007, Age calibration of the Fish Canyon sanidine  $^{40}\text{Ar}/^{39}\text{Ar}$  dating standard: *Geochimica et Cosmochimica Acta*, v. 71, p. 387-402.
- Jourdan, F., Verati, C., and Féraud, G., 2006, Intercalibration of the Hb3gr  $^{40}\text{Ar}/^{39}\text{Ar}$  dating standard: *Chemical Geology*, v. 231, p. 177-189.
- Kabengele, M., Tshimanga, K., Lubala, R.T., Kapenda, D., and Walraven, F., 1990, Geochronology of the calc-alkaline granitoids of the Marungu plateau (eastern Zaire - central Africa), 15th Colloquium of African Geology: Nancy, France, CIFEG - occasional publication, p. 51-55.
- Kaulina, T., Apanasevich, E., Savchenko, E., and Serov, P., 2006, U-Pb and Sm-Nd data for the late Archean eclogites of the Kola Peninsula (NE Baltic Shield): *Geophysical Research Abstracts*, v. 8.
- King, 1955, 198 Kibakwe South, Tanzanian Geology - quarter degree sheets: Dodoma, Tanzanian Geological Survey.
- Kinny, P.D., and Maas, R., 2003, Lu-Hf and Sm-Nd isotope systems in zircon, in Hanchar, J.M., and Hoskin, P.W.D., eds., *Zircon, Volume 53: Reviews in mineralogy and geochemistry*.
- Klerkx, J., Liegeois, J.P., Lavreau, J., and Claessens, W., 1987, Crustal evolution of the northern Kibaran Belt, eastern and central Africa, in Kroener, A., ed., *Proterozoic lithospheric evolution: Geodynamics Series*: Washington, DC, American Geophysical Union, p. 217-233.
- Kokonyangi, J., Armstrong, R., Kampunzu, A.B., Yoshida, M., and Okudaira, T., 2004, U-Pb zircon

- chronology and petrology of granitoids from Mitwaba (Katanga, Congo): implications for the evolution of the Mesoproterozoic Kibaran Belt.: *Precambrian Research*, v. 132, p. 79-106.
- Kokonyangi, J., Kampunzu, A.B., Poujol, M., Okudaira, T., Yoshida, M., and Shabeer, K.P., 2005, Petrology and geochronology of Mesoproterozoic mafic-intermediate plutonic rocks of Matwaba (D.R.Congo): implications for the evolution of the Kibaran belt in central Africa: *Geological Magazine*, v. 142, p. 109-130.
- Kopf, C.F., 2002, Archean and Early Proterozoic events along the Snowbird Tectonic Zone in Northern Saskatchewan, Canada: *Gondwana Research*, v. 5, p. 79-83.
- Koppers, A.A.P., 2002, ArArCALC-software for  $^{40}\text{Ar}/^{39}\text{Ar}$  age calculations: *Computers & Geosciences*, v. 28, p. 605-619.
- Krogh, T., 1988, The garnet-clinopyroxene Fe-Mg geothermometer: a reinterpretation of existing experimental data: *Contributions to Mineralogy and Petrology*, v. 99, p. 44-48.
- Kröner, A., 1981, Precambrian plate tectonics, *in* Kröner, A., ed., *Precambrian plate tectonics*, Volume 4: *Developments in Precambrian geology*: Amsterdam, Elsevier scientific publishing company, p. 57-90.
- Kröner, A., and Cordani, U., 2003, African, southern Indian and South American cratons were not part of the Rodinia supercontinent: evidence from field relationships and geochronology: *Tectonophysics*, v. 375, p. 325-352.
- Kröner, A., Cui, W.Y., Wang, S.Q., Wang, C.Q., and Nemchin, A.A., 1998, Single zircon ages from high-grade rocks of the Jianping Complex, Liaoning Province, NE China: *Journal of Asian Earth Sciences*, v. 16, p. 519-532.
- Kröner, A., Wilde, S.A., Li, J.H., and Wang, K.Y., 2005, Age and evolution of a late Archean to Paleoproterozoic upper to lower crustal section in the Wutaishan/Hengshan/Fuping terrain of northern China: *Journal of Asian Earth Sciences*, v. 24, p. 577-595.
- Kuiper, K.F., Deino, A., Hilgen, F.J., Krijgsman, W., Renne, P.R., and Wijbrans, J.R., 2008, Synchronising the rock clocks of Earth history: *Science*, v. 320, p. 500-504.
- Lambert, R.S.J., 1981, Earth tectonics and thermal history: review and a hot-spot model for the Archean, *in* Kröner, A., ed., *Precambrian plate tectonics*, Volume 4: Amsterdam, Elsevier, p. 453-468.
- Lapen, T.J., Mahlen, N.J., Johnson, C.M., Beard, B.L., and Baumgartner, L.P., 2002, Lu-Hf geochronology of UHP metamorphism in the Zermatt-Saas ophiolite, Lago di Cignana, Italy: *Geochimica et Cosmochimica Acta*, v. 66, p. A431-A431.
- Lau, V., 2009a, Geochemistry and Sm-Nd isotopic composition of eclogite and associated rocks in the Usagaran Orogen Belt, Tanzania [Honours thesis]: Adelaide, University of Adelaide.
- Lau, W.K., 2009b, Geochemistry and Sm-Nd isotopic composition of eclogite and associated rocks in the Usagaran Belt, Tanzania: Adelaide, University of Adelaide.
- Lenoir, J.-L., Liégeois, J.-P., Theunissen, K., and Klerkx, J., 1994a, The Palaeoproterozoic Ubendian shear belt in Tanzania: geochronology and structure: *Journal of African Earth Sciences*, v. 19, p. 169-184.
- Lenoir, J.-L., Liégeois, J.P., Theunissen, K., and Klerkx, J., 1994b, Origin and regional significance of Late Precambrian and early Paleozoic granitoids in the Pan-African belt of Somalia: *Geologische Rundschau*, v. 83, p. 624-641.
- Li, Z.X., Bogdanova, S.V., Collins Alan, S., Davidson, A., De Waele, B., Ernst, W.G., Fitzsimons, I.C.W., Fuck, R.A., Gladkochub, D.P., Jacobs, J., Karlstrom, K.E., Lu, S., Natapov, L.M., Pease, V., Pisarevsky, S.A., Thrane, K., and Vernikovsky, V., 2008, Assembly, configuration, and break-up history of Rodinia: a synthesis: *Precambrian Research*, v. 160, p. 179-210.
- Maas, R., Kinny, P.D., Williams, I.S., Froude, D.O., and Compston, W., 1992, The Earth's oldest known crust: a geochronological and geochemical study of 3900–4200 Ma old detrital zircons from Mt. Narryer and Jack Hills, Western Australia: *Geochimica et Cosmochimica Acta*, v. 56, p. 1281-1300.
- Maboko, M.A.H., Boelrijk, N.A.I.M., Priem, H.N.A., and Verdurmen, E.A.T., 1985, Zircon U-Pb and biotite Rb-Sr dating of the Wami River granulites, Eastern Granulites, Tanzania; evidence for approximately 715 ma old granulite-facies metamorphism and final Pan-African cooling approximately 475 ma ago.
- Maboko, M.A.H., and Nakamura, E., 1996, Nd and Sr isotopic mapping of the Archaean-Proterozoic boundary in southeastern Tanzania using granites as probes for crustal growth: *Precambrian Research*, v. 77, p. 105-115.
- Manya, S., Kobayashi, K., Maboko, M.A.H., and Nakamura, E., 2006, Ion microprobe zircon U-Pb dating of the late Archaean metavolcanics and associated granites of the Musoma-Mara Greenstone Belt, northeast Tanzania: implications for the geological evolution of the Tanzania Craton: *Journal of African Earth Sciences*, v. 45, p. 355-366.
- Manya, S., and Maboko, M.A.H., 2003, Dating basaltic volcanism in the Neoproterozoic Sukumaland Greenstone Belt of the Tanzania Craton using the Sm-Nd method: implications for the geological evolution of the Tanzania Craton: *Precambrian Research*, v. 121, p. 35-45.
- , 2008, Geochemistry and geochronology of Neoproterozoic volcanic rocks of the Iramba-Sekenke greenstone belt, central Tanzania: *Precambrian Research*, v. 163, p. 265-278.
- Marshak, S., 1999, Deformation style way back when: thoughts on the contrasts between Archean / Paleoproterozoic and contemporary orogens.: *Journal of Structural Geology*, v. 21, p. 1175-1182.
- Maruyama, S., and Liou, J.G., 1998a, Initiation of ultrahigh-pressure metamorphism and its significance on the Proterozoic-Phanerozoic boundary.: *The Island Arc*, v. 7, p. 6-35.
- , 1998b, Initiation of ultrahigh-pressure metamorphism and its significance on the Proterozoic-Phanerozoic boundary.: *The Island Arc*, v. 7, p. 6-35.

- Mawby, J., 2000, Metamorphic and geochronologic constraints on Palaeozoic tectonism in the eastern Arunta Inlier: Adelaide, University of Adelaide.
- McDougall, I., and Harrison, T.M., 1999, Geochronology and Thermochronology for the  $^{40}\text{Ar}/^{39}\text{Ar}$  method: Oxford, Oxford University Press, 269 p.
- McKenzie, D., and Weiss, N., 1975, Speculations on the thermal and tectonic history of the earth: *Geophysical Journal of the Royal Astronomical Society*, v. 42, p. 131-174.
- Medaris, L.G., Ghent, E.D., Wang, H.F., Fournelle, J.H., and Jelinek, E., 2006, The Spacice eclogite: constraints on the P-T-t history of the Gfohl granulite terrane, Moldanubian Zone, Bohemian Massif: *Mineralogy and Petrology*, v. 86, p. 203-220.
- Meinhold, K.-D., and Venzlaff, H., 1965, Geological map of Izazi - quarter degree sheet 197, German Geological Mission on Tanzania.
- Meyre, C., De Capitani, C., Zack, T., and Frey, M., 1999, Petrology of high-pressure metapelites from the Adula nappe (Central Alps, Switzerland): *Journal of Petrology*, v. 40, p. 199-213.
- Mezger, K., Essene, E.J., and Halliday, A.N., 1992, Closure temperatures of the Sm-Nd system in metamorphic garnets: *Earth and Planetary Science Letters*, v. 113, p. 397-409.
- Min, K., Mundil, R., Renne, P.R., and Ludwig, K.R., 2000, A test for systematic errors in  $^{40}\text{Ar}/^{39}\text{Ar}$  geochronology through comparison with U-Pb analysis of a 1.1 Ga rhyolite: *Geochimica et Cosmochimica Acta*, v. 64, p. 73-98.
- Miyashiro, A., 1973, *Metamorphism & metamorphic belts*: London, George, Allen & Unwin.
- Möller, A., Appel, P., Mezger, K., and Schenk, V., 1995, Evidence for a 2 Ga subduction zone; eclogites in the Usagaran Belt of Tanzania: *Geology (Boulder)*, v. 23, p. 1067-1070.
- Möller, A., Mezger, K., and Schenck, V., 2000, U-Pb dating of metamorphic minerals: Pan-African metamorphism and prolonged slow cooling of granulites in Tanzania, East Africa, *Precambrian Research*, v. 104, p. 123-146.
- Möller, A., Mezger, K., and Schenk, V., 1998a, Crustal age domains and the evolution of the continental crust in the Mozambique belt of Tanzania: combined Sm-Nd, Rb-Sr, and Pb-Pb isotopic evidence.: *Journal of Petrology*, v. 39, p. 749-783.
- , 1998b, Crustal Age Domains and the Evolution of the Continental Crust in the Mozambique Belt of Tanzania: combined Sm-Nd, Rb-Sr, and Pb-Pb Isotopic Evidence: *Journal of Petrology*, v. 39, p. 749-783.
- Moyen, J.-F., Stevens, G., and Kisters, A., 2006, Record of mid-Archaean subduction from metamorphism in the Barberton terrain, South Africa: *Nature*, v. 442, p. 559-562.
- Mruma, A.H., 1989a, Stratigraphy, metamorphism and tectonic evolution of the Early Proterozoic Usagaran Belt, Tanzania.: *Res Terrae*, v. Ser A, p. 193.
- , 1989b, Stratigraphy, Metamorphism and Tectonic Evolution of the Early Proterozoic Usagaran Belt, Tanzania: Finland, University of Oulu.
- , 1995, Stratigraphy and palaeodepositional environment of the Palaeoproterozoic volcano-sedimentary Konse Group in Tanzania: *Journal of African Earth Sciences*, v. 21, p. 281-290.
- Nanyaro, J.T., Basu, N.K., Muhongo, S.M., Mruma, A.H., Djare, S.A., Mwakalukwa, G.L., Mduma, I., Mudiguza, K.M., Van Straaten, P., Klerkx, J., Theunissen, K., and Liégeois, J.P., 1983, UNESCO geotraverse. Structural evolution of the Ubendian Belt: preliminary results of a traverse between Karema and Mpanda (Tanzania), Rapport annuel: Tervuren (Belgium), Department de Geologie et de Mineralogie du Musee Royal de l'Afrique Centrale.
- Nemchin, A.A., Pidgeon, R.T., and Whitehouse, M.J., 2006, Re-evaluation of the origin and evolution of >4.2 Ga zircons from the Jack Hills metasedimentary rocks: *Earth and Planetary Science Letters*, v. 244, p. 218-233.
- Newton, R.C., 1986, Metamorphic temperatures and pressures of Group B and C eclogites., in Evans, B.W., and Brown, E.H., eds., *Blueschists and eclogites*, Volume 164, Memoir (Geological Society of America), p. 17-30.
- O'Brien, P.J., 2008, Challenges in high-pressure granulite metamorphism in the era of pseudosections: reaction textures, compositional zoning and tectonic interpretation with examples from the Bohemian Massif: *Journal of Metamorphic Geology*, v. 26, p. 235-251.
- O'Brien, P.J., and Rötzler, J., 2003, High-pressure granulites: formation, recovery of peak conditions and implications for tectonics.: *Journal of Metamorphic Geology*, v. 12, p. 3-20.
- Okay, A.I., 1989, An exotic eclogite/blueschist slice in a Barrovian-style metamorphic terrain, Alanya Nappes, Southern Turkey: *Journal of Petrology*, v. 30, p. 107-132.
- Oliver, G.J.H., Johnson, S.P., Williams, I.S., and Herd, D.A., 1998, Relict 1.4 Ga oceanic crust in the Zambesi Valley, northern Zimbabwe: evidence for the Mesoproterozoic supercontinental fragmentation: *Geology*, v. 26, p. 571-573.
- Parkinson, C.D., 2000, Coesite inclusions and prograde compositional zonation of garnet in whiteschist of the HP-UHPM Kokchatev massif, Kazakhstan: a record of progressive UHP metamorphism.: *Lithos*, v. 52, p. 215-233.
- Patchett, P.J., Kuovo, O., Hedge, C.E., and Tatsumoto, M., 1981, Evolution of continental crust and mantle heterogeneity: evidence from Hf isotopes: *Contributions to Mineralogy and Petrology*, v. 78.
- Pearson, N.J., Griffin, W.L., and O'Reilly, S.Y., 2008, Mass fractionation correction in laser ablation-multiple collector ICP-MS: implications for overlap corrections and precise and accurate in situ isotope ratio measurement, in Sylvester, P., ed., *Laser-Ablation-ICP-MS in the Earth Sciences: Current Practices and Outstanding*. Mineralogical Association of Canada Short Course 40 Vancouver, B.C., Mineralogical Association of Canada, p. 93-116.

- Percival, 1992, Archean high-grade metamorphism, in Condie, K.C., ed., Archean crustal evolution, Volume 11: Amsterdam, Elsevier, p. 357-411.
- Pidgeon, R.T., 1992, Recrystallisation of oscillatory-zoned zircon: some geochemical and petrological implications: Contributions to Mineralogy and Petrology, v. 110, p. 463-472.
- Pidgeon, R.T., Nemchin, A.A., and Hatcher, G.J., 1998, Internal structures of zircons from Archean granites from the Darling Range batholith: implications for zircon stability and the interpretation of zircon U-Pb ages: Contributions to Mineralogy and Petrology, v. 132, p. 288-299.
- Pinna, P., Cocherie, A., Thieblemont, D., Jezequell, P., and Kayogoma, E., 1999, The Archean evolution of the Tanzanian Craton (2.93-2.53 Ga); , 11th international conference of the Geological Society of Africa; Earth resources for Africa.
- Pinna, P., Muhongo, S., Mchard, B.A., Le Goff, E., Deschamps, Y., Ralay, F., Milesi, J.P., Henry, C., Vinauger, P., and Chene, F., 2004, Geology and Mineral Map of Tanzania, BRGM.
- Pisarevsky, S.A., Wingate, M.T.D., Powell, C.M., Johnson, S.P., and Evans, D.A.D., 2003, Models of Rodinia assembly and fragmentation. , in Yoshida, M., Windley, B., F., and Dasgupta, S., eds., Proterozoic East Gondwana: supercontinent assembly and breakup, Volume Special Publication 206: London, Geological Society of London, p. 35-55.
- Platt, J.P., 1993, EXHUMATION OF HIGH-PRESSURE ROCKS - A REVIEW OF CONCEPTS AND PROCESSES: Terra Nova, v. 5, p. 119-133.
- Pohl, W., 1994, Kibaran (mid-Proterozoic) metatolony in Central and Southern Africa: Ore Geology Reviews, v. 9, p. 105-130.
- Priem, H.N.A., Boelrijk, N.A.I.M., Hebeda, E.H., Verdurmen, E.A.T., and Verschure, R.H., 1979, Isotopic age determinations on granitic and gneissic rocks from the Ubendian-Usagaran system in southern Tanzania: Precambrian Research, v. 9, p. 227-239.
- Proyer, A., 2003, The preservation of high-pressure rocks during exhumation: metagranites and metapelites: Lithos, v. 70, p. 183-194.
- Quennel, A.M., McKinley, A.C.M., and Aitken, W.F., 1956, Summary of the Geology of Tanganyika, Geological Survey of Tanganyika Memoirs, Volume 1(2): Dodoma, p. 264.
- Racek, N., Štípska, P., and Powell, R., 2008, Garnet-clinopyroxene intermediate granulites in the St. Leonhard massif of the Bohemian Massif: ultrahigh-temperature metamorphism or not?: Journal of Metamorphic Geology, v. 26, p. 253-271.
- Rainaud, C., 2003, A cryptic Mesoarchean terrane in the basement to the central African Copperbelt: Journal of the Geological Society London, v. 160, p. 11-14.
- Rainaud, C., Armstrong, R.A., Master, S., Robb, L.J. & Mumba, P.A.C.C., 2002, Contributions to the geology and mineralization of the Central African Copperbelt: I. Nature and geochronology of the pre-Katangan basement., 11th IAGOD Quadrennial Symposium and Geocongress: Windhoek, Namibia, Geological Survey of Namibia, p. 1427-1430.
- Rainaud, C., Master, S., Armstrong, R.A., and Robb, L.J., 2005, Geochronology and nature of the Palaeoproterozoic basement in the Central African Copperbelt (Zambia and the Democratic Republic of Congo), with regional implications, Recent advances in the geology and mineralization of the Central African Copperbelt dedicated to the memory and work of Henri Ali Basira Kampunzu.
- Rainaud, C.L., Armstrong, R.A., Master, S., and Robb, L.J., 1999, A fertile Palaeoproterozoic magmatic arc beneath the Central African Copperbelt, in Stanley, C.J., ed., Mineral Deposits: Processes to processing: London, Balkema, p. 1427-1430.
- Rainbird, R.H., Lehman, L.M., and Young, G., 1992, Sampling Laurentia: detrital zircon evidence offers evidence for an extensive Neoproterozoic river system originating from the Grenville orogen: Geology, v. 20, p. 324-354.
- Rainbird, R.H., McNicoll, V.J., Theriault, R.J., Heaman, L.M., Abbott, J.G., Long, D.G.F., and Thorkelson, D.J., 1997, Pan-continental river system draining Grenville Orogen recorded by U-Pb and Sm-Nd geochronology of Neoproterozoic quartz arenites and mudrocks, Northwestern Canada: Journal of Geology, v. 105, p. 1-17.
- Rammlmair, D., Hühndorf, A., Borg, G., and Hiza, G.N., 1990, Nouvelles datations isotopiques des granites et des gabbros de la region "greenstone"-granites du Sukumaland, N.W.-Tanzania 15th colloquium of African Geology (abstract volume) Nancy, p. 43.
- Ravna, E.J.K., and Terry, M.P., 2004, Geothermobarometry of UHP and HP eclogites and schists - an evaluation of equilibria among garnet-clinopyroxene-kyanite-phengite-coesite/quartz: Journal of Metamorphic Geology, v. 22, p. 579-592.
- Ray, G.E., 1974, The structural and metamorphic geology of northern Malawi: Journal of the Geological Society London, v. 130, p. 427-440.
- Reddy, S.M., Collins, A.S., and Buchan, C., 2004a, Structural and temporal framework of Palaeoproterozoic eclogites; Usagaran Orogen, Tanzania, in McPhie, J., and McGoldrick, P., eds., Dynamic Earth; past, present and future., Geological Society of Australia. Sydney, N.S.W., Australia. 2004.
- Reddy, S.M., Collins, A.S., Buchan, C., and Mruma, A., 2004b, Heterogeneous excess argon and Neoproterozoic heating in the Usagaran Orogen, Tanzania, revealed by single grain  $^{40}\text{Ar}/^{39}\text{Ar}$  thermochronology: Journal of African Earth Sciences, v. 39, p. 165-176.
- Reddy, S.M., Collins, A.S., Buchan, C., and Mruma, A.H., 2004c, Heterogeneous excess argon and Neoproterozoic heating in the Usagaran Orogen, Tanzania, revealed by single grain  $^{40}\text{Ar}/^{39}\text{Ar}$  thermochronology: Journal of African Earth Sciences, v. 39, p. 165-176.
- Reddy, S.M., Collins, A.S., and Mruma, A., 2003, Complex high-strain deformation in the Usagaran Orogen, Tanzania: structural setting of Palaeoproterozoic eclogites.: Tectonophysics, v. 375, p. 101-123.
- Reddy, S.M., Wheeler, J., and Cliff, R.A., 1999, The geometry and timing of orogenic extension: an

- example from the Western Italian Alps: *Journal of Metamorphic Geology*, v. 17, p. 573-589.
- Renne, P.R., Mundil, R., Balco, G., Min, K., and Ludwig, K.R., 2010, Joint determination of 40K Decay constants and 40Ar\*/39K for the Fish Canyon sanidine standard, and improved accuracy for 40Ar/39Ar geochronology: *Geochimica et Cosmochimica Acta*, v. 74, p. 5349-5367.
- Richter, F.M., 1985, Models for the Archean thermal regime: *Earth and Planetary Science Letters*, v. 68, p. 471-484.
- Riggs, N.R., Lehman, T.M., Gehrels, G.E., and Dickinson, W.R., 1996, Detrital zircon link between headwaters and terminus of the Upper Triassic Chinle-Dockum paleoriver system: *Science*, v. 272, p. 97-100.
- Ring, U., Kroener, A., and Toulkeridis, T., 1997, Palaeoproterozoic granulite-facies metamorphism and granitoid intrusions in the Ubendian-Usagaran Orogen of northern Malawi, east-central Africa: *Precambrian Research*, v. 85, p. 27-51.
- Ring, U., Kröner, A., Buchwaldt, R., Toulkeridis, T., and Layer, P.W., 2002, Shear-zone patterns and eclogite-facies metamorphism in the Mozambique belt of northern Malawi, east-central Africa: implications for the assembly of Gondwana.: *Precambrian Research*, v. 116, p. 19-56.
- Ring, U., Kröner, A., Layer, P., Buchwaldt, R., and Toulkeridis, T., 1999, Deformed A-type granites in northern Malawi, east-central Africa: pre- or syntectonic: *Journal of the Geological Society London*, v. 156, p. 695-714.
- Ringwood, A.E., and Green, D.H., 1966, An experimental investigation of gabbro-eclogite transformation and some geophysical implications: *Tectonophysics*, v. 3, p. 383.
- Robl, J., Hergarten, S., Stuwe, K., and Hauzenberger, C., 2007, THERMAL HISTORY: a new software to interpret diffusive zoning profiles in garnet: *Computers & Geosciences*, v. 33.
- Rubatto, D., 2002, Zircon trace element geochemistry: partitioning with garnet and the link between U-Pb ages and metamorphism: *Chemical Geology*, v. 184, p. 123-138.
- Rubatto, D., and Hermann, J., 2001, Exhumation as fast as subduction?: *Geology*, v. 29, p. 3-6.
- Rubie, D.C., 1986, The catalysis of mineral reactions by water and restrictions on the presence of aqueous fluid during metamorphism: *Mineralogical Magazine*, v. 50, p. 399-415.
- Schandelmeier, H., 1983, The geochronology of post-Ubendian granitoids and dolerites from the Mambwe area, Northern Province, Zambia, Report Institute Geological Sciences, Volume 83, p. 40-46.
- Scherer, E., Munker, C., and Mezger, K., 2001, Calibration of the lutetium-hafnium clock: *Science*, v. 293, p. 683-687.
- Scherer, E.E., Whitehouse, M.J., and Münker, C., 2007, Zircon as a monitor of crustal growth: *Elements*, v. 3, p. 19-24.
- Schmadicke, E., Okrusch, M., and Schmidt, W., 1992, Eclogite-facies rocks in the Saxonian Erzgebirge, Germany - high-pressure metamorphism under contrasting P-T conditions: *Contributions to Mineralogy and Petrology*, v. 110, p. 226-241.
- Schmitz, M.D., Vervoort, J.D., Bowring, S.A., and Patchett, P.J., 2002, Decoupling of the Lu-Hf and Sm-Nd isotopic systems in granulitic lower crust beneath southern Africa: *Geochimica et Cosmochimica Acta*, v. 66, p. A682-A682.
- Schulmann, K., Kroner, A., Hegner, E., Wendt, I., Konopasek, J., Lexa, O., and Stipska, P., 2005, Chronological constraints on the pre-orogenic history, burial and exhumation of deep-seated rocks along the eastern margin of the Variscan Orogen, Bohemian Massif, Czech Republic: *American Journal of Science*, v. 305, p. 407-448.
- Selway, K., Brick, R.A., Collins, A.S., Hand, M., Momburi, P.B., and Heinson, G., unpub, Magnetotelluric Transect Through the Tanzania Craton-Usagaran Orogen Boundary: Adelaide, University of Adelaide.
- Selway, K., Heinson, G., and Hand, M., 2006a, Electrical evidence of continental accretion: steeply-dipping crustal-scale conductivity contrast: *Geophysical Research Letters*, v. 33.
- Selway, K.M., Hand, M., Heinson, G., and Payne, J., 2006b, Magnetotelluric constraints on subduction polarity: turning reconstruction models for Proterozoic Australia back to front: *Geology*.
- Shellnutt, J.G., Wang, C.Y., Zhou, M.-F., and Yang, Y., 2009, Zircon Lu-Hf isotopic compositions of metaluminous and peralkaline A-type granitic plutons of the Emeishan large igneous province (SW China): constraints on the mantle source: *Journal of Asian Earth Sciences*, v. 35, p. 45-55.
- Sizova, E., Gerya, T.V., Brown, M., and Perchuk, L.L., 2010, Subduction styles in the Precambrian; insight from numerical experiments: *Lithos*, v. 116, p. 209-229.
- Sklyarov, E., Theunissen, K., Melnikov, A., Klerkx, J., Gladkochub, D.P., and Mruma, A., 1997, Paleoproterozoic eclogites of the Ubende Belt (Tanzania), in Anonymous, ed., Fifth international eclogite conference; abstracts., Volume 1: Terra Abstracts. 9, Suppl: Oxford, International, Blackwell Scientific Publications, p. 35.
- Sklyarov, E.V., Theunissen, K., Melnikov, A.I., Klerkx, J., Gladkochub, D.P., and Mruma, A., 1998, Paleoproterozoic eclogites and garnet pyroxenites of the Ubende Belt (Tanzania), in Anonymous, ed., IEC 97; Fifth international eclogite conference., Volume 78; 2: Schweizerische Mineralogische und Petrographische Mitteilungen = Bulletin Suisse de Mineralogie et Petrographie: Zurich, Switzerland, Staebli Verlag AG, p. 257-271.
- Slabunov, A.I., Volodichev, O.I., Bibikova, E.V., Shchipansky, A.A., Stepanov, V.S., and Konilov, A.N., 2003, Archean ophiolitic sequences and eclogites of the Baltic/Fennoscandian Shield, EGS - AGU - EUG Joint Assembly: Nice, France.
- Smulikowski, 1964, In: *Stern* 1996.
- Snoeyenbos, D.R., Williams, M.L., and Sanmer, S., 1995, Archean high-pressure metamorphism in the western Canadian Shield.: *European Journal of Mineralogy*, v. 7, p. 1251-1272.



- Sommer, H., Kroner, A., Hauzenberger, C., and Muhongo, S., 2005a, Reworking of Archaean and Palaeoproterozoic crust in the Mozambique belt of central Tanzania as documented by SHRIMP zircon geochronology: *Journal of African Earth Sciences*, v. 43, p. 447-463.
- Sommer, H., Kroner, A., Muhongo, S., and Hauzenberger, C., 2005b, SHRIMP zircon ages for post-Usagaran granitoid and rhyolitic rocks from the Palaeoproterozoic terrain of southwestern Tanzania: *South African Journal of Geology*, v. 108, p. 247-256.
- Songnian, L., Chunliang, Y., Huaikun, L., and Humin, L., 2002, A group of rifting events in the terminal Paleoproterozoic in the North China Craton.: *Gondwana Research*, v. 5, p. 123-131.
- Spear, F.S., 1991, On the interpretation of peak metamorphic temperatures in light of garnet diffusion during cooling: *Journal of Metamorphic Geology*, v. 9, p. 379-388.
- , 1995, Metamorphic phase equilibria and pressure-temperature-time paths: Washington, Mineralogical Society of America, 799 p.
- Spear, F.S., Kohn, M.J., Florence, F.P., and Menard, T., 1990, A model of garnet and plagioclase growth in pelitic schists: implications for thermobarometry and P-T path determination: *Journal of Metamorphic Geology*, v. 8, p. 683-696.
- Steiger, R.H., and Jäger, E., 1977, Subcommittee on geochronology: convention on the use of decay constants in geo- and cosmochronology. : *Earth and Planetary Science Letters*, v. 36, p. 359-362.
- Stern, R.J., 1994a, Arc assembly and continental collision in the Neoproterozoic East-African orogen - implications for the consolidation of Gondwanaland: *Annual Review of Earth and Planetary Sciences*, v. 22, p. 319-351.
- , 1994b, Arc Assembly and Continental Collision in the Neoproterozoic East African Orogen: Implications for the Consolidation of Gondwanaland: *Annual Reviews Earth Planetary Sciences*, v. 22, p. 319-351.
- , 2005a, Evidence from ophiolites, blueschists, and ultrahigh-pressure metamorphic terranes that the modern episode of subduction tectonics began in Neoproterozoic time: *Geology*, v. 33, p. 557-560
- , 2005b, Evidence from ophiolites, blueschists, and ultrahigh-pressure metamorphic terranes that the modern episode of subduction tectonics began in Neoproterozoic time.: *Geology*, v. 33, p. 557-560.
- Štípska, P., P., P., and Powell, R., 2006a, Separate or shared metamorphic histories of eclogites and surrounding rocks? An example from the Bohemian Massif: *Journal of Metamorphic Geology*, v. 24, p. 219-240.
- Štípska, P., Pitra, P., and Powell, R., 2006b, Separate or shared metamorphic histories of eclogites and surrounding rocks? An example from the Bohemian Massif: *Journal of Metamorphic Geology*, v. 24, p. 219-240.
- Štípska, P., and Powell, R., 2005, Constraining the P-T path of a MORB-type eclogite using pseudosections, garnet zoning and garnet-clinopyroxene thermometry: an example from the Bohemian Massif: *Journal of Metamorphic Geology*, v. 23, p. 725-743.
- Stipska, P., Schulmann, K., and Powell, R., 2008, Contrasting metamorphic histories of lenses of high-pressure rocks and host migmatites with a flat orogenic fabric (Bohemian Massif, Czech Republic): a result of tectonic mixing within horizontal crustal flow?: *Journal of Metamorphic Geology*, v. 26, p. 623-646.
- Storey, C.D., Brewer, T.S., and Parrish, R.R., 2003, Grenvillian age decompression of eclogites in the Glenelg-Attadale inlier, NW Scotland: *Geophysical Research Abstracts*, v. 5, p. 06080.
- Sutton, J., Watson, J., and James, T.C., 1954, Metamorphic rocks of Karema and Kungwe Bay, western Tanganyika, Tanganyika Geological Survey Department.
- Tack, L., De Paepe, P., Liegeois, J.P., Nimpagaritse, G., Ntugicimpaye, A., and Midente, G., 1990, Kibaran magmatism in Burundi: *Journal of African Earth Sciences*, v. 10, p. 733-738.
- Tack, L., Fernandez-Alonso, M., Tahon, M., Wingate, M.T.D., and Barritt, S., 2002, The "northeastern Kibaran belt" (NKB) and its mineralisations reconsidered: new constraints from a revised lithostratigraphy, a GIS compilation of existing geological maps and a review of recently published as well as unpublished igneous emplacement ages in Burundi, 11th IAGOD Quadrennial Symposium and Geocongress: Windhoek, Namibia, Geological Survey of Namibia, p. 6.
- Tack, L., Liegeois, J.P., Deblond, A., and Duchesne, J.C., 1994, Kibaran A-type granitoids and mafic rocks generated by two mantle sources in a late orogenic setting (Burundi): *Precambrian Research*, v. 68, p. 323-356.
- Tikoff, B., and Greene, D., 1997, Stretching lineations in transpressional shear zones: and example from the Sierra Nevada Batholith, California: *Journal of Structural Geology*, v. 19, p. 29-39.
- Timmerman, H., Štedra, V., Gerdes, A., Noble, S.R., Parrish, R.R., and Dörr, W., 2004, The problem of dating high-pressure metamorphism: a U-Pb isotope and geochemical study on eclogites and related rocks of the Mariánské Lázně Complex, Czech Republic.: *Journal of Petrology*, v. 45, p. 1311-1338.
- Timmermann, H., Štedra, V., Gerdes, A., Noble, S.R., Parrish, R.R., and Dörr, W., 2004, The problem of dating high-pressure metamorphism: a U-Pb isotope and geochemical study on eclogites and related rocks of the Mariánské Lázně Complex, Czech Republic: *Journal of Petrology*, v. 45, p. 1311-1338.
- Tracey, R.J., Robinson, P., and Thomas, A.B., 1976, Garnet composition and zoning in the determination of temperature and pressure of metamorphism, central Massachusetts: *American Mineralogist*, v. 61, p. 767-775.
- Tropper, P., Deibl, I., Finger, F., and Kaindl, R., 2006, P-T-t evolution of spinel-cordierite-garnet gneisses from the Sauwald Zone (Southern Bohemian Massif, Upper Austria): is there evidence for two independent late-Variscan low-P/high-T events in the Moldanubian Unit?: *International Journal of Earth Sciences*, v. 95, p. 1019-1037.

- Tsujimori, T., Matsumoto, K., Wakabayashi, J., and Liou, J.G., 2006, Franciscan eclogite revisited: reevaluation of the P-T evolution of tectonic blocks from Tiburon Peninsula, California, U.S.A.: *Mineralogy and Petrology*, v. 88, p. 243-267.
- Tuisku, P., and Huhma, H., 1998, Eclogite from the SW-marginal zone of the Lapland Granulite belt: evidence from the 1.90-1.88 Ga subduction zone., *in* Hanski, E., and Vuollo, J., eds., *International Ophiolite Symposium and Field Excursion: Generation and emplacement of ophiolites through time: Oulo, Finland*, Geological Survey of Finland, p. 61.
- Turner, G., Huneke, J.C., Podosec, F.A., and Wasserburg, G.J., 1971,  $^{40}\text{Ar}/^{39}\text{Ar}$  ages and cosmic ray exposure ages of Apollo 14 sample: *Earth and Planetary Science Letters*, v. 12, p. 19-15.
- Van Achterbergh, E., Ryan, C.G., Jackson, S.E., and Griffin, W.L., 2001, Data reduction software for LA-ICPMS: Appendix, *in* Sylvester, P.J., ed., *Laser ablation-ICP-mass spectrometry in the Earth Sciences: principles and applications*, Volume 29, Mineralogical Association of Canada, p. 239-243.
- Vavra, G., Schmid, R., and Gebaur, D., 1999, Internal morphology, habit and U-Th -Pb microanalysis of amphibolite-to-granulite facies zircons: geochronology of the Ivrea Zone (Southern Alps): *Contributions to Mineralogy and Petrology*, v. 134, p. 380-404.
- Versmeech, P., 2004, How many grains are needed for a provenance study? : *Earth and Planetary Science Letters*, v. 224, p. 351-441.
- Vervoort, J., D., and Blichert-Toft, J., 1999, Evolution of the depleted mantle: Hf isotopic evidence from juvenile rocks through time: *Geochimica et Cosmochimica Acta*, v. 63, p. 533-556.
- Vogt, M., Kröner, A., Poller, U., Sommer, H., Muhongo, S., and Wingate, M.T.D., 2006, Archaean and Palaeoproterozoic gneisses reworked during a Neoproterozoic (Pan-African) high-grade event in the Mozambique belt of East Africa: structural relationships and zircon ages from the Kidatu area, central Tanzania: *Journal of African Earth Sciences*, v. 45, p. 139-155.
- Volodichev, O.I., 1977, Metamorphic evolution of the polycyclic Belomorian Complex, Recurrence and direction of regional metamorphism: *Leningrad, Nauka*, p. 57-79.
- , 1990, Belomorian complexes of Karelia: *Leningrad, Nauka*.
- , 1997, Geological and petrological traces of the subduction stage of Belomorian Collision Structure in the Late Archean, *International Conference "Belomorian Mobile Belt": Petrozavodsk*, p. 23-24.
- Volodichev, O.I., Slabunov, A.I., Bibikova, E.V., Konilov, A.N., and Kuzenko, T.I., 2004, Archean eclogites in the Belomorian mobile belt, Baltic shield.: *Petrology*, v. 12, p. 540-560.
- Wade, B.P., Hand, M., Maidment, D.W., Close, D.F., and Scrimgeour, I.R., 2008, Origin of metasedimentary and igneous rocks from the Entia Dome, eastern Arunta region, central Australia: a U-Pb LA-ICPMS, SHRIMP and Sm-Nd isotope study: *Australian Journal of Earth Sciences*, v. 55, p. 703-719.
- Walsh, E.O., and Hacker, B.R., 2004, The fate of subducted continental margins: two stage exhumation of the high-pressure to ultrahigh-pressure Western Gneiss REgion, Norway: *Journal of Metamorphic Geology*, v. 22, p. 671-687.
- Wark, D.A., and Watson, E.B., 2006, TitaniQ: a titanium-in-quartz geothermometer: *Contributions to Mineralogy and Petrology*, v. 152, p. 743-754.
- Watson, E.B., Hayden, L.A., Wark, D.A., Cherniak, D.J., Thomas, J.B., and Manchester, J.E., 2006a, New crystallisation thermometers for zircon, rutile and sphene: calibrations, diffusion considerations, and applications., *Geological Society of America, Volume 38*, Geological Society of America, p. 5.
- Watson, E.B., Wark, D.A., and Thomas, J.B., 2006b, Crystallization thermometers for zircon and rutile *Contributions to Mineralogy and Petrology*, v. 151, p. 413-433.
- Wei, C., and Powell, R., 2006, Calculated phase relations in the system NCKFMASH ( $\text{Na}_2\text{O}-\text{CaO}-\text{K}_2\text{O}-\text{FeO}-\text{MgO}-\text{Al}_2\text{O}_3-\text{SiO}_2-\text{H}_2\text{O}$ ) for high-pressure metapelites.: *Journal of Petrology*, v. 47, p. 385-408.
- Wei, C.J., Li, Y.J., Yu, Y., and Zhang, J.S., 2010, Phase equilibria and metamorphic evolution of glaucophane-bearing UHP eclogites from the Western Dabieshan Terrane, Central China: *Journal of Metamorphic Geology*, v. 28, p. 647-666.
- Weidenback, M., Alle, P., Corfu, F., Griffin, W.L., Meier, M., Oberli, F., Von Quadt, A., Roddick, J.C., and Spiegel, W., 1995, Three natural standards for U-Th-Pb, Lu-Hf, trace element and REE analyses: *Geostandards Newsletter*, v. 19, p. 1-24.
- Weidenback, M., Hanchar, J.M., Peck, W.H., Sylvester, P., Valley, J.W., Whitehouse, M., Kronz, A., Mirshita, Y., and Nasdala, L., 2004, Further characterisation of the 91500 zircon crystal: *Geostandards and Geoanalytical Research*, v. 28, p. 9-39.
- Wendt, I., Besang, C., Harre, W., Kreuzer, H., Lenz, H., and Müller, P., 1972, Age determinations of granitic intrusions and metamorphic events in the early Precambrian of Tanzania., *International Geological Congress: Montreal*, p. 295-314, section 1.
- Whittingham, J.K., 1959, *The geology of the Nyanzwa Area*, 58 p.
- Wilde, S.A., Valley, J.W., Peck, W.H., and Graham, C.M., 2001, Evidence from detrital zircons for the existence of continental crust and oceans on the Earth 4.4 Ga ago: *Nature*, v. 409, p. 175-178.
- Williams, H., Hoffman, P.F., Lewry, J.F., Monger, J.W.H., and Rivers, T., 1991, *Anatomy of North America: thematic geologic portrayals of the continent: Tectonophysics*, v. 187, p. 117-134.
- Williams, I.S., Buick, I.S., and Cartwright, I., 1996, An extended episode of early Mesoproterozoic metamorphic fluid flow in the Reynolds Range, central Australia: *Journal of Metamorphic Geology*, v. 14, p. 29-47.
- Williams, M.L., Hanmer, S., Kopf, C., and Darrach, M., 1995, Syntectonic generation and segregation of tonalitic melts from amphibolite dikes in the lower crust, Striding-Athabasca mylonite zone, North

- Saskatchewan: *Journal of Geophysical Research-Solid Earth*, v. 100, p. 15717-15734.
- Williams, M.L., Melis, E.A., Kopf, C.F., and Hanmer, S., 2000, Microstructural tectonometamorphic processes and the development of gneissic layering: a mechanism for metamorphic segregation: *Journal of Metamorphic Geology*, v. 18, p. 41-57.
- Windley, B.F., and Garde, A.A., 2009, Arc-generated blocks with crustal sections in the North Atlantic craton of West Greenland: crustal growth in the ARchaeon with modern analogues: *Earth Science Reviews*, v. 93, p. 1-30.
- Winslow, D.M., Chamberlain, C.P., and Zeitler, P.K., 1995, Metamorphism and melting of the lithosphere due to rapid denudation, Nanga Parbat Massif, Himalaya: *Journal of Geology*, v. 103, p. 395-409.
- Wirth, K.R., Vervoort Jeffrey, D., Weisberger, B., and Anonymous, 2004a, Origin and evolution of the Kilimafedha greenstone belt, eastern Tanzania Craton; evidence from Nd and Pb isotopes.; Geological Society of America, 2004 annual meeting.
- Wirth, K.R., Vervoot, J.D., and Weisberger, B., 2004b, Origin and evolution of the Kilimafedha greenstone belt, eastern Tanzania Craton: evidence from Pb isotopes: Geological Society of America Abstracts with Programs, v. 36.
- Wordsworth, G.J., 1977, Homogenization of zoned garnets from pelitic schists: *Canadian Mineralogist*, v. 15, p. 230-242.
- Xiao, Y.L., Hoefs, J., Van den Kerkhof, A.M., and Li, S.G., 2001, Geochemical constraints of the eclogite and granulite facies metamorphism as recognized in the Raobazhai complex from North Dabie Shan, China: *Journal of Metamorphic Geology*, v. 19, p. 3-19.
- Yardley, 1977, An empirical study of diffusion in garnet: *American Mineralogist*, v. 62, p. 793-800.
- Zack, T., and Luvizottow, G., 2006, Application of rutile thermometry to eclogites: *Mineralogy and Petrology*, v. 88, p. 69-85.
- Zeh, A., Gerdes, A., Klemm, R., and Barton Jr., J.M., 2008, U-Pb and Lu-Hf isotope record of detrital zircon grains from the Limpopo Belt - evidence for crustal recycling at the Hadean to early-Archean transition: *Geochimica et Cosmochimica Acta*, v. 72, p. 5304-5329.
- Zhang, J.X., Yang, J.S., Mattinson, C.G., Xu, Z.Q., Meng, F.C., and Shi, R.D., 2005a, Two contrasting eclogite cooling histories, North Qaidam HP/UHP terrane, western China: petrological and isotopic constraints: *Lithos*, v. 84, p. 51-76.
- Zhang, Z., Xiao, Y., Liu, F., Liou, J.G., and Hoefs, J., 2005b, Petrogenesis of UHP metamorphic rocks from Qinglongshan, southern Sulu, east-central China: *Lithos*, v. 81, p. 189-207.
- Zhang, Z.M., Shen, K., Wang, J.L., and Dong, H.L., 2009, Petrological and geochronological constraints on the formation, subduction and exhumation of the continental crust in the southern Sulu orogen, eastern-central China: *Tectonophysics*, v. 475, p. 291-307.
- Zhao, G., Cawood, P.A., Wilde, S.A., and Lu, L., 2001, High-pressure granulites (retrograded eclogites) from the Hengshan Complex, North China Craton: petrology and tectonic implications.: *Journal of Petrology*, v. 42, p. 1141-1170.
- Zhao, G., Cawood, P.A., Wilde, S.A., Sun, M., and Lu, L., 2000, Metamorphism of basement rocks in the Central Zone of the North China Craton: implications for Paleoproterozoic tectonic evolution.: *Precambrian Research*, v. 103, p. 55-88.

Appendix 1, Chapter 2 Table 1. U-Pb analytical results for Albidon Ltd sample analysed at GEMOC.

Zircon No.	Isotope Ratios - Common Pb corrected						Ages (Ma) - Common Pb corrected						Conc <sup>1</sup>
	<sup>207</sup> Pb/ <sup>206</sup> Pb	± 2s	<sup>207</sup> Pb/ <sup>235</sup> U	± 2s	<sup>206</sup> Pb/ <sup>238</sup> U	± 2s	<sup>207</sup> Pb/ <sup>206</sup> Pb	2σ	<sup>207</sup> Pb/ <sup>235</sup> U	2σ	<sup>206</sup> Pb/ <sup>238</sup> U	2σ	
ALBSONG-05													
AS05-94	0.07265	0.00200	1.68323	0.04592	0.16804	0.00364	1004	58	1002	18	1001	20	100
AS05-69	0.10954	0.00444	4.30476	0.15102	0.28502	0.00574	1792	76	1694	28	1617	28	95
AS05-46	0.1111	0.00332	4.67483	0.10800	0.30518	0.00580	1817	56	1763	20	1717	28	97
AS05-91	0.11127	0.00606	4.94507	0.24434	0.32232	0.00736	1820	102	1810	42	1801	36	99
AS05-76	0.1116	0.00474	4.61683	0.16930	0.30003	0.00640	1826	78	1752	30	1691	32	96
AS05-52	0.11248	0.00352	4.96378	0.11798	0.32007	0.00654	1840	58	1813	20	1790	32	99
AS05-10	0.11255	0.00322	4.92906	0.10714	0.31762	0.00592	1841	54	1807	18	1778	28	98
AS05-79	0.11262	0.00468	5.04436	0.18028	0.32485	0.00692	1842	78	1827	30	1813	34	99
AS05-65	0.11274	0.00294	4.7132	0.12472	0.30322	0.00666	1844	48	1770	22	1707	32	96
AS05-70	0.11308	0.00458	4.96045	0.16970	0.31815	0.00686	1849	74	1813	28	1781	34	98
AS05-09	0.11321	0.00248	5.04079	0.10246	0.32294	0.00604	1852	40	1826	18	1804	30	99
AS05-06	0.11339	0.00370	4.96223	0.12536	0.31738	0.00652	1855	60	1813	22	1777	32	98
AS05-83	0.11384	0.00310	4.76215	0.09394	0.30341	0.00568	1862	50	1778	16	1708	28	95
AS05-74	0.11409	0.00366	4.98044	0.12098	0.31661	0.00664	1866	60	1816	20	1773	32	97
AS05-104	0.11412	0.00252	5.23622	0.11028	0.33277	0.00646	1866	40	1859	18	1852	32	100
AS05-98	0.11421	0.00374	5.16424	0.13508	0.32794	0.00650	1868	60	1847	22	1828	32	99
AS05-55	0.11449	0.00390	5.13855	0.14416	0.32551	0.00630	1872	62	1843	24	1817	30	98
AS05-48	0.11515	0.00330	5.09047	0.14884	0.32063	0.00738	1882	52	1835	24	1793	36	98
AS05-03	0.11522	0.00260	5.37291	0.11962	0.33824	0.00694	1883	42	1881	20	1878	34	100
AS05-04	0.11531	0.00250	5.25028	0.10296	0.33026	0.00598	1885	40	1861	16	1840	28	99
AS05-02	0.11547	0.00250	5.43606	0.11516	0.34146	0.00684	1887	40	1891	18	1894	32	100
AS05-50	0.11551	0.00242	5.26795	0.10992	0.33079	0.00664	1888	38	1864	18	1842	32	99
AS05-41	0.11567	0.00264	5.31659	0.12126	0.33339	0.00690	1890	42	1872	20	1855	34	99
AS05-67	0.11565	0.00248	5.28848	0.11058	0.33168	0.00658	1890	40	1867	18	1847	32	99
AS05-89	0.11566	0.00266	5.44561	0.11962	0.3415	0.00674	1890	42	1892	18	1894	32	100
AS05-93	0.11566	0.00274	5.3823	0.12932	0.33753	0.00726	1890	44	1882	20	1875	34	100
AS05-80	0.11578	0.00252	5.35906	0.11222	0.33574	0.00662	1892	40	1878	18	1866	32	99
AS05-72	0.11584	0.00266	5.45229	0.12364	0.34139	0.00702	1893	42	1893	20	1893	34	100
AS05-73	0.11581	0.00314	5.4489	0.14996	0.34126	0.00774	1893	50	1893	24	1893	38	100
AS05-78	0.11622	0.00250	5.42761	0.11690	0.33874	0.00694	1899	40	1889	18	1881	34	99
AS05-86	0.11623	0.00254	5.09654	0.10708	0.31806	0.00622	1899	40	1836	18	1780	30	97
AS05-84	0.11631	0.00262	5.41826	0.12166	0.33789	0.00694	1900	42	1888	20	1877	34	99
AS05-90	0.11664	0.00252	5.47879	0.11178	0.34071	0.00654	1905	40	1897	18	1890	32	100
AS05-77	0.11721	0.00280	5.53941	0.12632	0.3428	0.00674	1914	44	1907	20	1900	32	100
AS05-58	0.12128	0.00282	5.81643	0.13228	0.34787	0.00706	1975	42	1949	20	1924	34	99
AS05-66	0.12141	0.00264	5.71212	0.11696	0.34128	0.00650	1977	40	1933	18	1893	32	98
AS05-63	0.12146	0.00286	5.70306	0.13480	0.34059	0.00712	1978	42	1932	20	1890	34	98
AS05-61	0.12445	0.00282	6.19948	0.13934	0.36133	0.00738	2021	42	2004	20	1988	34	99
AS05-53	0.12539	0.00268	6.45673	0.13588	0.3735	0.00746	2034	38	2040	18	2046	36	100
AS05-92	0.16971	0.00794	10.05654	0.41392	0.42976	0.00962	2555	80	2440	38	2305	44	95
AS05-85	0.17697	0.00412	12.4951	0.29118	0.51214	0.01076	2625	40	2642	22	2666	46	101
AS05-49	0.18162	0.00396	12.66475	0.26254	0.50578	0.00976	2668	36	2655	20	2639	42	100
AS05-88	0.18404	0.00588	12.21454	0.30170	0.48135	0.00978	2690	54	2621	24	2533	42	97
AS05-99	0.18439	0.00414	12.88682	0.27586	0.50691	0.00982	2693	38	2671	20	2643	42	99
AS05-62	0.18501	0.00430	12.09581	0.28518	0.47422	0.01006	2698	40	2612	22	2502	44	97
AS05-68	0.18607	0.00594	12.47507	0.29848	0.48625	0.01026	2708	54	2641	22	2554	44	98
AS05-54	0.18828	0.00400	13.27018	0.26950	0.51124	0.00990	2727	36	2699	20	2662	42	99
AS05-82	0.18828	0.00552	13.21142	0.28332	0.50892	0.01016	2727	50	2695	20	2652	44	99
AS05-97	0.19009	0.00440	13.3045	0.28376	0.50766	0.00950	2743	38	2702	20	2647	40	99
AS05-95	0.19936	0.00448	15.04535	0.31170	0.54738	0.01020	2821	38	2818	20	2814	42	100

**Appendix 1, Chapter 2 Table 2.** Lu-Hf analytical results Albidon Ltd sample analysed at GEMOC. Calculations of  $^{176}\text{Hf}/^{177}\text{Hf}(t)$ ,  $\epsilon\text{Hf}(t)$ ,  $T_{\text{DM}(\text{Ga})}$  and  $T_{\text{DM}(\text{crustal})}$  are based on the  $^{176}\text{Lu}$  decay constant =  $1.865 \times 10^{-11}$  (Scherer et al., 2001)

Zircon No.	$^{176}\text{Yb}/^{177}\text{Hf}$	$^{176}\text{Lu}/^{177}\text{Hf}$	$^{176}\text{Hf}/^{177}\text{Hf}$	$\pm 2\sigma$	$^{176}\text{Hf}/^{177}\text{Hf}(t)$	$\epsilon\text{Hf}(t)$	$\pm 2\sigma$	$T_{\text{DM}(\text{Ga})}$	$T_{\text{DM}(\text{crustal})}$
<b>ALBSONG-05</b>									
AS05-94	0.059620	0.001510	0.282380	0.000012	0.282351	7.34	0.42	1.25	1.40
AS05-69	0.022619	0.000645	0.281606	0.000010	0.281584	-2.12	0.3395	2.29	2.61
AS05-46	0.006212	0.000215	0.281412	0.000010	0.281405	-7.92	0.3465	2.52	3.00
AS05-76	0.039199	0.000940	0.281582	0.000011	0.281549	-2.57	0.385	2.34	2.67
AS05-52	0.010058	0.000285	0.281442	0.000014	0.281432	-6.42	0.49	2.48	2.93
AS05-79	0.013911	0.000449	0.281256	0.000014	0.281240	-13.19	0.49	2.75	3.35
AS05-65	0.051915	0.001176	0.281441	0.000017	0.281400	-7.47	0.595	2.54	2.99
AS05-70	0.010493	0.000314	0.281584	0.000013	0.281573	-1.21	0.455	2.30	2.60
AS05-83	0.039933	0.001342	0.281412	0.000020	0.281365	-8.32	0.7	2.60	3.06
AS05-74	0.273469	0.008009	0.282002	0.000020	0.281718	4.34	0.7	2.16	2.26
AS05-55	0.049917	0.001383	0.281586	0.000010	0.281537	-1.97	0.3395	2.36	2.67
AS05-48	0.039498	0.001019	0.281591	0.000012	0.281555	-1.12	0.42	2.33	2.62
AS05-03	0.008968	0.000269	0.281387	0.000009	0.281377	-7.39	0.329	2.56	3.02
AS05-02	0.028166	0.000725	0.281490	0.000007	0.281464	-4.22	0.231	2.45	2.82
AS05-50	0.013077	0.000371	0.281424	0.000011	0.281411	-6.09	0.385	2.51	2.94
AS05-67	0.034172	0.001016	0.281499	0.000014	0.281463	-4.20	0.49	2.45	2.82
AS05-89	0.033119	0.000928	0.281429	0.000010	0.281396	-6.58	0.3395	2.54	2.97
AS05-80	0.009874	0.000297	0.281409	0.000011	0.281398	-6.44	0.385	2.53	2.97
AS05-72	0.015327	0.000448	0.281381	0.000012	0.281365	-7.60	0.42	2.58	3.04
AS05-73	0.004780	0.000166	0.281308	0.000011	0.281302	-9.83	0.385	2.66	3.18
AS05-78	0.019268	0.000550	0.281418	0.000013	0.281398	-6.28	0.455	2.53	2.96
AS05-86	0.014624	0.000420	0.281430	0.000010	0.281415	-5.69	0.343	2.51	2.92
AS05-84	0.039178	0.001208	0.281602	0.000009	0.281558	-0.57	0.322	2.32	2.60
AS05-90	0.015854	0.000446	0.281457	0.000010	0.281441	-4.63	0.35	2.48	2.86
AS05-77	0.014104	0.000404	0.281415	0.000011	0.281400	-5.87	0.385	2.53	2.95
AS05-58	0.038893	0.001101	0.281467	0.000010	0.281426	-3.57	0.35	2.50	2.85
AS05-66	0.029774	0.000832	0.281540	0.000015	0.281509	-0.58	0.525	2.39	2.66
AS05-63	0.022525	0.000677	0.281589	0.000012	0.281564	1.39	0.42	2.31	2.54
AS05-61	0.017030	0.000460	0.281127	0.000010	0.281109	-13.76	0.35	2.92	3.53
AS05-53	0.031010	0.000828	0.281344	0.000017	0.281312	-6.27	0.595	2.65	3.07
AS05-92	0.012440	0.000352	0.281081	0.000011	0.281064	-3.13	0.385	2.97	3.27
AS05-85	0.052625	0.001340	0.281152	0.000017	0.281085	-0.76	0.595	2.95	3.17
AS05-49	0.008414	0.000231	0.281064	0.000010	0.281052	-0.92	0.35	2.99	3.21
AS05-88	0.015613	0.000459	0.281068	0.000010	0.281044	-0.69	0.35	3.00	3.22
AS05-99	0.038571	0.001141	0.281130	0.000013	0.281071	0.33	0.455	2.97	3.15
AS05-62	0.014960	0.000389	0.281099	0.000011	0.281079	0.72	0.385	2.95	3.13
AS05-68	0.038046	0.001086	0.281090	0.000010	0.281034	-0.66	0.35	3.02	3.23
AS05-54	0.012088	0.000360	0.281021	0.000011	0.281002	-1.34	0.385	3.05	3.29
AS05-82	0.006798	0.000226	0.281017	0.000010	0.281005	-1.23	0.336	3.05	3.28
AS05-97	0.007579	0.000228	0.281070	0.000008	0.281058	1.02	0.2695	2.98	3.15
AS05-95	0.031915	0.000877	0.281150	0.000010	0.281103	4.42	0.35	2.92	2.99



Chapter 5 - Table 1. Representative AX output file. File is for sample T01-22, peak assemblage

```

% thermocalc file (requires editing before use)
  phl      0.068      0.0107      ann      0.025      0.0057      east      0.058      0.0098
   py      0.0051      0.00158      gr      0.0017      0.00058      alm      0.30      0.023
spss      0.000058      0.0000240
  an      0.28      0.0218      ab      0.80      0.0201
  ilm      0.96      0.048      pnt      0.019      0.0043      geik      0.0070      0.0020
  mu      0.74      0.037      cel      0.0062      0.0027      fcel      0.0077      0.0034
  pa      0.10      0.0143
  ky      1.0
  q      1.0
H2O

% add your other end-members here
*

```

Chapter 5 -Table 2. Representative THERMOCALC output file. File is for sample T01-22, peak assemblage

```

calculation type :
  0 = table of thermodynamic data of end-members
  1 = phase diagram calculations
  2 = average pressure-temperature calculations
  3 = calculations on all reactions between end-members
  4 = list end-member names and compositions
control code : 2
data filename: suffix in 'tcd.txt' : t01-22
datafile being read: "tcdt01-22.txt"
reading phase info from this file ...
phl ann east py gr alm spss an ab ilm pnt geik mu cel fcel pa
ky q H2O
log output is in "tclog.txt"
main output is in the file, "tcot01-22.txt"
other (eg drawpd) output is in the file, "tcdr.txt"

THERMOCALC 3.26 running at 7.59 on Tue 28 Oct,2008, with
tcds55.txt produced at 19:29:59 on 22 Nov 2003 (with sigma fit = 1.067)

phl ann east py gr alm spss an ab ilm pnt
geik mu cel fcel pa ky q H2O
which end-members : (nothing input)

type of rock calculation:
  1 : average P
  2 : average T
  3 : average PT
code : 3

          phl      ann      east      py      gr      alm      spss      an      ab
ilm
  a  0.0680  0.0250  0.0580  0.00510  0.00170  0.300  5.80e-5  0.280  0.800
0.960
  sd(a)  0.0107  0.00570  0.00980  0.00158  0.000580  0.0450  4.50e-5  0.0218  0.0400
0.0480

          pnt      geik      mu      cel      fcel      pa      ky      q      H2O
  a  0.0190  0.00700  0.740  0.00620  0.00770  0.100  1.00  1.00
  sd(a)  0.0100  0.0100  0.0740  0.0100  0.0100  0.0143  0  0

these data ok ? no
names of end-members to be excluded : mu cel fcel pa
these are the only changes you want to make ? yes
rock was fluid-bearing ? yes

specification of PT window:
PT window within which average PT expected to lie
T low,high, P low,high : 100 1200 1 100

```

---

fluid just H2O ? yes

Reactions must be reasonably linear within the window;  
allowed angle change of reaction per kbar (try 1) : 1  
reactions :  
|X|X|0|0|0|X|-----|0X|00X

an independent set of reactions has been calculated

Activities and their uncertainties

	phl	ann	east	py	gr	alm	spss
a	0.0680	0.0250	0.0580	0.00510	0.00170	0.300	5.80e-5
sd(a)/a	0.15735	0.22800	0.16897	0.30980	0.34118	0.15000	0.77502

	an	ilm	pnt	geik
a	0.280	0.960	0.0190	0.00700
sd(a)/a	0.07786	0.05000	0.52632	1.42857

	ky	q	H2O
a	1.00	1.00	1.00
sd(a)/a	0	0	

Independent set of reactions

- 1)  $gr + 2ky + q = 3an$
- 2)  $3east + py + 4q = 3phl + 4ky$
- 3)  $phl + alm = ann + py$
- 4)  $3east + alm + 3geik + 4q = 3phl + 3ilm + 4ky$
- 5)  $2phl + ann + 4gr + 3pnt + 12ky = 3east + spss + 12an + 3ilm$

Calculations for the independent set of reactions

(for  $x(H2O) = 1.0$ )

	P(T)	sd(P)	a	sd(a)	b	c	ln_K	sd(ln_K)
1	10.5	0.56	67.19	0.57	-0.14782	5.785	2.558	0.413
2	8.9	3.33	-94.76	1.12	0.06530	-1.781	5.756	0.759
3	23.9	13.08	43.76	0.92	-0.01199	0.269	-5.075	0.442
4	32.6	19.83	-114.66	1.60	0.04585	-1.684	16.444	4.347
5	10.6	0.82	311.30	6.52	-0.67196	24.638	12.769	2.502

Average PT (for  $x(H2O) = 1.0$ )

Single end-member diagnostic information

avP, avT, sd's, cor, fit are result of doubling the uncertainty on ln a :  
a ln a suspect if any are v different from lsq values.  
e\* are ln a residuals normalised to ln a uncertainties :  
large absolute values, say >2.5, point to suspect info.  
hat are the diagonal elements of the hat matrix :  
large values, say >0.38, point to influential data.  
For 95% confidence, fit (= sd(fit)) < 1.61  
however a larger value may be OK - look at the diagnostics!

	avP	sd	avT	sd	cor	fit
lsq	9.9	1.6	622	78	0.927	1.28

	P	sd(P)	T	sd(T)	cor	fit	e*	hat
phl	9.19	1.91	584	97	0.952	1.21	-0.46	0.31
ann	10.37	1.55	647	75	0.937	1.13	-0.77	0.09
east	9.34	1.43	590	71	0.933	1.06	1.07	0.15
py	10.38	2.12	649	107	0.959	1.25	-0.30	0.39
gr	9.58	1.94	618	79	0.854	1.26	0.19	0.65
alm	10.13	1.59	635	77	0.933	1.20	0.50	0.04
spss	9.85	1.62	621	78	0.927	1.26	-0.23	0.00
an	9.72	1.79	620	79	0.885	1.27	-0.13	0.30
ilm	9.86	1.63	622	78	0.927	1.28	0.00	0.00
pnt	9.84	1.60	621	77	0.927	1.25	0.47	0.00
geik	9.97	1.37	628	66	0.928	1.07	-1.39	0.01
ky	9.86	1.63	622	78	0.927	1.28	0	0
q	9.86	1.63	622	78	0.927	1.28	0	0

---

T = 622;C, sd = 78,  
P = 9.9 kbars, sd = 1.6, cor = 0.927, sigfit = 1.28

more calculations with this rock ? no

more rock calculations ? no  
all done ? yes

---

## Appendix 3 – Chapter 6 Supplementary data

Table 1. U-Pb data for samples AlbSong-01 – AlbSong-04

Core/ Rim	Isotope Ratios - Common Pb corrected						Ages (Ma) - Common Pb corrected						Conc <sup>1</sup> %
	<sup>207</sup> Pb/ <sup>206</sup> Pb	± 2s	<sup>207</sup> Pb/ <sup>235</sup> U	± 2s	<sup>206</sup> Pb/ <sup>238</sup> U	± 2s	<sup>207</sup> Pb/ <sup>206</sup> Pb	2σ	<sup>207</sup> Pb/ <sup>235</sup> U	2σ	<sup>206</sup> Pb/ <sup>238</sup> U	2σ	
ALBSONG-01													
01-034	0.07306	0.00176	1.64571	0.03384	0.16338	0.00274	1016	50	988	12	976	16	97
01-103	0.0733	0.00170	1.68797	0.03436	0.16702	0.00292	1022	48	1004	12	996	16	98
01-015	0.1194	0.00338	5.80913	0.16188	0.35287	0.00758	1947	52	1948	24	1948	36	100
01-047	0.07343	0.00178	1.75431	0.03772	0.17327	0.00308	1026	50	1029	14	1030	16	100
01-006	0.11956	0.00256	5.71672	0.10346	0.34682	0.00582	1950	40	1934	16	1919	28	99
01-001	0.11927	0.00320	5.77002	0.15558	0.35088	0.00772	1945	50	1942	24	1939	36	100
01-046	0.12084	0.00274	5.96993	0.12392	0.35832	0.00666	1969	42	1971	18	1974	32	100
01-043	0.12369	0.00360	6.1201	0.15592	0.35892	0.00626	2010	52	1993	22	1977	30	99
01-010	0.12021	0.00276	5.85141	0.11420	0.35308	0.00590	1959	42	1954	16	1949	28	100
01-096	0.12027	0.00262	5.81902	0.10620	0.35092	0.00584	1960	40	1949	16	1939	28	99
01-082	0.12562	0.00340	6.28724	0.14758	0.36301	0.00626	2038	48	2017	20	1996	30	99
01-105	0.12018	0.00274	5.79826	0.11700	0.34994	0.00622	1959	42	1946	18	1934	30	99
01-056	0.12052	0.00292	5.74258	0.13016	0.34558	0.00662	1964	44	1938	20	1913	32	99
01-038	0.1201	0.00308	5.75467	0.13896	0.34753	0.00686	1958	46	1940	20	1923	32	99
01-013	0.12431	0.00314	6.10404	0.14500	0.35616	0.00700	2019	46	1991	20	1964	34	99
01-020	0.12066	0.00300	5.84115	0.13312	0.35111	0.00664	1966	46	1953	20	1940	32	99
01-011	0.12011	0.00396	5.62072	0.18260	0.33941	0.00782	1958	60	1919	28	1884	38	98
01-122	0.12434	0.00326	6.00017	0.13394	0.35004	0.00590	2019	48	1976	20	1935	28	98
01-106	0.12035	0.00346	5.96282	0.16882	0.35936	0.00780	1961	52	1970	24	1979	36	100
01-009	0.1151	0.00270	5.1354	0.10248	0.32363	0.00544	1881	44	1842	16	1807	26	98
01-071	0.12028	0.00320	5.84386	0.13072	0.35237	0.00580	1960	48	1953	20	1946	28	100
01-042	0.12276	0.00308	6.14841	0.13044	0.3633	0.00604	1997	46	1997	18	1998	28	100
01-099	0.11997	0.00312	5.66905	0.12570	0.34272	0.00584	1956	48	1927	20	1900	28	99
01-28R	0.11859	0.00378	5.22818	0.13270	0.31974	0.00620	1935	58	1857	22	1788	30	96
01-28C	0.12038	0.00292	5.55151	0.12968	0.3345	0.00666	1962	44	1909	20	1860	32	97
01-005	0.12026	0.00282	5.7204	0.12322	0.34502	0.00650	1960	42	1934	18	1911	32	99
01-033	0.1199	0.00276	5.72634	0.11202	0.34643	0.00580	1955	42	1935	16	1918	28	99
01-049	0.11921	0.00298	5.78497	0.12712	0.35199	0.00628	1944	46	1944	20	1944	30	100
01-108	0.125	0.00378	6.38571	0.17364	0.37052	0.00684	2029	54	2030	24	2032	32	100
01-114	0.12018	0.00312	5.76054	0.13562	0.34767	0.00644	1959	48	1941	20	1923	30	99
01-112	0.11535	0.00268	5.16205	0.10166	0.32457	0.00542	1885	42	1846	16	1812	26	98
01-036	0.1197	0.00274	5.71004	0.11344	0.346	0.00600	1952	42	1933	18	1915	28	99
01-134	0.12416	0.00292	6.05652	0.12304	0.3538	0.00612	2017	42	1984	18	1953	30	98
01-113C	0.11964	0.00360	5.51554	0.14402	0.33435	0.00574	1951	56	1903	22	1859	28	98
01-007	0.11896	0.00276	5.64828	0.11812	0.34439	0.00628	1941	42	1923	18	1908	30	99
01-073	0.11964	0.00282	5.67735	0.11792	0.3442	0.00610	1951	44	1928	18	1907	30	99
01-060	0.11147	0.00268	4.83166	0.09618	0.31438	0.00502	1824	44	1790	16	1762	24	98
01-113R	0.11467	0.00488	5.02608	0.20806	0.31792	0.00814	1875	78	1824	36	1780	40	97
01-087	0.11257	0.00312	4.93215	0.12746	0.31779	0.00648	1841	52	1808	22	1779	32	98
01-117	0.1189	0.00278	5.41416	0.11058	0.33028	0.00576	1940	42	1887	18	1840	28	97
01-030	0.11466	0.00304	5.1403	0.11640	0.32519	0.00546	1875	48	1843	20	1815	26	98
01-083C	0.11551	0.00350	5.34374	0.13936	0.33549	0.00568	1888	56	1876	22	1865	28	99
01-132	0.11272	0.00258	5.01181	0.09764	0.32246	0.00548	1844	42	1821	16	1802	26	99
01-139	0.11259	0.00292	5.08992	0.12132	0.32791	0.00622	1842	48	1834	20	1828	30	100
01-083R	0.11284	0.00308	4.68707	0.12026	0.30129	0.00600	1846	50	1765	22	1698	30	96
01-022	0.09768	0.00230	3.20203	0.07040	0.23778	0.00456	1580	46	1458	18	1375	24	92

01-133	0.11722	0.00458	5.38075	0.20792	0.33294	0.00830	1914	72	1882	34	1853	40	98
01-149	0.11932	0.00290	5.74364	0.11970	0.34911	0.00594	1946	44	1938	18	1930	28	100
01-125	0.12007	0.00330	5.78941	0.15124	0.34973	0.00730	1957	50	1945	22	1933	34	99
01-150	0.12007	0.00304	5.8977	0.13002	0.35627	0.00620	1957	46	1961	20	1964	30	100
01-129	0.12055	0.00332	5.5532	0.13474	0.33413	0.00610	1964	50	1909	20	1858	30	97
01-144	0.12052	0.00306	5.74559	0.13080	0.3458	0.00630	1964	46	1938	20	1915	30	99
01-136	0.12067	0.00328	6.02601	0.15550	0.36223	0.00736	1966	50	1980	22	1993	34	101
01-076	0.12159	0.00328	5.82159	0.14834	0.34727	0.00696	1980	50	1950	22	1922	34	98
01-121	0.12226	0.00280	6.07912	0.11872	0.36065	0.00608	1989	42	1987	18	1985	28	100
01-124	0.12527	0.00346	5.72748	0.14808	0.33164	0.00658	2033	50	1936	22	1846	32	95



Core/ Rim	Isotope Ratios - Common Pb corrected						Ages (Ma) - Common Pb corrected						Conc <sup>1</sup> %
	<sup>207</sup> Pb/ <sup>206</sup> Pb	± 2s	<sup>207</sup> Pb/ <sup>235</sup> U	± 2s	<sup>206</sup> Pb/ <sup>238</sup> U	± 2s	<sup>207</sup> Pb/ <sup>206</sup> Pb	2σ	<sup>207</sup> Pb/ <sup>235</sup> U	2σ	<sup>206</sup> Pb/ <sup>238</sup> U	2σ	
ALBSONG-02													
02-98	0.0619	0.00164	0.91791	0.02248	0.10757	0.00202	671	58	661	12	659	12	99
02-104	0.06274	0.00184	0.96261	0.02644	0.11128	0.00220	699	64	685	14	680	12	98
02-100	0.07229	0.00180	1.62566	0.03850	0.16311	0.00322	994	52	980	14	974	18	99
02-88	0.06444	0.00354	0.97234	0.05052	0.10945	0.00272	756	118	690	26	670	16	91
02-93	0.0708	0.00156	1.46696	0.03026	0.15028	0.00286	952	46	917	12	903	16	96
02-09	0.07606	0.00168	1.96486	0.03864	0.18737	0.00336	1097	46	1104	14	1107	18	101
02-76	0.0741	0.00164	1.73202	0.03606	0.16954	0.00326	1044	46	1021	14	1010	18	98
02-87	0.0592	0.00136	0.75637	0.01644	0.09268	0.00180	574	52	572	10	571	10	100
02-62	0.07321	0.00174	1.73731	0.03852	0.17213	0.00328	1020	50	1022	14	1024	18	100
02-103	0.07203	0.00318	1.56999	0.06780	0.1581	0.00410	987	92	958	26	946	22	97
02-55	0.07358	0.00164	1.72875	0.03566	0.17041	0.00320	1030	46	1019	14	1014	18	99
02-07	0.07222	0.00158	1.65043	0.03380	0.16576	0.00314	992	46	990	12	989	18	100
02-96	0.07123	0.00240	1.56612	0.05002	0.15949	0.00334	964	70	957	20	954	18	99
02-22	0.07275	0.00172	1.64808	0.03748	0.16431	0.00328	1007	50	989	14	981	18	98
02-05	0.07104	0.00166	1.58421	0.03430	0.16176	0.00304	959	48	964	14	967	16	101
02-71	0.07074	0.00190	1.55459	0.03844	0.15939	0.00304	950	56	952	16	953	16	100
02-18	0.0725	0.00162	1.63442	0.03412	0.16352	0.00310	1000	46	984	14	976	18	98
02-01	0.07065	0.00166	1.51842	0.03248	0.15588	0.00290	947	50	938	14	934	16	99
02-15	0.07284	0.00184	1.70401	0.03986	0.16968	0.00326	1010	52	1010	14	1010	18	100
02-53	0.07182	0.00170	1.62597	0.03574	0.16422	0.00314	981	50	980	14	980	18	100
02-51	0.07154	0.00166	1.60039	0.03490	0.16226	0.00314	973	48	970	14	969	18	100
02-25	0.07206	0.00172	1.64942	0.03652	0.16602	0.00314	988	50	989	14	990	18	100
02-73	0.07233	0.00190	1.64531	0.03932	0.16498	0.00310	995	54	988	16	984	18	99
02-102	0.11564	0.00334	5.34724	0.15026	0.3354	0.00738	1890	54	1876	24	1865	36	99
02-97	0.10996	0.00246	4.25842	0.08922	0.28089	0.00538	1799	42	1685	18	1596	28	94
02-23	0.11771	0.00324	5.54939	0.15408	0.34193	0.00774	1922	50	1908	24	1896	38	99
02-74	0.07211	0.00156	1.65646	0.03410	0.16661	0.00322	989	46	992	14	993	18	100
02-58	0.12042	0.00266	5.73101	0.11866	0.34519	0.00656	1962	40	1936	18	1912	32	99
02-08	0.07336	0.00164	1.74876	0.03522	0.1729	0.00312	1024	46	1027	14	1028	18	100
02-83	0.11796	0.00276	5.69311	0.13258	0.35007	0.00726	1926	42	1930	20	1935	34	100
02-101	0.0747	0.00178	1.80856	0.04068	0.1756	0.00340	1060	50	1049	14	1043	18	99
02-17	0.11157	0.00250	4.87121	0.09628	0.31669	0.00558	1825	42	1797	16	1774	28	98
02-82	0.14643	0.00354	8.53035	0.20878	0.42255	0.00908	2305	42	2289	22	2272	42	99
02-60	0.07178	0.00180	1.62923	0.03826	0.16463	0.00316	980	52	982	14	982	18	100
02-68	0.11247	0.00242	5.03029	0.10032	0.32442	0.00610	1840	40	1824	16	1811	30	99
02-21	0.11494	0.00256	5.36812	0.11476	0.33876	0.00664	1879	42	1880	18	1881	32	100
02-99	0.10883	0.00248	4.42249	0.09238	0.29477	0.00550	1780	42	1717	18	1665	28	96
02-19	0.07326	0.00164	1.74724	0.03602	0.17299	0.00324	1021	46	1026	14	1029	18	100
02-20	0.07196	0.00162	1.65772	0.03460	0.16708	0.00314	985	46	993	14	996	18	101
02-54	0.07233	0.00180	1.66016	0.04108	0.16647	0.00352	995	52	993	16	993	20	100
02-78	0.07618	0.00692	1.70282	0.14828	0.16212	0.00552	1100	186	1010	56	969	30	92
02-95	0.107	0.00310	3.95839	0.11678	0.26833	0.00626	1749	54	1626	24	1532	32	93
02-24	0.07313	0.00212	1.67632	0.04416	0.16626	0.00314	1018	60	1000	16	991	18	98
02-10	0.0864	0.00306	2.3831	0.08446	0.20007	0.00500	1347	70	1238	26	1176	26	92
02-91	0.07316	0.00164	1.73233	0.03614	0.17176	0.00326	1018	46	1021	14	1022	18	100
02-84	0.07245	0.00202	1.60886	0.04142	0.16108	0.00310	999	58	974	16	963	18	97
02-13	0.07254	0.00198	1.64711	0.04150	0.1647	0.00318	1001	56	988	16	983	18	99
02-90	0.07047	0.00316	1.36384	0.05840	0.14038	0.00322	942	94	874	26	847	18	93
02-16	0.0723	0.00172	1.66913	0.03734	0.16745	0.00322	994	50	997	14	998	18	100
02-81	0.09362	0.00244	2.89663	0.07722	0.22441	0.00500	1500	50	1381	20	1305	26	92
02-52	0.07286	0.00158	1.71353	0.03460	0.17059	0.00320	1010	44	1014	12	1015	18	100

02-56	0.07126	0.00232	1.11759	0.03630	0.11376	0.00264	965	68	762	18	695	16	79
02-02	0.07485	0.00178	1.78697	0.03978	0.17316	0.00334	1064	48	1041	14	1029	18	98
02-63	0.07421	0.00188	1.70002	0.03998	0.16616	0.00320	1047	52	1009	16	991	18	96
02-94	0.07102	0.00194	1.6229	0.04184	0.16575	0.00330	958	58	979	16	989	18	102
02-03	0.0808	0.00856	2.27868	0.23464	0.20452	0.00518	1217	214	1206	72	1200	28	99

Core/ Rim	Isotope Ratios - Common Pb corrected						Ages (Ma) - Common Pb corrected						Conc <sup>1</sup> %
	<sup>207</sup> Pb/ <sup>206</sup> Pb	± 2s	<sup>207</sup> Pb/ <sup>235</sup> U	± 2s	<sup>206</sup> Pb/ <sup>238</sup> U	± 2s	<sup>207</sup> Pb/ <sup>206</sup> Pb	2σ	<sup>207</sup> Pb/ <sup>235</sup> U	2σ	<sup>206</sup> Pb/ <sup>238</sup> U	2σ	
ALBSONG-03													
03-19	0.06392	0.00152	1.04112	0.02288	0.11815	0.00224	739	52	724	12	720	12	98
03-80	0.07319	0.00190	1.6674	0.04140	0.16525	0.00334	1019	54	996	16	986	18	98
03-72	0.073	0.00170	1.67769	0.03700	0.16668	0.00322	1014	48	1000	14	994	18	99
03-05	0.07241	0.00162	1.64646	0.03354	0.16495	0.00304	997	46	988	12	984	16	99
03-61	0.07353	0.00186	1.65239	0.03810	0.163	0.00306	1029	52	990	14	973	16	96
03-75	0.07043	0.00170	1.48202	0.03388	0.15263	0.00296	941	50	923	14	916	16	98
03-25	0.07212	0.00174	1.58422	0.03506	0.15934	0.00300	989	50	964	14	953	16	97
03-31	0.07246	0.00162	1.67572	0.03436	0.16774	0.00312	999	46	999	14	1000	18	100
03-85	0.0727	0.00178	1.63381	0.03764	0.16301	0.00316	1006	50	983	14	973	18	98
03-20	0.0724	0.00164	1.64823	0.03448	0.16513	0.00310	997	48	989	14	985	18	99
03-23	0.07296	0.00164	1.72503	0.03652	0.17149	0.00328	1013	46	1018	14	1020	18	100
03-03	0.07205	0.00152	1.63943	0.03172	0.16504	0.00304	987	44	985	12	985	16	100
03-74	0.11186	0.00256	4.78618	0.10486	0.31034	0.00610	1830	42	1782	18	1742	30	97
03-11	0.11953	0.00260	5.77195	0.11636	0.35025	0.00654	1949	40	1942	18	1936	32	100
03-60	0.10949	0.00260	4.42596	0.09496	0.2932	0.00536	1791	44	1717	18	1658	26	96
03-43	0.11317	0.00244	5.08973	0.10270	0.32623	0.00618	1851	40	1834	18	1820	30	99
03-24	0.10086	0.00214	3.43665	0.06848	0.24714	0.00468	1640	40	1513	16	1424	24	92
03-04	0.07261	0.00154	1.67643	0.03274	0.16746	0.00308	1003	44	1000	12	998	18	100
03-21	0.11074	0.00250	4.61317	0.09400	0.30216	0.00554	1812	42	1752	18	1702	28	97
03-78	0.07395	0.00188	1.64236	0.03906	0.16108	0.00314	1040	52	987	16	963	18	95
03-27	0.11965	0.00252	5.79256	0.11224	0.35116	0.00650	1951	38	1945	16	1940	32	100
03-37	0.07254	0.00170	1.62193	0.03532	0.16218	0.00308	1001	48	979	14	969	18	98
03-50	0.11028	0.00238	4.50126	0.09028	0.29606	0.00560	1804	40	1731	16	1672	28	96
03-79	0.11943	0.00272	5.56526	0.11894	0.33801	0.00648	1948	42	1911	18	1877	32	98
03-63	0.11953	0.00260	5.69174	0.11386	0.34536	0.00642	1949	40	1930	18	1912	30	99
03-40	0.1196	0.00294	5.56319	0.14052	0.33739	0.00742	1950	44	1910	22	1874	36	98
03-22	0.07286	0.00168	1.67867	0.03600	0.1671	0.00318	1010	48	1000	14	996	18	99
03-68	0.1171	0.00282	5.33114	0.12250	0.33018	0.00654	1912	44	1874	20	1839	32	98
03-59	0.11025	0.00234	4.81923	0.09662	0.31706	0.00604	1804	40	1788	16	1775	30	99
03-01	0.1103	0.00236	4.68236	0.09096	0.30794	0.00564	1804	40	1764	16	1731	28	98
03-07	0.1109	0.00240	4.44975	0.09118	0.29103	0.00558	1814	40	1722	16	1647	28	95
03-28	0.11002	0.00320	4.67417	0.13758	0.30815	0.00722	1800	54	1763	24	1732	36	98
03-44	0.11858	0.00296	5.64338	0.14134	0.34522	0.00740	1935	46	1923	22	1912	36	99
03-02	0.10996	0.00238	4.66995	0.09270	0.30806	0.00574	1799	40	1762	16	1731	28	98
03-51	0.12157	0.00284	5.84627	0.12512	0.3488	0.00654	1979	42	1953	18	1929	32	99
03-33	0.11148	0.00346	4.9144	0.15270	0.31976	0.00752	1824	58	1805	26	1789	36	99
03-17	0.12051	0.00258	5.88295	0.11924	0.35408	0.00680	1964	40	1959	18	1954	32	100
03-49	0.12091	0.00278	5.78706	0.12522	0.34716	0.00670	1970	42	1944	18	1921	32	99
03-47	0.10806	0.00244	4.16786	0.08910	0.27977	0.00540	1767	42	1668	18	1590	28	94
03-53	0.12075	0.00300	5.6951	0.12656	0.3421	0.00622	1967	46	1931	20	1897	30	98
03-08	0.07269	0.00182	1.65966	0.03794	0.16561	0.00310	1005	52	993	14	988	18	99
03-34	0.1079	0.00304	4.36206	0.11064	0.29323	0.00544	1764	52	1705	20	1658	28	97
03-13	0.10485	0.00220	3.74055	0.07216	0.25876	0.00480	1712	40	1580	16	1483	24	92
03-46	0.11229	0.00256	4.49713	0.09784	0.29049	0.00568	1837	42	1730	18	1644	28	94
03-38	0.10309	0.00258	3.5392	0.09064	0.24902	0.00550	1680	48	1536	20	1433	28	91
03-41	0.13799	0.00290	7.65056	0.14972	0.40216	0.00756	2202	38	2191	18	2179	34	100
03-09	0.11043	0.00240	4.35831	0.08814	0.28627	0.00538	1806	40	1704	16	1623	26	94
03-36	0.10783	0.00270	4.06242	0.09116	0.27326	0.00498	1763	46	1647	18	1557	26	93
03-30	0.12024	0.00254	5.80416	0.11348	0.35015	0.00654	1960	38	1947	16	1935	32	99
03-73	0.11132	0.00312	4.50526	0.09500	0.29352	0.00538	1821	52	1732	18	1659	26	95
03-06	0.07067	0.00206	1.56906	0.04276	0.16104	0.00318	948	62	958	16	963	18	101

03-52	0.0714	0.00232	1.33942	0.04370	0.13608	0.00322	969	68	863	18	822	18	89
03-18	0.07018	0.00160	1.47022	0.03104	0.15196	0.00286	934	48	918	12	912	16	98
03-15	0.0827	0.00804	2.2814	0.21530	0.20007	0.00474	1262	194	1207	66	1176	26	96
03-12	0.08312	0.00542	2.04106	0.12474	0.1781	0.00400	1272	130	1129	42	1057	22	89
03-14	0.08792	0.01160	2.80154	0.36220	0.23111	0.00620	1381	262	1356	96	1340	32	98
03-69	0.106	0.00232	3.95343	0.07780	0.2705	0.00490	1732	42	1625	16	1543	24	94
03-70	0.11374	0.00524	5.09808	0.20890	0.32507	0.00682	1860	86	1836	34	1814	34	99
03-45	0.11505	0.00278	4.93891	0.11496	0.3114	0.00626	1881	44	1809	20	1748	30	96
03-64	0.12059	0.00278	5.73157	0.12330	0.34472	0.00662	1965	42	1936	18	1909	32	99

Core/ Rim	Isotope Ratios - Common Pb corrected						Ages (Ma) - Common Pb corrected						Conc <sup>1</sup> %
	<sup>207</sup> Pb/ <sup>206</sup> Pb	± 2s	<sup>207</sup> Pb/ <sup>235</sup> U	± 2s	<sup>206</sup> Pb/ <sup>238</sup> U	± 2s	<sup>207</sup> Pb/ <sup>206</sup> Pb	2σ	<sup>207</sup> Pb/ <sup>235</sup> U	2σ	<sup>206</sup> Pb/ <sup>238</sup> U	2σ	
ALBSONG-04													
04-53	0.06431	0.00146	1.06607	0.02334	0.12023	0.00236	752	50	737	12	732	14	98
04-31	0.06433	0.00146	1.09138	0.02362	0.12305	0.00240	752	50	749	12	748	14	100
04-93	0.06438	0.00298	1.06921	0.04758	0.12046	0.00292	754	100	738	24	733	16	98
04-68	0.06316	0.00362	1.06223	0.05984	0.12198	0.00368	714	124	735	30	742	22	103
04-65	0.07189	0.00316	1.21651	0.05236	0.12274	0.00324	983	92	808	24	746	18	82
04-70	0.06495	0.00168	1.0676	0.02614	0.11922	0.00236	773	56	738	12	726	14	95
04-69	0.06391	0.00160	1.05384	0.02606	0.11961	0.00248	739	54	731	12	728	14	99
04-77	0.06418	0.00148	1.0364	0.02318	0.11714	0.00234	748	50	722	12	714	14	97
04-63	0.06382	0.00194	1.0654	0.03218	0.12108	0.00272	736	66	736	16	737	16	100
04-92	0.06408	0.00160	1.05269	0.02508	0.11916	0.00236	744	54	730	12	726	14	98
04-94	0.06409	0.00156	1.07071	0.02472	0.12118	0.00238	745	52	739	12	737	14	99
04-79	0.06429	0.00206	1.0693	0.03330	0.12065	0.00266	751	70	738	16	734	16	98
04-76	0.0669	0.00190	1.10479	0.03028	0.11978	0.00252	835	60	756	14	729	14	91
04-74	0.0649	0.00176	1.07242	0.02818	0.11986	0.00250	771	58	740	14	730	14	96
04-21	0.06491	0.00200	1.08004	0.03290	0.12069	0.00272	771	66	744	16	735	16	96
04-08	0.11957	0.00322	5.51473	0.10846	0.3345	0.00616	1950	50	1903	16	1860	30	98
04-50	0.12431	0.00282	6.23329	0.13756	0.36369	0.00728	2019	42	2009	20	2000	34	100
04-28	0.12024	0.00254	5.65832	0.11276	0.34134	0.00648	1960	38	1925	18	1893	32	98
04-02	0.11984	0.00270	5.69836	0.12666	0.34489	0.00700	1954	42	1931	20	1910	34	99
04-04	0.12633	0.00264	6.3553	0.12430	0.36487	0.00688	2048	38	2026	18	2005	32	99
04-06	0.11999	0.00256	5.7417	0.11244	0.34708	0.00644	1956	38	1938	16	1921	30	99
04-40	0.11953	0.00250	5.8204	0.11838	0.35319	0.00694	1949	38	1949	18	1950	34	100
04-37	0.12129	0.00254	5.97393	0.12024	0.35725	0.00696	1975	38	1972	18	1969	34	100
04-41	0.12606	0.00286	6.20998	0.13076	0.35731	0.00674	2044	42	2006	18	1969	32	98
04-42	0.12066	0.00252	5.8586	0.11746	0.35219	0.00684	1966	38	1955	18	1945	32	99
04-46	0.12515	0.00290	6.25579	0.14734	0.36258	0.00772	2031	42	2012	20	1994	36	99
04-27	0.12233	0.00410	5.78648	0.15826	0.34307	0.00666	1990	62	1944	24	1901	32	98
04-19	0.12581	0.00292	6.36604	0.15530	0.36704	0.00814	2040	42	2028	22	2015	38	99
04-47	0.12021	0.00280	5.74174	0.12324	0.34646	0.00650	1959	42	1938	18	1918	32	99
04-96	0.12017	0.00270	5.75264	0.12480	0.34724	0.00688	1959	42	1939	18	1921	32	99
04-09	0.11731	0.00250	5.36544	0.10528	0.33173	0.00618	1916	40	1879	16	1847	30	98
04-29	0.12025	0.00258	5.67887	0.11694	0.34254	0.00668	1960	40	1928	18	1899	32	98
04-03	0.11698	0.00456	4.92528	0.15852	0.30535	0.00672	1911	72	1807	28	1718	34	95
04-83	0.11902	0.00256	5.73235	0.11644	0.34935	0.00670	1942	40	1936	18	1931	32	100
04-15	0.12049	0.00266	5.82497	0.12484	0.35065	0.00694	1963	40	1950	18	1938	34	99
04-80	0.12077	0.00268	5.86868	0.12262	0.35247	0.00676	1968	40	1957	18	1946	32	99
04-18	0.12149	0.00302	6.03363	0.14994	0.36023	0.00758	1978	46	1981	22	1983	36	100
04-20	0.11363	0.00564	5.17905	0.23356	0.33058	0.00680	1858	92	1849	38	1841	32	100
04-34	0.12119	0.00304	5.87689	0.14502	0.35173	0.00742	1974	46	1958	22	1943	36	99
04-35	0.11835	0.00264	5.56858	0.12404	0.34127	0.00702	1931	40	1911	20	1893	34	99
04-45	0.1201	0.00264	5.72212	0.12092	0.34559	0.00684	1958	40	1935	18	1914	32	99
04-16	0.11553	0.00248	5.00784	0.10240	0.31439	0.00606	1888	40	1821	18	1762	30	96
04-30	0.10314	0.00346	3.27283	0.08774	0.23014	0.00466	1681	64	1475	20	1335	24	88
04-25R	0.12059	0.00296	5.8465	0.14624	0.35167	0.00770	1965	44	1953	22	1943	36	99
04-17	0.11895	0.00254	5.30855	0.10676	0.32372	0.00614	1941	40	1870	18	1808	30	96
04-25C	0.12528	0.00284	6.29901	0.12882	0.36468	0.00664	2033	42	2018	18	2004	32	99
04-57	0.12349	0.00348	6.15688	0.18234	0.3616	0.00876	2007	52	1998	26	1990	42	100
04-52	0.11858	0.00288	5.67101	0.12798	0.34688	0.00664	1935	44	1927	20	1920	32	100
04-64	0.11856	0.00294	5.44568	0.13358	0.33317	0.00704	1935	46	1892	22	1854	34	98
04-55	0.11901	0.00294	5.70961	0.13788	0.34797	0.00716	1941	46	1933	20	1925	34	100
04-60	0.11928	0.00266	5.64662	0.12228	0.34337	0.00688	1945	40	1923	18	1903	34	99



04-56	0.11991	0.00270	5.77329	0.12560	0.34923	0.00694	1955	42	1942	18	1931	34	99
04-61	0.12028	0.00258	5.71157	0.11886	0.34442	0.00676	1960	40	1933	18	1908	32	99
04-67	0.12048	0.00268	5.85634	0.11986	0.35258	0.00660	1963	40	1955	18	1947	32	100
04-58	0.12062	0.00268	5.81364	0.12874	0.34959	0.00716	1965	40	1948	20	1933	34	99
04-48	0.12093	0.00282	5.8441	0.13654	0.35054	0.00732	1970	42	1953	20	1937	34	99

Table 2. Lu-Hf data for samples AlbSong-01 – AlbSong-04

	$\frac{^{176}\text{Yb}}{^{177}\text{Hf}}$	$\frac{^{176}\text{Lu}}{^{177}\text{Hf}}$	$\frac{^{176}\text{Hf}}{^{177}\text{Hf}}$	$\pm 2\sigma$	$\frac{^{176}\text{Hf}}{^{177}\text{Hf}}(t)$	$\epsilon\text{Hf}(t)$	$\pm 2\sigma$	$T_{\text{DM}}(\text{Ca})$	$T_{\text{DM}}$ (crustal)
<b>ALBSONG-01</b>									
01-034	0.031594	0.000857	0.283182	0.000013	0.283166	36.46	0.455	0.10	-0.49
01-103	0.021168	0.000644	0.282010	0.000006	0.281998	-4.80	0.1925	1.73	2.19
01-015	0.088415	0.002397	0.281724	0.000008	0.281635	3.23	0.2905	2.23	2.39
01-047	0.032898	0.000870	0.281919	0.000011	0.281902	-8.10	0.385	1.87	2.40
01-006	0.010680	0.000253	0.281625	0.000008	0.281616	2.60	0.273	2.24	2.44
01-001	0.048318	0.001357	0.281649	0.000011	0.281599	1.89	0.385	2.27	2.48
01-046	0.064159	0.001691	0.281647	0.000010	0.281584	1.90	0.35	2.29	2.50
01-043	0.019579	0.000474	0.281572	0.000007	0.281554	1.78	0.259	2.32	2.54
01-010	0.034736	0.000916	0.281602	0.000014	0.281568	1.11	0.49	2.31	2.54
01-096	0.008158	0.000244	0.281570	0.000010	0.281561	0.89	0.35	2.31	2.55
01-082	0.035955	0.000951	0.281569	0.000008	0.281532	1.65	0.287	2.35	2.57
01-105	0.025206	0.000763	0.281582	0.000009	0.281554	0.60	0.3045	2.33	2.57
01-056	0.073723	0.001608	0.281612	0.000012	0.281552	0.66	0.42	2.34	2.57
01-038	0.026876	0.000695	0.281564	0.000008	0.281538	0.03	0.28	2.35	2.61
01-013	0.070407	0.001931	0.281590	0.000010	0.281516	0.64	0.343	2.39	2.62
01-020	0.030173	0.000812	0.281562	0.000011	0.281532	-0.02	0.385	2.36	2.62
01-011	0.030307	0.000731	0.281554	0.000008	0.281527	-0.37	0.2625	2.36	2.63
01-122	0.044848	0.001261	0.281545	0.000009	0.281497	-0.05	0.301	2.41	2.66
01-106	0.050270	0.001438	0.281567	0.000009	0.281513	-0.78	0.322	2.39	2.66
01-009	0.035356	0.001009	0.281572	0.000009	0.281536	-1.80	0.3045	2.35	2.66
01-071	0.059369	0.001656	0.281564	0.000011	0.281502	-1.19	0.385	2.41	2.69
01-042	0.031054	0.000920	0.281520	0.000009	0.281485	-0.96	0.3255	2.42	2.70
01-099	0.010169	0.000280	0.281506	0.000010	0.281496	-1.53	0.3395	2.40	2.70
01-28R	0.018771	0.000485	0.281519	0.000012	0.281501	-1.81	0.42	2.39	2.71
01-28C	0.043249	0.001161	0.281534	0.000010	0.281491	-1.56	0.336	2.42	2.71
01-005	0.002433	0.000051	0.281492	0.000007	0.281490	-1.63	0.2555	2.40	2.71
01-033	0.019945	0.000580	0.281510	0.000016	0.281488	-1.80	0.56	2.41	2.72
01-049	0.015988	0.000418	0.281505	0.000009	0.281490	-2.01	0.2975	2.41	2.73
01-108	0.043756	0.001258	0.281511	0.000011	0.281462	-1.03	0.385	2.45	2.73
01-114	0.013086	0.000377	0.281497	0.000008	0.281483	-1.90	0.273	2.42	2.73
01-112	0.008168	0.000201	0.281512	0.000010	0.281505	-2.82	0.35	2.39	2.73
01-036	0.006240	0.000156	0.281489	0.000008	0.281483	-2.06	0.2905	2.41	2.73
01-134	0.044186	0.001390	0.281513	0.000008	0.281460	-1.41	0.28	2.46	2.74
01-113C	0.010044	0.000279	0.281479	0.000009	0.281469	-2.59	0.308	2.43	2.77
01-007	0.005671	0.000139	0.281476	0.000010	0.281471	-2.74	0.3395	2.43	2.77
01-073	0.010389	0.000272	0.281467	0.000010	0.281457	-3.01	0.3395	2.45	2.79
01-060	0.005748	0.000129	0.281488	0.000008	0.281484	-4.96	0.2625	2.41	2.82
01-113R	0.008575	0.000241	0.281476	0.000007	0.281467	-4.37	0.245	2.44	2.82
01-087	0.002319	0.000057	0.281479	0.000008	0.281477	-4.80	0.2765	2.42	2.82
01-117	0.042249	0.001262	0.281492	0.000011	0.281445	-3.67	0.385	2.48	2.83
01-030	0.017546	0.000399	0.281474	0.000007	0.281460	-4.64	0.259	2.45	2.84
01-083C	0.002627	0.000061	0.281447	0.000008	0.281445	-4.88	0.266	2.46	2.86
01-132	0.006974	0.000209	0.281465	0.000011	0.281458	-5.42	0.385	2.45	2.86
01-139	0.007417	0.000204	0.281442	0.000005	0.281435	-6.28	0.189	2.48	2.92

01-083R 0.002707 0.000061 0.281413 0.000007 0.281411 -7.04 0.231 2.51 2.97

	$^{176}\text{Yb}/^{177}\text{Hf}$	$^{176}\text{Lu}/^{177}\text{Hf}$	$^{176}\text{Hf}/^{177}\text{Hf}$	$\pm 2\sigma$	$^{176}\text{Hf}/^{177}\text{Hf}(t)$	$\epsilon\text{Hf}(t)$	$\pm 2\sigma$	$T_{\text{DM}}(\text{Ga})$	$T_{\text{DM}}$ (crustal)
02-98	0.043456	0.001232	0.282394	0.000016	0.282379	0.61	0.56	1.22	1.56
02-104	0.023548	0.000737	0.282351	0.000007	0.282342	-0.24	0.2555	1.26	1.63
02-100	0.008418	0.000332	0.282182	0.000010	0.282176	0.44	0.35	1.48	1.82
02-88	0.036918	0.001049	0.282274	0.000017	0.282261	-3.32	0.595	1.38	1.82
02-93	0.022989	0.000764	0.282176	0.000009	0.282163	-1.60	0.3255	1.51	1.89
02-09	0.005296	0.000135	0.282072	0.000009	0.282069	-0.59	0.3045	1.63	1.98
02-76	0.000813	0.000020	0.282047	0.000010	0.282047	-2.57	0.343	1.65	2.06
02-87	0.035019	0.001224	0.282171	0.000009	0.282158	-9.16	0.301	1.53	2.11
02-62	0.005587	0.000155	0.282018	0.000012	0.282015	-4.23	0.42	1.70	2.15
02-103	0.014114	0.000510	0.282036	0.000011	0.282027	-5.46	0.385	1.69	2.17
02-55	0.006558	0.000192	0.281986	0.000012	0.281982	-5.17	0.42	1.75	2.22
02-07	0.088097	0.002310	0.282024	0.000012	0.281981	-6.13	0.42	1.79	2.25
02-96	0.005117	0.000179	0.281988	0.000011	0.281985	-6.78	0.385	1.74	2.26
02-22	0.004435	0.000113	0.281960	0.000014	0.281958	-6.55	0.49	1.78	2.29
02-05	0.004217	0.000110	0.281926	0.000012	0.281924	-8.64	0.42	1.82	2.39
02-71	0.016407	0.000453	0.281930	0.000010	0.281922	-9.03	0.35	1.83	2.40
02-18	0.040593	0.001099	0.281903	0.000010	0.281882	-9.38	0.35	1.90	2.46
02-01	0.039269	0.000981	0.281873	0.000010	0.281856	-11.80	0.35	1.94	2.56
02-15	0.007182	0.000201	0.281837	0.000010	0.281833	-10.90	0.336	1.95	2.56
02-53	0.031657	0.000795	0.281854	0.000011	0.281839	-11.33	0.385	1.95	2.57
02-51	0.031155	0.000796	0.281855	0.000010	0.281840	-11.56	0.35	1.95	2.57
02-25	0.049916	0.001301	0.281853	0.000008	0.281829	-11.50	0.2765	1.98	2.59
02-73	0.036023	0.000948	0.281822	0.000008	0.281804	-12.50	0.2905	2.01	2.64
02-102	0.018665	0.000556	0.281551	0.000015	0.281531	-1.77	0.525	2.35	2.67
02-97	0.030627	0.000909	0.281573	0.000010	0.281542	-3.45	0.3465	2.35	2.71
02-23	0.024352	0.000612	0.281520	0.000012	0.281498	-2.23	0.42	2.40	2.72
02-74	0.017587	0.000514	0.281773	0.000006	0.281763	-13.75	0.1995	2.05	2.73
02-58	0.034725	0.000878	0.281509	0.000009	0.281476	-2.07	0.308	2.43	2.74
02-08	0.005394	0.000122	0.281740	0.000010	0.281738	-13.97	0.35	2.07	2.77
02-83	0.002001	0.000050	0.281477	0.000011	0.281475	-2.93	0.385	2.42	2.77
02-101	0.005030	0.000130	0.281716	0.000012	0.281713	-14.03	0.42	2.11	2.80
02-17	0.026586	0.000679	0.281514	0.000009	0.281490	-4.69	0.2975	2.41	2.80
02-82	0.011959	0.000420	0.281354	0.000011	0.281336	0.78	0.385	2.61	2.83
02-60	0.003107	0.000072	0.281724	0.000013	0.281723	-15.49	0.455	2.09	2.83
02-68	0.018315	0.000492	0.281489	0.000009	0.281472	-5.01	0.2975	2.43	2.84
02-21	0.009401	0.000248	0.281455	0.000012	0.281446	-5.04	0.42	2.47	2.87
02-99	0.010071	0.000289	0.281477	0.000007	0.281467	-6.54	0.245	2.44	2.89
02-19	0.001464	0.000034	0.281672	0.000010	0.281671	-16.39	0.3325	2.16	2.92
02-20	0.017011	0.000419	0.281682	0.000013	0.281674	-16.85	0.455	2.17	2.92
02-54	0.035327	0.000861	0.281673	0.000012	0.281657	-17.48	0.42	2.21	2.96
02-78	0.018942	0.000518	0.281604	0.000008	0.281593	-17.39	0.2695	2.28	3.04
02-95	0.012388	0.000332	0.281410	0.000011	0.281399	-9.66	0.385	2.53	3.06
02-24	0.013283	0.000367	0.281607	0.000010	0.281600	-18.99	0.3325	2.27	3.07
02-10	0.022688	0.000625	0.281520	0.000012	0.281504	-15.01	0.42	2.40	3.08
02-91	0.001624	0.000044	0.281596	0.000010	0.281595	-19.16	0.35	2.26	3.09
02-84	0.004161	0.000136	0.281612	0.000007	0.281610	-19.88	0.2555	2.25	3.09

02-13	0.010495	0.000314	0.281593	0.000011	0.281587	-19.82	0.385	2.28	3.11
02-90	0.011190	0.000362	0.281628	0.000011	0.281622	-22.01	0.385	2.24	3.13
02-16	0.009727	0.000298	0.281576	0.000010	0.281570	-20.48	0.3395	2.31	3.15
02-81	0.004024	0.000121	0.281412	0.000012	0.281409	-14.96	0.42	2.51	3.20
02-52	0.001167	0.000026	0.281531	0.000011	0.281531	-21.63	0.385	2.35	3.23
02-56	0.031208	0.000798	0.281533	0.000009	0.281519	-23.06	0.315	2.39	3.29
02-02	0.009946	0.000254	0.281455	0.000009	0.281450	-23.28	0.329	2.47	3.38
02-63	0.005442	0.000131	0.281451	0.000010	0.281448	-23.71	0.3395	2.46	3.39
02-94	0.003575	0.000133	0.281465	0.000013	0.281463	-24.51	0.455	2.44	3.39

---



	$^{176}\text{Yb}/$ $^{177}\text{Hf}$	$^{176}\text{Lu}/$ $^{177}\text{Hf}$	$^{176}\text{Hf}/$ $^{177}\text{Hf}$	$\pm 2\sigma$	$^{176}\text{Hf}/$ $^{177}\text{Hf}(t)$	$\epsilon\text{Hf}(t)$	$\pm 2\sigma$	$T_{\text{DM}}(\text{Ga})$	$T_{\text{DM}}$ (crustal)
ALBSONG-03									
03-19	0.012808	0.000380	0.282290	0.000010	0.282285	-1.36	0.35	1.34	1.73
03-80	0.015092	0.000474	0.282063	0.000013	0.282054	-2.88	0.455	1.65	2.06
03-72	0.021031	0.000625	0.281952	0.000010	0.281940	-7.02	0.3325	1.81	2.32
03-05	0.052433	0.001438	0.281949	0.000008	0.281922	-8.32	0.2905	1.85	2.38
03-61	0.027738	0.000731	0.281898	0.000017	0.281884	-8.68	0.595	1.89	2.44
03-75	0.035017	0.001056	0.281927	0.000009	0.281909	-10.32	0.2975	1.87	2.45
03-25	0.024199	0.000688	0.281883	0.000009	0.281871	-10.84	0.315	1.91	2.52
03-31	0.030289	0.000865	0.281869	0.000011	0.281853	-10.45	0.385	1.94	2.53
03-85	0.020178	0.000623	0.281855	0.000010	0.281843	-10.63	0.3465	1.94	2.54
03-20	0.029283	0.000833	0.281860	0.000008	0.281845	-11.05	0.294	1.95	2.55
03-23	0.019533	0.000567	0.281847	0.000009	0.281836	-10.73	0.322	1.95	2.55
03-03	0.036735	0.001088	0.281864	0.000008	0.281844	-11.08	0.273	1.96	2.55
03-74	0.008337	0.000248	0.281605	0.000009	0.281596	-0.81	0.2975	2.26	2.56
03-11	0.032013	0.000900	0.281590	0.000009	0.281557	0.49	0.2975	2.32	2.57
03-60	0.032670	0.000985	0.281633	0.000010	0.281600	-1.59	0.35	2.27	2.58
03-43	0.012413	0.000338	0.281588	0.000009	0.281576	-1.06	0.3115	2.29	2.59
03-24	0.031835	0.000879	0.281664	0.000009	0.281637	-3.70	0.3115	2.22	2.60
03-04	0.018528	0.000464	0.281827	0.000007	0.281818	-11.59	0.2485	1.97	2.60
03-21	0.011207	0.000322	0.281594	0.000007	0.281583	-1.70	0.231	2.28	2.60
03-78	0.026583	0.000779	0.281821	0.000010	0.281806	-11.20	0.336	2.00	2.61
03-27	0.037728	0.001041	0.281577	0.000008	0.281538	-0.12	0.28	2.35	2.61
03-37	0.019254	0.000550	0.281819	0.000011	0.281809	-11.97	0.385	1.99	2.62
03-50	0.013270	0.000382	0.281580	0.000010	0.281567	-2.45	0.3325	2.31	2.65
03-79	0.007456	0.000254	0.281526	0.000013	0.281517	-0.96	0.455	2.37	2.66
03-63	0.029569	0.000861	0.281547	0.000012	0.281515	-0.99	0.42	2.38	2.66
03-40	0.029969	0.000847	0.281544	0.000014	0.281513	-1.06	0.49	2.38	2.67
03-22	0.002942	0.000064	0.281785	0.000007	0.281784	-12.65	0.245	2.01	2.67
03-68	0.003529	0.000110	0.281524	0.000010	0.281520	-1.66	0.35	2.36	2.68
03-59	0.031155	0.000962	0.281585	0.000011	0.281552	-2.98	0.385	2.33	2.68
03-01	0.009552	0.000277	0.281556	0.000009	0.281547	-3.18	0.301	2.33	2.69
03-07	0.029101	0.000779	0.281568	0.000009	0.281541	-3.14	0.3045	2.35	2.70
03-28	0.007070	0.000191	0.281542	0.000013	0.281535	-3.66	0.455	2.34	2.72
03-44	0.008266	0.000206	0.281499	0.000009	0.281491	-2.15	0.308	2.40	2.73
03-02	0.009178	0.000274	0.281539	0.000008	0.281530	-3.89	0.2765	2.35	2.73
03-51	0.006386	0.000153	0.281479	0.000008	0.281473	-1.79	0.287	2.43	2.74
03-33	0.002558	0.000064	0.281514	0.000009	0.281512	-3.96	0.3185	2.37	2.76
03-17	0.005848	0.000150	0.281465	0.000009	0.281459	-2.63	0.322	2.45	2.78
03-49	0.019156	0.000531	0.281472	0.000009	0.281452	-2.75	0.3255	2.46	2.79
03-47	0.003442	0.000098	0.281515	0.000008	0.281512	-5.25	0.273	2.38	2.79
03-53	0.030418	0.000887	0.281480	0.000007	0.281447	-3.01	0.252	2.47	2.81
03-08	0.022355	0.000583	0.281731	0.000011	0.281720	-15.02	0.385	2.11	2.82
03-34	0.002678	0.000068	0.281502	0.000009	0.281500	-5.75	0.329	2.39	2.82
03-13	0.002809	0.000081	0.281515	0.000009	0.281512	-6.48	0.308	2.37	2.83
03-46	0.023859	0.000650	0.281492	0.000008	0.281469	-5.17	0.273	2.44	2.84
03-38	0.029052	0.000861	0.281540	0.000009	0.281513	-7.20	0.322	2.39	2.85
03-41	0.013534	0.000398	0.281368	0.000008	0.281351	-1.03	0.287	2.59	2.86

03-09	0.013695	0.000387	0.281480	0.000010	0.281467	-5.96	0.3325	2.44	2.87
03-36	0.014279	0.000392	0.281482	0.000008	0.281469	-6.86	0.2625	2.44	2.89
03-30	0.023155	0.000573	0.281429	0.000008	0.281408	-4.56	0.2765	2.52	2.90
03-73	0.003283	0.000093	0.281452	0.000009	0.281449	-6.26	0.315	2.46	2.90
03-06	0.000121	0.000003	0.281590	0.000009	0.281590	-20.57	0.3185	2.27	3.13
03-52	0.004300	0.000137	0.281531	0.000007	0.281529	-22.61	0.2485	2.36	3.26
03-18	0.001591	0.000043	0.281533	0.000009	0.281532	-23.75	0.315	2.35	3.29

	$^{176}\text{Yb}/$ $^{177}\text{Hf}$	$^{176}\text{Lu}/$ $^{177}\text{Hf}$	$^{176}\text{Hf}/$ $^{177}\text{Hf}$	$\pm 2\sigma$	$^{176}\text{Hf}/$ $^{177}\text{Hf}(t)$	$\epsilon\text{Hf}(t)$	$\pm 2\sigma$	$T_{\text{DM}}(\text{Ga})$	$T_{\text{DM}}$ (crustal)
ALBSONG-04									
04-53	0.034986	0.000764	0.282423	0.000017	0.282412	3.43	0.595	1.17	1.44
04-31	0.029193	0.000779	0.282339	0.000018	0.282328	0.80	0.63	1.28	1.62
04-93	0.018070	0.000546	0.282285	0.000014	0.282277	-1.33	0.49	1.35	1.74
04-68	0.015287	0.000358	0.282270	0.000008	0.282265	-1.57	0.2765	1.36	1.77
04-65	0.017212	0.000563	0.282261	0.000011	0.282253	-1.90	0.385	1.38	1.79
04-70	0.019904	0.000468	0.282258	0.000011	0.282252	-2.40	0.385	1.38	1.81
04-69	0.028699	0.000683	0.282256	0.000010	0.282247	-2.53	0.35	1.39	1.82
04-77	0.011471	0.000346	0.282249	0.000008	0.282244	-2.93	0.2625	1.39	1.83
04-63	0.019408	0.000488	0.282233	0.000012	0.282226	-3.08	0.42	1.42	1.86
04-92	0.013844	0.000437	0.282232	0.000007	0.282226	-3.31	0.259	1.42	1.86
04-94	0.020189	0.000644	0.282212	0.000013	0.282203	-3.88	0.455	1.45	1.91
04-79	0.010612	0.000283	0.282204	0.000010	0.282200	-4.05	0.3465	1.45	1.92
04-76	0.009355	0.000249	0.282175	0.000013	0.282172	-5.17	0.455	1.49	1.98
04-74	0.009821	0.000251	0.282135	0.000009	0.282132	-6.57	0.3115	1.54	2.07
04-21	0.016994	0.000434	0.282105	0.000014	0.282099	-7.61	0.49	1.59	2.14
04-08	0.157870	0.003947	0.281854	0.000018	0.281708	5.88	0.63	2.13	2.23
04-50	0.098759	0.002410	0.281687	0.000013	0.281595	3.43	0.455	2.28	2.44
04-28	0.187161	0.004805	0.281762	0.000020	0.281583	1.67	0.7	2.32	2.50
04-02	0.037584	0.000971	0.281567	0.000010	0.281531	-0.31	0.35	2.36	2.63
04-04	0.070420	0.001687	0.281563	0.000016	0.281497	0.64	0.56	2.41	2.64
04-06	0.039127	0.000942	0.281558	0.000010	0.281523	-0.55	0.343	2.37	2.64
04-40	0.040362	0.000946	0.281560	0.000008	0.281525	-0.64	0.294	2.37	2.64
04-37	0.070239	0.001878	0.281577	0.000009	0.281507	-0.70	0.315	2.40	2.67
04-41	0.038124	0.000958	0.281516	0.000013	0.281479	-0.11	0.455	2.43	2.68
04-42	0.015693	0.000350	0.281515	0.000012	0.281502	-1.07	0.42	2.39	2.68
04-46	0.058459	0.001478	0.281531	0.000012	0.281474	-0.58	0.42	2.44	2.70
04-27	0.041625	0.001044	0.281523	0.000009	0.281484	-1.18	0.2975	2.42	2.71
04-19	0.062783	0.001649	0.281531	0.000008	0.281467	-0.62	0.2765	2.45	2.71
04-47	0.029358	0.000693	0.281513	0.000016	0.281487	-1.75	0.56	2.41	2.72
04-96	0.012517	0.000384	0.281500	0.000009	0.281486	-1.81	0.322	2.41	2.72
04-09	0.016659	0.000390	0.281508	0.000009	0.281494	-2.50	0.329	2.40	2.74
04-29	0.021669	0.000589	0.281496	0.000009	0.281474	-2.20	0.301	2.43	2.75
04-03	0.035527	0.000895	0.281521	0.000008	0.281489	-2.80	0.2905	2.42	2.75
04-83	0.009198	0.000274	0.281480	0.000009	0.281470	-2.76	0.322	2.43	2.77
04-15	0.019962	0.000520	0.281481	0.000009	0.281462	-2.57	0.3115	2.45	2.78
04-80	0.013716	0.000447	0.281473	0.000013	0.281456	-2.65	0.455	2.45	2.78
04-18	0.038031	0.000948	0.281487	0.000009	0.281451	-2.59	0.329	2.47	2.79
04-20	0.015787	0.000389	0.281498	0.000010	0.281484	-4.16	0.35	2.42	2.80
04-34	0.013025	0.000300	0.281450	0.000006	0.281439	-3.13	0.21	2.48	2.82
04-35	0.016423	0.000367	0.281454	0.000007	0.281441	-4.05	0.2345	2.47	2.85
04-45	0.016297	0.000398	0.281446	0.000011	0.281431	-3.77	0.385	2.49	2.85
04-16	0.020519	0.000487	0.281464	0.000009	0.281447	-4.82	0.2975	2.47	2.86
04-30	0.032218	0.000743	0.281525	0.000017	0.281501	-7.57	0.595	2.40	2.87
04-25R	0.022523	0.000543	0.281432	0.000014	0.281412	-4.30	0.49	2.52	2.89
04-17	0.022752	0.000529	0.281434	0.000007	0.281415	-4.75	0.2555	2.51	2.90
04-25C	0.022343	0.000599	0.281374	0.000010	0.281351	-4.91	0.343	2.60	2.98

04-57    0.245275    0.005377    0.281427    0.000015    0.281222    -10.08    0.525    2.88    3.29